THE UNIVERSITY OF MANITOBA

PRELIMINARY INVESTIGATIONS OF A SYSTEM COMPRISING A SELF-EXCITED INDUCTION GENERATOR ASYNCHRONOUSLY COUPLED THROUGH A D.C. LINK TO AN ISOLATED A.C. LOAD

by

Trevor Lorne Maguire

A thesis

presented to the University of Manitoba

in partial fulfillment of the

requirements for the degree of

Master of Science

in the

Department of Electrical Engineering

ISBN Ø-315-33952-7

PRELIMINARY INVESTIGATIONS OF A SYSTEM COMPRISING A SELF-EXCITED INDUCTION GENERATOR ASYNCHRONOUSLY COUPLED THROUGH A D.C. LINK TO AN ISOLATED A.C. LOAD

BY

TREVOR LORNE MAGUIRE

A thesis submitted to the Faculty of Graduate Studies of the University of Manitoba in partial fulfillment of the requirements of the degree of

MASTER OF SCIENCE

I hereby declare that I am the sole author of this thesis.

I authorize the University of Manitoba to lend this thesis to other institutions or individuals for the purpose of scholarly research.

Trevor Lorne MAGUIRE

I further authorize the University of Manitoba to reproduce this thesis by photocopying or by other means, in total or in part, at the request of other institutions or individuals for the purpose of scholarly research.

Trevor Lorne MAGUIRE

The University of Manitoba requires the signatures of all persons using or photo-copying this thesis. Please sign below , and give address and date.

ABSTRACT

This thesis reports on investigations into utilizing a self-excited induction generator asynchronously coupled through a D.C. link to an isolated A.C. load. A basic algorithm is developed for determining the capacitance and machine speed required to support self-excitation to a specified voltage level at a specified frequency. For given ranges of machine speed and real power load, the minimum capacitance required by the machine to maintain excitation at a given voltage level occurs at minimum speed and at maximum power. A program is discussed for generating families of curves descriptive of characteristic quantities of self-excited states as functions of machine speed and real and reactive loading. An additional algorithm is discussed for describing rectifier firing delay angle and rectifier I_d and V_d associated with maintaining machine voltage at a specified level over ranges of machine speed and power. Account is taken of commutating reactance, rectifier transformer magnetizing reactance, and minimum rectifier firing angle and also the extra terminal capacitance required because of these considerations. Novel chopper-inverter apparatus is discussed for interposing between the rectifier output and the A.C. load in order to match the required rectifier I_d and V_d to the requirements of the load over given ranges of machine speed and power. As an alternative apparatus, a dual arrangement of series capacitor commutated Graetz bridge inverters is briefly discussed. Preliminary proposals and studies are presented for appropriate control systems.

ACKNOWLEDGEMENTS

The author expresses appreciation to his thesis advisor Dr. A. M. Gole´ for his many suggestions and valued discussions and to Dr. R. W. Menzies for his instruction on non-linear search techniques.

The author is grateful to the University of Manitoba for support from it's Fellowship program and to the Natural Sciences and Engineering Research Council for financial support from the Post Graduate Scholarship program.

CONTENTS

CHAPTER ONE

INTRODUCTION

1.1. STATEMENT OF GENERAL OBJECTIVES

There has been considerable interest for the past several years in the utilization of self-excited induction generators in power system applications. That interest has been focused primarily upon two types of systems. On the one hand, a number of investigations [1,2,3] have looked into use of self-excited induction generators in isolated systems wherein an a.c. load is supplied directly from the machine a.c. output. Such systems require speed control for frequency regulation and reactive power control for voltage regulation. On the other hand, several investigations [4,5] have focused upon supplying power into a strong a.c. system through a d.c. link from a self-excited induction generator. Furthermore, some investigators [6,7] have looked into supplying an isolated d.c. load from the rectified output of a self-excited induction generator. In addition, articles [8] have been presented describing the process of self-excitation in induction generators and the steady state analysis [9,10] of such self-excited machines. In view of the considerable body of earlier work, this dissertation will focus upon preliminary investigations of a system comprising a self-excited induction generator asynchronously coupled through a d.c. link to an isolated a.c. load.

A number of steps were required in the course of this preliminary investigation. As a first step, a procedure was developed for producing an alternative set of operating curves descriptive of the operation of a self-excited induction generator. Next, a procedure was developed for producing a reduced set of curves. This reduced set of

curves describes the steady state quantities associated with the operation of a self-excited machine at a specific level of terminal voltage. The quantities are given as a function of machine speed and power level. One quantity described is the reactive loading that the rectifier must place upon the self-excited machine at a given combination of machine speed and power in order to maintain the machine voltage at the specified level.

Conclusions are presented concerning the effect of rectifier generated harmonics upon the typical self-excited machine.

Descriptions are presented concerning the nature of compatible devices for connection between the rectifier output and the isolated a.c. load. The positioning of these compatible devices in the circuit under consideration is as illustrated in Figure 1. The devices described are intended to complement the reactive power requirements of a self-excited induction generator and to permit the generator to be asynchronously coupled through a d.c. link to an isolated a.c. load. The devices are intended to permit a broad range of machine operating speeds. Suggestions are presented in respect of control strategy. The results of computer simulations are presented in order to confirm the suitability of certain aspects of the control strategy and to determine the response of the self-excited machine to changes in rectifier delay angle.

1.2 A REVIEW OF SOME PERTINENT ARTICLES

1.2.1 THE BENEFITS OF OPERATING A TURBINE AND GENERATOR UNIT AT VARIABLE SPEED

R. Nair [11] has reviewed the potential advantages of a system comprising an hydraulic turbine operable at varying speed driving a synchronous generator connected through a d.c. link to an a.c. system. Two advantages that he points out are increased turbine efficiency and simplified turbine equipment.

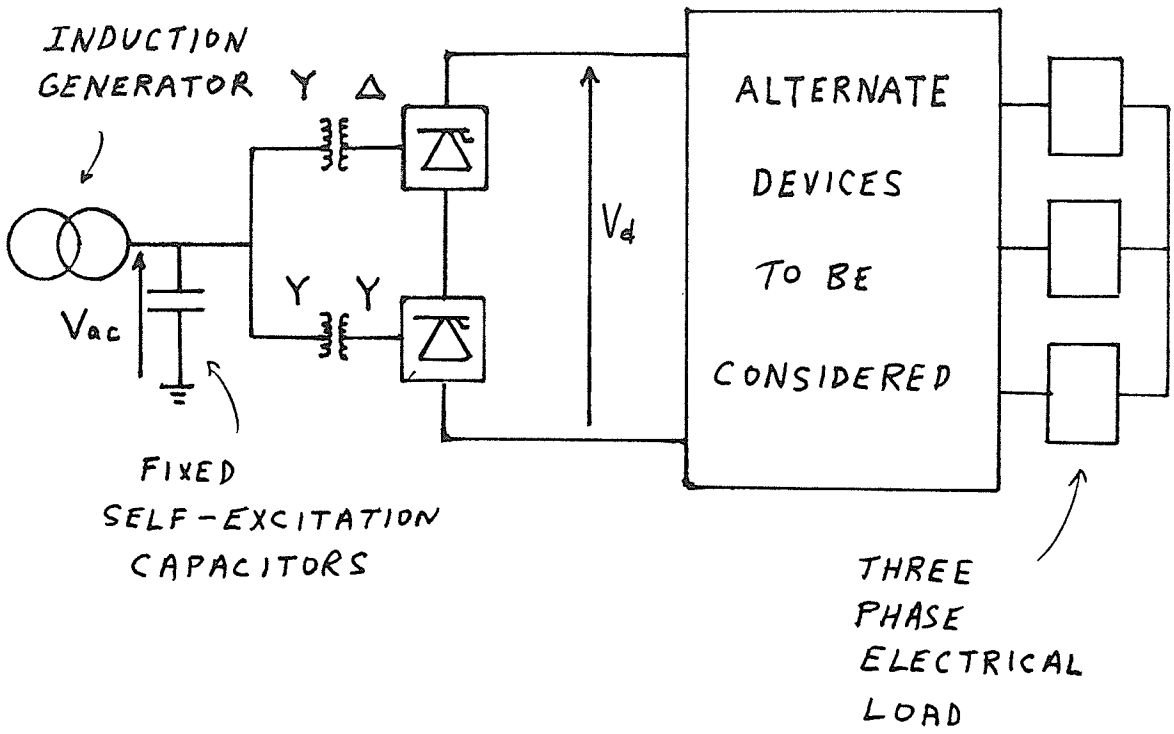

Figure 1 Circuit Configuration Under Consideration

Nair's remarks as to efficiencies are directed particularly to propeller turbines. Nair notes that high efficiencies can be maintained for propeller turbines operated under varying head conditions by operating the propeller turbine at an optimum load and speed for any particular head condition. The efficiencies thus obtained are said to be comparable to the efficiencies which can be obtained from a Kaplan turbine operable only at constant speed. Speed variation is necessary for this method of maintaining efficiencies. However, it should be noted that the efficiency of a propeller turbine operated in a variable speed mode will not be as high as for a Kaplan turbine when the propeller turbine is operated at loads which depart from the optimum load for a given head. This speed variation method of maintaining efficiencies allows propeller turbines to operate efficiently under more variable head conditions than can be accommodated by a propeller turbine operated at constant speed.

Nair suggests that the speed maintaining qualities of the turbine governor can be significantly reduced if asynchronous coupling of the generator to the load is provided. In such a system, the mechanical speed of the generator does not affect the frequency regulation of the voltage supplied to the customer. Thus, with asynchronous coupling, if the load decreases then the turbine governor can be allowed to accelerate up to it's runaway speed under light electrical load conditions. Runaway speed, for a given head, is the speed to which a turbine will go before hydraulic and frictional losses completely dissipate the power of the water passing through the turbine. At such a speed there is no additional water power to accelerate the turbine to a faster speed. If an electrical load was then placed on the runaway generator, the generator torque would cause the turbine to slow until at full electrical load the turbine would be running at a relatively efficient speed. Runaway speeds vary with turbine type but are usually 2 to 3 times faster than normal efficient running speeds. In such an unusual configuration no governor would be required.

However, for large turbines, Nair concludes that at least slow acting gate control would likely be required for several reasons, namely: to limit flow because of excess head; to give some limited flow control for operation with well defined heads; to facilitiate load sharing between units; to limit the duration of overspeed conditions; to reduce any hydraulic instability at light loads; and to improve efficiency.

It is submitted that Nair has in general demonstrated the potential advantages of being able to operate an hydraulic turbine at variable speed. In addition, Monition, Le Nir, and Roux [12] have presented an efficiency chart which shows maximum efficiency for a Pelton turbine to occur at a particular speed per metre of head.

In relation to wind turbines, Watson et al [6] present a graph which illustrates that the optimally efficient rotor speed of a wind turbine increases with increasing wind speed. In addition, Moretti and Divone [13] present a set of curves relating the

efficiencies of various types of wind turbines to the ratio of blade tip speed to wind speed. The curves show that for each type of wind turbine the maximum efficiency occurs at a fixed ratio of tip speed to wind speed.

1.2.2 THE INDUCTION GENERATOR

Various authors [9,10] have listed the characteristics of induction generators which create the potential for their more frequent use in power systems. Briefly, the wound rotor of a synchronous generator is usually not present in an induction machine because most induction machines use the less elaborate and more sturdy squirrel cage rotor. The use of the squirrel cage rotor eliminates the need for brushes and a separate source of d.c. excitation current. Also unit costs and maintenance costs for induction generators are generally lower than those for synchronous generators.

The simplest method for utilizing an induction generator is for it to be connected directly to a strong a.c. system. Such an approach has several inherent disadvantages, namely: large inrush currents may occur upon connection of the induction generator to the system; fault levels on the system may rise; and the induction generator must operate at the frequency of the a.c. system. Capacitor banks may be provided at the terminals of the induction generator to compensate some of the reactive load that the generator places on the system. However, if an attempt is made to compensate the entire reactive load of the generator with fixed capacitors, then the induction generator could suffer a destructive overvoltage due to uncontrolled self-excitation in the event of an unintended opening of the generator feeder.

1.2.3 AN EXISTING SCHEME FOR THE APPLICATION OF INDUCTION GENERATORS UTILIZING A D.C. LINK

Arrillaga, Watson et al [5,6] suggest that the above mentioned difficulties associated with induction generators can be overcome by connecting a self-excited induc-

tion generator to an a.c. system by means of a d.c. link as shown in Figure 2.

With reference to Figure 2, the voltage $V_{a.c.}$ indicates the induction generator voltage while the voltage V_d indicates the rectifier output voltage. Both $V_{a.c.}$ and the ratio $\frac{V_d}{V_{a.c.}}$ are inversely related to the firing delay angle α of the rectifier.

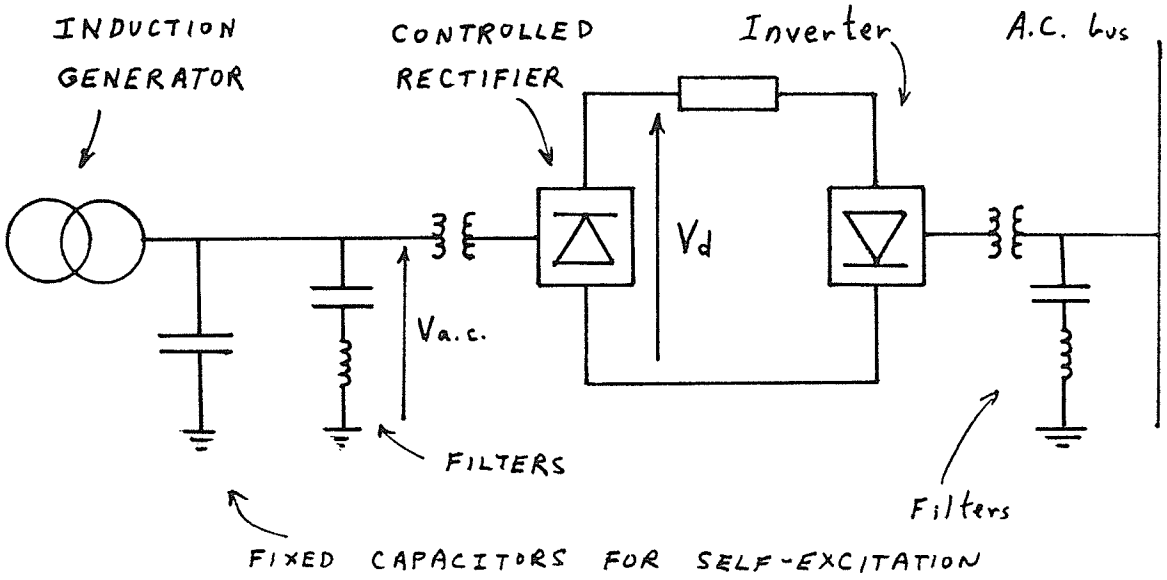

Figure 2 Connection of an Induction Generator to an A.C. System Through a D.C. Link

The induction generator voltage $V_{a.c.}$ will decrease due to an increase in α toward 90° because the rectifier will exhibit an increased demand for reactive power and that demand will restrict the induction generator excitation current.

The ratio $\frac{V_d}{V_{a.c.}}$ will also decrease with increasing α . This relation exists because, as a first order approximation appropriate for Graetz bridge rectifiers, d.c. voltage V_d is related to a.c. voltage $V_{a.c.}$ by the well known equation [14]:

$$V_d = K\ V_{a.c.} \cos \alpha \ . \qquad (1.1)$$

Thus V_d can be controlled in the configuration of Figure 2 because both $V_{a.c.}$ and cos α are inversely related to α for angles of α appropriate for rectification.

Arrillaga et al have verified the above described method of controlling V_d by assembling and testing a model consisting of a self-excited induction generator with fixed capacitors feeding a controlled rectifier which in turn was supplying a resistive load as illustrated in Figure 3. The flexibility of the system is demonstrated by the fact that a change in the resistive load R_l does not affect the ability of the apparatus to provide a constant controlled d.c. voltage to the load resistance.

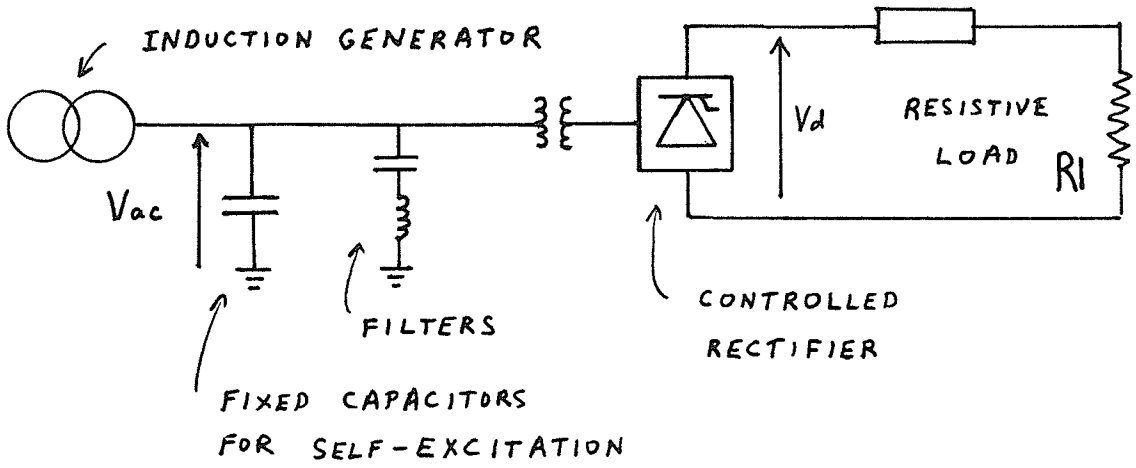

Figure 3 A Self-Excited Induction Generator Supplying a D.C. Resistive Load Through a Controlled Rectifier

Arrillaga et al confirmed that while providing a constant voltage to a constant resistive load in Figure 3 the apparatus could accommodate increases or decreases in the induction generator speed by means of variation of the firing delay angle α. However, for a given capacitance and load resistance only a 10 to 20 % variation in machine speed could be accommodated by variation of α between 0° and 50°. The limited speed range is due to the fact that increased machine speed and frequency cause the susceptance of excitation capacitors to rise which in turn causes $V_{a.c.}$ to tend to rise. For small values of α, an increase in α is an acceptable method of

controlling V_d to a constant value. However, as α reflects the ratio $\frac{V_{a.c.}}{V_d}$, high α also reflects high $V_{a.c.}$ for a constant V_d. Thus, in maintaining constant V_d, increasing α only remains an option as long as the induction generator voltage does not reach a maximum allowable level. Arrillaga et al also demonstrated that the machine speed range could be extended by switching in the excitation capacitors in stages. In this dissertation the approach of switching capacitors will be avoided.

It will be shown in this thesis that a wide range of machine operating speed can be obtained for any given load between zero and rated power by causing the d.c. link current to increase with increasing machine speed. For a given power level there will of course be an accompanying decrease in d.c. link voltage when the d.c. link current rises. By this method it will be shown that machine voltage can be maintained at 1.0 p.u. for machine speeds between, for example, 0.9 and 1.8 p.u. and machine power anywhere between zero and rated.

1.2.4 A RECENTLY DEVELOPED SCHEME FOR SUPPLYING A D.C. LOAD FROM A SELF-EXCITED INDUCTION GENERATOR

Rocha, Watanabe, and Carneiro [7] have recently suggested the use of a scheme as illustrated in Figure 4. In the circuit a load is supplied with a d.c. current I_o at a desired d.c voltage V_o according to a load voltage reference signal $V_{loadreference}$. The exact details of the chopper circuit do not appear to have been given in the article but the nature of the chopper and it's operation have been deduced by an analysis of the waveforms which were presented. The chopper appears to be functionally as shown in Figure 5.

The operation of the apparatus disclosed by Rocha et al will be described in relation to Figure 5 and the waveforms illustrated in Figure 6.

Referring to Figure 5, when switch 1 is closed, switch 2 is open and vice versa. Each of the switches are operated at a frequency which is 6 times that of the

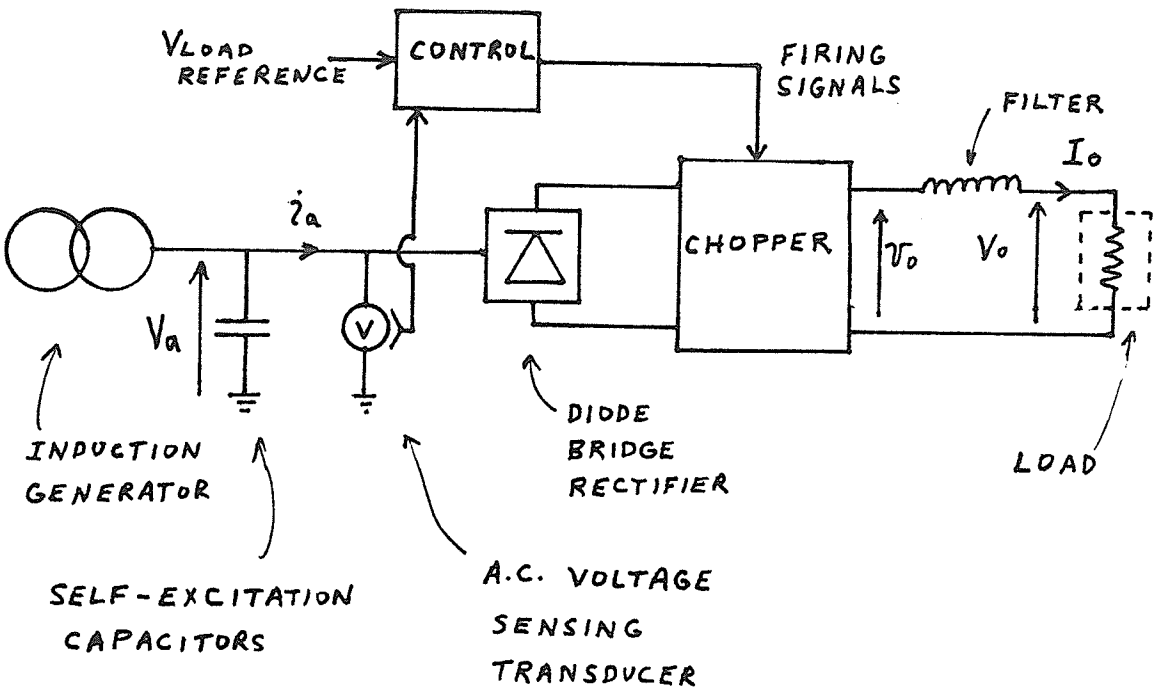

Figure 4 A Self-Excited Induction Generator Supplying a D.C. Resistive Load Through an Uncontrolled Rectifier With Chopper .

induction generator output voltage and the switches are precisely synchronized with the waves of induction machine voltage. When switch 2 is open, switch 1 is closed and current I_o passes through switch 1 to the load from the diode rectifier. However, when switch 1 is open, no current passes through it or the rectifier and the load current I_o circulates through a closed switch 2.

Figure 6 herein illustrates the waveforms associated with the Rocha et al apparatus. The fundamental component of current into phase "a" of the rectifier can be made to lead the induction machine voltage V_a by 15° (ϕ in Figure 6) by closing switch 1 at the instant that V_a becomes larger than V_b . The rectifier in that mode of operation appears as a source of reactive power to the induction machine and will promote higher self-excitation of the machine. The current into phase "a" of the rectifier can be made to lag behind V_a by 15° by delaying the closed period of switch 1 by 30° with respect to the phase relationship illustrated in Figure 6. The

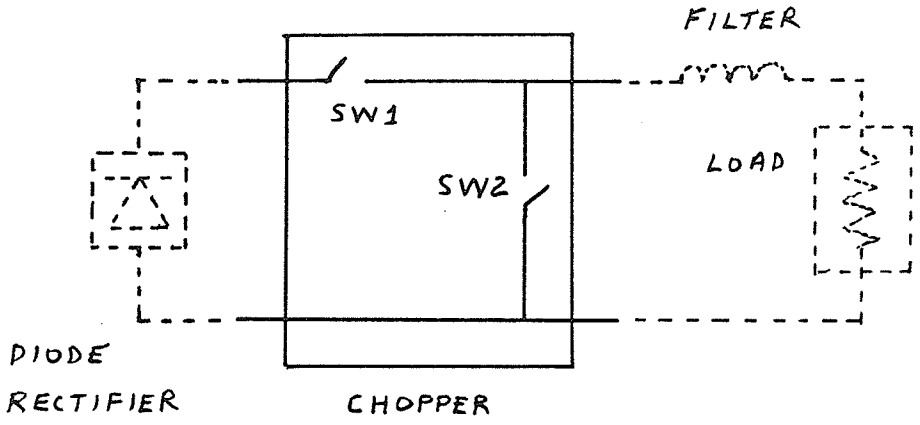

Figure 5 Chopper Circuit Deduced to be as in Fig. 4

rectifier in that mode of operation appears as a reactive load and inhibits the capacitors in exciting the induction machine. This manner of restricting excitation current to the induction machine can be used during higher speed operation so as to help limit machine voltage. Phases "b" and "c" of the rectifier present similar impedances to the induction machine.

It can be noted that the rectifier in the Rocha apparatus always draws low a.c. current when the d.c. load current is low. When the rectifier draws low a.c. current it will neither absorb nor produce significant reactive power. One can thus conclude that the practise in the Rocha et al apparatus of phase shifting the closed interval of switch 1 with respect to the induction machine voltage can only have an effect on machine voltage at those times when a d.c. load current is present. Thus, without a load current, the machine voltage will rise quickly with increasing machine speed.

I have given a rather detailed explanation of the Rocha et al apparatus because their original publication is in Portugese and also because the block diagram of their

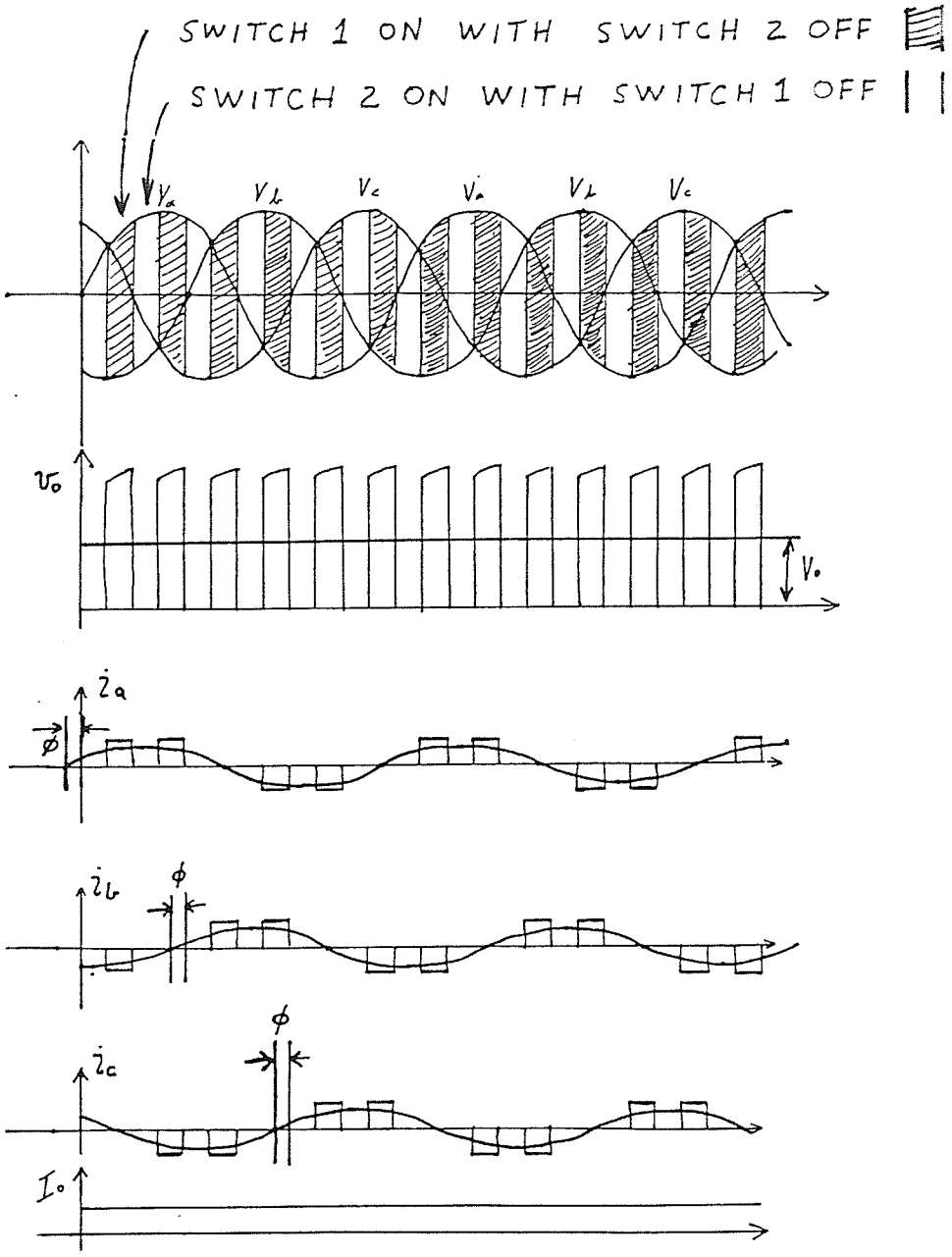

Figure 6 The Waveforms for Apparatus Illustrated in Figure 4

apparatus gives the inaccurate impression that their apparatus is very close to apparatus presented in this dissertation.

1.2.5 BIBLIOGRAPHY

In addition to those articles already mentioned, references [15] to [30] describe various ancillary aspects of self-excitation in induction machines.

1.3 OUTLINE OF THE THESIS

Chapter one gives a brief introduction to prior art; presents a bibliography of pertinent articles; presents a brief review of certain articles; and gives an outline of the thesis. One reviewed article plus additional references demonstrate the benefits of running a wind or hydraulic turbine at variable speed. A number of prior schemes are discussed to illustrate the state of the art in utilizing d.c. links fed from self-excited induction generators.

Chapter two presents a brief review of the process of self-excitation; discusses basic modelling techniques developed by others; presents the procedure for developing a program for estimating suitable terminal capacitance; presents the procedure for obtaining a novel set of steady state operating curves for a self-excited induction machine supplying real and reactive load; and presents a comparison of calculated operating curves to those obtained in the laboratory. The operating curves developed are families of constant value curves in the terminal voltage VT versus load resistance RL plane. Quantities plotted in the VT versus RL plane are: frequency F, machine speed MSPD, machine terminal current, capacitor current, total load current, load power, and slip S. For each quantity several planes must be developed corresponding to different values of load reactance XL.

Chapter three addresses a number of issues. The voltage of operation for the induction machine in the proposed system is chosen at 1.0 p.u. voltage. A procedure is developed for producing a reduced set of operating curves which describe steady state quantities associated with operation at a specific level of terminal voltage (ex. 1.0 p.u.). In the reduced set of curves each quantity of interest is described in a

plane as a function of machine speed and power level. The quantities which are considered are: total load current, load power factor angle, the real component of current into the load, the reactive component of current into the load, the machine terminal current, magnetizing current, and airgap voltage.

Section 3.5 demonstrates that commutating reactance, rectifier minimum α setting, and rectifier transformer magnetizing reactance all require the provision of additional capacitance at the terminals of the self-excitation machine. A procedure is demonstrated for determining that extra capacitance and then for modifying the reduced set of curves discussed earlier in the chapter.

The apparatus between the rectifier and the load in Figure 1 must act to match the output of the rectifier to the requirements of the load while maintaining the machine voltage at 1.0 p.u. The necessity to have a specific I_d and V_d for each combination of machine speed and power is pointed out in section 3.6.

Section 3.7 discusses the harmonic currents which can be expected in the induction machine and the reduction to be expected from using a 12 pulse rectifier instead of a 6 pulse rectifier.

Section 3.8 presents two alternative configurations of apparatus for connection between the rectifier and the load. The first alternative is a chopper and inverter circuit which includes an inverter which is intended to produce balanced voltages. The second alternative comprises a dual arrangement of series capacitor commutated inverters. Both alternatives are discussed with respect to their steady state condition. In addition a control strategy is proposed for the first alternative and a discussion is presented as to disturbances from the steady state. Ripple on the smoothing inductor current and the smoothing capacitor voltage for the first alternative is discussed in section 3.8.2.3. Proposed controllers for the first alternative are discussed in section 3.8.2.4. The second alternative is discussed in section 3.8.3. That section proposes that a dual arrangement of series capacitor commutated Graetz bridge inverters could be

used in place of the chopper-inverter apparatus. It is demonstrated that the Graetz bridge inverter valves and capacitors must have increased voltage ratings to accommodate variable d.c. current operation.

Chapter four consists of three related sections.

Section 4.2 presents the results of a transient simulation of a chopper and inverter apparatus of chapter 3 supplying a load through filters. The rectifier output voltage and the chopper duty cycle are constant during the simulation so that the simulation in fact represents operation with the controls momentarily frozen. The method of creating the simulation subroutine for the chopper and inverter is also discussed.

Section 4.3 presents the results of a transient simulation of controllers which are based on the principles described in section 3.8.2.4. The simulation confirms that the capacitor voltage controller and the inductor current controller can be made to operate simultaneously.

Section 4.3 presents a simulation to demonstrate that the load suppression of self-excitation voltage is a comparatively slow phenomena even if the machine in question is operating with light saturation and undergoes a large immediate load increase.

CHAPTER 2

DEVELOPING CHARACTERISTIC CURVES OF A SELF-EXCITED INDUCTION GENERATOR WITH LOAD

2.1 INTRODUCTION

Self-excitation in induction machines can occur when sufficient terminal capacitance is connected to the output of an induction machine which is being mechanically driven at sufficient speed. The process of self-excitation has been analyzed in terms of a permanent magnet machine which converts to an asynchronous generator as the induced currents circulating between the generator and the capacitors grow in magnitude [8]. At very low levels of induced currents it is believed that the residual flux of the rotor causes the machine to act like a permanent magnet generator. In the permanent magnet mode the induced currents in the machine will tend to grow if the terminal capacitance on the machine is sufficient. When the currents have grown to a sufficient level they begin to coercise the residual flux on the rotor and the induction machine transforms from permanent magnet operation to asynchronous operation as a self-excited induction generator.

In this chapter, methods will be described for obtaining a novel set of operating curves descriptive of the steady state operation of a self-excited induction generator connected with terminal capacitors and supplying real and reactive load. As a preliminary step a program is developed which is used to determine the capacitance and machine speed required in order to provide a specified voltage and frequency at the machine terminals for a given load.

2.2 A MODEL OF THE SELF-EXCITED INDUCTION GENERATOR

2.2.1 THE EQUIVALENT CIRCUIT REPRESENTATION

The approach used in obtaining the operating curves is based upon the solution of transcendental equations similar to those described by S. S. Murthy et al [9,10].

The basic circuit configuration is as illustrated in Figure 7. In the analysis to follow circuit element parameters illustrated in Figure 7 including RL, XL, XC, RS, XS, XM, RI, XR, and RR all express impedance magnitudes at 1.0 p.u. frequency. XC has units of (ohms × p.u. freq.). XL, RL, RS, RI, and RR have units of (ohms). Finally, XS, XM, and XR have units of (ohms / p.u. freq.)

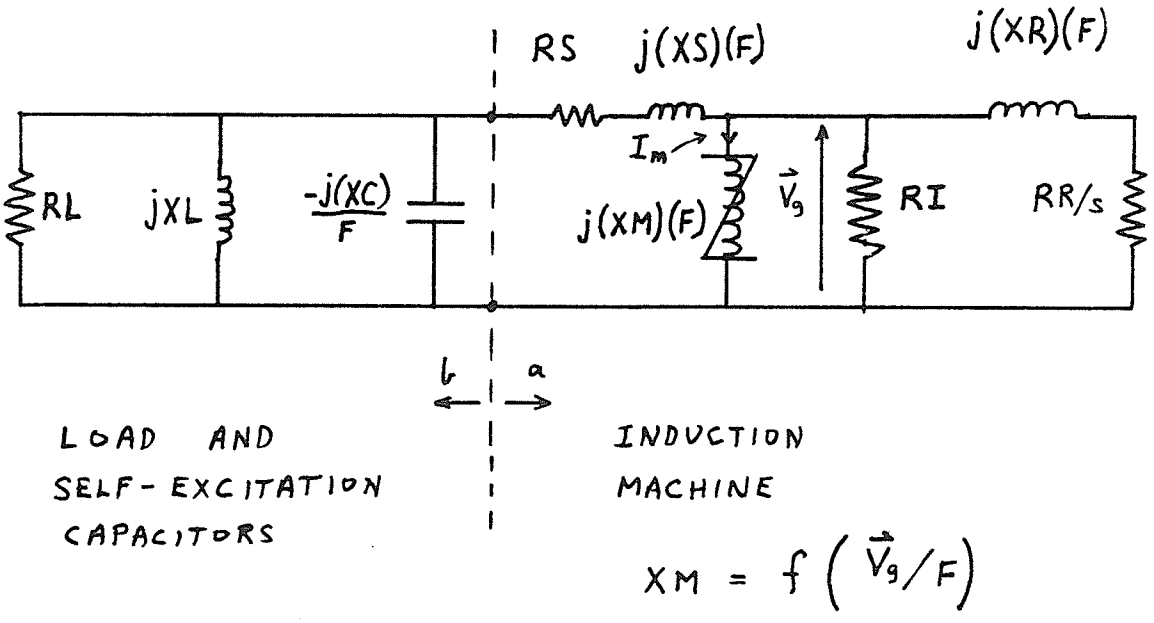

Figure 7 Steady State Single Phase Representation of a Three Phase Self-Excited Induction Machine with Load

The reactive load XL is shown in Figure 7 as being frequency independant. This approach has been taken because the load is intended to represent a rectifier and as a first approximation the power factor of a rectifier is determined by α and does not

depend heavily upon frequency.

In the analysis to follow the circuit parameters XS and XR representative of stator and rotor leakage are assumed to be independant of the magnitude of stator and rotor currents. The assumption is justified by the premise that a self-excited induction generator should never be operated at levels of stator or rotor current which could cause saturation of the flux leakage paths. Such currents and saturation normally occur in induction motors only during starting when one would normally expect several times normal running current to be present in both the stator and the rotor coils.

The circuit element parameter XM in Figure 7 is not a constant but varies with the saturation level of the machine's air gap flux path. Saturation of the airgap flux is of course dependant upon the magnitude of airgap flux linkage. Airgap flux linkage in turn is determined by airgap voltage and electrical frequency.

The relation $XM = f\,(V_g/F)$ indicated in Figure 7 relates XM (ohms / p.u. freq.) to V_g/F (volts / p.u. freq.). XM represents the machine magnetizing reactance at 1.0 p.u. frequency. V_g represents the magnitude of the airgap voltage phasor in r.m.s. volts and F represents electrical frequency in p.u.. The relation $XM = f\,(V_g/F)$ is developed for a given machine by consideration of the machine's magnetization curve obtained at one frequency.

The magnetizing curve typically relates the magnitude of the airgap voltage phasor at 1.0 p.u. frequency $V_{g1.0}$, to the magnitude of the magnetizing current phasor I_m. The magnetizing curve is usually obtained by applying a range of voltage magnitudes at 1.0 p.u. frequency to an induction machine driven at 1.0 p.u. speed in a synchronous speed test. The magnetizing curve $V_{g1.0}$ versus I_m can be plotted given the results of the synchronous speed test and reliable values of stator resistance and stator leakage impedance at 1.0 p.u. frequency (i.e. RS and XS respectively).

The magnetizing curve $V_{g1.0}$ versus I_m obtained in the above specified manner actually relates airgap voltage per p.u. frequency to the magnetizing current. If the frequency of the airgap voltage goes up then $V_{g1.0}$ must be multiplied times F (p.u. freq.) / 1.0 (p.u. freq.) to get the actual airgap voltage V_g for a given magnetizing current I_m . Clearly this relationship can be expressed as $V_{g1.0} = V_g/F$. Thus, as an alternative , one can express the magnetizing curve in terms of V_g/F (volts / p.u. frequency) versus I_m (amps). The magnitudes obtained for the V_g/F axis will be 60 $\times 2\pi$ times the actual flux linkage phasors for a base frequency of 60 hertz because V_g/F has a denominator which is in p.u. rather than actual electrical radians / second.

Given the V_g/F (volts / p.u. freq.) versus I_m (amps) curve, one can then relate the XM (ohms / p.u. freq.) to I_m (amps) due to the relation:

$$XM = \frac{V_G/F}{I_m} \tag{2.1}$$

It is a simple matter to plot a V_g/F versus XM curve once curves have been obtained relating V_g/F to I_m and XM to I_m . The actual magnetizing impedance at any XM and F is obtainable by multiplying XM (ohms / p.u. frequency) times F (p.u. freq.). Also, using the V_g/F versus XM curve, the actual airgap voltage V_g (volts) for a given XM and F is obtainable by multiplying the given F (p.u.) times the V_g/F which corresponds to the given XM.

A typical V_g/F versus XM curve is illustrated in Figure 8. The curve in Figure 8 is for motor # 1 as described in Appendix 1.

It is useful to note that each XM on the curve of Figure 8 corresponds to a particular magnetizing current level and thus to a corresponding particular saturation level.

One notable aspect of the curve illustrated in Figure 8 is that V_g/F is not a single valued function of XM. In particular, one can note with some difficulty that

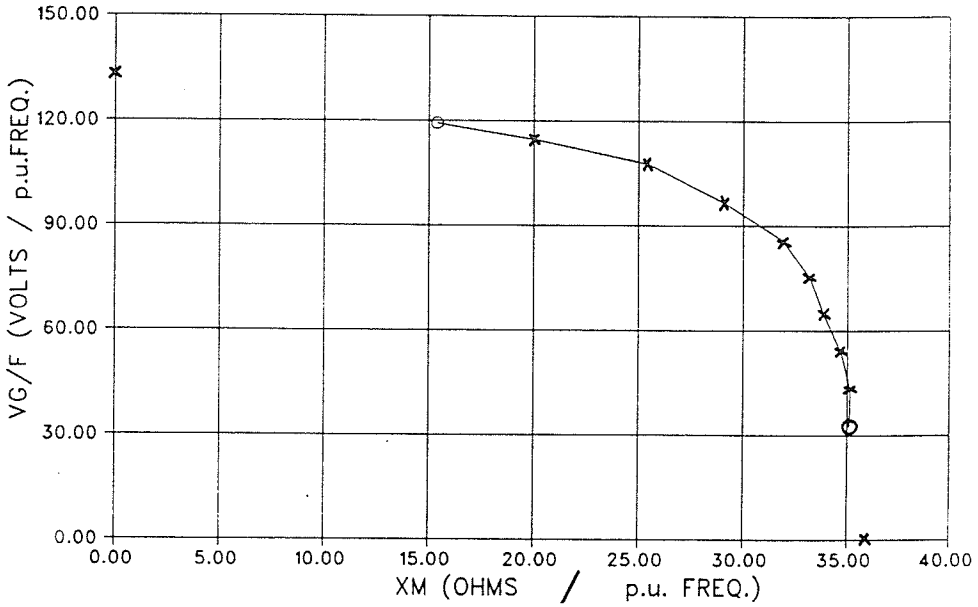

Figure 8 The V_g/F versus XM Curve for the Laboratory Machine Described in Appendix 1

tracing the curve from the minimum illustrated V_g/F causes XM to increase slightly and subsequently to decrease. Elder et al [8] have demonstrated that this should be expected.

Using a technique for measuring magnetizing inductance at low levels of magnetizing current, Elder et al were able to obtain a curve of magnetizing inductance versus magnetizing current which they illustrated as their Figure 2. From the information in that curve the magnetizing curve for their machine is illustrated in Figure 9. From Figure 9 a V_g/F versus XM curve can be obtained and is illustrated as Figure 10.

Only those points on the curve of Figure 10 disposed above the "x" can be stable operating points. Those points below the "x" cannot be stable operating points. For illustrative purposes consider point "A" on Figure 10 and assume that the machine is operating at a particular frequency. Then assume that there is just sufficient

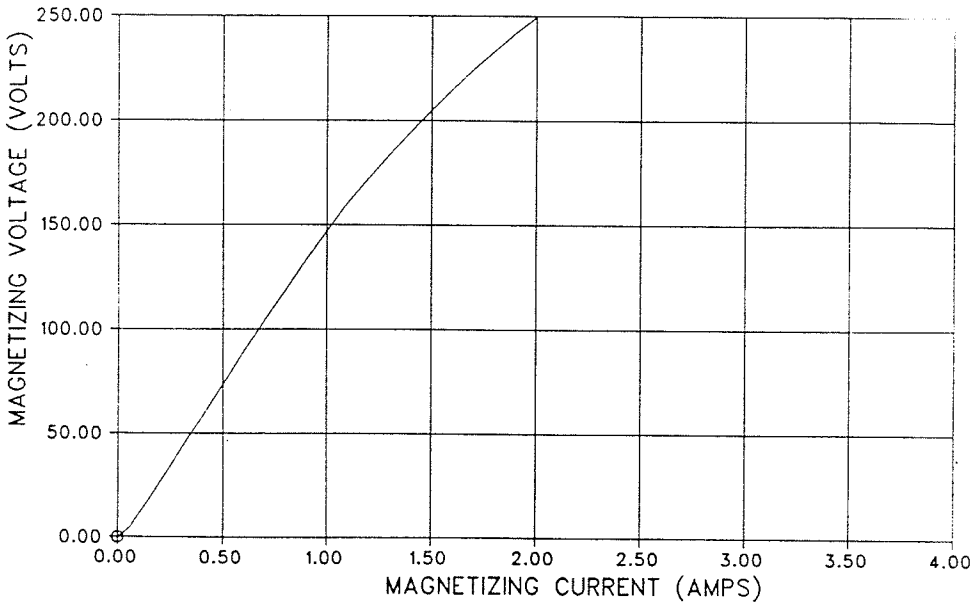

Figure 9 The Magnetizing Curve for the Elder et al [8] Machine

capacitive susceptance connected on the machine terminals to support self-excitation of the machine when XM is equal to 135.0 (ohms / p.u. freq.) which corresponds to the XM for point "A". If under those circumstances the machine is operating at the airgap voltage level of point "A" then the slightest increase in airgap voltage will cause XM to increase. Such an increase in XM will reduce the magnetizing current. The resulting surplus reactive power provided by the terminal capacitors drives the airgap voltage higher until a stable point is encountered in the vicinity of point "B". Likewise, if the machine is operating at the airgap voltage level of point "A" under the above circumstances then the slightest decrease in airgap voltage will cause XM to decrease. Such a decrease in XM will increase the magnetizing current. The resulting deficit in reactive power provided by the self-excitation capacitors causes the airgap voltage to collapse to negligible levels. Similar arguments can be used to demonstrate that point "B" in Figure 10 can be a stable operating point for self-excitation.

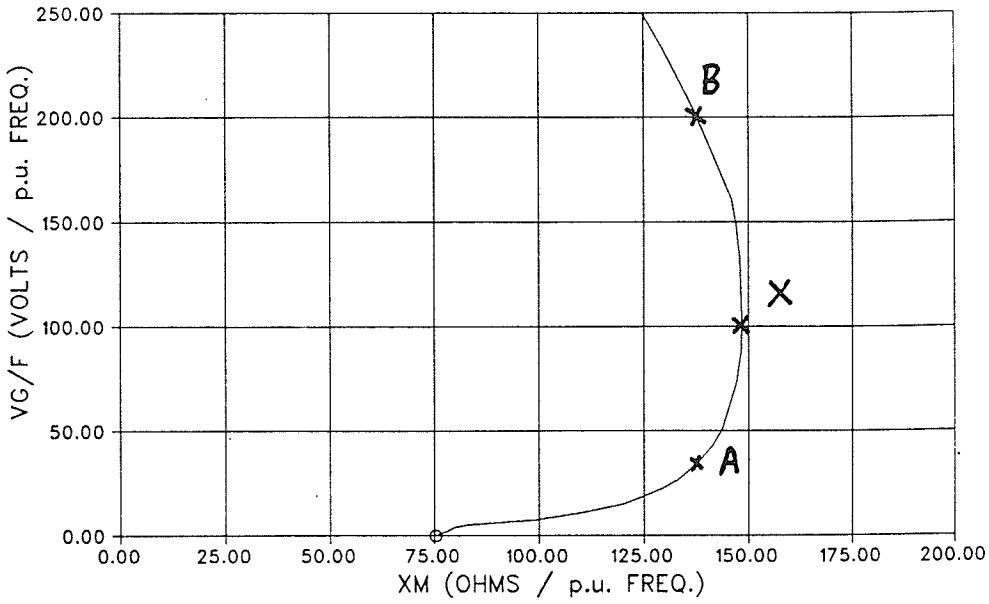

Figure 10 The V_g/F versus XM Curve for the Elder et al [8] Machine

The point "x" in Figure 10 represents a boundary for the loss of self-excitation. For illustrative purposes, assume that the self-excited machine is in a stable operating condition at point "B" supplying a load represented by RL and XL in the single line diagram of Figure 7. Assume the machine speed is adjusted to maintain one operating frequency. The capacitor XC supplies the reactive power to the machine and the load. If the load begins to draw more reactive power there will be less reactive power for the machine. The result is that the machine will become less self-excited; the saturation of the airgap flux will reduce and XM will increase. By this means the machine can come to a stable operating point at a reduced voltage level somewhere between points "B" and "x" in Figure 10. However, if the load current into RL and XL continues to increase the machine will reach it's maximum XM. If the load current is increased further there will be a deficit of reactive power which will not be corrected because the machine cannot come further out of saturation to reduce it's reactive power requirements. Under this final circumstance self-excitation will be

lost and the machine voltage will drop to negligible levels.

Turning again to Figure 10 it can be concluded that, in determining the stable operating points of a self-excited induction machine, one need only consider the negatively sloped portion of a V_g/F versus XM curve.

2.2.2 THE INDICIA OF A STEADY STATE OPERATING CONDITION

Four criteria indicative of a validly calculated steady state operating condition for a self-excited induction generator are as follows:

(1) The generator must operate at negative slip. Slip (p.u.) is indicated by "S" in Figure 7.

(2) The apparatus must of course operate at positive frequency. Frequency (p.u.) is indicated by "F" in Figure 7.

(3) The only permissible values for XM (ohms / p.u. freq.) are those positive values that are under the V_g/F versus XM curve. Furthermore, a lower bound may be specified for XM because each XM corresponds to a particular magnetizing current level. For the machine described in Figure 8, an XM of 14.0 (ohms / p.u. freq.) corresponds to a magnetizing current of 8 amps. The machine is only rated for 6.4 amps of stator current so that one can safely omit consideration of XM less than 14.0 (ohms / p.u. freq.) when considering feasible operating points for that machine.

(4) The impedance looking into the terminals of the induction machine (as at "a" in Figure 7) must be equal in magnitude but 180° out of phase with the impedance looking into the parallel arrangement of capacitor and load (as at "b" in Figure 7). This last requirement assures that the power absorbed by the load is equal to the power produced by the generator and that the reactive power absorbed by the generator is equal to the reactive power produced by the combined load and self-excitation capacitors.

2.2.3 FINDING STEADY STATE OPERATING CONDITIONS

Turning again to Figure 7, it is clear that for a given load (RL and XL) and capacitance (XC), all equivalent circuit impedances are fixed by S (slip in p.u.), F (terminal frequency in p.u.), and XM (magnetizing impedance in ohms / p.u. freq.). However, a real solution (S_1, F_1, XM_1) to the circuit equations will not always exist for every set of XC, RL, and XL. For instance, when RL = 0.0 ohms, the capacitor voltage and current must go to zero and the induction machine loses it's source of excitation current.

In looking for steady state operating conditions the mismatch in impedance in the fourth requirement is used as an objective function which must be minimized by search techniques. The first three requirements impose bounds on the values of S, F, and XM which can be legitimately searched.

The objective function is given by an equation as follows:

$$F = \left| R_{in} + R_{out} \right| + \left| X_{in} + X_{out} \right| \tag{2.2}$$

wherein:

R_{in} is the real part of the impedance looking into the machine terminals in Figure 7;

R_{out} is the real part of the impedance looking out of the machine terminals of Figure 7;

X_{in} is the imaginary part of the impedance looking into the machine terminals in Figure 7; and

X_{out} is the imaginary part of the impedance looking out of the machine terminals in Figure 7.

The result of the search converges to a true result as the objective function is reduced to zero. Suitable search techniques include simplex search and pattern search methods. However, simplex allowed a more reliable and faster convergence of

the objective function to zero for those cases with a real solution.

In cases where the above four criteria can be met, the negatively sloped portion of the V_g/F versus XM curve is used to determine the airgap voltage level. The airgap voltage level can then be used to determine all other voltages and currents in the circuit of Figure 7.

2.3 A PROGRAM FOR ESTIMATING SUITABLE TERMINAL CAPACITANCE

Most a.c. generators are required to supply a given terminal voltage at a given frequency to a given load. In order to accomplish that result with a self-excited induction machine it is necessary to connect a particular size of terminal capacitance to the induction machine and then to drive the machine at a particular speed. In order to determine the required capacitance and speed in advance it is necessary to solve the equations for the equivalent circuit network illustrated in Figure 7. That is the purpose of the program described in this section and referred to as program I.

The magnitude of terminal voltage and frequency are specified at the beginning of the program. However, XC is unknown and thus terminal current is unknown. Because terminal current is unknown the airgap voltage V_g is also unknown. V_g is related to the saturation level of the airgap flux and thus XM is unknown. The power which must be transferred across the airgap is also unknown because iron losses and stator copper losses are unknown. The fact that airgap power and airgap voltage are unknown dictates that slip S is unknown.

Because of the above considerations, the search variables in this program are slightly different from those described in section 2.2. In this program it is not necessary to search over F because we merely set F to the desired value. However, in place of F, XC (ohms × p.u. freq.) is a unknown and is used as a search variable. Slip S (p.u.) and magnetizing reactance XM (ohms / p.u. freq.) remain as the other variables.

Also in this program we are not satisfied just to find any steady state operating point. We in fact wish to find a steady state operating point with a certain level of terminal voltage. Thus the objective function described in Eqn 2.2 must be supplemented with a term which will go to zero as the terminal voltage approaches the desired value. The new objective function is as follows:

$$F_1 = F + (WT) \times \left| V_t - V_{desired} \right| \tag{2.3}$$

wherein:

F is given by Eqn. 2.2;

WT is a weighting factor;

$V_{desired}$ is the desired terminal voltage; and

V_t is the terminal voltage calculated for each set of variables (XC,S,XM) tested in the search routine.

A copy of program I, complete with exemplary input and output files, is included in App. 2 of [43]. In the example, the program calculated the XC (ohms × p.u. freq.) and machine speed (p.u.) required for the machine of Appendix 1 to supply a load of 38.6 ohms with a voltage of 120 volts r.m.s. l-n at 1.0 p.u. frequency.

2.4 A PROGRAM FOR OBTAINING STEADY STATE OPERATING CURVES FOR A SELF-EXCITED INDUCTION MACHINE - PROGRAM II

2.4.1.1 GENERAL DESCRIPTION

Most a.c. generators, including self-excited induction generators, typically supply a load which varies in impedance magnitude and power factor. Because of the normal variability of load, it was decided to develope a computer program to generate a set of curves descriptive of the steady state operating characteristics of a self-excited induction machine. The program which has been developed generates curves which describe the equivalent circuit voltages, currents, and frequency as a function of real

and reactive load for all feasible machine speeds.

The program was developed in three parts all of which are included in App. 3 of [43] with directions. Parts 1 and 2 of program II generate data on the steady state operating points and part 3 of program II converts that data into a form which can be plotted.

In developing parts 1 and 2 it was necessary to arrive at a procedure which would allow the recording of solutions over the ranges of permissible RL, XM, and XL. Search variables were F and S. It can be noted that a self-excited induction generator is on the verge of losing self-excitation when it is run with a minimum of saturation of the airgap flux. In for example Figure 8, maximum XM under the V_g/F versus XM curve corresponds to the minimum saturation. It can also be noted that each value of XM corresponds to a specific magnitude of magnetizing current I_m . By these considerations, a minimum XM can also be determined corresponding to the maximum allowable magnetizing current I_m . XM is thus bounded between minimum and maximum values. We can canvas the entire range of feasible operating points by considering a large number of values of XM in the bounded zone.

In the discussion to follow it is assumed that a particular machine is being considered and that XC has already been chosen perhaps using program I.

With reference to Figure 7, it is apparent that if we fix RL and XL, then for each value of XM the only two unknowns are frequency F and slip S. Thus for a given XM we can have a search routine search over F and S for a valid steady state operating condition as described in section 2.2.

2.4.1.2 DUPLICITY OF SOLUTIONS (F,S) FOR A GIVEN (RL, XL, XM, XC)

When searching over (F,S) for a solution corresponding to a given (RL, XM, XL, XC), it is necessary to consider whether any solution encountered is unique.

Study of simplified admittance circle diagrams leads to the conclusion that the existence of one true solution (F,S) for a given (RL, XM, XL) with XC fixed implies that a second solution (F,S) also exists.

A simplified admittance circle diagram can be considered for the circuit of Figure 7. The simplified circuit is illustrated in Figure 11 and is identical to the circuit of Figure 7 except that stator resistance and stator leakage reactance are excluded from Figure 11.

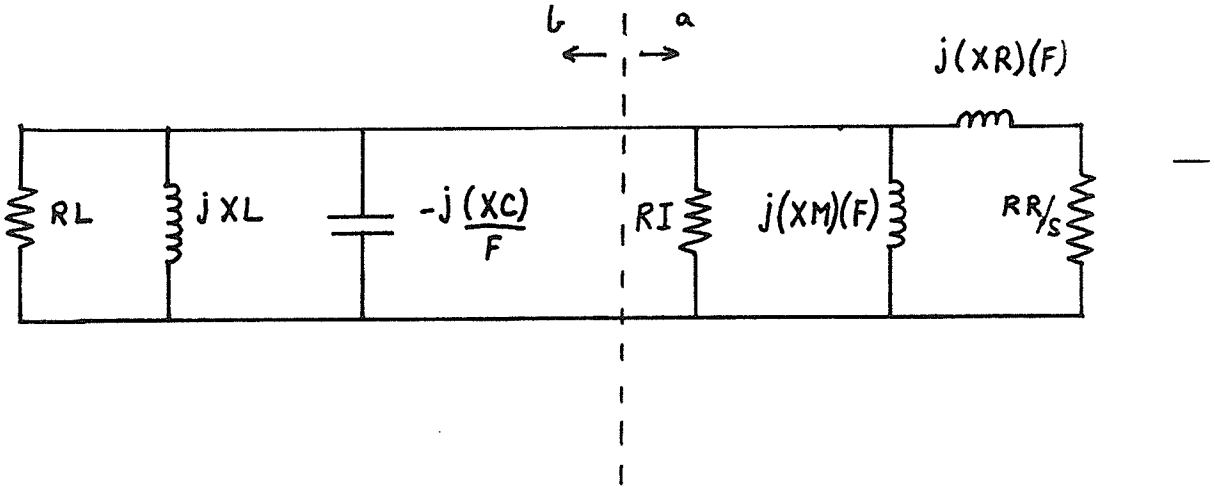

Figure 11 Simplified Equivalent Circuit for Constructing Admittance Circle Diagrams

When preparing an admittance circle diagram it is convenient first of all to consider the rotor circuit. In Figure 12, the impedance of the rotor is shown above the real axis and the admittance of the same circuit is shown below the real axis.

A typical admittance circle diagram is as illustrated in Figure 13. Ignoring the conductance of the iron loss resistance RI, it is plain that solutions can only exist for those values of F which satisfy the following conditions:

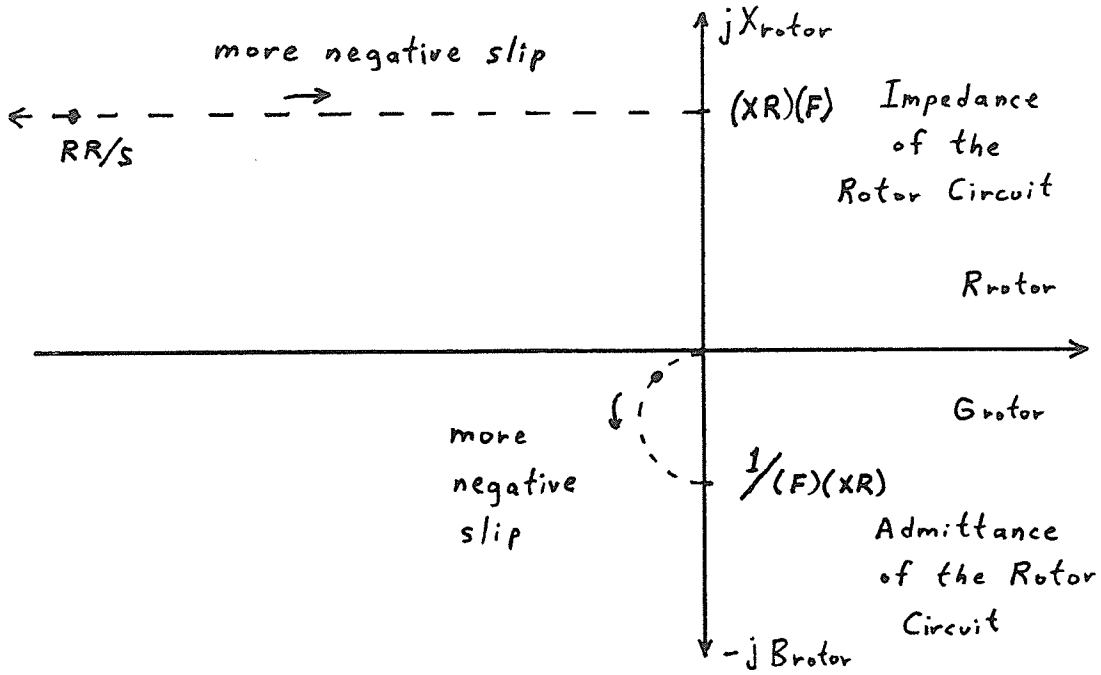

Figure 12 Admittance and Impedance Diagram of the Rotor Circuit for One Frequency

$$F/XC > \frac{1}{F \times XM} + \frac{1}{XL} \tag{2.4}$$

and

$$F/XC < \frac{1}{F \times XM} + \frac{1}{F \times XR} + \frac{1}{XL} . \tag{2.5}$$

Furthermore, if we assume that the load is exclusively real then the above conditions can be re-written as:

$$F^2 > \frac{XC}{XM} \tag{2.6}$$

and

$$F^2 < \frac{XC\ (XR + XM)}{XR \times XM} . \tag{2.7}$$

If reactive load is added, the band of frequency F for which solutions exist will be shifted upwards. At this point , it is useful to refer to simplified circle diagrams for a real machine. In that regard reference is made to the 900 h.p. machine described in Appendix 2.

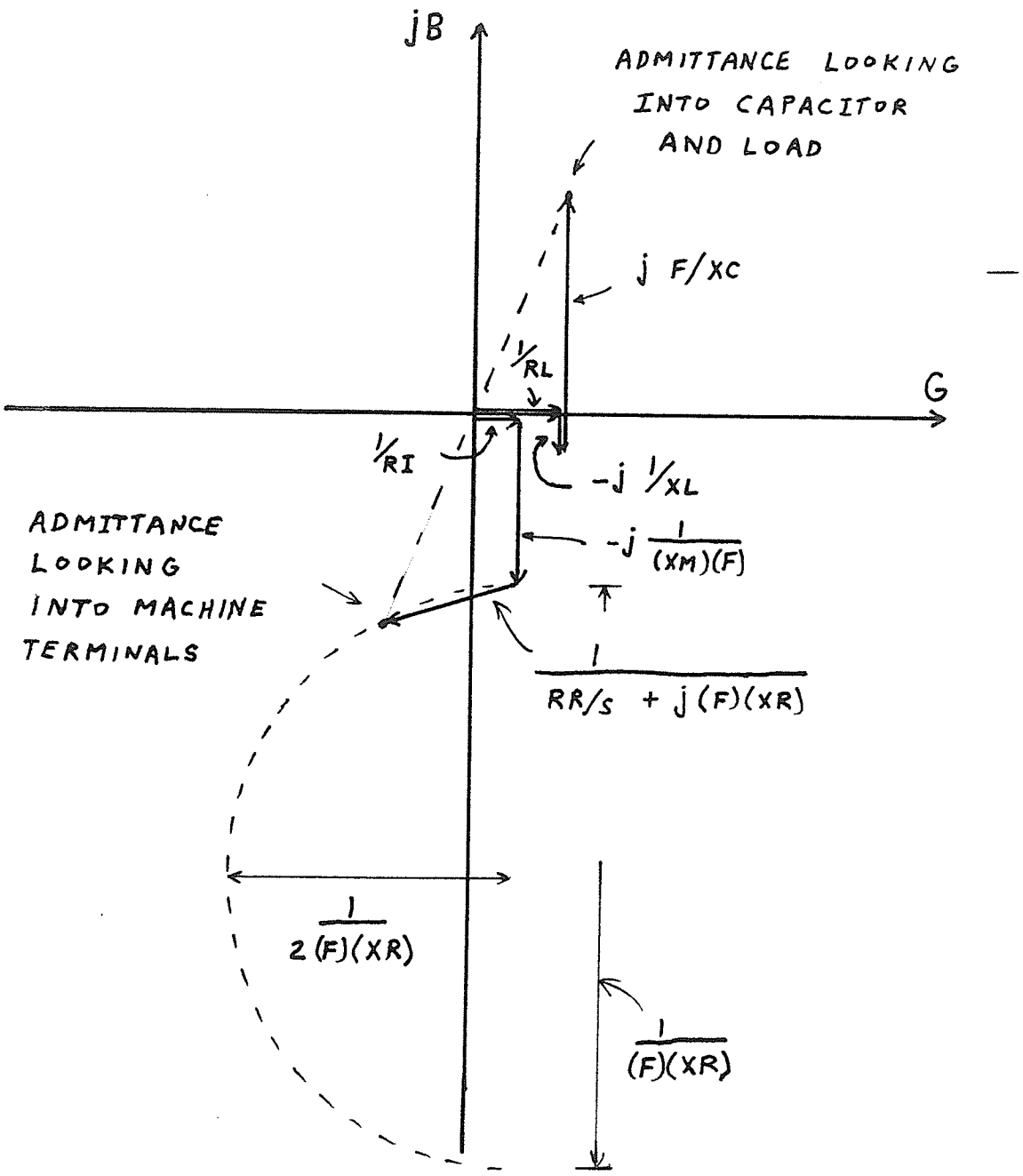

Figure 13 A Typical Admittance Circle Diagram For a Self-Excited Machine

We are interested in determining the number of solutions for a given set of (RL, XM, XL) with XC fixed. To keep the explanation clear we assume XL that is very large so that the load susceptance can be ignored. The machine of Appendix 2 has a maximum XM of 136.87 (ohms / p.u. freq.) and that value is acceptable as an example of XM for a search. The machine has a rotor leakage reactance of 3.827

(ohms / p.u. freq.) and a rotor resistance of 0.175 (ohms × p.u. slip). Program I as described earlier herein, was used to choose XC. XC was chosen as 44.13 (ohms × p.u. freq.) which corresponds to a sufficiently large capacitance to maintain 1.0 p.u. voltage (2309 volts r.m.s. l-n) at 0.9 p.u. frequency while supplying approximately rated resistive load (i.e. RL = 25.0 ohms) and negligible reactive load (i.e. XL very large).

For the above parameters an approximate range of F can be determined as described by the relation:

$$\frac{XC}{XM} < F^2 < \frac{XC(XR + XM)}{XR \times XM} \tag{2.8}$$

or

$$0.5678 < F < 3.715 . \tag{2.9}$$

Circle diagrams to the same scale have been constructed for the five values of frequency F given in Table I with XC = 44.13 (ohms × p.u. freq.), XM = 136.87 (ohms / p.u. freq.) and XR = 3.827 (ohms / p.u. freq.). In each of the circle diagrams

Table I Admittance Circle Diagram Dimensions

Freq. (p.u.)	Magnitude of the Admittance of the Capacitor $\frac{F}{XC}$	Magnitude of the Admittance of the Magnetizing Inductance $\frac{1}{XM \times F}$	Radius of the Rotor Admittance Circle $\frac{1}{2 \times F \times XR}$	$\frac{1}{RL}$	RL
0.7	0.01586	0.01044	0.2173	0.0483	20.69
0.9	0.02039	0.00812	0.1690	0.0633	15.79
1.8	0.04079	0.00406	0.0845	0.0683	14.63
2.7	0.06118	0.00271	0.0563	0.0567	17.65
3.6	0.08158	0.00203	0.0423	0.0167	60.00

of Figure 14 a) to e), XL and XM remain at the same value. Only F, S, and RL change from diagram to diagram. Figure 15 is a sketch of RL versus F for the solutions illustrated in Figure 14 a) to e). Figure 15 illustrates that, for any RL for which there is a corresponding true F value, there will in fact be two true solutions for F and thus two true solutions (F,S). To summarize, for any (RL, XM, XL) for which there is one true solution (F,S) there will in fact be two true solutions (F,S). This

means that for a given flux level, if there is a solution for a given (RL,XL), there will in fact be two such solutions. However, the two solutions are different. One solution will be for operation at relatively low speed and voltage while the other solution will be for operation at a higher speed and higher voltage.

Several other observations can be made in respect of the circle diagrams of figure 14. Figure 14 d) illustrates the admittance circle diagram for F = 2.7 p.u.. It happens that, for this machine at this saturation level and XC, F = 2.7 p.u. is of particular interest. In studying Figure 14 d), assume that frequency F remains fixed but that XM saturates to one half of the value illustrated in the figure. Under that circumstance, the saturation of XM could be accommodated by a small reduction in negative slip with virtually no change in RL. Thus, for both RL and F fixed, there will be a broad range of saturation and slip possible. For F a constant, saturation of XM is accompanied by an increase in V_g according to the V_g/F versus XM curve. This wide range of V_g for essentially a fixed RL and F shows up in the operating curves illustrated later herein.

It is notable as well that the RL of Figure 14 d) does not represent the minimum RL in respect of the XM used in drawing the circle diagrams of Figure 14. Figure 14 c) corresponds to an RL which is less than the RL of Figure 14 d). The smaller RL of Figure c) is due to the larger radius of the rotor admittance circle in Figure 14 c) as compared to Figure 14 d). The rotor admittance circle in Figure 14 c) is larger because F is smaller in Figure 14 c) than in Figure 14 d).

Referring again to the two solutions (F,S) for a given (RL, XM, XL), it is fortunate that the two solutions are readily distinguishable. The lower frequency solution corresponds to a circulation of current which is predominantly between the capacitors and the magnetizing branch. On the other hand, the higher frequency solution corresponds to a circulation of current which is predominantly between the capacitors and rotor circuit. For ease of indication herein, the lower frequency solu-

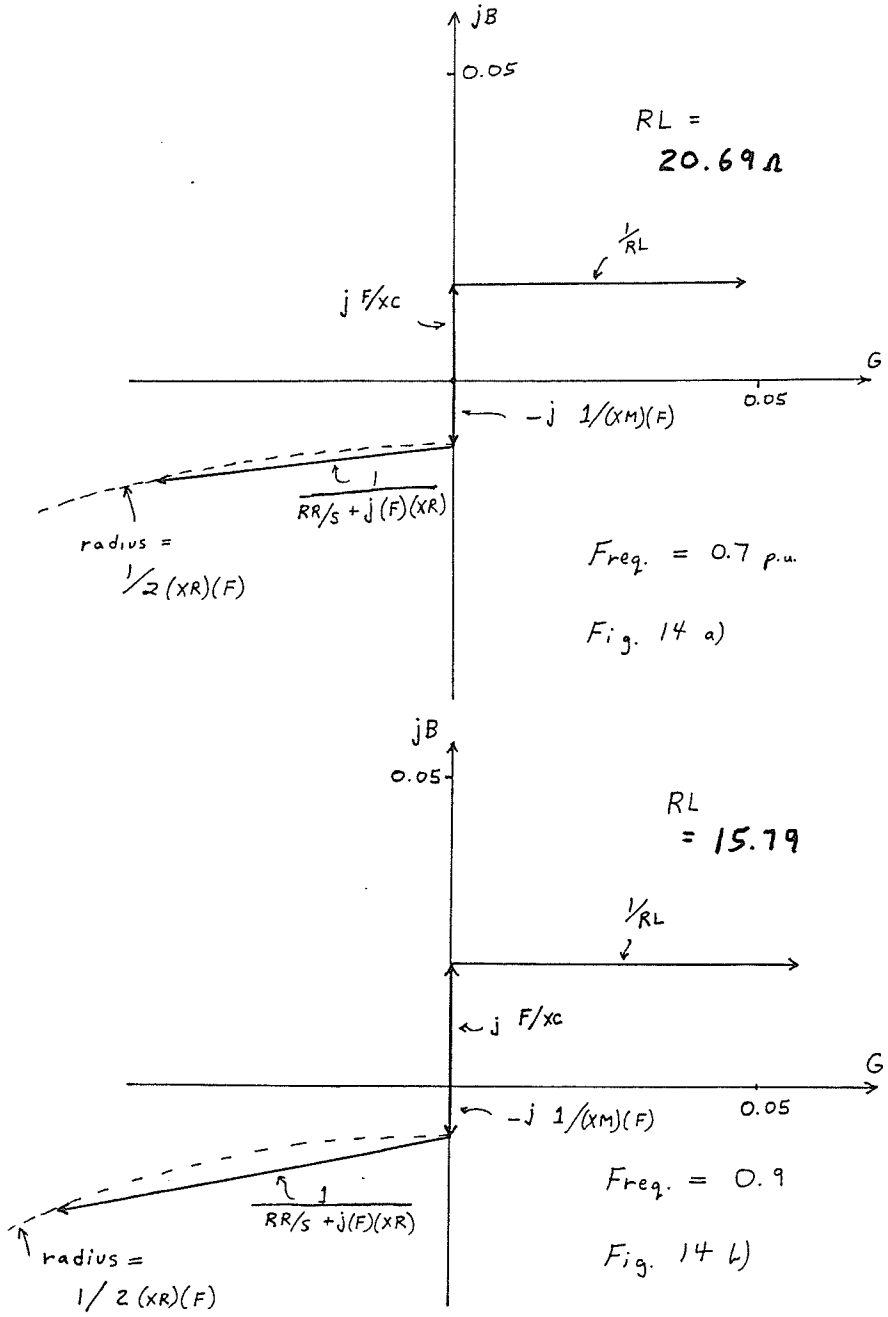

Figure 14 Simplified Admittance Circle Diagrams for Fixed XC, XL, XM and Various F, S, RL for the Example System

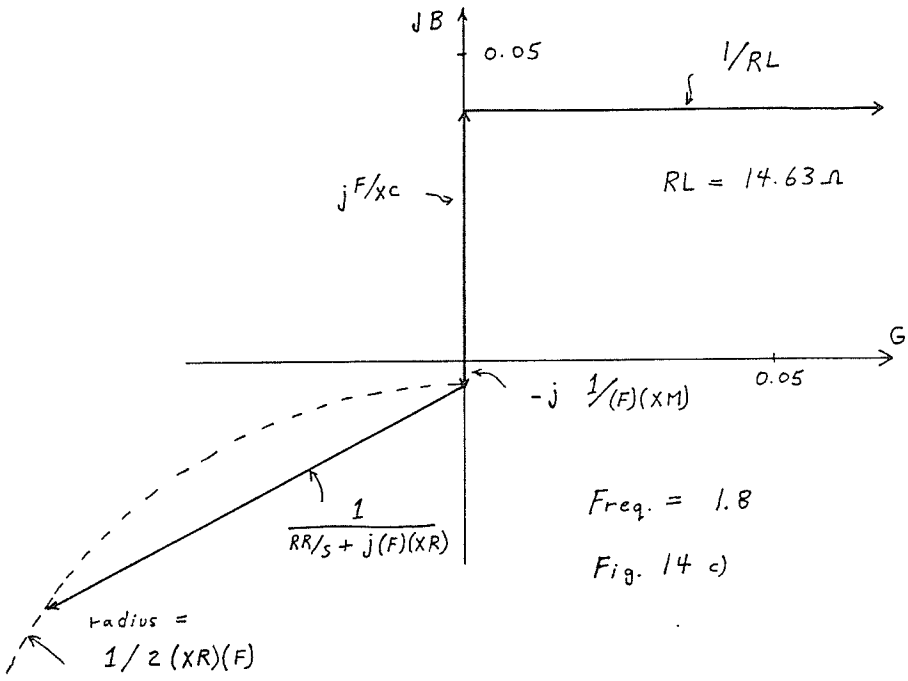

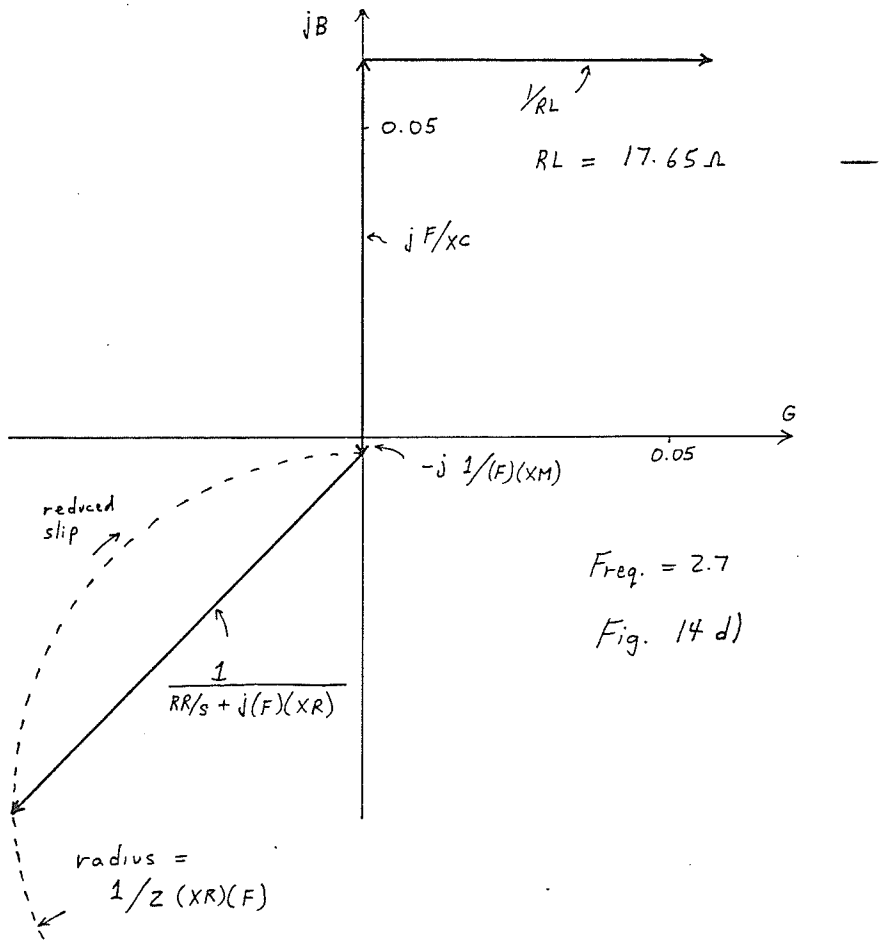

Figure 14 continued

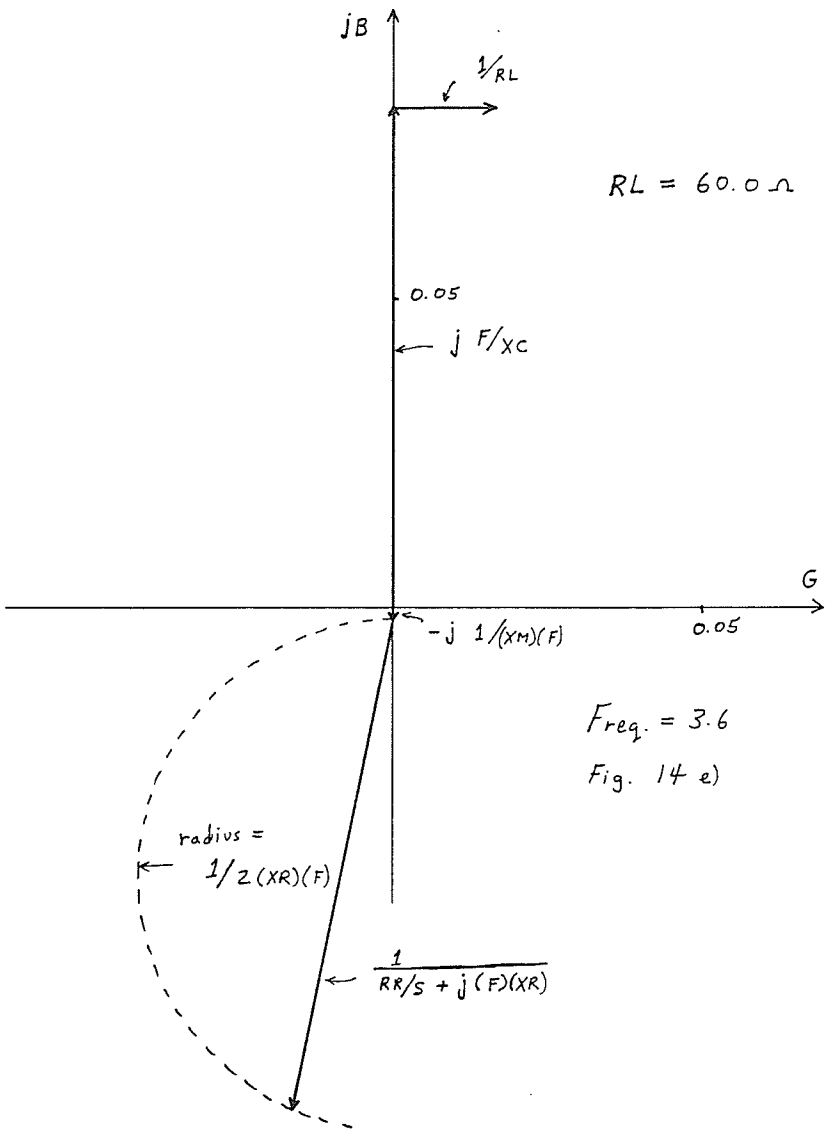

Figure 14 continued

tion for a given (RL, XM, XL) will be referred to as a mode I solution while the higher frequency solution will be referred to as a Mode II solution.

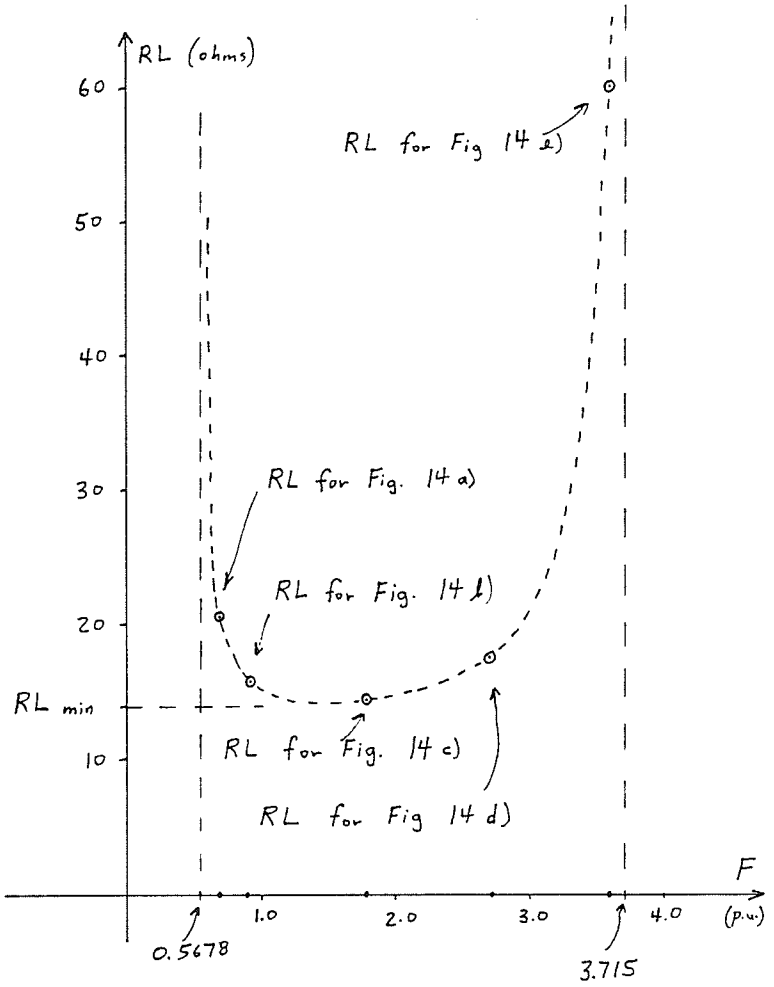

Figure 15 RL versus F for Solutions Illustrated in Figure 14

2.4.1.3 INVESTIGATING THE TWO MODES OF SOLUTION

RL and XL in Figure 7 define the load on the induction machine. Self-excitation is more likely to occur when the real and reactive load on the machine is small because under that circumstance the terminal capacitance has it's greatest effect. The conclusion can thus be drawn that we should begin a search for valid operating points with large RL and XL if we wish our search routine to find a valid steady state operating point. If the search is successful with respect to a given (RL, XL, XM) then the program must calculate and record the equivalent circuit currents, voltages, frequency and machine speed for that combination of RL, XM, and XL.

Once either a mode I solution or a mode II solution is found for the largest RL for a given XM then RL can gradually be reduced in steps. A gradual stepwise reduction in RL will allow the search routine to continue to converge to the same mode of solution provided that at each step the initial values for (F,S) are the solution of the search for the last previous values of (RL, XL, XM). Thus mode I and mode II solutions can be investigated separately. The program must search for a steady state operating condition at each value of RL and record a description of the steady state condition if one is found. The program should continue to reduce RL in a stepwise fashion until the search routine ceases to converge to a steady state operating condition. Referring back to Figure 15, RL_{min} represents the resistance below which no true solution for F will be available for the conditions described for Figure 15. The negatively sloped portion of the curve in Figure 15 represents mode I solutions for F while the positively sloped portion of the curve in Figure 15 represents mode II solutions for F.

In order to look at mode I solutions and mode II solutions separately it became necessary to find means to cause the search routine to selectively converge for large RL to either a mode I solution or a mode II solution. Such a selective convergence has been accomplished for large RL by using different initial values for (F,S) in the

search routine depending upon whether it is desired to begin investigating mode I solutions or mode II solutions.

2.4.1.4 SELECTIVELY CONVERGING TO MODE I SOLUTIONS

Convergence of the search routine to a mode I solution for large RL can be expedited by an appropriate initial approximation of the search variables (F,S). When RL is large both resistive load current and rotor current will be small for the mode I solution. Thus, for mode I solutions and large RL, the reactive power produced by the terminal capacitors will be almost entirely consumed in the machine's magnetizing branch. Given the above premises, the leakage impedances and the stator resistance will have only a secondary effect in determining the nature of the steady state operating condition. Ignoring the effect of the leakage impedance and the stator resistance reduces the single line diagram of Figure 7 to the simplified single line diagram of Figure 16. The circuit of Figure 16 can be solved (according to section 2.2.2) for F and S resulting in the following equations:

$$F = \frac{XC/XL + ((XC/XL)^2 + 4 \times (XC/XM))^{1/2}}{2} \tag{2.10}$$

and

$$S = -\frac{RR \times (RL + RI)}{RL \times RI} \tag{2.11}$$

These initial estimates for F and S are used in the part 1 search routine each time part 1 begins searching for a mode I steady state operating condition in respect of the largest RL considered for a given XM. When the search routine converges to a true solution (F,S) for a given RL, then a small reduction in RL will cause the next search routine to converge to values of (F,S) which are only slightly different from their prior values. Thus, when RL is reduced for a given XM, a good initial estimate for (F,S) will be the (F,S) found by the last prior search. As long as RL is not reduced drastically in one step this method will produce reasonable estimates for initial values of (F,S) for both the largest and subsequent reduced values of RL in

respect of a given XM.

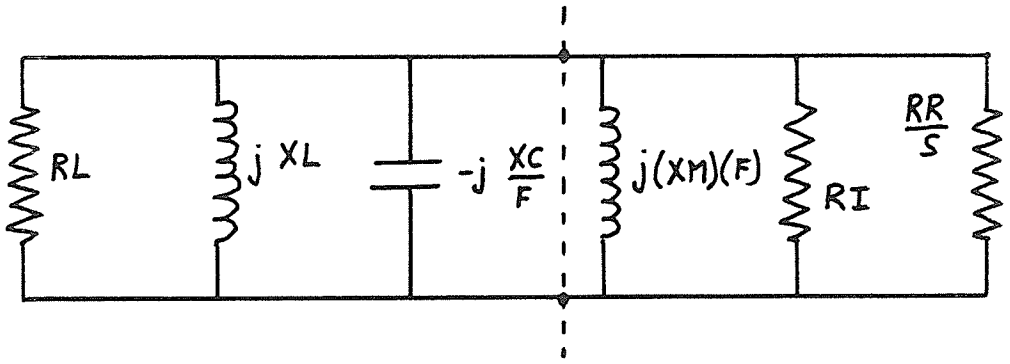

Figure 16 Simplified Equivalent Circuit for Estimating Mode I F and S for Large RL

2.4.1.5 SELECTIVELY CONVERGING TO MODE II SOLUTIONS

In order to investigate mode II solutions it is necessary to be able to cause the search routine to converge to a mode II solution for large RL. Magnetizing branch current is small with respect to rotor current for a mode II solution. Thus reasonable initial search values for (F,S) are derived by considering a single line equivalent circuit with the magnetizing branch deleted. Such a circuit is illustrated in Figure 17. In Figure 17 the imaginary component of the impedance looking out of the machine terminals is given by the following equation:

$$X_t = \frac{(RL)^2 \times X_{ct}}{RL^2 + X_{ct}^2} \tag{2.12}$$

wherein:

$$X_{ct} = \frac{XL \times XC/F}{XC/F - XL} . \tag{2.13}$$

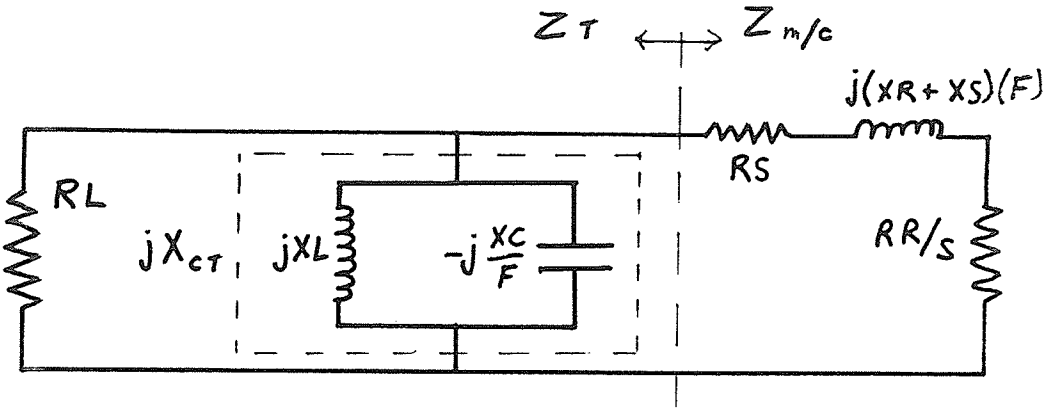

$$Z_T = R_T + j X_T$$

$$Z_{m/c} = R_{m/c} + j X_{m/c}$$

Figure 17 Simplified Equivalent Circuit for Estimating Mode II F and S for Large RL

X_{ct} is negative (i.e. capacitive) for F > XC/XL; X_{ct} goes toward minus infinity for F going to $\left(\frac{XC}{XL}\right)^+$; and X_{ct} goes to zero as F goes toward infinity. A plot of the locus of Z_T is given in Figure 18. In addition a plot of X_T versus F for $F > \frac{XC}{XL}$ is given in Figure 19. Figure 19 also includes plots of X_{ct} versus F and $-X_{m/c}$ versus F.

A suitable initial pair of (F,S) for commencement of a search for a mode II solution can be derived from the condition that Z_T plus $Z_{m/c}$ should equal zero in Figure 17. This implies that $X_T = -X_{m/c}$ at suitable F. Points 1 and 2 in Figure 19 illustrate two points at which $X_T = -X_{m/c}$. The values of F corresponding with points 1 and 2 in Figure 19 can be found by solving a cubic equation in F. If there is a positive real solution for F, there will be a corresponding value for S which will result in $R_T = -R_{m/c}$ and thus $Z_T = Z_{m/c}$.

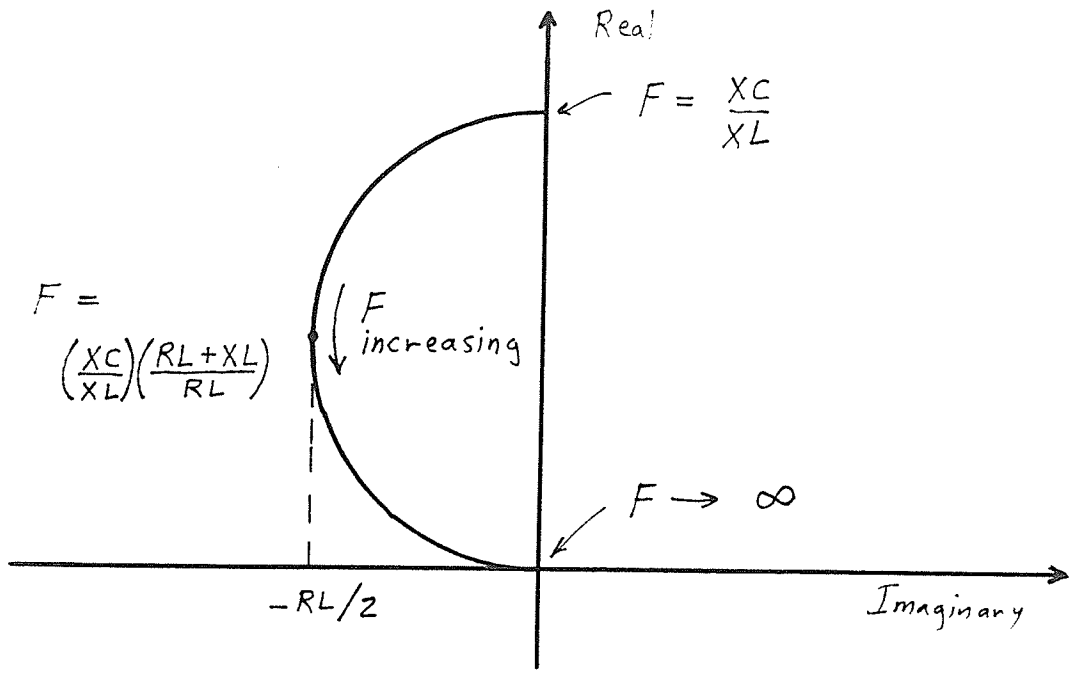

Figure 18 Locus of Z_T for Figure 17

At this point it is useful to recall the main premise for using Figure 17. To use the circuit of Figure 17, it is necessary to consider the magnetizing impedance to be high due to a high frequency of operation F. Turning again to Figure 19, point 2 is more likely to lead to a valid mode II operating point because F is a good deal larger at point 2 than at point 1.

When RL is large a reasonable choice of initial F can also be obtained based on the solution of a quadratic equation. Note that:

$$X_T = \frac{RL^2 \times X_{ct}}{RL^2 + X_{ct}^2} \tag{2.14}$$

and that when RL is large X_T is approximately equal to X_{ct}. When RL is large , a reasonable choice for initial F would thus be the most positive solution for F in the quadratic equation:

$$X_{ct} + X_{m/c} = 0$$

or

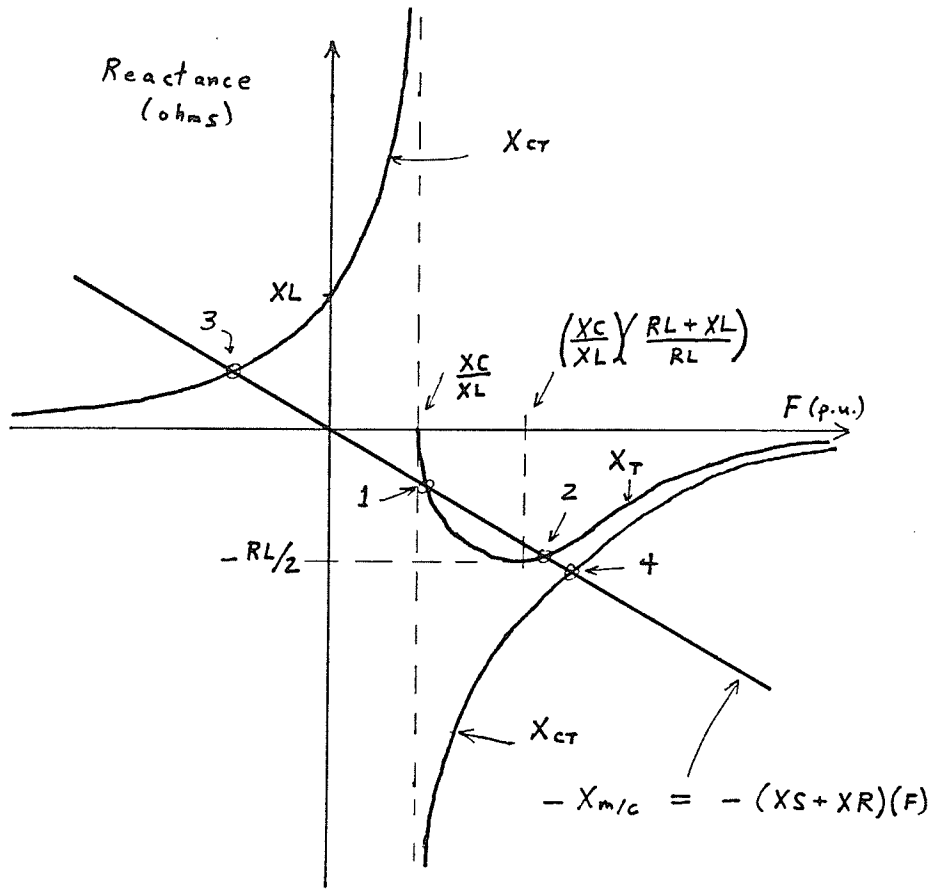

Figure 19 Plot of X_T, X_{CT}, and $-X_{m/c}$ versus F

$$\frac{XL \times (XC/F)}{XC/F - XL} + (XS + XR) \times F = 0$$

or

$$F^2 - \left(\frac{XC}{XL}\right) \times F - \frac{XC}{XS + XS} = 0. \tag{2.15}$$

The solutions for F are of course:

$$F = \frac{\left(\frac{XC}{XL}\right) \pm \left[\left(\frac{XC}{XL}\right)^2 + 4 \times \left(\frac{XC}{XS + XR}\right)\right]^{1/2}}{2}. \tag{2.16}$$

Both solutions are always real and only one is positive. The positive solution for F corresponds to point 4 in Figure 19.

With reference again to Figure 17, $R_T + R_{m/c} = 0$ when:

$$\frac{RL \times (X_{ct})^2}{RL^2 + X_{ct}^2} + (RS + RR/S) = 0 \qquad (2.17)$$

wherein:

$$X_{ct} = \frac{XL \times (XC/F)}{XC/F - XL}. \qquad (2.18)$$

The above equation can be re-written as:

$$S = - \frac{RR}{RS + \frac{RL \times (X_{ct})^2}{RL^2 + (X_{ct})^2}}. \qquad (2.19)$$

In this form it is apparent that for any F (or X_{ct}) there is always an S which will provide that $R_T = - R_{m/c}$. Thus once we estimate F for a mode II search we can easily derive a complementary estimate of S.

Once the first mode II solution for large RL has been obtained the program reduces RL in small steps so as to permit investigation of the mode II solutions in a manner similar to that used for investigating mode I solutions. When the program is set up to investigate mode II solutions then it is referred to as part 2 of program II.

2.4.1.6 FINDING SOLUTIONS (F,S) FOR A GIVEN MODE OVER A RANGE OF RL AND XM

To this point means have been presented for obtaining solutions (F,S) for selectively either mode I or mode II over a range of RL but for fixed (XL, XM, XC). It is, of course, necessary to consider a range of XM as well as RL in order to find a range of solutions (F,S) with respect to a given XL.

In order to cover the full range of XM the program has been arranged to reduce XM in steps from maximum XM to minimum XM for a given value of XL. At each value of XM the program repeats the process of reducing RL in steps from a large value. Of course, at each value of RL the program is arranged to search for a steady state operating condition and to store a description of the condition each time that one is found. The result of the process is that, for a given XL, a large number

of steady state operating conditions are stored and each steady state condition will correspond to a particular pair of RL and XM.

Part 1 and part 2 of program II each follow the above described process. Part 1 gives mode I solutions while part 2 gives mode II solutions. For a given mode of solution the following information is stored at each valid steady state operating point associated with a given (RL, XM) pair:

1) Frequency (F)

2) Machine Speed (MSPD)

3) Machine Terminal Current

4) Capacitor Current

5) Total Load Current

6) Load Power

7) Slip (S)

8) Terminal Voltage (VT)

From the above data it is possible to plot a curve of terminal voltage VT versus RL for each of several values of XM. Figure 20 illustrates two such curves. The lower curve is for XM = 136.9 (ohms / p.u. freq.) and the upper curve is for XM = 130.0 (ohms / p.u. freq.). The lower half of each curve corresponds to mode I solutions while the upper half corresponds to mode II solutions.

For a given mode we are not limited to plotting curves of constant XM in the VT versus RL plane. In Figure 20 each dot in the VT versus RL plane represents a known steady state operating condition for which the above 8 items of information have been stored. Thus, by interpolating between dots, constant value curves can be drawn in the VT versus RL plane for each of the first seven characteristics listed above. A segment of an example curve is illustrated in Figure 20 for machine speed equal to 0.65 p.u.. The purpose of part 3 of program II is to conduct the

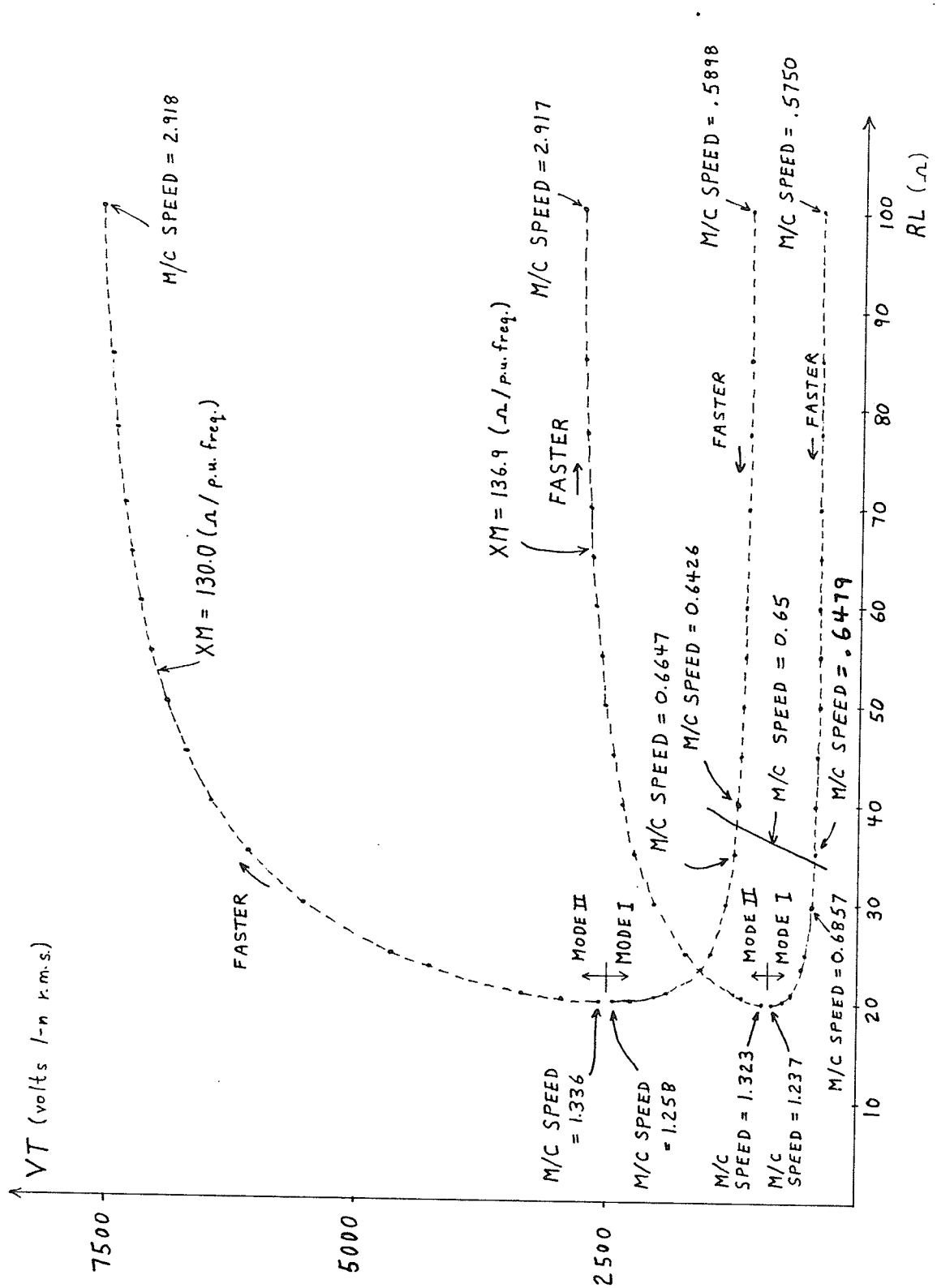

Figure 20 VT versus RL for Two Values of XM with Large XL

interpolation between calculated steady state conditions and to prepare an output file descriptive of a set of constant values curves in the VT versus RL plane.

For either mode of solution, program II can be re-executed for a few additional values of XL in order to get a complete family of curves covering a range of RL and XL.

2.4.1.7 PLOTTING

When either part 1 (mode I solutions) or part 2 (mode II solutions) of program II is executed it reads all required data from input files. Part 3, on the other hand, takes the output files from part 1 or part 2 and then accepts additional instructions that the user enters in response to questions displayed on the monitor. The user of part 3 must tell the program the type of curves required, the number of constant value curves on a graph and the magnitude associated with each constant value curve. There are additional questions as to scaling and titles for the graphs. When the output file from part 3 is completed, it is in a form acceptable to plotting utilities available on the Department of Electrical Engineering computer (DG MV8000) at the University of Manitoba.

2.4.1.8 ANALYSIS OF PROGRAM II OUTPUT CURVES

Appendix 3 contains two sets of graphs descriptive of mode I and mode II solutions for the machine of Appendix 2 with XC = 44.13 (ohms × p.u. freq.) and XL very large. That configuration of machine and capacitors is the same as was studied with the simplified admittance diagrams described in Figures 14 and 15. Figures A1 a) to g) describe the mode I solution and Figures A2 a) to g) describe the mode II solution. Figures A1 a) and Figures A2 a) have been included in this chapter for ease of reference as Figures 21 and 22.

Each set of graphs contained in Appendix 3 comprises seven separate graphs corresponding to a particular XL and XC. Each graph of a set describes a quantity

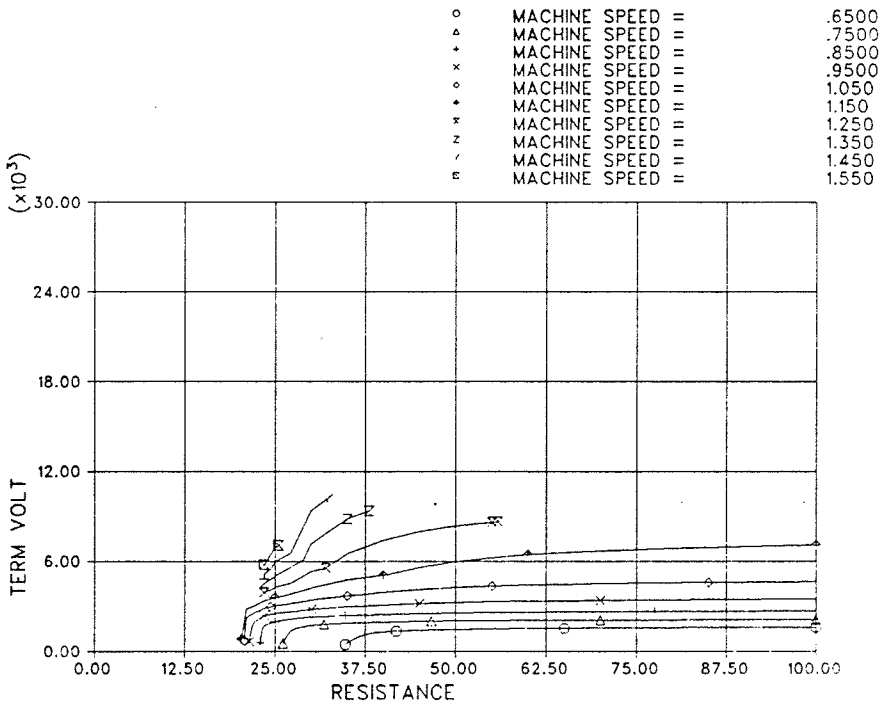

Figure 21 Constant Machine Speed Curves in the VT versus RL Plane for Mode I and Large XL

of interest and consists of a family of constant value curves in the terminal voltage versus load resistance plane. In a set each coordinate in the VT versus RL plane corresponds to a particular state of self-excitation. Thus seven characteristics of a particular state of self-excitation can be determined by looking at a particular VT versus RL coordinate in the seven graphs. The seven graphs describe machine speed, frequency, machine terminal current, capacitor current, total load current, load power and slip.

Given a combination of machine speed and RL it is possible to determine if there is a mode I solution or a mode II solution in the two sets of graphs which describe operating states for a given XL and XC. Figures 21 and 22 are the machine

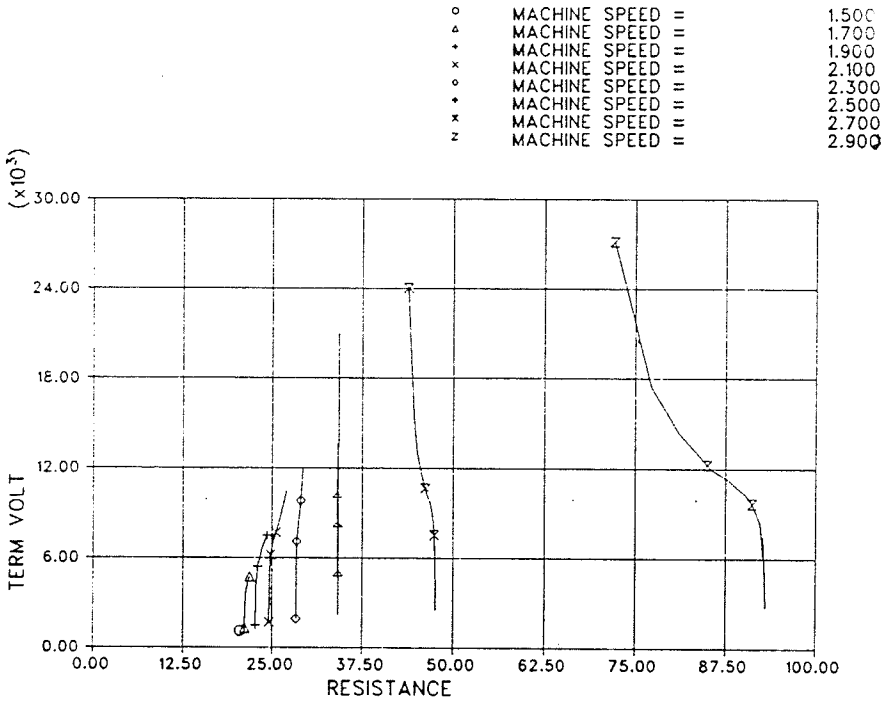

Figure 22 Constant Machine Speed Curves in the VT versus RL Plane for Mode II and Large XL

speed graphs from the two sets of graphs for a given XL and XC. Figure 21 describes mode I solutions for a given XL and XC. Figure 22 describes mode II solutions for the same XL and XC. Examination of Figures 21 and 22 indicates that, except for one case described below, a solution corresponding to a given machine speed and RL will be unique in the two sets of graphs for a given XL and XC.

As an example, the mode II solutions for RL = 25.0 ohms in Figure 22 all occur at a higher speed than any of the mode I solutions in Figure 21 for RL = 25.0 ohms.

The above discussion agrees with the expected result for a self-excited machine driven at a given speed supplying a given resistive load. One expects only one possible state of self-excitation.

Figures 21 and 22 are reasonably accurate for machine voltages below 6000 volts l-n (2.6 p.u.) because the machine current graphs in Appendix 3 show the terminal current is below 390 amps (3.5 p.u.) in that voltage range. However, above that voltage level saturation of the leakage reactances XR and XS will occur.

It is expected that there will be a transition from a mode I type solution to a mode II type solution for RL = 25.0 ohms. However, Figures 21 and 22 do not show the transition. Some consideration of the mechanism of the possible transition is in order. It is interesting to note that at RL = 25.0 ohms in Figure 22 voltage drops with increasing machine speed. Consideration of an admittance circle diagram such as Figure 14 e) is helpful at this point. The dropping of voltage with an increase in frequency must mean that XM increases as speed increases in mode II for RL = 25.0. Therefore, at lower voltages in Figure 22, the magnetizing admittance $\frac{1}{XM \times F}$ will be relatively small as in Figure 14 e). In Figure 14 e) a saturated value of XR would accommodate a smaller value of RL such as RL = 25.0 ohms because the diameter of the rotor admittance circle would be increased. It is suspected that saturation of leakage may accommodate a transition from mode I to mode II for RL = 25.0 ohms and XL large. Further work could be done in this area but I have left it because the transition would occur at a level of voltage (i.e. > 3.0 p.u) which would likely destroy the machine insulation.

The resolution of Figures 21 and 22 is low because the graphs describe operation to about 25 kV l-n for a machine rated at 2.309 kV l-n. Such a high voltage was chosen in order to illustrate the nature of the mode II solution.

The exceptional case noted above can be seen in the mode II operation described in Figure 22. Figure 22 indicates that terminal voltage is extremely sensitive to any small change in RL or machine speed at machine speed of approximately 2.5 p.u. and RL of 34.0 ohms. It would not be practical to use the curves to try to predict terminal voltage for this exceptional case. The vertical line in Figure 22 which

corresponds to the exceptional case can be related as well to the simplified admittance diagram of Figure 14 d). It is recalled at this point that the simplified admittance diagrams are only roughly accurate because stator leakage reactance and resistance were neglected in their preparation. At least under light load, neglecting stator leakage reactance can be expected to lead to a high prediction for frequency at a given XM. This occurs because neglecting stator leakage leads to the requirement that XC/F should approximately equal $XM \times F$ rather than $(XM + XS) \times F$. See Figure 23. Review of Figure 14 d) and

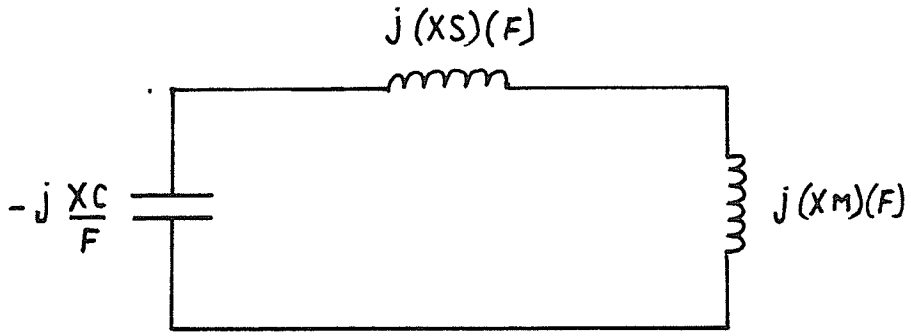

Figure 23 Primitive Circuit for Estimating F

the prior discussion thereon indicates that prediction of XM and thus VT should become difficult for frequency equal to 2.7 p.u. and RL equal to 17.65 ohms. There is a fairly close correlation between the frequencies predicted by simplified admittance diagrams and the more complete model represented by the sets of graphs of Appendix 3. As expected, the simplified admittance diagram predicted a frequency which was too high (i.e. 2.7 p.u. versus 2.5 p.u.). The prediction of resistance RL for the anomalous case by the simplified admittance diagrams was very inaccurate when compared against the RL predicted by the curves of Figure A2 b). The curves of Figure A2 b) can be expected to be accurate because they were developed to include stator

reactance and resistance.

The families of curves for capacitor current, machine terminal current, and total load current can be used to ensure that the elements of the circuit configuration will not be overloaded in any proposed operating state. Such an facility is useful in rating the elements of a circuit configuration during the design of a practical circuit.

In concluding this section it is submitted that the curves which can be generated by program II present adequate information for sizing components to handle fundamental frequency components of current and voltage. The accuracy of the curves was checked in the laboratory for the machine of Appendix 1 and the results of that check are presented in the next section.

2.4.2 VERIFICATION OF THE OPERATING CURVES GENERATED BY PROGRAM II

Program II allows the creation of a set of steady state operating curves descriptive of the operation of a self-excited induction machine. Four sets of operating curves have been reproduced in App. 6 of [43] for the machine described in Appendix 1. Two sets of curves are for capacitance XC equal to 16.8 (ohms × p.u. freq.) (i.e. 158 μ F) and the other two sets of curves are for capacitance XC equal to 18.5 (ohms × p.u. freq.) (i.e. 143 μ F). In each case, one of the two sets of curves is for XL = 9999.0 (ohms) and the other is for XL equal to 40.0 (ohms). Verification of the curves was undertaken by means of laboratory testing and a comparison with program I results.

The machine described in Appendix 1 was self-excited in the laboratory in order to check the capabilities of program II. A brief summary of procedure and results is included hereunder.

The induction machine was driven by a d.c machine and was excited by means

of excitation capacitors having a nameplate rating of 150 μ F. The induction machine was driven at three speeds and at each speed it supplied a manually variable purely resistive load. The three speeds of operation were 0.9, 1.0, and 1.1 p.u. speed based on a base p.u. speed of 1200 r.p.m.. For operating speeds of 0.9 p.u. and 1.0 p.u., RL was gradually reduced in steps until self-excitation was lost. For operation at 1.1 p.u. speed, RL was reduced until the d.c. prime mover overloaded. The laboratory tests resulted in the experimental constant value machine curves given in Figure 24. The experimental curves have linear segments connecting experimental values of RL.

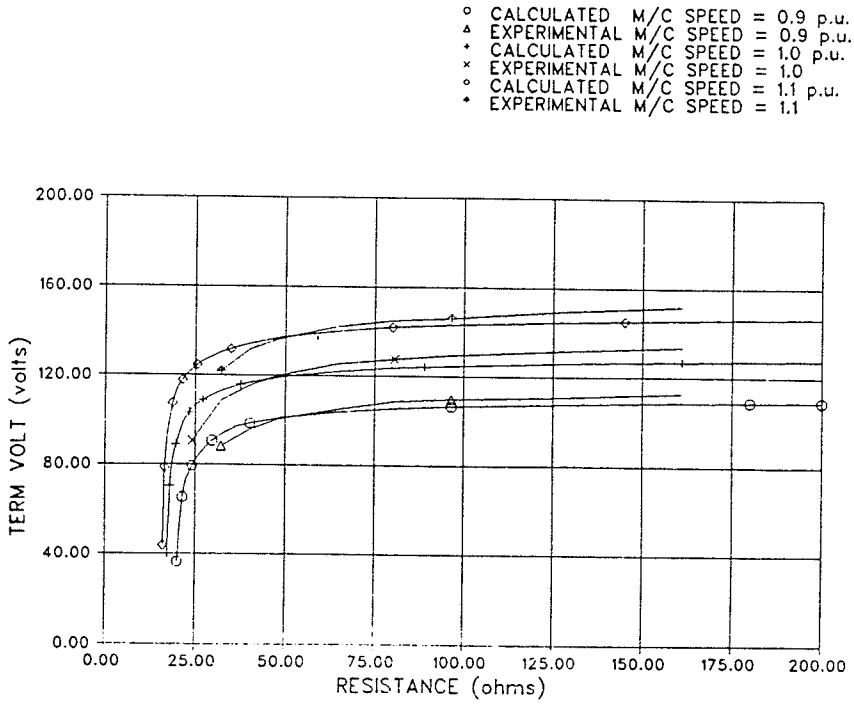

Figure 24 Comparison of Experimentally Derived Operating Curves to Those Generated by Program II

The first calculated constant value curves were somewhat different from those shown in Figure 24. A low value of calculated no load voltage was initially calculated but this was traced to the fact that the calculation relied upon an inaccurate nameplate rating on the self-excitation capacitors. The capacitors actually presented 158 μF (i.e. XC = 16.8 ohms × p.u. freq.) of capacitance to the machine terminals

rather than their nameplate rating of 150 μF. Use of XC = 16.8 (ohms × p.u. freq.) in program II resulted in the calculated constant machine speed curves in Figure 24. It can be noted that the calculated values of voltage are within 7 % of the experimentally determined values except at low values of RL at which terminal voltage drops rapidly with lowering of load resistance.

The calculated curves in Figure 24 are quit sensitive to variations in machine parameters. Small variations in RS, XS, XR1, and RI were used in calculating curves in order to see if inaccuracy in machine parameters could account for the 7 % discrepancies discussed above. The machine parameters from Appendix 1 indicate a stator leakage reactance XS of 1.6 (ohms / p.u. freq.) and a cage 1 leakage reactance XR1 of 2.78 (ohms / p.u. freq.). It was decided to transfer 0.5 (ohms / p.u. freq.) of leakage reactance from cage 1 to the stator in order to reduce the capacitive impedance presented by the series stator inductance and the self-excitation capacitor. The effect was to increase the no load voltage. An iron loss resistance of 400 ohms (approximately 11 times magnetizing reactance) was included in the model to account for possible iron losses. Finally, stator resistance was increased from 1.32 ohms to 1.82 ohms to account for possible contact resistance in the laboratory set-up. The resulting calculated curves are compared with the experimental curves in Figure 25. Although these calculated curves more closely match the experimental curves it appears that reasonable variations in machine parameters do not completely account for variations between the calculated and experimentally derived curves. However, the effort demonstates how sensitive the curves are to small variations in machine parameters.

As a small digression, Figure 26 and Figure 27 illustrate respectively, calculated constant value machine speed curves for the double cage representation and the single cage representation of the machine of Appendix 1 for large XL and XC = 16.8 (ohms × p.u. freq.). As expected, there is almost no difference at light loads (high

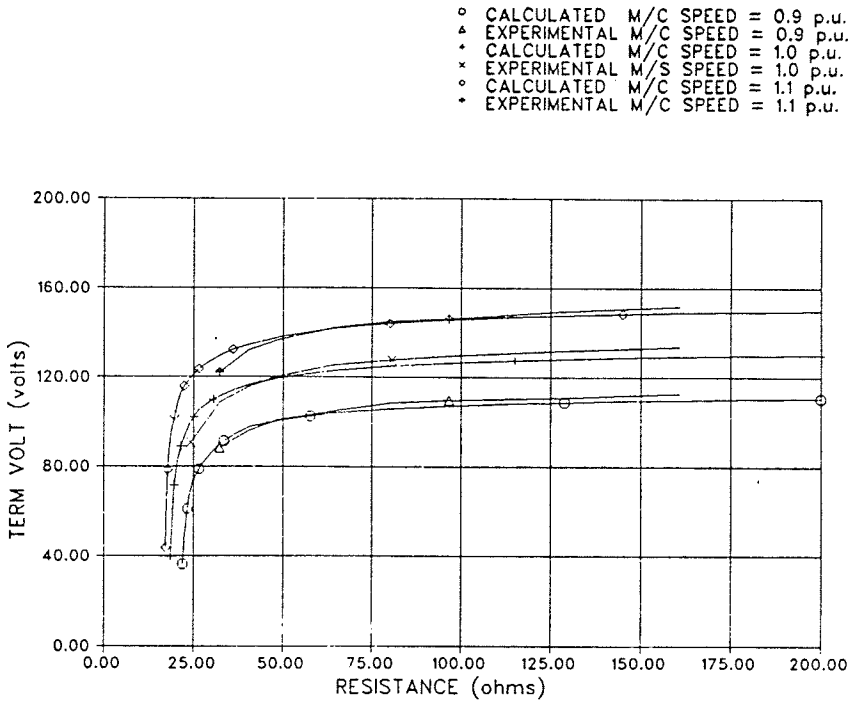

Figure 25 Curves as in Figure 24 with Small Variations in the Parameters Used in Generating Calculated Curves

RL). At high loads the machine voltage collapses in the single cage representation at a slightly lower value of RL than for the double cage representation. However, reasonable results can still be be expected from program II if only single cage parameters are available.

Program I, as presented in App. 2 of [43], was used to predict the capacitance XC and the machine speed required in order to have the machine of Appendix 1 supply 120 volts r.m.s. l-n at 1 p.u. frequency to a load of RL = 38.6 ohms with XL open. The prediction was that XC should be equal to 18.5 (ohms × p.u. freq.) and the machine speed should be 1.036 p.u.. Figures 28 and 29 are part of the set of curves in App. 6 of [43] for XC = 18.5 (ohms × p.u. freq.) and XL = 9999.0 ohms (i.e. XL practically open). These curves confirm the program I prediction in that the frequency equals 1.0 p.u. curve and the slip equals -0.036 curve intersect in the VT versus RL plane at VT equals 120 volts r.m.s. l-n and RL equals approximately 38.6

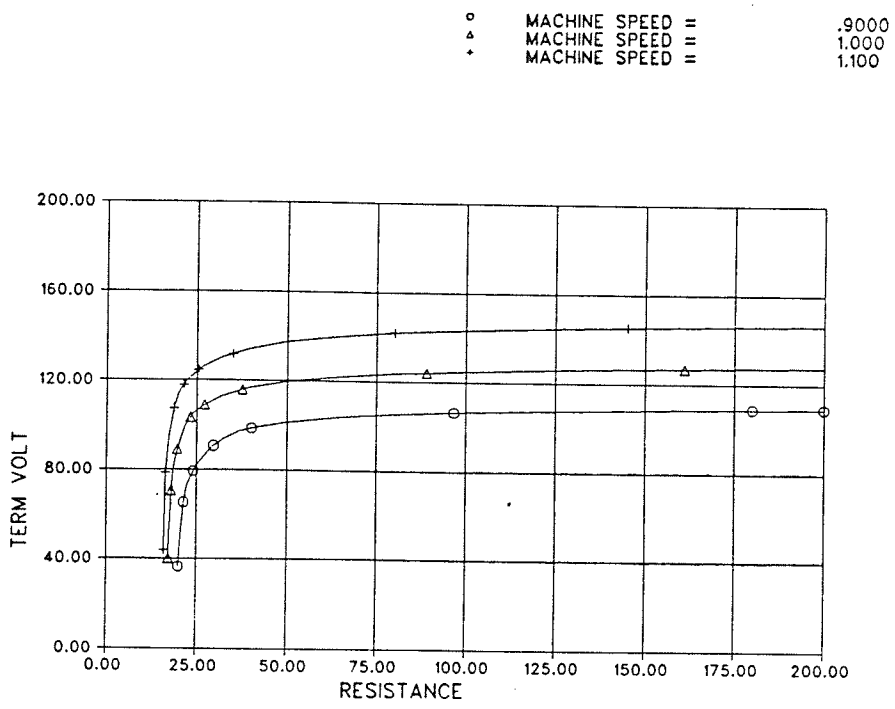

Figure 26 Constant Speed Curves for the Double Cage Representation

ohms. This check guards only against programming error because each program is based on the same model.

2.5 GENERAL OBSERVATIONS ARISING OUT OF LABORATORY WORK

While conducting the laboratory work some general observations were made. The machine described in Appendix 1 could be made to self-excite merely by disconnecting the resistive load and running the machine up to the testing speed with terminal capacitance connected of XC equals 16.8 (ohms × p.u. freq.). When the load resistance RL was decreased to the point of collapsing the machine voltage, the machine voltage could be reliably restored merely by removing the resistive load.

Restoration of self-excitation voltage is not that easy with all induction

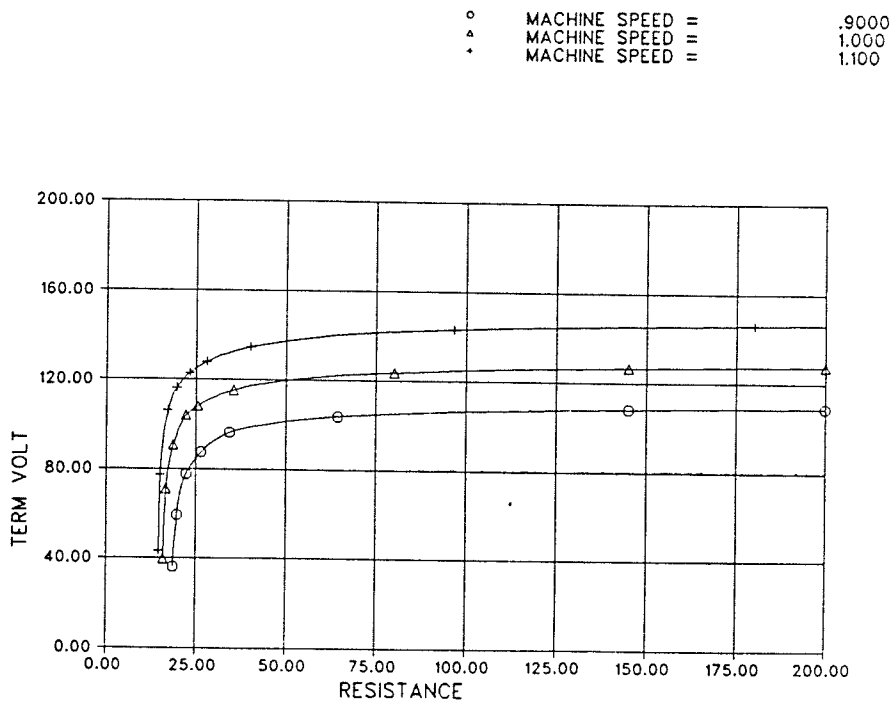

Figure 27 Constant Speed Curves for the Single Cage Representation

machines. A 900 r.p.m. laboratory machine characterized by low magnetizing reactance and high leakage reactance would not restore itself to self-excitation at reasonable operating speeds after a collapse of voltage and subsequent removal of the resistive load. In order to cause the 900 r.p.m. machine to self-excite, it was first necessary to stop the machine and pass a few amps of d.c. current through two stator phases.

The 900 r.p.m. induction machine was quit hard to self-excite after it's residual magnetism had been coerced to low values. Closing a fully charged capacitor onto the machine at speed would not cause self-excitation even with no load. Also, driving the induction machine at 30 % overspeed with load removed would not cause self-excitation. However, the approach of passing d.c. current through the stator windings of the stationary machine always allowed the 900 r.p.m. machine to be self-excited at

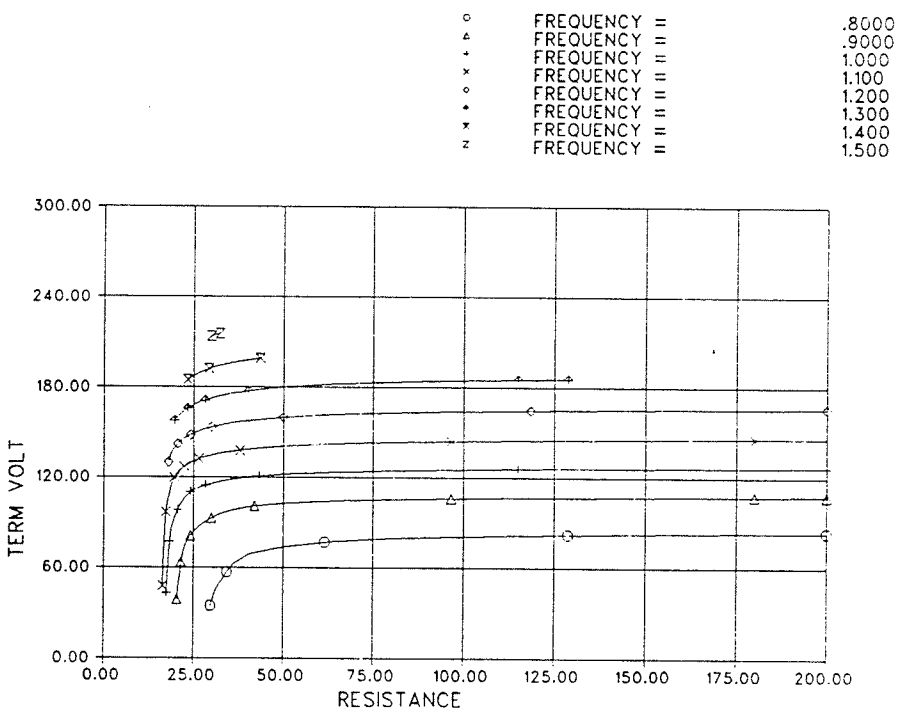

Figure 28 Constant Frequency Curves in the VT versus RL Plane for the Machine of Appendix 1 with Large XL and XC = 18.5 (ohms × p.u. freq.)

reasonable speeds. The most reliable start-up sequence was as follows:

1. reinforce the residual magnetism of the stationary rotor with d.c. current passed through stator windings;

2. open circuit the stator windings;

3. run the machine up to speed;

4. close uncharged capacitors onto the running machine and finally;

5. apply the load.

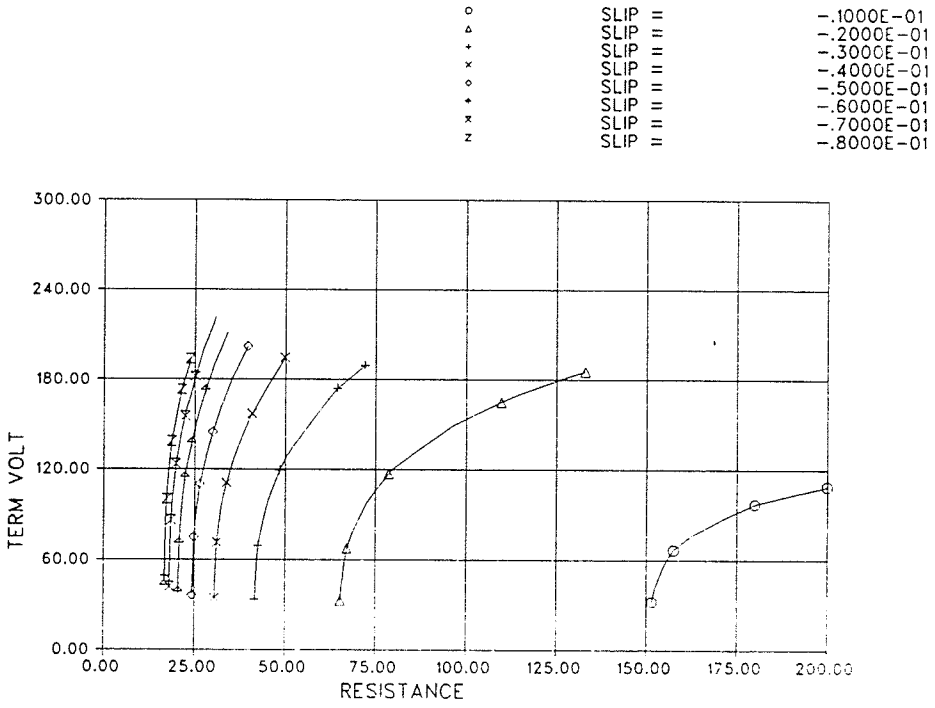

Figure 29 Constant Slip Curves in the VT versus RL Plane for the Machine of Appendix 1 with Large XL and XC = 18.5 (ohms × p.u. freq.)

CHAPTER 3

RECTIFYING AND INVERTING APPARATUS COMPLEMENTARY TO A SELF-EXCITED INDUCTION GENERATOR

3.1 INTRODUCTION

Figure 1 in chapter 1 illustrates the basic configuration under study in this thesis. As indicated in Figure 1, there are alternate devices which can be interposed between the rectifier circuitry and the three phase electrical load. This chapter will describe the steady state performance requirements of the interposed apparatus and will present and discuss alternate implementations.

3.2 PERFORMANCE REQUIREMENTS DICTATED BY THE NATURE OF THE LOAD

An inverter bridge is required in order to supply the load with the three phase electrical power. The nature of that bridge is dictated partially by the nature of the load.

The phase impedances of a 3 phase electrical load can be either balanced or unbalanced and the type of inverter which should be used partially depends on that characteristic of the load. Approximately balanced 3 phase voltages can be obtained using a forced commutated Graetz bridge inverter only for the case where the phase impedances are approximately balanced. The well known Graetz bridge inverter can be commutated using series capacitors[36,37,38]. In the case where a 3 phase load is heavily unbalanced the Graetz bridge inverter will produce heavily unbalanced

voltages and imbalance in currents may impede proper operation of a series capacitor commutated inverter. It can therefore be advantageous to use a different type of inverter than the Graetz bridge inverter for loads which can be heavily unbalanced. Such unbalance often occurs in small isolated systems at times when the loads on all phases are light.

A possible alternative exists in a voltage inverter which is adapted to supply balanced 3 phase voltage waveforms to the load regardless of the balanced or unbalanced condition of the load. The fundamental difference between a Graetz bridge inverter and a voltage inverter rests in the fact that the Graetz bridge inverter supplies balanced 3 phase fundamental currents while the voltage inverter supplies balanced 3 phase fundamental voltages.

In a Graetz bridge inverter each phase receives a waveform of current as illustrated in Figure 30. Shunt filters are used to remove characteristic current harmonics from the waveform.

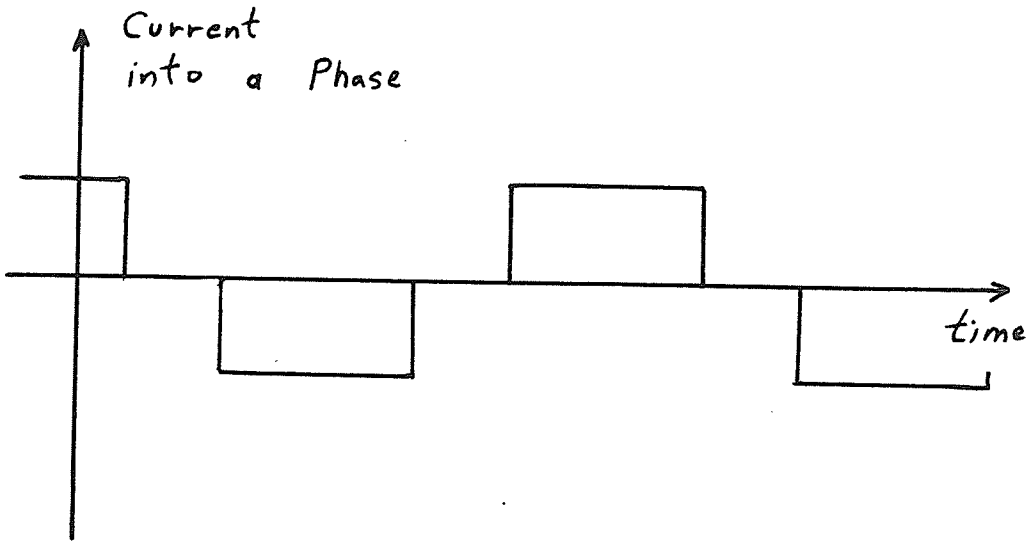

Figure 30 Current Out of a Graetz Bridge Inverter Without Overlap

In a typical voltage type inverter each phase receives a waveform of voltage as illustrated in Figure 31. It is convenient to note at this point that voltage type invert-

ers generally include an element such as a continually replenished capacitor bank which acts as a source of d.c. voltage. Use of series filters or pulse width modulation can be used to reduce the characteristic voltage harmonics.

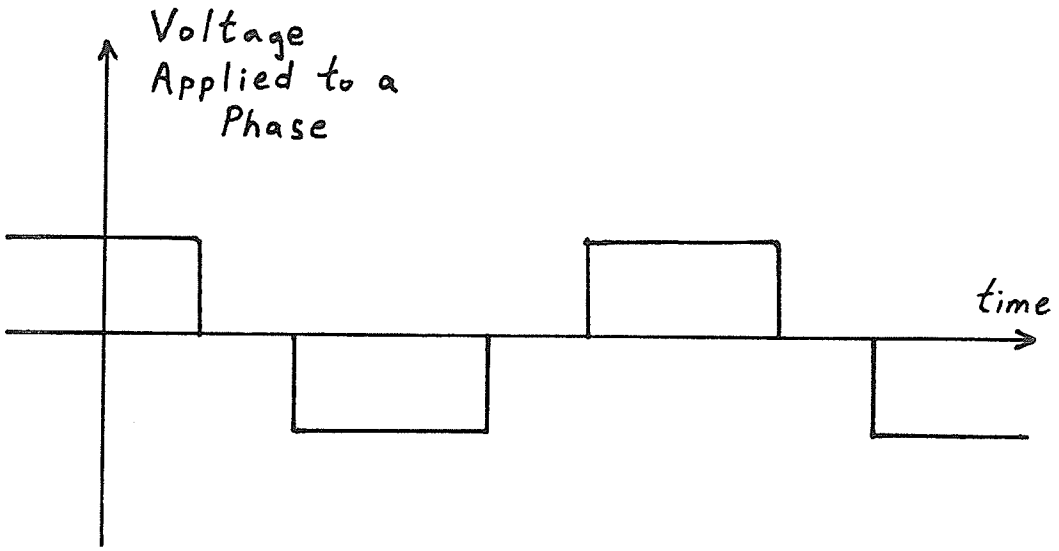

Figure 31 Voltage Waveforms Out of a Voltage type Inverter

Regardless of the type of inverter, it is necessary that the voltage waveforms applied to the separate phases should be equal and that they as a group, should be closely regulated in magnitude and frequency.

3.3 THE CHOICE OF MACHINE OPERATING VOLTAGE

As discussed in chapters 1 and 2, induction machines can be operated in a self-excited state by placing adequate capacitance on the terminals of the machine having regard to the speed of operation and the load on the machine.

It is advantageous to operate a machine at the voltage level for which the stator insulation is designed, namely rated voltage. A higher operating voltage would cause stator insulation to deteriorate more quickly than it would at rated voltage. A lower operating voltage would indicate that the machine is being operated closer than necessary to the verge of losing self-excitation. Also at reduced voltage the machine will not provide the same level of power without increased current.

Arguably one ought to reduce operating voltage to below rated levels when machine speed is reduced below rated generator speed in order to keep the machine flux at design levels. Such a step would be taken with the intention of avoiding overcurrent at full load due to increased magnetizing current.

On the other hand, it may be possible to accept a fractionally higher magnetizing current than normal if the machine is designed to have a relatively high power factor for normal operation. Such a fractionally higher magnetizing current in a high power factor machine might be acceptable for two reasons.

On the one hand, a given percentage increase in magnetizing current in a high power factor machine would be a smaller absolute increase than a similar percentage increase in a low power factor machine. Furthermore, a small increase in magnetizing current in a loaded high power factor machine will result in very little increase in terminal current. This is due to the fact that the extra magnetizing current phasor will be closer to being in quadrature to the high power factor machine current phasor than it would be to being in quadrature with the to the low power factor machine current phasor.

The second reason stems from a consideration of the losses to be expected during a lower frequency operation occurring simultaneously with higher levels of flux. Hysterisis and eddy current losses at a given level of flux tend to be reduced due to operation at a lower frequency level. Therefore, from a loss standpoint, higher losses expected due to operation at a higher flux level will be somewhat reduced due to the lower frequency of operation.

Consideration of the above points indicates that, at slightly reduced machine speeds (ex. 0.9 p.u.), machine terminal overcurrent due to high magnetizing current should not be objectionably large in a high power factor machine operated at full load and rated voltage. If some objectionable overcurrent developes the real component of current can be reduced slightly with a corresponding slight reduction in

output power or as an alternative the minimum machine speed at full load can be raised slightly.

At this point in the presentation it remains to be considered how much over rated speed a machine might be driven at full load and rated voltage before overcurrent would arise due to poor power factor resulting from the increased leakage impedances associated with high frequency operation.

On the basis of the above discussion it is proposed to operate the self-excited machine at rated voltage over an allowable range of machine speeds and power levels. The minimum power level will, of course, be zero output. The proposed maximum generator power output is the electrical output level which would be generated if the the machine were run at rated speed with an input torque equal to the rated motor torque of the machine. A proposed minimum speed at the proposed maximum output power is used to pick the self-excitation capacitors using program I described in chapter 2. A check must be conducted to make sure that the machine will not be in overcurrent at the proposed minimum speed when it is producing the proposed maximum output. If it is in overcurrent either the proposed minimum speed should be increased or the proposed maximum power should be decreased. The maximum speed at the proposed maximum power will be determined by the speed to which the machine can be driven before overcurrent arises due to poor power factor as discussed above.

The above choices as to operating voltage, speed, and power ranges must be checked by looking at the characteristics of the particular machine to be used.

3.4 OPERATING CURVES RELATED TO A SPECIFIC LEVEL OF TERMINAL VOLTAGE

Program III, listed in App. 7 in [43], was developed and used to investigate machine terminal current and reactive load current associated with operating a typi-

cal self-excited machine at rated voltage in the range of power levels and machine speeds as noted above.

Program III can investigate one combination of power and machine speed in a given program execution. With reference to Figure 7, program III accepts desired machine speed, desired terminal voltage, RL, XC, and the data on the machine including it's V_g/F versus XM curve. The program then searches over frequency, XM, and XL until the search converges on a valid operating point at the desired terminal voltage. Specifying machine speed, desired terminal voltage and RL fixes the output power at the particular machine speed in question. Once the search converges on a valid operating point, it is a matter of simple calculation to produce all the equivalent circuit impedances, voltages, and currents.

Output from program III was used to generate curves, as a function of machine speed and power, which describe the magnitude of the total load current; load power factor angle; the real component of current into the load; the reactive component of current into the load; machine terminal current; capacitor current; magnetizing current; and airgap voltage.

Program III at present converges only with difficulty and for extended use it should be improved by converting the search technique from a pattern search routine to a simplex search routine as was done for programs I and II. The simplex routine used was based upon the algorithm of Nelder and Mead and was programmed several years ago by Dr. A. M. Gole.

A full set of curves generated using output from program III is illustrated in Appendix 4. The curves relating to load current magnitude, real load current, reactive load current, load power factor angle, frequency, and machine terminal current are illustrated in Figures 32 a) to f). Figure 32 b) is trivial but is included for the sake of completeness. The curves relate to the machine described in Appendix 2 operating between 0.9 and 1.8 p.u. speed and 0 and 1 p.u. power. XC was chosen as

44.13 (ohms × p.u. freq.) based on minimum speed of 0.9 p.u..

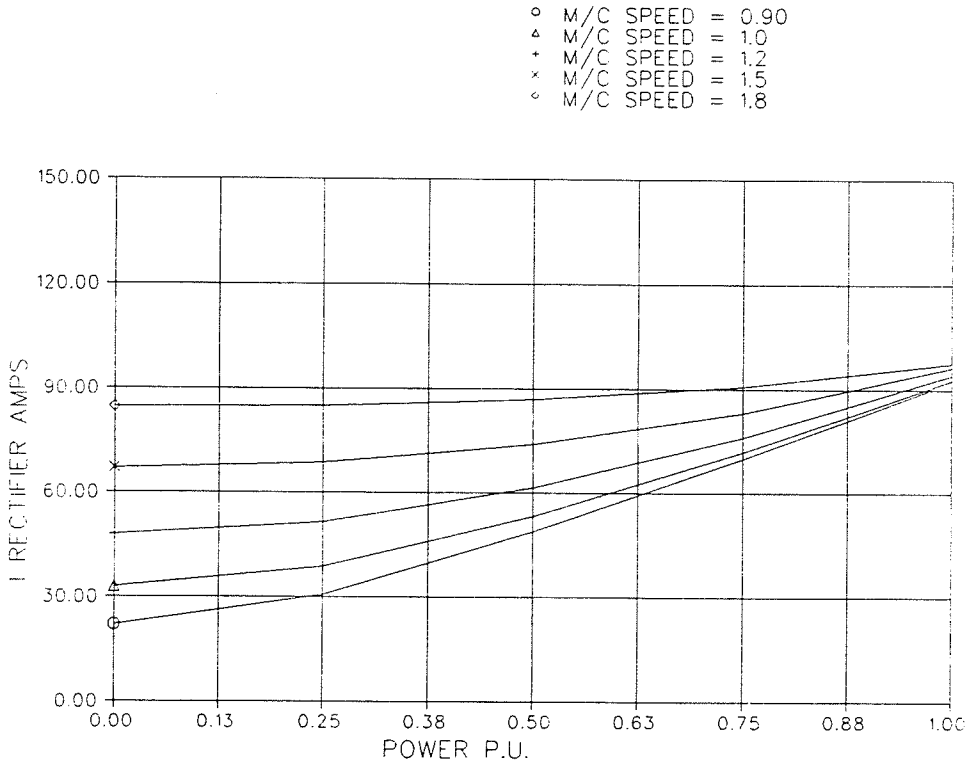

Figure 32 a) Load Current Magnitude Corresponding to the Machine of Appendix 2 at 1.0 p.u. Voltage for XC = 44.31 (ohms × p.u. freq.)

I will digress at this point to clarify the correspondence between a program III solution and the curves generated by program II. RL, as defined in Figure 7, is used as input to program III. XL, as defined in Figure 7, can be obtained from the output of program III specifically by calculation using machine terminal voltage and the reactive component of current illustrated in Figure 32 c). Given a value of XL, program II can be used to generate mode I and mode II operating curves which cover all levels of voltage at the specified value of XL. Once the curves are generated, the RL and machine speed used as input to program III can be used to select the operating point in the curves generated by program II.

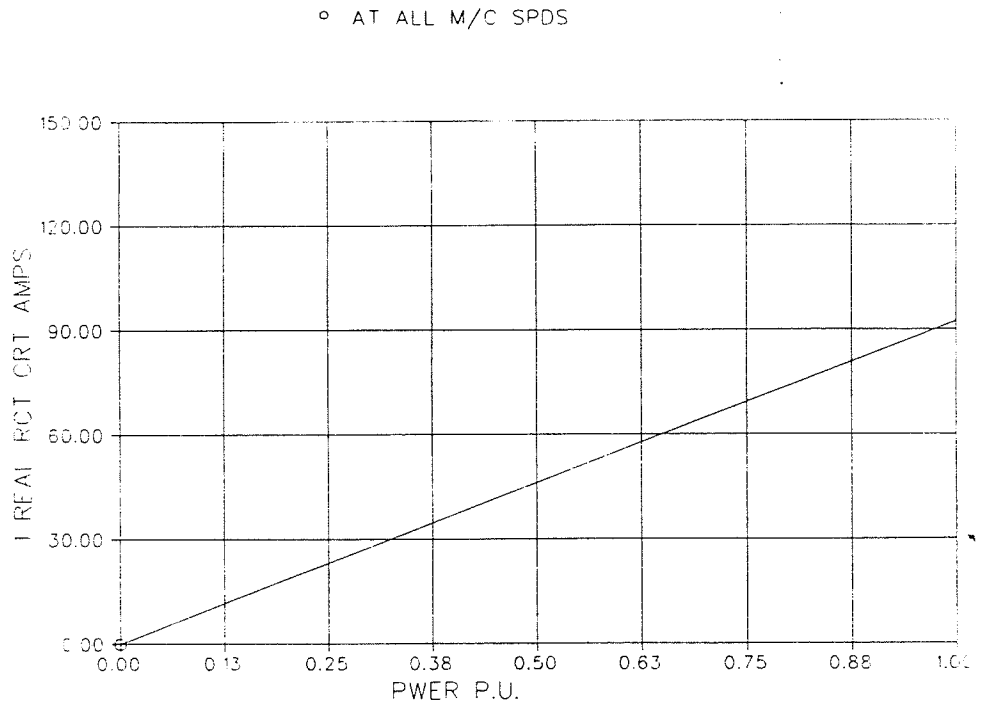

Figure 32 b) Real Load Current Corresponding to the Machine of Appendix 2 at 1.0 p.u. Voltage for XC = 44.31 (ohms × p.u. freq.)

3.5 CONSIDERATIONS ARISING OUT OF RECTIFIER MINIMUM FIRING ANGLE AND COMMUTATION REACTANCE

Use of a non-ideal Graetz bridge rectifier with transformer requires in practise that more capacitance should be provided at the terminals of the machine than that indicated by consideration of the machine alone. See Figure 33 illustrating the extra capacitance element.

In program I, it was assumed that the firing delay angle α of the rectifier could be reduced to 0° and further that, at $\alpha = 0°$, the power factor into the load would be 1.0 (i.e. $\phi = 0°$). In practise rectifiers are operated with a minimum firing angle (α_{min}) of about 5 ° . Furthermore, the commutation reactance causes a commuta-

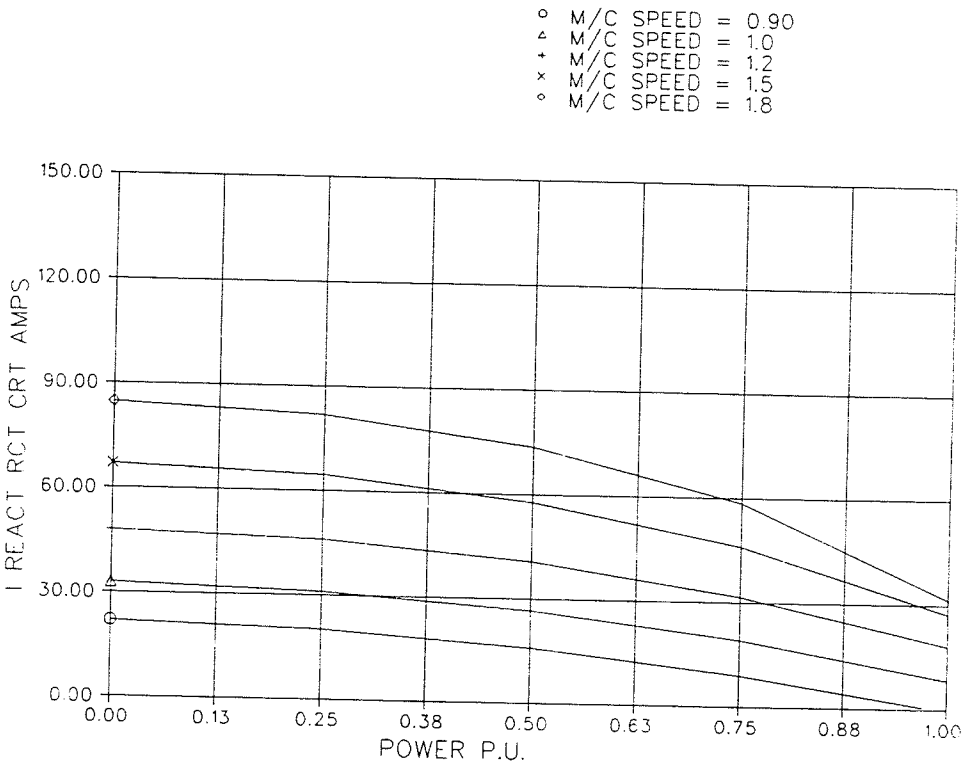

Figure 32 c) Reactive Load Current Corresponding to the Machine of Appendix 2 at 1.0 p.u. Voltage for XC = 44.31 (ohms × p.u. freq.)

tion angle μ which further reduces the power factor of the current into the converter transformer.

In the analysis of Graetz bridge rectifiers it is often assumed that the converter transformer is lossless. Based on that assumption, standard approximate equations [31] are available in respect of the circuit of Figure 34. They are as follows:

$$V_d = V_{do} \cos \alpha - R_c I_d \tag{3.20}$$

$$V_{do} = \frac{3\sqrt{6}\, V_{l-n}}{\pi} \ (r.m.s.) \tag{3.21}$$

$$R_c = \frac{3 X_L \ (F \ p.u.)}{\pi} \tag{3.22}$$

$$I_{L1} \ (r.m.s.) = \frac{\sqrt{6}\, I_d}{\pi} \tag{3.23}$$

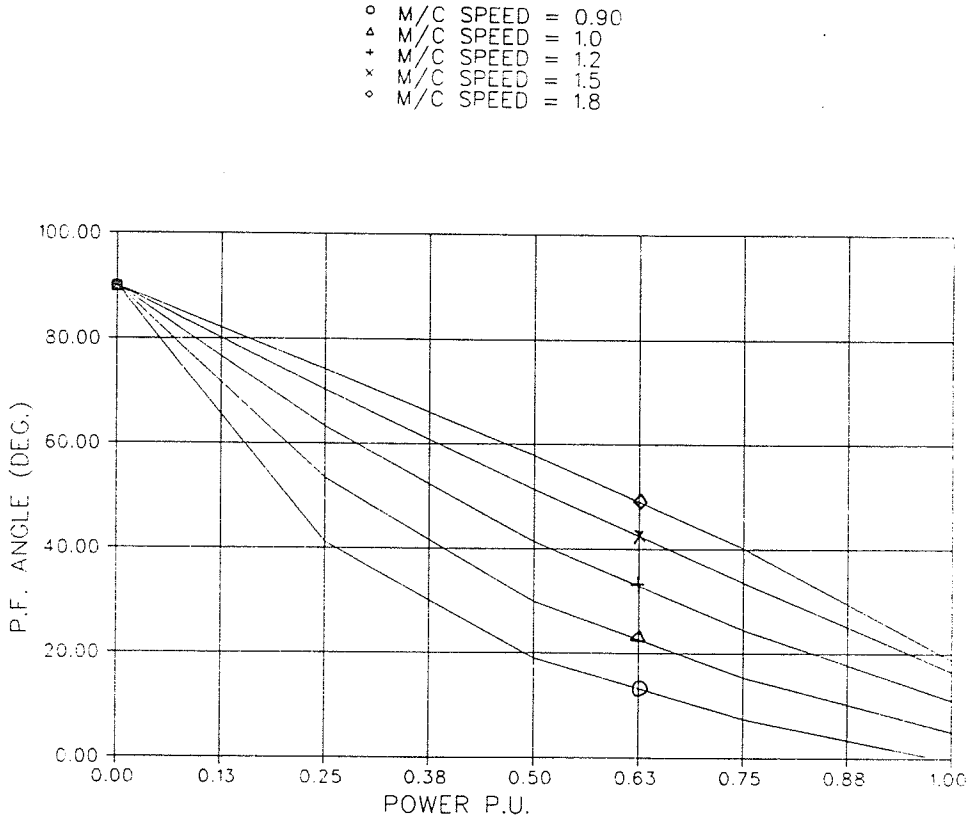

Figure 32 d) Load Power Factor Angle Corresponding to the Machine of Appendix 2 at 1.0 p.u. Voltage for XC = 44.31 (ohms × p.u. freq.)

$$I_{real} = I_{L1} \cos \phi \tag{3.24}$$

$$V_d \, I_d = 3 \, V_{l-n} \, I_{L1} \cos \phi \tag{3.25}$$

The above equations can be combined to give:-

$$3 \, V_{l-n} \, I_{L1} \cos \phi = V_{do} \, I_d \cos \alpha - R_c \, {I_d}^2 \tag{3.26}$$

The left hand side is recognizable as the real power into the converter transformer. V_{do} is a constant for a given a.c. voltage (ex. V_{do} = 5401 volts for V_{L-L} = 4000 volts r.m.s.). R_c is not a constant but varies in proportion to F p.u. for a given transformer. With reference to the curves of section 3.4, the real component, the reactive component, and the frequency of the load current are known for each power level and machine speed at the given machine voltage. By setting α to α_{min} = 5° in equation 3.26 we can solve for I_d for each machine speed and power level. In turn, it is

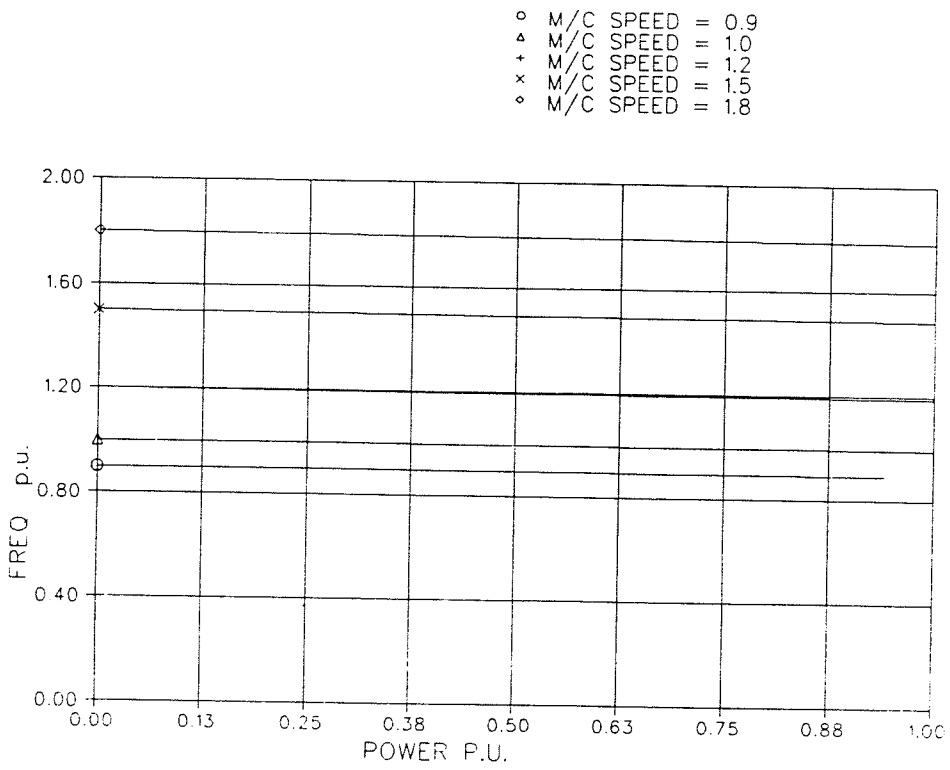

Figure 32 e) Frequency Corresponding to the Machine of Appendix 2 at 1.0 p.u. Voltage for XC = 44.31 (ohms × p.u. freq.)

possible to solve for reactive current into the commutating reactance for each machine speed and power level. Allowance can also be made for the magnetizing current of the transformer which is assumed to have a linear saturation curve to above the maximum operating flux level.

It is thus possible to search through all machine speeds and power levels to find just how small X_{cx} must be in order to augment the reactive power provided by the apparatus in the block diagram on the left of Figure 33. In order to do that a converter transformer was arbitrarily chosen having a magnetizing current of 2.1% and a leakage reactance of 11.8% (both at 1.0 p.u. freq.) on an mva base of 1000 kva with a $V_{baseL-L}$ equal to 4 kv.

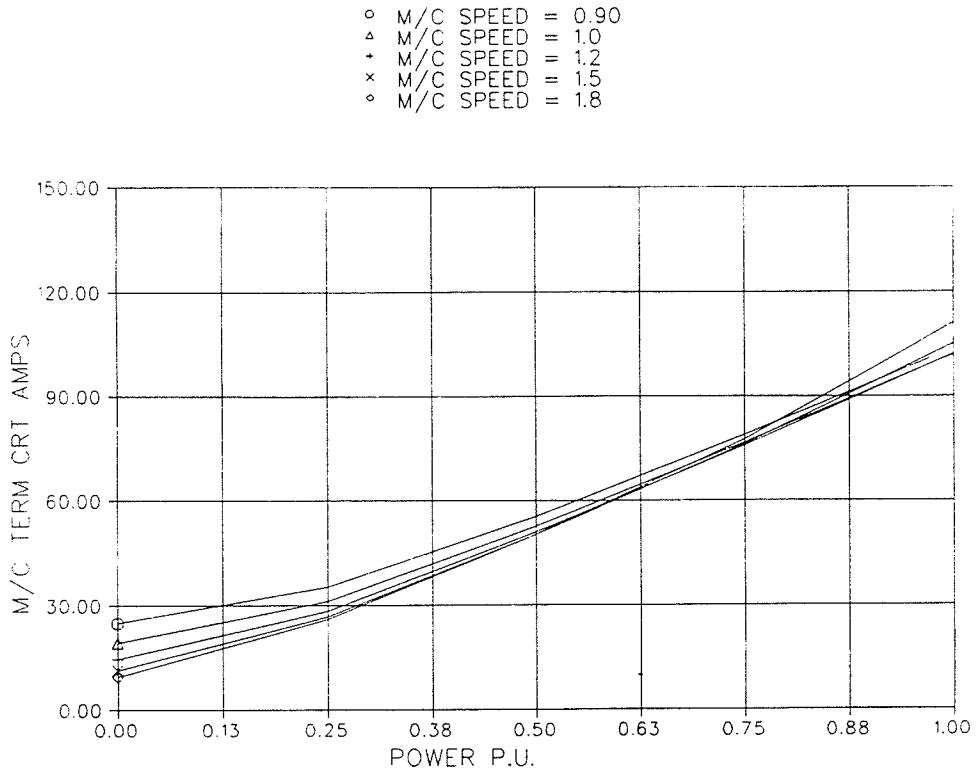

Figure 32 f) Machine Terminal Current Corresponding to the Machine of Appendix 2 at 1.0 p.u. Voltage for XC = 44.31 (ohms × p.u. freq.)

As might be expected X_{cx} was smallest at the lowest machine speed with the highest power level and turned out to be 67.9 (ohms × p.u.freq.). The reactance of the self-excitation capacitors is 44.13 (ohms × p.u. freq.) in parallel with 67.9 (ohms × p.u. freq.) for a total of 26.7 (ohms × p.u. freq.).

With reference to Figure 33, once X_{cx} is known it is possible to determine the real and reactive current into the commutating reactance of Figure 34 for each machine speed and power level. In turn, the α and I_d required in order to keep the induction machine at 1.0 p.u. voltage can be obtained once the real and reactive current are known. Curves of I_{ct} (i.e. total capacitor current), I_{cvt} (i.e. current into the converter transformer), V_d, I_d, and α are given in Figure 35 a) to e).

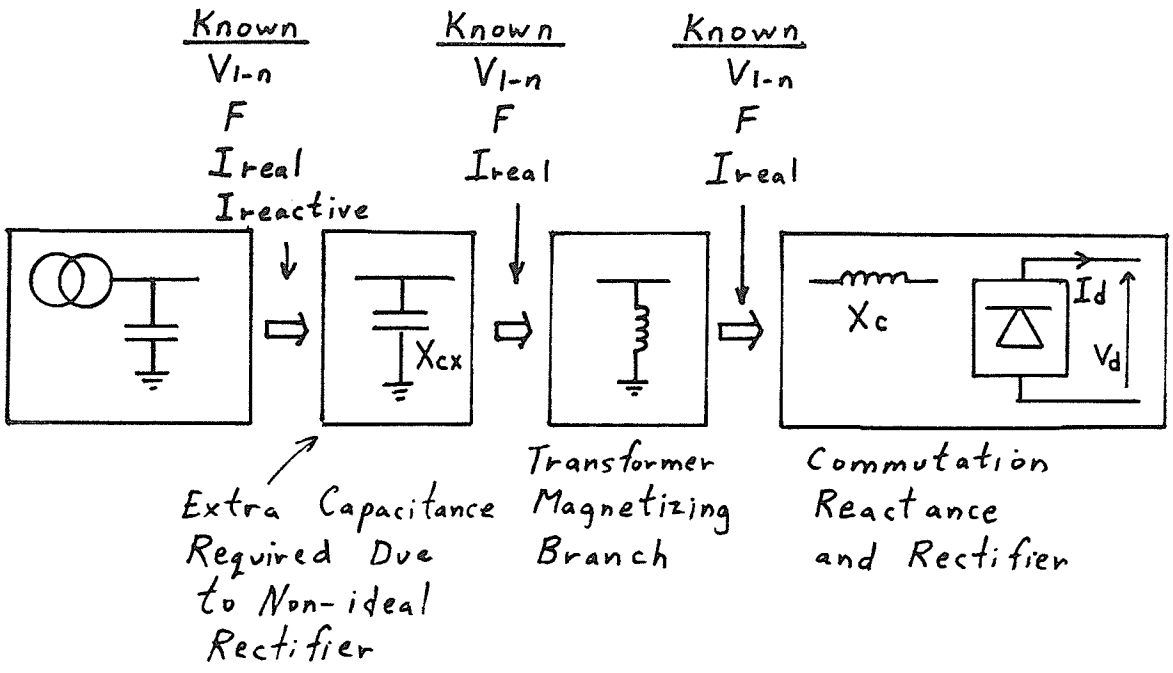

Figure 33 Equivalent Circuit for Considering the Effect of Commutating Reactance

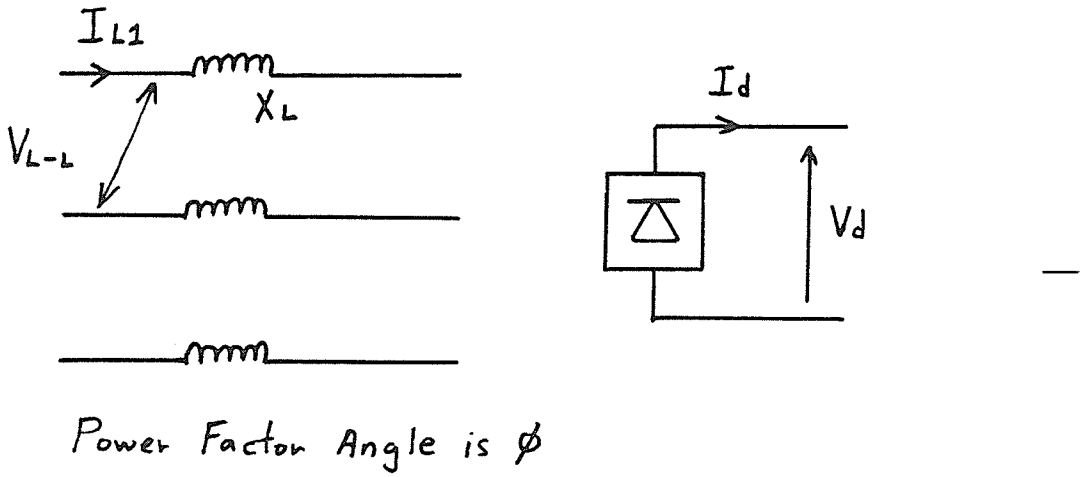

Figure 34 Definitions for Equations 3.20 to 3.26

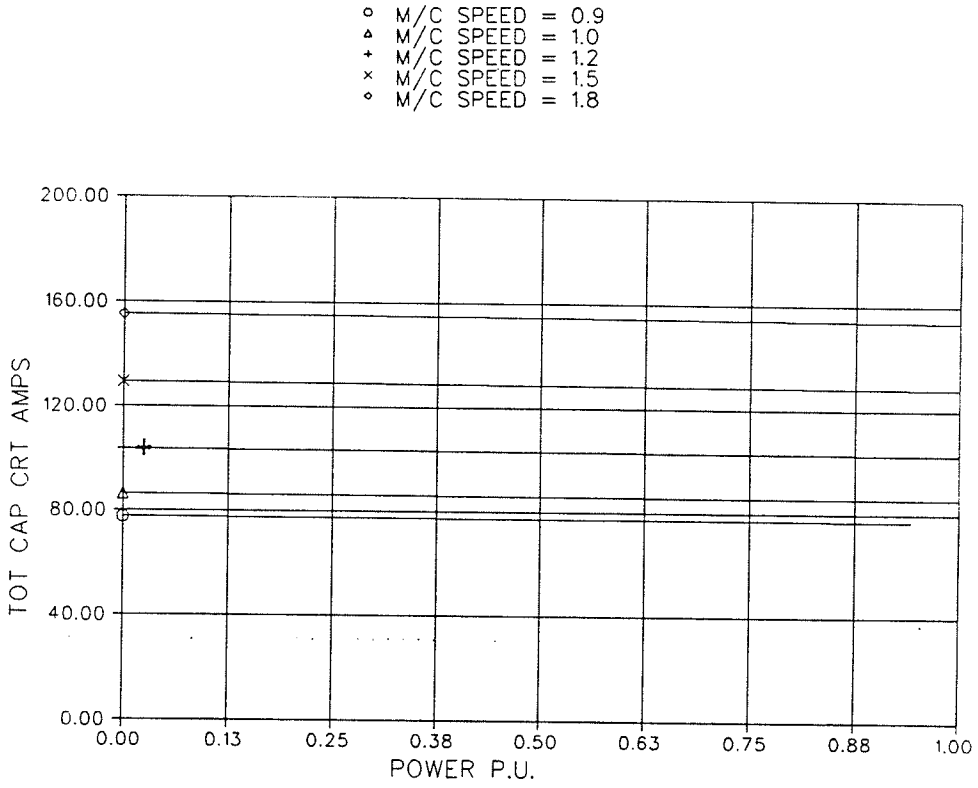

Figure 35 a) Capacitor Current Magnitude for the Machine of Appendix 2 at 1.0 p.u. Voltage with XC = 26.7 (ohms × p.u. freq.) and Including Commutating Reactance

Figure 32 b), e), and f), describing real load current, frequency and machine terminal current respectively remain applicable to the case with a non-ideal rectifier. The capacitor currents for the non-ideal rectifier, as illustrated in Figure 35 a), are approximately 65% larger than the capacitor currents for the ideal rectifier. This larger capacitor current is needed because of the reactive load of the non-ideal rectifier at low speed and high power. The higher capacitor current translates into higher converter transformer and rectifier ratings. In that regard, the converter transformer currents of Figure 35 b) can be seen to be larger than the a.c. load currents of Figure 32 a).

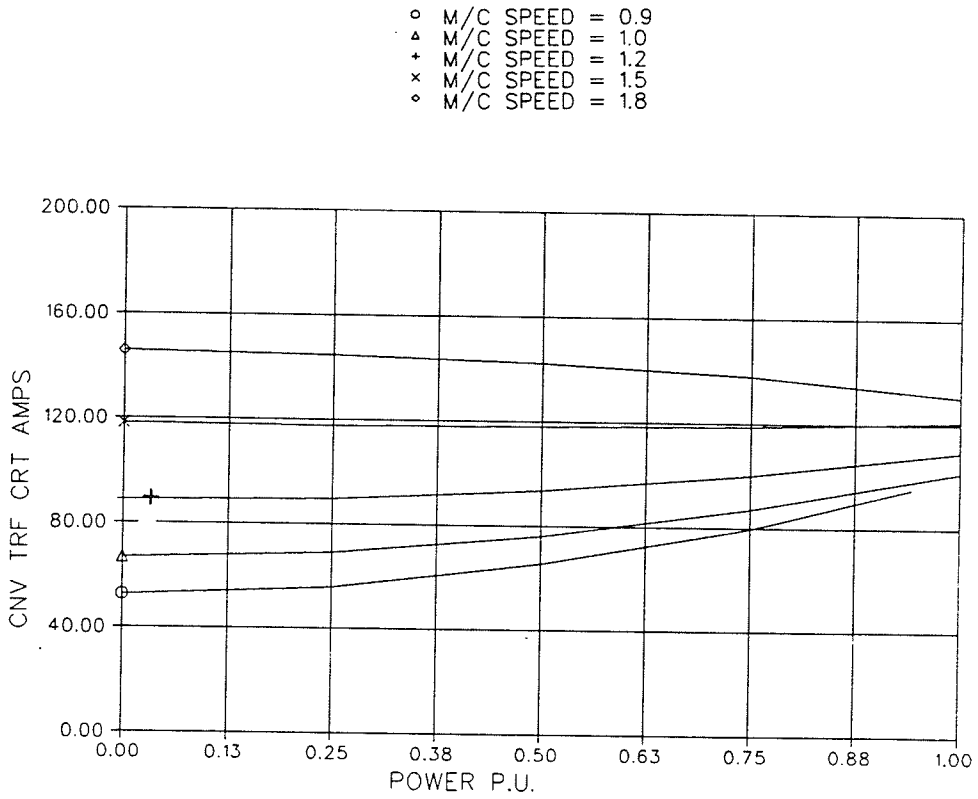

Figure 35 b) Converter Transformer Current for the Machine of Appendix 2 at 1.0 p.u. Voltage with XC = 26.7 (ohms × p.u. freq.) and Including Commutating Reactance

From the above discussion we can make several comments on choosing the minimum delay angle and the transformer leakage reactance.

Minimum α should be kept as small as possible so as to minimize the excitation capacitor, converter transformer and rectifier capacity ratings. Reduced α may be feasible because of the small number of series thyristors and snubber circuits required for each valve group at the relatively low voltages contemplated in this application.

The converter transformer leakage reactance should be kept relatively small. Even at minimum speed, a large commutating reactance (corresponding to 11.8 % transformer leakage impedance) causes a significant demand for reactive power at

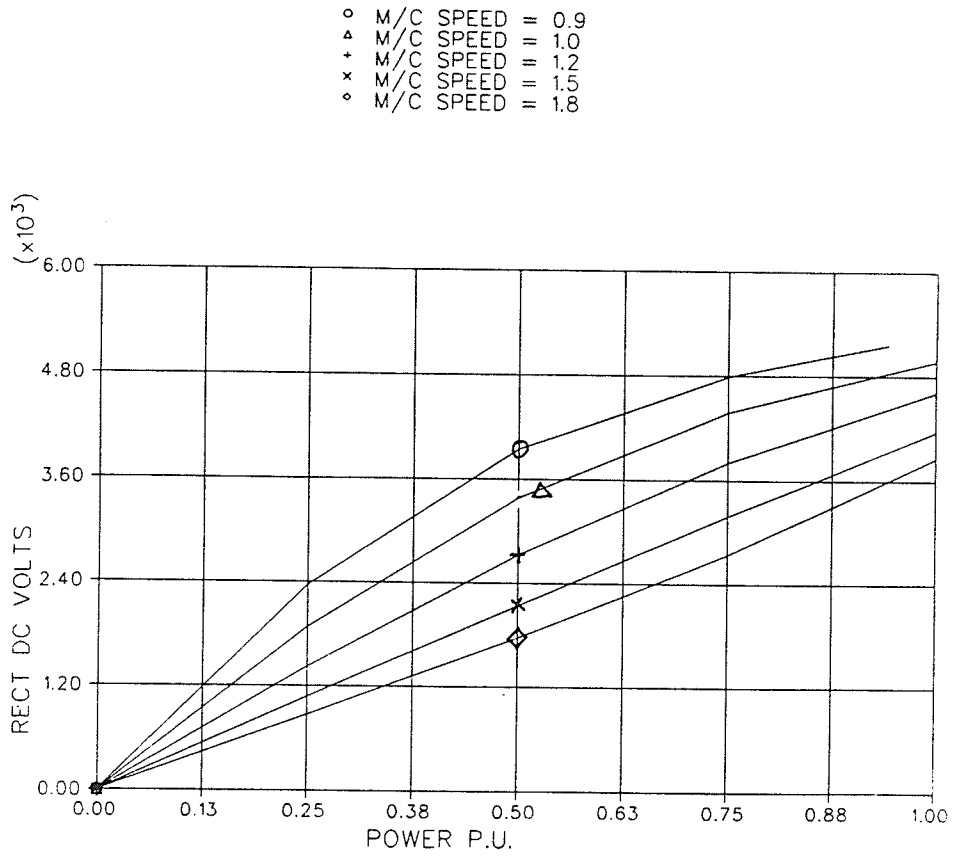

Figure 35 c) D.C. Voltage for the Machine of Appendix 2 at 1.0 p.u. Voltage with XC = 26.7 (ohms × p.u. freq.) and Including Commutating Reactance

1.0 p.u. real power. In turn, reactive demand at 1.0 p.u. power and minimum speed determines the minimum allowable size of the excitation capacitors.

3.6 PERFORMANCE REQUIREMENTS DICTATED BY THE NATURE OF THE RECTIFIER AND THE INDUCTION MACHINE

Several remarks can be made based on the curves of Figure 35.

Figure 35 d) illustrates that the rectifier d.c. current I_d should certainly not be held constant if we wish to be able to operate the generator over a broad range of power and machine speeds while maintaining 1.0 p.u. machine voltage. On the contrary, a very specific level of current I_d is required for each combination of machine speed and power. Corresponding required levels of V_d for each machine speed and

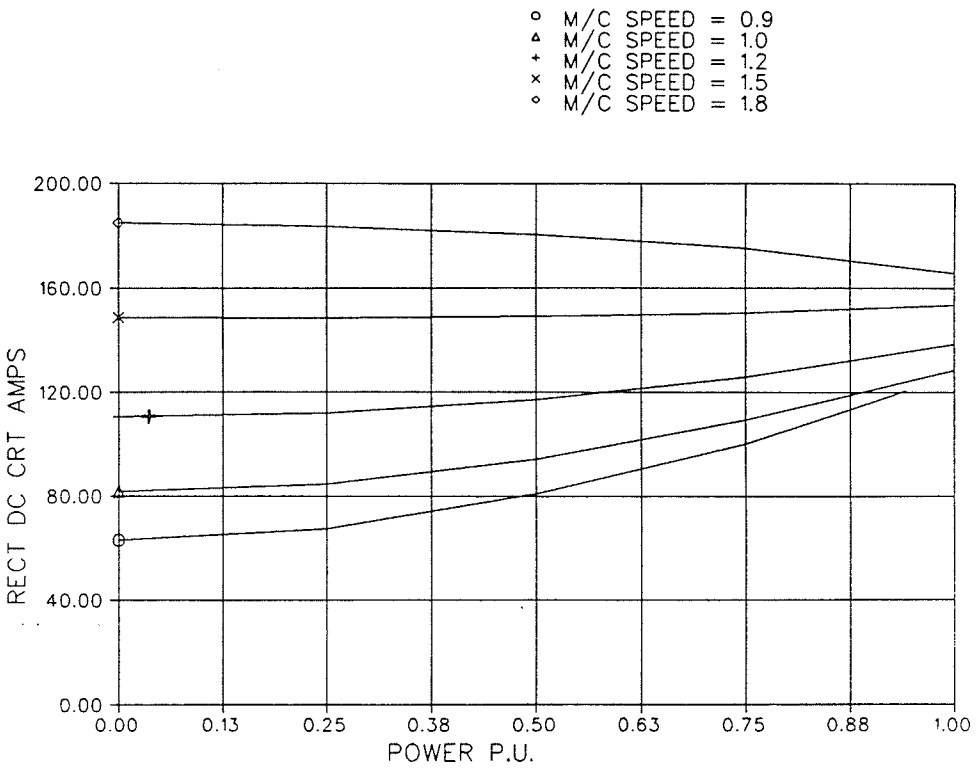

Figure 35 d) D.C. Current for the Machine of Appendix 2 at 1.0 p.u. Voltage with XC = 26.7 (ohms × p.u. freq.) and Including Commutating Reactance

power level are illustrated in Figure 35 c). In addition, the rectifier firing delay angles α required to give these particular levels of V_d and I_d are illustrated in Figure 35 e). These values of α allow for the effect of the commutation reactance for the example system which includes the machine of Appendix 2.

The necessity for a particular level of V_d and I_d for each combination of machine speed and rectifier output power dictates that the apparatus connected on the d.c. output of the rectifier must be able to receive power at the various levels of I_d and V_d.

For the example system, I_d will vary from about 65 amps to a high of about 185 amps as illustrated in Figure 35 d). At a particular power level, a relatively fast

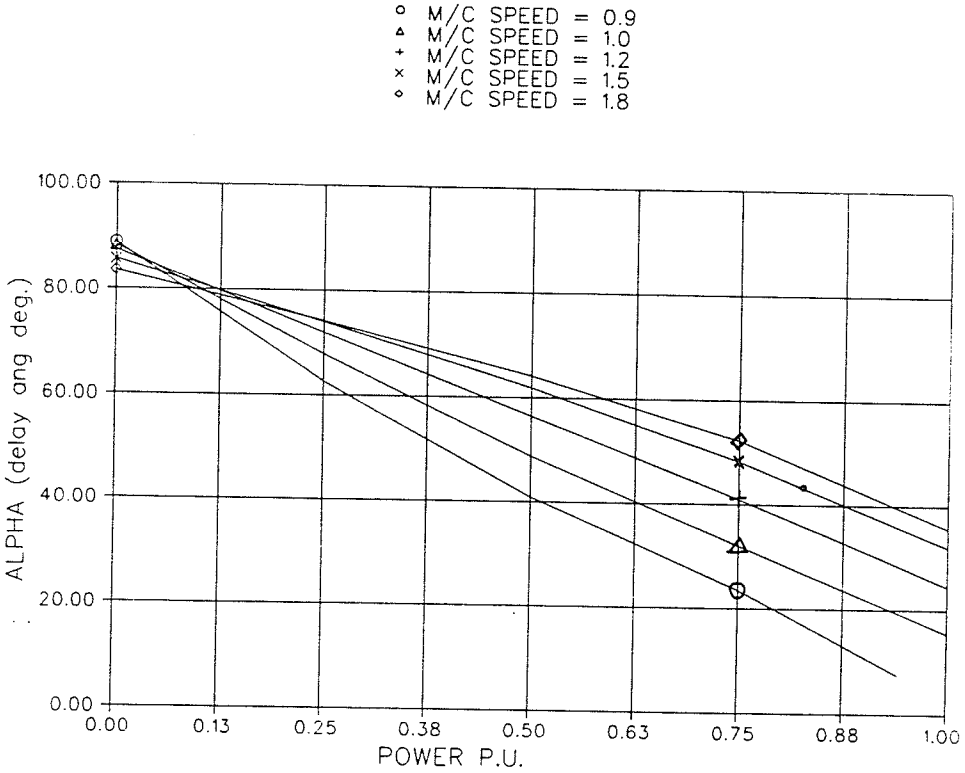

Figure 35 e) Rectifier Firing Angle for the Machine of Appendix 2 at 1.0 p.u. Voltage with XC = 26.7 (ohms × p.u. freq.) and Including Commutating Reactance

machine speed corresponds to a relatively high I_d and a relatively low V_d.

As illustrated in Figure 35 e), rectifier delay angle reduces as the power level increases regardless of the speed of operation. Figure 35 e) also confirms that α must be increased with machine speed at high power. This corresponds with a need to absorb reactive power into the rectifier. It is perhaps worth while however to note that α must be decreased away from 90° as speed increases at or near zero load. This latter effect can be attributed to an increased commutation angle at high speed and low power. That large commutation angle is due to the high commutating reactance associated with high frequency and the high current which must be commutated at high speed and low power. The effect does not occur at high power because the

current to be commutated at high power does not change as drastically with speed as it does for low power operation.

3.7 THE CHOICE BETWEEN 6 AND 12 PULSE RECTIFIERS

A.c. harmonic currents created by the rectifier apparatus could adversely affect the induction machine by causing heating in the machine. This problem could potentially be worsened by a parallel resonance between the machine and capacitor bank. Furthermore, it would be difficult to use tuned filters to eliminate the harmonic currents because it is intended that the induction machine should be operated at variable speed.

Figure 36 illustrates an equivalent circuit which was used to consider the effect of harmonic currents.

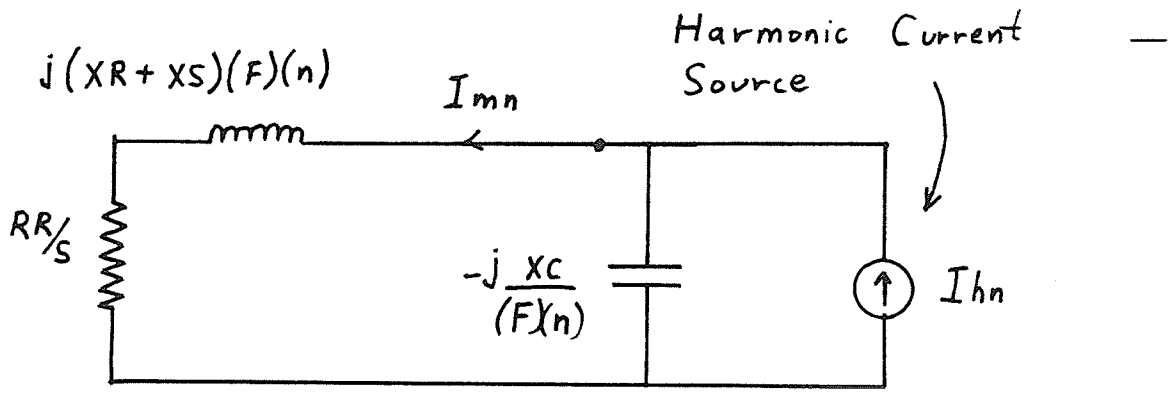

Figure 36 A Circuit for Considering the Effect of Rectifier Generated Harmonic Currents on the Machine

Induction machines used as generators normally have low slip characteristics in order to minimize losses. Slip for any harmonic is given by:

$$S = \frac{\textit{Harmonic Synchronous Mech. Speed} - \textit{Actual Mech. Speed}}{\textit{Harmonic Synchronous Mechanical Speed}} \qquad (3.27)$$

If the fundamental electrical frequency is given by ω_s then to a first approximation

the actual mechanical speed is given by $\frac{2\,\omega_s}{p}$ where p is the number of poles. The harmonic synchronous mechanical speed is identified by the sequence and identifying number of the harmonic. For instance, in the case of the 5th harmonic, the harmonic synchronous speed is given by:

$$-\frac{5\,\omega_s\,2}{p} \tag{3.28}$$

because the 5th harmonic current is negative sequence. Thus, for the fifth harmonic, slip stays at approximately 1.2 regardless of the variation of fundamental electrical frequency or the slip for fundamental frequency. Likewise, the 7th, 11th, and 13th harmonics have slips of 0.85, 1.09, and 0.92 respectively. Slips for higher harmonics will be even closer to equaling 1.0. Low slip induction machines have low values of rotor resistance RR. Low rotor resistance combined with near unity slip allows us to neglect the effect of rotor resistance when determining the approximate magnitudes of harmonic currents in the machine.

Referring back to Figure 36, for a given harmonic current I_{hn} introduced by the rectifier, the nth harmonic current into the machine I_{mn} is given by the equation:

$$I_{mn} = \frac{I_{hn}}{1 - \left(\frac{XR + XS}{XC}\right)(n\,F)^2} \tag{3.28}$$

Note that the harmonic current in the machine can be larger than that introduced by the source due to a parallel resonance between the capacitor bank and the machine.

Consideration of a typical machine illustrates that high power factor machines are more subject to resonance with the capacitor bank than would be low power factor machines. For an example consider a machine with a high power factor of 0.92 at 60 Hz. A capacitor bank would need to have an impedance of approximately 2.55 p.u. in order to provide the reactive power required by the machine at 60 Hz. We can assume leakage reactance XR + XS of 0.167 p.u. for an induction machine with a

starting current of 6 p.u.. Using the above formula, the 5th harmonic current in the machine for a minimum F of 1.0 is:-

$$I_{m5} = -1.56\, I_{h5} \tag{3.29}$$

In the case of a machine with a low power factor of 0.8 and leakage impedance of 0.2 p.u., the relation would be:-

$$I_{m5} = -0.5\, I_{h5} \tag{3.30}$$

From these relations we can conclude that in certain circumstances the presence of the capacitor bank could amplify the 5th and possibly the 7th harmonic currents into the machine. The high power factor machines are particularly susceptible to this problem because of the higher capacitor bank impedance and lower leakage impedance associated with such machines.

The supply side current to a 6 pulse rectifier can be approximated by the following equation [32] if commutation angle is assumed as zero:

$$i_a = 1.103\, I_d \left(\cos\theta + \frac{1}{5}\cos 5\theta - \frac{1}{7}\cos 7\theta - \frac{1}{11}\cos 11\theta + \frac{1}{13}\cos 13\theta + \frac{1}{17}\cos 17\theta - \frac{1}{19}\cos 19\theta - \cdots \right) \tag{3.31}$$

In the above equation i_a is the actual instantaneous current. Thus the 5th harmonic current into the 6 pulse rectifier is 20 % of the fundamental. For the high power factor machine considered above, the 5th harmonic current in the machine would be amplified to 30 % and that would be unacceptable in most cases. In the machine with 0.8 power factor, the 5th harmonic current would be cut to 10 % of the fundamental.

Consideration of a real machine and rectifier leads to a slightly less pessimistic view for high power factor machines. In that regard, reference can be made to the machine of Appendix 2 with XC = 26.7 (ohms × p.u. freq.). That value of capacitive impedance provides the extra capacitance required by a practical rectifier as calculated in section 3.5. The extra capacitance was required because a practical rectifier

always absorbs some reactive power due to commutation angle and minimum firing delay angle. The increased capacitance diverts rectifier harmonic current away from the machine. For the machine of Appendix 2, the leakage impedance XR + XS equals 5.747 (ohms / p.u. freq.).

Table 2 was prepared for the machine of Appendix 2 supplying the practical rectifier described in section 3.5. The XC and (XR + XS) used in the calculation of the table are those for the example system namely: 26.7 (ohms × p.u.freq.) and 5.747 (ohms / p.u. freq.). The table gives the approximate magnitudes for machine harmonic currents as a percentage of the fundamental current into the rectifier.

The values in the table are for the lowest frequency of operation contemplated (0.9 p.u.). The percentages of machine harmonic

Table II

Harmonic	Approximate Magnitudes of Machine Harmonic Currents in Percentage of the Fundamental Current in the Rectifier
5	6.0
7	2.0
11	0.45
13	0.27
17	0.001
19	0.0008

current would be further reduced for harmonics of order greater than 19. It is intended that fundamental a.c. currents to the rectifier should be larger at high machine speeds in order to control fundamental voltage magnitude. In spite of that, it is anticipated that the machine harmonic currents would actually be lower during high speed operation due to the fact that at higher frequencies of operation a larger fraction of each rectifier harmonic current would be diverted through the capacitor bank. It appears that the worst situation would arise at full load power and low speed because that condition requires the largest rectifier current for any low speed operation.

Commutation reactance in the converter transformers increases the capacitance

necessary at the machine terminals as discussed in section 3.5. The presence of commutation reactance can be expected to reduce all machine harmonic currents to below the values shown in Table II for yet another reason. Commutation can reduce a.c. side current harmonics forced into the machine and capacitor bank to below 1/n of the fundamental rectifier current as illustrated by well known graphs [33] of rectifier harmonic current as a function of firing delay angle and commutation angle. However, the reduction of the 5th and 7th harmonic currents attributable to this cause can be expected to be small during low frequency operation. Low frequency operation implies that commutation reactance and thus commutation angle will be relatively small for reasonable values of 60 Hz. converter transformer leakage impedance. A small commutation angle corresponds to only minor reductions in the lower order current harmonics (5th and 7th) as illustrated in the above mentioned graphs [34].

Based on the above analysis, the percentages in Table II are reasonable approximations for maximum harmonic currents for the machine of Appendix 2 supplying the example rectifier. Furthermore, the fundamental a.c. rectifier current to be used as a reference value to Table II should be the a.c. rectifier current at minimum speed and maximum power. In that regard, Figure 35 d) illustrates a value of approximately 100 amps at 0.9 p.u. speed and 1.0 p.u. power. Whether or not these levels of harmonic machine currents are acceptable will depend on the design of the machine. Krishnayya [35] has related a machine's ability to accept harmonic currents to it's negative sequence current rating.

In the event that the predicted levels of 5th and 7th harmonic currents are unacceptable for a given machine, those harmonics could be almost entirely eliminated by going to a 12 pulse rectifier. The remaining harmonics of order 11 or higher would then only have a minor effect on the machine. That may be noted by observing the small values in Table II corresponding to those harmonics.

3.8 ALTERNATIVES IN APPARATUS COMPLEMENTARY TO THE REQUIREMENTS OF THE LOAD, INDUCTION MACHINE, AND RECTIFIER

3.8.1 INTRODUCTION

Two alternative configurations of apparatus are presented for connection between the rectifier and the a.c. load. The first alternative is a chopper inverter circuit which includes a voltage inverter to accommodate unbalanced loads. The second alternative comprises a dual arrangement of series capacitor forced commutated inverters [36,37,38]. The latter alternative allows d.c. voltages sufficiently high for transmission purposes because it allows the arrangemnt of thyristors in series in a bridge arm.

Both alternatives are discussed as to their steady state condition. In addition a control strategy is proposed for the first alternative and a discussion is presented as to disturbances from steady state. The control strategy is the subject of a simplified simulation the results of which are discussed in chapter 4.

3.8.2 ALTERNATIVE 1 - THE CHOPPER INVERTER APPARATUS

The schematic shown in Figure 37 illustrates a chopper inverter apparatus for conditioning the output of the rectifier to match a 3 phase load.

3.8.2.1 THE INVERTER

Figure 38 presents a schematic of an example voltage inverter apparatus. In Figure 38, the symbol of a junction in a circle refers to a one way current device which can be blocked such as a gate turn off (GTO) thyristor. The turn on order is 1-2-3-4-5-6 and the conduction states lasts 180° for each bridge arm (i.e. GTO thyristor plus anti-parallel diode). The resultant output waveforms which are applied to the primary windings of T3, T4, and T5 are illustrated in Figure 39. The input voltage to the inverter V_{cap} must be kept essentially constant because the fundamental com-

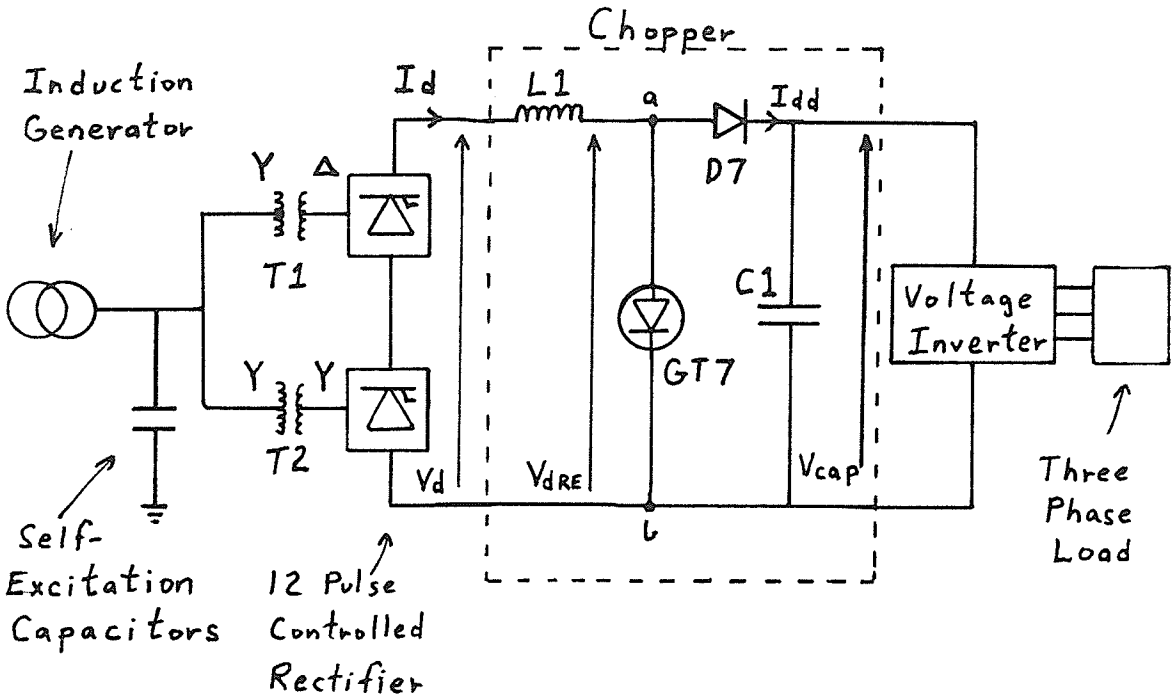

Figure 37 The Chopper Inverter Apparatus

ponent of a.c. output voltage will be some factor times V_{cap}. That factor can be picked by a choice of the turns ratio of transformers T3, T4, and T5 in Figure 38. The choice of the constant value of V_{cap} will be made based upon the requirements of the induction machine and the chopper. This will be discussed in relation to the chopper.

The output voltage waveforms illustrated in Figure 39 have no even or triplen harmonics and thus it is necessary to block 5th, 7th, 11th, 13th, and higher voltage harmonics. No attempt has been made to completely optimize the filters illustrated in Figure 38. It is recognized that other voltage inverters [39] such as pulse width modulated inverters may be more suitable for creating a balanced set of phase voltage waveforms with reduced harmonics.

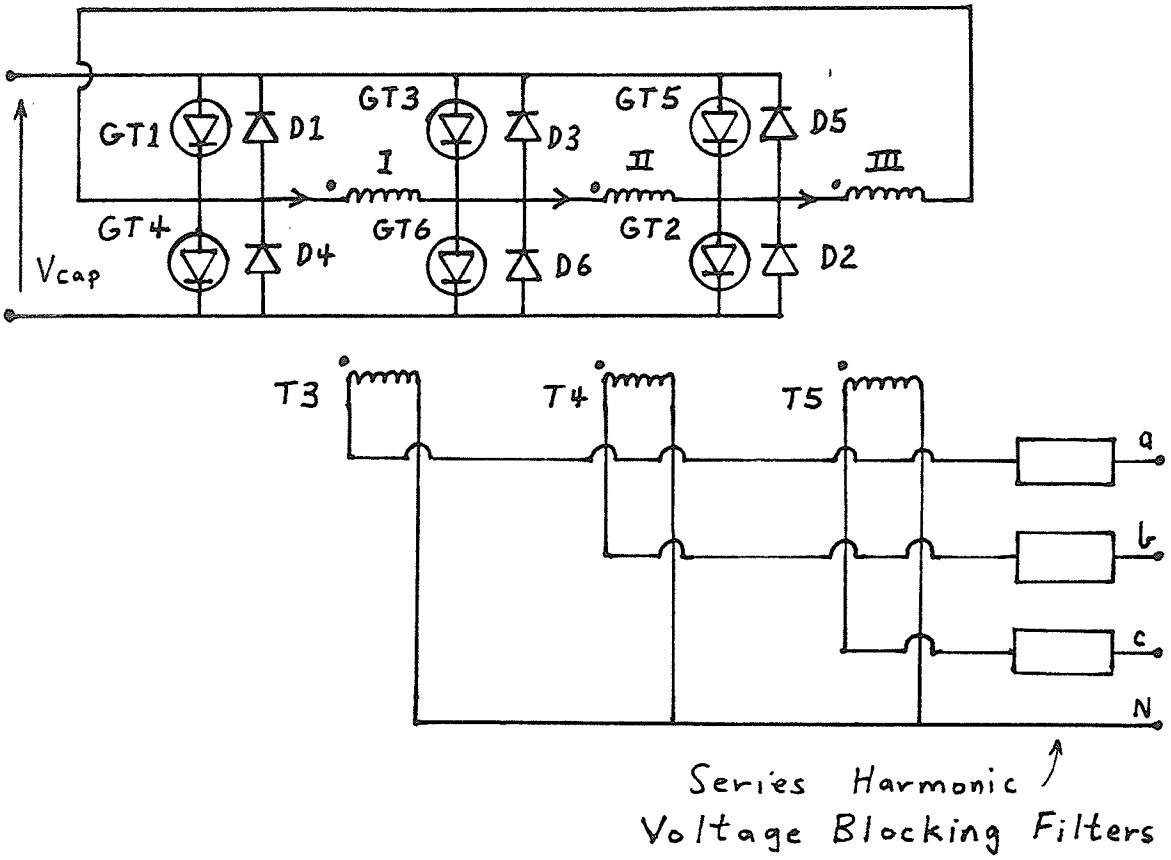

Figure 38 A Voltage Inverter

3.8.2.2 THE CHOPPER

The chopper circuit can be considered from the standpoint of steady state operation.

As a premise for analyzing the circuit it is assumed that the inductor L1 in Figure 37 is sufficiently large to smooth the current through it to almost a constant d.c. level. Choice of inductor L1 will be affected by the superimposed voltage ripple from the two ends of the inductor as compared to allowable current ripple. However, it is understood that a higher level of inductance may be required due to consideration of system stability and system control.

From the proposed operation of the chopper it can be deduced that V_{cap} must be larger than the maximum steady state rectifier output voltage. In the steady state, V_d in Figure 37 will be positive on average and on average I_d will be neither

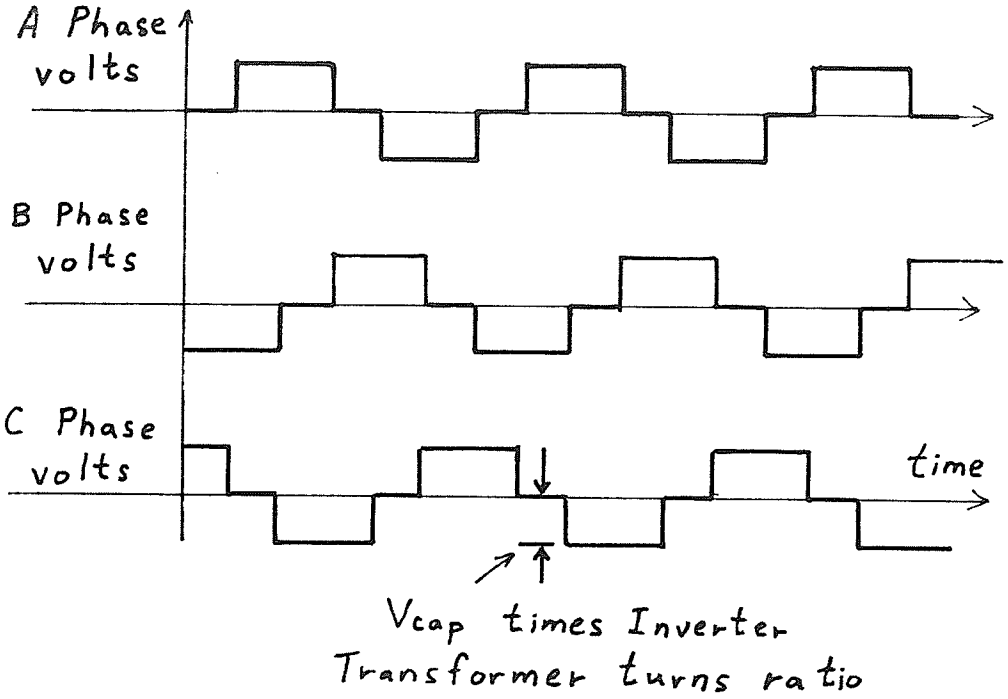

Figure 39 The Voltage Waveforms from the Output of the Voltage Inverter of Figure 37

increasing or decreasing. GT7 will turn "on" and "off" at a fairly high frequency for power of perhaps 1000 Hz. When GT7 is "on", current in L1 will grow. When GT7 is "off", it is necessary that the current in L1 should drop in order that I_d should be at a fixed average level. In order for I_d to drop when GT7 is "off", V_{cap} should always be greater than V_d. For the example system including the machine of Appendix 2, the maximum V_d is approximately 5200 volts and thus the choice of operating level for V_{cap} would need to be higher than that level.

The chopper, in effect, acts as a variable matching circuit in order that the necessary rectifier voltage and current output levels (see Figures 35 c) and d)) can be matched to the voltage of and the average current into the capacitor bank C1. The variability of the matching circuit is introduced by varying the duty cycle of the switching of GT7. For explanation purposes, the fraction of each chopper cycle during which GT7 is blocked will be referred to as T_{froff}.

The variability of T_{froff} can enable the chopper to act as a matching circuit. In the steady state, and given a certain level of V_{cap}, the average voltage V_{dRE} at the load end of the inductor L1 will be given by the equation:

$$V_{dRE} = T_{froff}\ V_{cap} \tag{3.32}$$

Furthermore, in steady state, the average value of I_d will not be increasing or deceasing. Therefore, in Figure 37, the average voltage V_d at the rectifier end of the inductor L1 must be equal to V_{dRE}. Thus, in steady state, the above equation can be altered to:

$$V_d = T_{froff}\ V_{cap} \tag{3.33}$$

A similar approach can be taken in respect of currents. Given that the inductor current I_d is approximately constant for a given operating condition we can conclude that the average current into the capacitor bank C1 is given by:

$$I_{dd} = T_{froff}\ I_d \tag{3.34}$$

Re-written, the above current equation becomes:

$$I_d = \frac{I_{dd}}{T_{froff}} \tag{3.35}$$

When the re-written equation is associated with

$$V_d = T_{froff}\ V_{cap} \tag{3.36}$$

it becomes clear that the chopper circuit does in fact act as a matching circuit. The power balance can be seen plainly by noting the equation:

$$V_d\ I_d = \left(\frac{I_{dd}}{T_{froff}}\right) T_{froff}\ V_{cap} = I_{dd}\ V_{cap}\ . \tag{3.37}$$

This final equation represents a lossless chopper.

There is significance to equation 3.36 in that for the steady state we can calculate the required duty cycle T_{froff} from the rectifier output voltage V_d as:

$$T_{froff} = \frac{V_d}{V_{cap}}. \tag{3.38}$$

Proper choice of V_{cap} was discussed above, and V_d is available from Figure 35 c) for

each combination of machine speed and power level.

3.8.2.3 THE EFFECT OF HARMONICS ON THE CHOICE OF THE SMOOTHING INDUCTOR AND SMOOTHING CAPACITOR

3.8.2.3.1 THE SMOOTHING INDUCTOR

The smoothing inductor between the rectifier and the chopper should have sufficient inductance to maintain the harmonic current content to below maximum allowable levels. The harmonic voltages applied at both ends of the inductor as well as the magnitude of harmonic current to be allowed must all be considered in order to get an upper limit on the inductance required for harmonic current suppression.

The effect of the rectifier generated voltage harmonics will be considered first. Maximum voltage harmonics generated at the d.c. output of the rectifier are listed in Table III. The listed values are maximum values for the complete available ranges of commutation angle and firing delay angle [40]. A maximum magnitude will be obtained for each individual current harmonic caused by the rectifier voltage if the minimum intended operating frequency is considered during calculation. A maximum peak magnitude of current ripple due to the rectifier can then be obtained by assuming that all current harmonics are in the worst possible phase relation and then adding the magnitudes of all the individual current harmonics. The equation for the worst case maximum peak current induced by the rectifier can then be given as follows:

$$I_p\ (rect.) = \frac{1}{L}\left[\frac{\sqrt{2}\,V_{do}}{(F_{\min})\ (377)\ (100)}\sum_{n\ =\ 6,\ 12,\ 18,\ 24,\ldots}\frac{\%\ \text{for}\ nth}{n}\right] \qquad (3.39)$$

Table III	
Harmonic Order	R.M.S. Voltage Magnitude as a Percentage of V_{do}
6	24
12	12
18	8
24	6

On the other hand, the peak ripple in the inductor current due to the chopper is as follows:

$$I_p\ (ch.) = \frac{1}{L}\left(\frac{V_d}{2\,f_{chop}}\right)\left(1 - T_{froff}\right). \tag{3.40}$$

Equation 3.40 can be derived based on constant current charging of the capacitor during the charging portion of the chopper period (i.e. T_{froff}). Furthermore, the maximum peak chopper induced current can be found by recalling that $T_{froff} = V_d / V_{cap}$ (Eqn. 3.38) during steady state operation and then differentiating with respect to V_d. The result indicates a maximum as follows:

$$I_p\ (ch.max.) = \frac{V_{cap}}{8\,f_{chop}\,L}. \tag{3.41}$$

An understanding of the relative importance of the contributions to inductor current can be obtained by considering the machine of Appendix 2 supplying a suitable rectifier and chopper circuit. Suitable input data for equations 3.39 to 3.41 is given in Table III and by the values below:

$V_{cap} = 5500\ volts$

$f_{chop} = 1000\ Hz$

$F_{\min} = 0.9\ p.u.$

$V_{do} = 5401\ volts$

When these values are inserted equation 3.39 becomes:

$$I_p\ (rect.) = \frac{1}{L}\left[\,0.900 + 0.225 + 0.100 + 0.056 + \cdots\,\right]. \tag{3.42}$$

Likewise, equation 3.40 becomes:

$$I_p\ (ch.max.) = \frac{1}{L}\left[\,0.688\,\right]. \tag{3.43}$$

From this analysis it can be noted that the chopper will induce a peak value of ripple current which is less than that which would be induced by the 6th harmonic voltage. Thus we are able to conclude that the chopper will not generate a prohibitive level of harmonics if it is operated at a frequency in the range of 1000 Hz.

From the perspective of harmonic current suppression, the smoothing induc-

tance could be very significantly reduced but for the presence of the chopper harmonic voltages and the 6th harmonic voltage. The rectifier 6th harmonic voltage is easily reduced by using a 12 pulse rectifier. Increasing chopper frequency beyond the 1000 Hz used in the the example would reduce the ripple induced by the chopper. However, increasing the chopper frequency beyond 1000 Hz will also cause increased switching losses in the switching devices used in the chopper. Furthermore, some switching devices, such as GTO (gate turn off) thyristors, require several tens of microseconds to turn off and if frequency is raised much beyond 1000 Hz then the turn-on and turn-off time for the switching device will become a significant portion of the chopper period.

For the example system including the machine of Appendix 2 a maximum inductor current ripple might suitably be specified as some fraction of the minimum d.c. component of inductor current associated with any combination of machine speed and power level. From Figure 35 d) the minimum d.c. operating current for the example is approximately 65 amps. If maximum peak d.c. current ripple was taken as 10 % of that value then a ripple of 6.5 peak amps would be allowed. An upper limit on the required smoothing inductance for harmonic current suppression can be determined as 0.149 henries for the example system by considering chopper induced currents and rectifier induced currents (excluding the 6th and 18th) cumulatively.

The smoothing inductor will have effects on the system beyond the suppression of harmonic currents. In particular a large smoothing inductor will tend to slow the response of the system to load changes or generator speed changes. However, a larger inductor may be required from the point of view of system stability. In conclusion, a complete simulation of the entire system would be required in order to optimize the inductor size having regard to response, stability, and harmonic suppression. A discussion of control and response is presented later herein.

3.8.2.3.2 THE SMOOTHING CAPACITOR

The smoothing capacitor at the output of the chopper should have sufficient capacitance to maintain the ripple voltage on the capacitor to below a maximum allowable level. The ripple in the current to the capacitor both from the chopper and the inverter as well as the magnitude of the allowable voltage ripple must be considered in order to obtain an upper limit on the capacitance required for ripple voltage suppression.

The effect of chopper ripple currents will be considered first. In steady state operation an average current of $T_{froff}\ I_d$ goes to the inverter from the smoothing capacitor. The capacitor is only replenished when the chopper switching device is blocked. The time during which the capacitor is replenished is equal to $T_{froff}\ / f_{chop}$ during each chopper cycle. During that time the current from the chopper into the smoothing capacitor is I_d. During the replenishing, an excess charge flows into the capacitor above the charge going to the inverter. That excess charge causes an increase in the capacitor voltage. During the remainder of the chopper period the voltage on the capacitor and thus the excess charge drop to minimum levels. The excess charge on the capacitor which causes the capacitor voltage to climb during each cycle is given by the equation:

$$Q\ (ch.) = I_d\ (1 - T_{froff})\left(\frac{1}{f_{chop}}\right)(T_{froff})\ . \tag{3.44}$$

Recalling that in steady state operation:

$$T_{froff} = \frac{V_d}{V_{cap}} \tag{3.38}$$

allows the equation for Q (ch.) to be re-written as:

$$Q\ (ch.) = \frac{I_d\ (V_{cap} - V_d)\ V_d}{f_{chop}\ (V_{cap})^2}\ . \tag{3.45}$$

Figures 35 c) and 35 d) show that there are unique values of machine V_d and I_d for each combination of machine speed and power. Thus the value of chopper induced

ripple charge Q (ch.) can be obtained for each power level and machine speed. Table IV gives the magnitudes of ripple charge induced by the chopper over a range of power levels and machine speeds for the example system associated with the machine of Appendix 2 and for an f_{chop} equal to 1000 Hz. The maximum value of ripple charge detected by the simple search is 0.0438 coulombs.

Table IV Coulombs of Ripple Charge for Various Combinations of Machine Speed and Power Level

		Power Levels (p.u. of rated)				
		0.0	0.25	0.5	0.75	1.0
Machine Speed (p.u.)	0.9	0.0	0.0166	0.0164	0.0113	0.0050
	1.0	0.0	0.0191	0.0224	0.177	0.0111
	1.2	0.0	0.0215	0.0293	0.0268	0.0187
	1.5	0.0	0.0234	0.0355	0.0367	0.0281
	1.8	0.0	0.0244	0.0394	0.0438	0.0347

The required capacitance of the smoothing capacitor is also affected by the action of the inverter. Various types of inverters might be employed. For illustrative purposes the inverter of Figure 38 has been considered supplying a three phase load.

Reference is made to the various portions of Figure 40 in order to determine the shape of the current waveform out of the capacitor to the inverter positive bus. Figure 40 a) illustrates the sinusoidal load voltage waveforms assumed to be obtained by filtering the voltage waveform initially applied to windings I, II, and III in Figure 38. The rectangular voltage waveform applied to winding I is shown as a dotted line. Figure 40 b) illustrates a resultant sinusoidal phase current. Figure 40 c) tabulates the effect that each winding current has on current out of the capacitor to the positive inverter bus during a complete inverter period. Figure 40 d) illustrates the current out of the capacitor to the inverter positive bus for an a.c load with a power factor of 0.707 lagging ($\phi = 45°$).

From study of Figure 40 d) it is apparent that the lowest harmonic is the 6th order harmonic current. We can thus conclude that to determine ripple we need only consider the first 1/6 th of an inverter period. Furthermore, the current waveform to the inverter is directly analagous to the d.c. side output voltage of an ideal 6 pulse

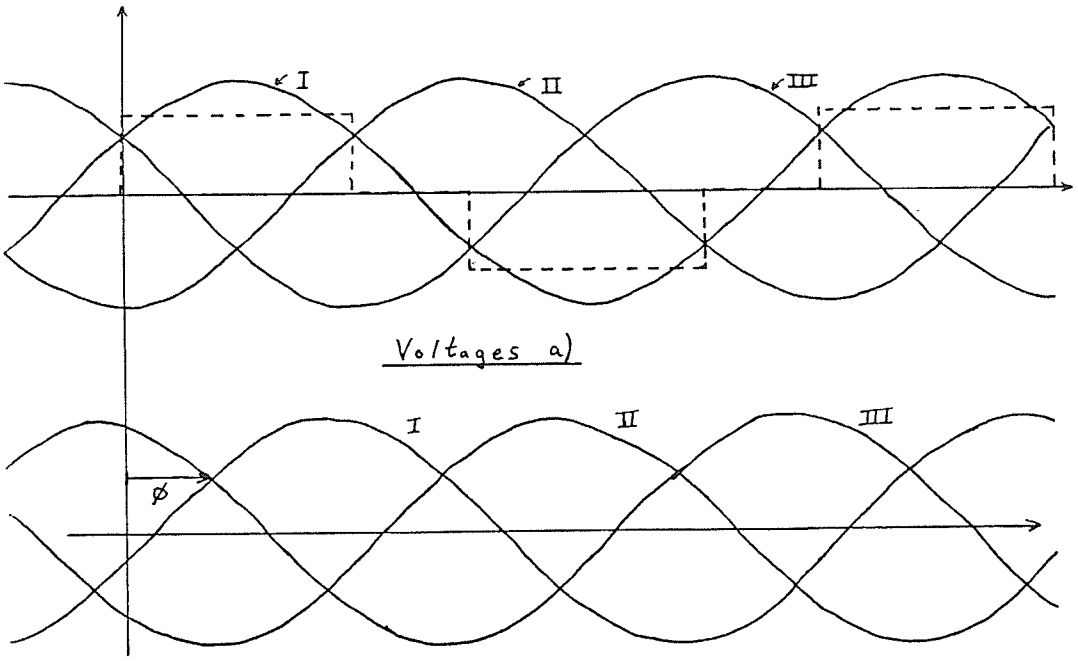

Phase						
I	+	+	o	−	−	o
II	−	o	+	+	o	−
III	o	−	−	o	+	+

- a "+"ve sign signifies current out of the capacitor to the +ve inverter bus.
- a "−"ve sign signifies current into the capacitor from the +ve inverter bus.
- a "o" signifies no current flowing to the capacitor

Load Current Connection Chart c)

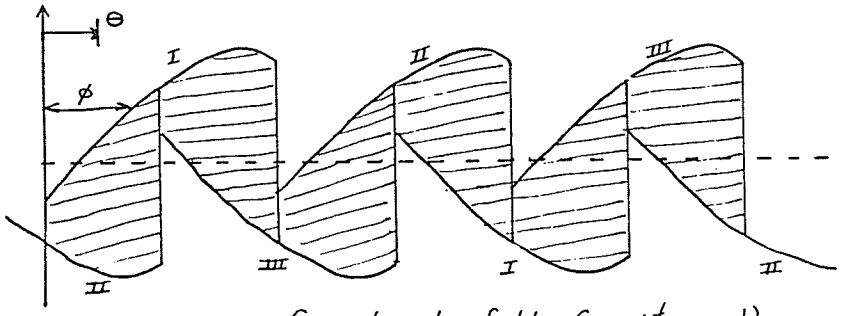

Current out of the Capacitor d)
(Shaded Area)

Figure 40 Analysis of Inverter Harmonic Currents for the Inverter of Figure 38 with 45° Lagging Load

Graetz bridge inverter. Therefore, the average current to the inverter is given by the equation:

$$I_{AV} = I_{RMS} \frac{3\sqrt{6}}{\pi} \cos\phi \ . \qquad (3.46)$$

The smoothing capacitor in a steady running condition will get I_{AV} from the chopper. On the other hand, during the first 1/6 th of the inverter period, the current to the inverter is given by the equation:

$$i(t) = \sqrt{2}\, I_{RMS} \left[\sin(\theta + 30 - \phi) - \sin(\theta - 90 - \phi) \right] . \qquad (3.47)$$

wherein θ is as illustrated in Figure 40 d). Charge on the smoothing capacitor climbs when I_{AV} is greater than $i(t)$; remains stable when I_{AV} is equal to $i(t)$; and falls when I_{AV} is less than $i(t)$. Therefore, it is only necessary to integrate the surplus of the current during the time that I_{AV} is greater than $i(t)$ in order to determine the ripple charge. For any ϕ ($0° < \phi < 90°$), it is possible to determine the particular θ for which $i(t)$ is equal to I_{AV}. For instance, if ϕ is 45° then I_{AV} is equal to $i(t)$ at $\theta = 27.45°$. Thus, for $\phi = 45°$, the ripple charge can be determined by integrating $(I_{AV} - i(t))$ between $\theta = 0°$ and $\theta = 27.45°$.

For the example circuit associated with the machine of Appendix 2 and for 60 Hz inverter operation the ripple charge due to the inverter can be calculated as 0.0436 coulombs at full inverter load (70.35 amps r.m.s.) with a power factor of 0.707. Any load imbalance at full load would increase the capacitor voltage ripple.

The total ripple charge can be obtained by adding the ripple charge due to the chopper to that due to the inverter. Given the total ripple charge and the allowable ripple voltage magnitude, the required capacitance is calculated as:

$$C_S = \frac{Q_{total}}{V_{ripple}} \ . \qquad (3.48)$$

For the example system, a V_{ripple} of 330 volts corresponds to a variation of V_{cap} of $\pm$ 3 % for $V_{cap} = 5500\ volts$. The total ripple charge is $Q_{total} = Q\ (ch.) + Q\ (inv.)$ and equals 0.0874 coulombs. Calculation of the

smoothing capacitance yields $C_S = 264.9\ \mu F$. The capacitor would need an a.c. voltage rating of $6000 / \sqrt{2}$ in order to handle a maximum capacitor voltage of 6000 volts.

The required current rating of the capacitor would not be fixed by it's capacitance because we are not dealing with 60 Hz voltages. The largest component of voltage on the capacitor would be d.c. voltage which would not cause any current. However, the r.m.s. current in the capacitor due to the inverter and the chopper could easily be determined because we know the current waveshapes from the above discussion.

3.8.2.4 PROPOSED CONTROLLERS

In the system illustrated in Figure 37, controllers will be required for controlling the level of current in the smoothing inductor and the level of voltage on the smoothing capacitor. In addition, a governor may be required for certain types of prime movers. In this preliminary investigation discussions will focus on the performance required of these controllers and suggestions for implementation of the controls. Some of the basic control principles have been tested in simplified simulations discussed in chapter 4.

Prime mover speed is generally controlled by a governor. However, precise speed regulation may not be required in this proposed generation scheme because of the scheme's variable speed capability. For instance, the runaway speed of some Francis turbines is in the range of 1.8 p.u. speed. As the turbine approaches runaway speed, it becomes so inefficient that it can only supply the windage and friction torque to the generator. Thus, the generator output electrical power must be zero if the generator is to reach run-away speed. From the graphs of Figure 35, a typical example of the proposed generation scheme is intended to accept any power level between 0 and 1.0 p.u. power at any speed between 0.9 and 1.8 p.u. speed. Thus, steady state considerations indicate that in certain cases the generator could accept

acceleration to the runaway speed as electrical load dropped to zero. Any increase in electrical load above zero would cause the turbine and generator to slow to some value of speed below runaway speed. Thus, no governor would be required. Slow variation of gate position could be adopted to save water and reduce speed during extended periods of light loading. This approach would only be feasible provided that a particular turbine could survive prolonged overspeed.

As mentioned previously, controllers will be required to control smoothing inductor current and smoothing capacitor voltage. In the proposed control scheme illustrated in Figure 41, it is intended that the capacitor voltage controller adjusts the duty cycle of the chopper and the inductor current controller adjusts the firing delay angle of the rectifier. Operation of the controls in response to disturbances from a steady state condition will be discussed.

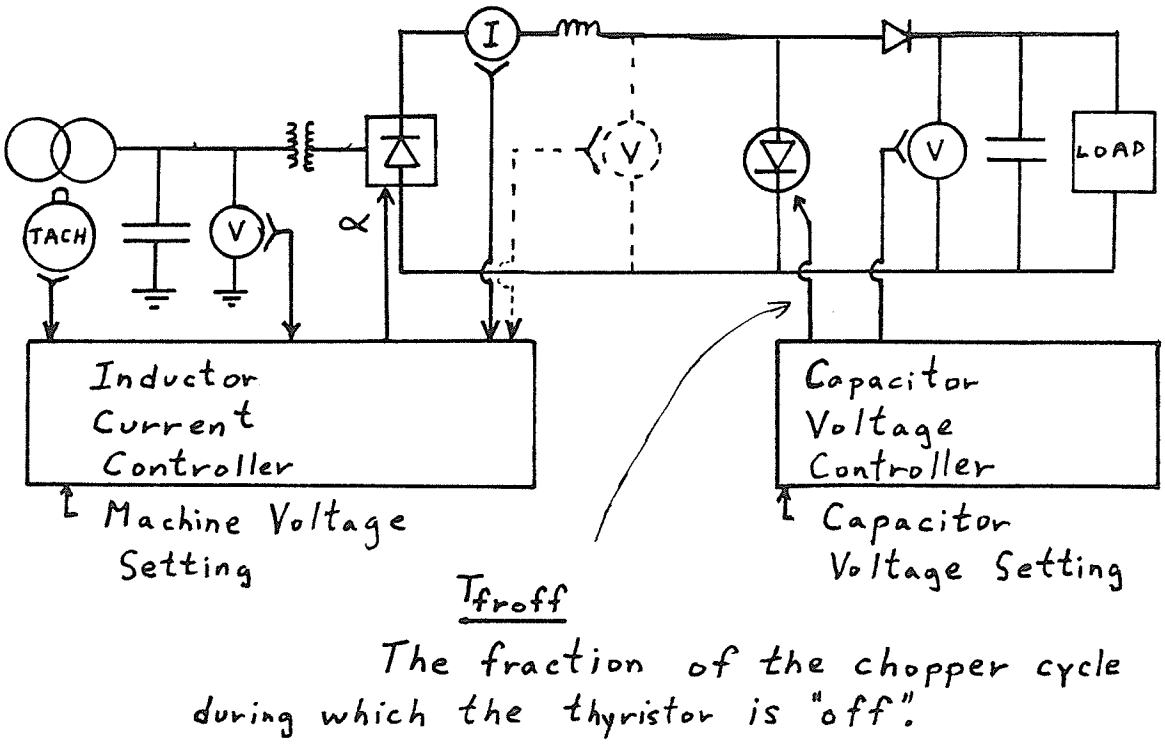

Figure 41 Schematic of the Overall Control Layout

As was discussed previously, the chopper is intended to act as a variable matching circuit to match the output of the rectifier to the load. It will be necessary to provide a fast acting capacitor voltage controller if close control of smoothing capacitor voltage is desired. A preliminary sketch for such a controller is given in Figure 42.

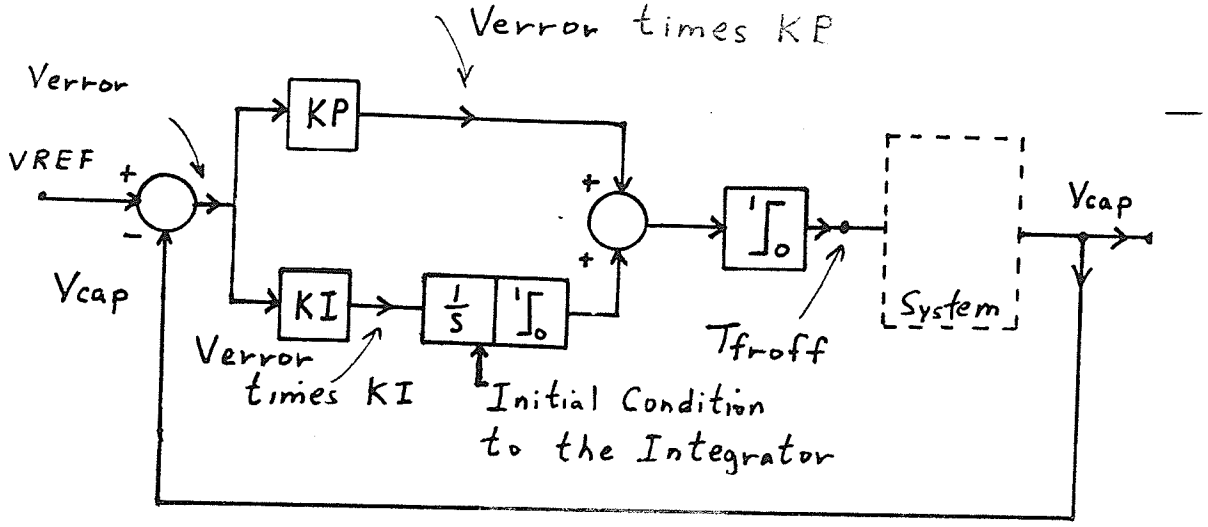

Figure 42 Schematic of the Proposed Voltage Controller

In response to a capacitor voltage signal, the controller should adjust the duty cycle of the chopper so that the appropriate fraction of I_d will be diverted into the smoothing capacitor in order to maintain the capacitor voltage at a set level. For instance, if the load goes up, T_{froff} will increase in response to falling capacitor voltage and more of the smoothing inductor current I_d will flow into the smoothing capacitor. The accompanying effect of increasing T_{froff} is that the average voltage V_{dRE} at the load end of the smoothing inductor will go up. On the other hand, if load on the inverter goes down, T_{froff} drops and V_{dRE} will be reduced. Thus, if rectifier delay angle is not adjusted from the steady operating angle, then an increase in load will tend to reduce I_d and a decrease in load will tend to increase I_d.

The above tendencies have been considered in respect of the converter

transformer current magnitudes illustrated in Figure 35 b) for low speed (0.9 p.u.) and high speed (1.8 p.u.) operation.

High speed operation is discussed first. At high speed V_g/F is low and XM is large as can be seen from a V_g/F versus XM curve. Large XM corresponds with very little saturation. With low saturation we expect relatively large changes in machine voltage to result from relatively small changes in converter real or reactive current. Figure 35 d) shows that the inductor current must drop when load increases during high speed operation. If the decrease does not occur, excitation may drop heavily due to the already unsaturated nature of the machine magnetizing reactance. It is thus beneficial that the capacitor voltage controller will tend to provide the decrease in I_d which the machine requires during a load increase. Figure 35 d) shows that the inductor current must increase when load decreases during high speed operation. If the increase does not occur, the machine may suffer over excitation. Therefore, it is also beneficial that the capacitor voltage controller will tend to provide the increase in I_d which the machine requires during a load decrease.

Consideration will now be directed toward slow operation. At slow speed, V_g/F is high and XM is considerably lower than during high speed operation. The machine will thus be considerably more saturated during low speed operation. As a result, the machine voltage will not be so sensitive to changes in available excitation current. This relative insensitivity is fortunate because the capacitor voltage controller will tend to change the inductor current magnitude contrary to the change which is actually required by the machine as illustrated in Figure 35 d). Thus, in the time before the rectifier control can respond, a load increase at low speed will cause a certain rise in machine voltage and a load decrease at low speed will cause a certain decrease in machine voltage.

The inductor current controller controlling the rectifier must be capable of responding to inappropriate changes to smoothing inductor current occurring during

load changes. At high speed the inappropriate changes will be of the right sign but perhaps of the wrong magnitude. On the other hand, at low speed the inappropriate changes will even have the wrong sign. These specific comments are based upon an interpretation of the characteristics of the example system including the machine of Appendix 2 and should therefore be taken as appropriate for systems similar to the example system.

Before moving on to the inductor current controller I will discuss a few aspects of the capacitor voltage controller. In Figure 42 T_{froff} is limited to between 0 and 1. A value of T_{froff} close to 0 or 1 could cause problems with the operation of the chopper switching device. For instance, if T_{froff} is close to zero that means that the chopper thyristor is only meant to turn off for a very short time. In practise, it takes about 60 μsec to turn a gate turn off (GTO) thyristor off and then turn it back on. Thus, if a chopper operates at 1000 Hz, it is impractical to call for $T_{froff} < 0.06$. Thus, in Figure 42, logic needs to be incorporated in the chopper firing circuit so that if the controller calls for $T_{froff} < 0.06$ then the chopper thyristor will remain "on" for the complete chopper period. This will temporarily stop current from reaching the smoothing capacitor from the chopper and V_{cap} will begin to fall. However, the fall of voltage V_{cap} will be gradual because, at small T_{froff} the inverter load current must be quite small. After a few chopper cycles the voltage on the capacitor will sink to a level which will cause T_{froff} to rise above 0.06 and short periodic pulses of current will again flow to the capacitor from the chopper. Using this scheme the chopper could be expected to regularly skip sending periodic pulses of current to the smoothing capacitor during light load operation. Also, no such periodic pulses would be delivered if the inverter load was steady at zero.

A similar strategy can be adopted when T_{froff} is called for which is greater than 0.94. In that case, the chopper thyristor should be left "off" all the time until the controller calls for a T_{froff} less than 0.94. However, the requirement to operate

with $T_{froff} > 0.94$ can be avoided by recalling that $T_{froff} = \frac{V_d}{V_{cap}}$ and then by picking V_{cap} sufficiently large to avoid $T_{froff} > 0.94$.

The inductor current controller is intended to stabilize I_d and to provide for variation in I_d to control machine voltage.

The stabilization of I_d is required because of the rapid variation of voltage V_{dRE} at the load end of the inductor brought about by the operation of the capacitor voltage controller. For instance, a step increase in inverter electrical load at a given value of I_d will cause a rapid increase in the average voltage V_{dRE} at the load end of the smoothing inductor. In that case I_d will fall unless rectifier output voltage V_d is made to track the increase in V_{dRE} with some precision. The variation in V_{dRE} can be made available to the inductor current controller in two ways. V_{dRE} could be measured directly with a voltage transducer. As a alternative, V_{dRE} could be observed indirectly by measuring the rate of change of inductor current which a change in V_{dRE} will tend to produce. The latter scheme could allow operation without ancillary communication between the rectifier and load end of the inductance. Such operation would be beneficial for schemes in which a transmission forms part of the inductance. However, observing the rate of change of I_d to determine V_{dRE} introduces an inherent time delay. Direct observation has the advantage of providing a signal for V_{dRE} more quickly. Furthermore, the capacitor voltage controller can be made to give advance notice to the inductor current controller of an upcoming change in V_{dRE}. For instance, if the capacitor voltage controller makes some increase ΔT_{froff} to T_{froff} for the upcoming chopper cycle then the capacitor voltage controller can predict that V_{dRE} will increase by $\Delta T_{froff} \times V_{cap}$ in that chopper cycle. The availability of V_{dRE} allows the inductor current controller to adjust $V_d(ordered)$ so as to bring about a quick approximate stabilization of I_d. It is useful to note that there will always be some error in the measured value for V_{dRE}.

The inductor current controller must be able to accept this slightly erroneous signal for V_{dRE} and complete the formulation of a V_d order.

In formulating a V_d order the inductor current controller must fulfill two functions. It must be able to accomplish a fast gross adjustment to the V_d order based upon a slightly erroneous estimate of V_{dRE}. Secondly, the inductor current controller must be able to provide feedback control of the machine voltage while compensating for errors in measuring V_{dRE} and errors in implementing the V_d order.

Figure 43 illustrates a preliminary schematic which can serve as a starting point in the future design of a functional inductor current controller. V_{dRE} is the dominant component of the V_d (*ordered*) illustrated in in Figure 43. Additional signals must be added to V_{dRE} to cause I_d to increase or decrease in order to keep the machine voltage at the set level. The control circuit path through blocks "-1", "K_4", and "L" is intended to convert a machine voltage error signal into a proportional signal to be added to V_{dRE} in producing V_d (*ordered*). This proportional signal is intended to provided a certain level of $\frac{di}{dt}$ for a given machine voltage error. The integral path through block "K_5" is intended to compensate for error in reading V_{dRE} and error in responding to V_d (*ordered*). The control path through blocks "filtered differentiator" and "K_3" is intended to adjust the voltage error signal depending on whether the machine voltage is approaching or departing from the desired machine voltage. Finally, The block containing the equation:

$$\alpha = \cos^{-1}\left(\frac{V_d\ (ordered) + R_c\ I_d}{V_{do}}\right) \tag{3.49}$$

produces the final α order to the rectifier. The α order would normally be limited to the range between approximately 5° and 90° .

The inductor current controller must respond to changes in machine speed. For instance, increasing machine speed will cause the machine voltage to start to climb unless corrective control occurs. In the preliminary inductor current controller, an

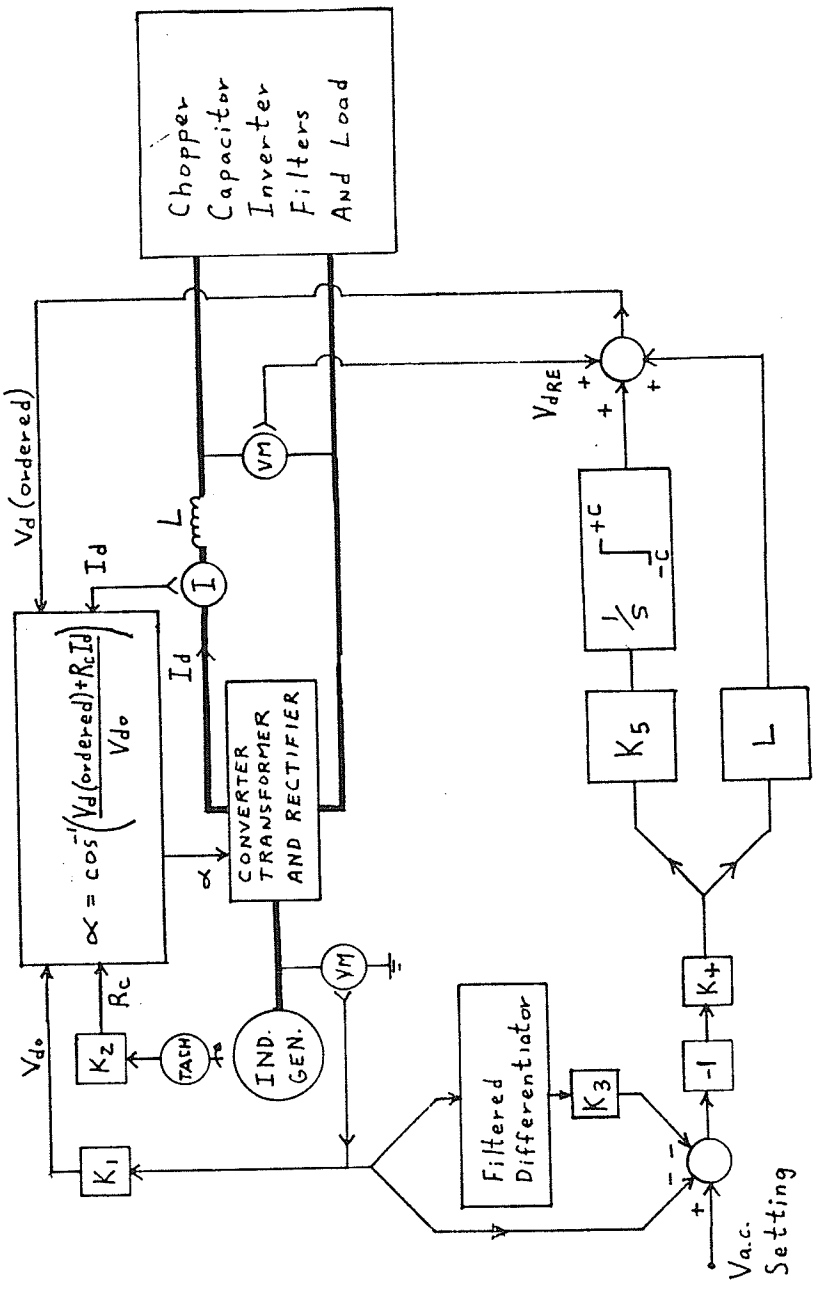

Figure 43 Preliminary Schematic for the Proposed Inductor Current Controller

increasing machine voltage would be sensed and V_d (*ordered*) would be increased for a time until the machine voltage began to settle toward a proper value.

The actual dynamics of the proposed control system cannot be thoroughly checked without a complete simulation of the system including controls, machine, rectifier, chopper, inverter, and load. The complete simulation and optimization of a system is left for future work. However, preliminary work toward developing a chopper and inverter model is presented in chapter 4. The remaining components are presently available in the developed subroutine library of Manitoba Hydro's electromagnetics transients simulation program known as EMTDC.

3.8.3 ALTERNATIVE 2 - THE DUAL ARRANGEMENT OF SERIES CAPACITOR COMMUTATED GRAETZ BRIDGE INVERTERS

3.8.3.1 GENERAL DESCRIPTION

This arrangement is put forward as an alternative to the chopper inverter apparatus discussed above. A schematic for the dual arrangement of series capacitor commutated Graetz bridge inverters is illustrated in Figure 44. The particular utility of the dual arrangement in this system arises due to the variability of the ratio of I_{LOAD} to I_d in Figure 44. However, in order to facilitate a broad range of possible I_d, it is necessary to provide thyristors and series capacitors with increased voltage ratings. The operation of the circuit has been discussed by others [36,38] and the discussion herein will be limited to an examination of the above points.

The variability of the ratio of I_{LOAD} to I_d arises out of the practise of firing the two Graetz bridge inverters with different delay angles with respect to the load voltage. Figure 45 illustrates a phasor diagram of phase voltage and currents and also includes the delay angle α_1 and α_2 for the two Graetz bridge inverters. In Figure 45, I_{LOAD} represents phase current into the load. The other currents in the figure all refer to currents into the load side of the converter transformers. The converter

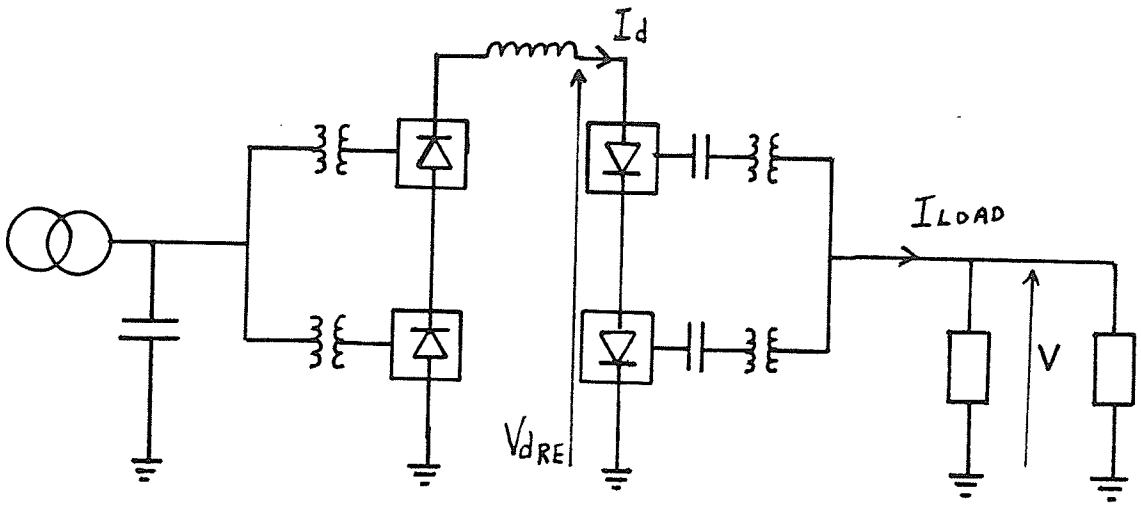

Figure 44 Alternate System Including a Dual Arrangement of Series Capacitor Commutated Graetz Bridge Inverters

currents are related to I_d by the equation:

$$| I_{CONV1} | = | I_{CONV2} | = \frac{\sqrt{6}}{\pi} I_d \ . \tag{3.50}$$

Therefore, for constant I_d, increases in $| I_{LOAD}' |$ can be accommodated by adjusting α_1 and α_2 so as to decrease β in Figure 45. Furthermore, if the angle of I_{LOAD} becomes more lagging then α_1 and α_2 can be increased to handle the change. On the other hand, if it is necessary to increase I_d, then β in Figure 45 can be increased to maintain I_{LOAD}' as a constant. Given $| I_{CONV1} |$, $| I_{CONV2} |$, and the load p.f. angle ϕ, it is possible to determine the first and second inverter firing delay angles with respect to the load voltage to be as follows:

$$\alpha_1 = 180 - \phi - \beta \tag{3.51}$$

and

$$\alpha_2 = 180 - \phi + \beta \tag{3.52}$$

wherein:

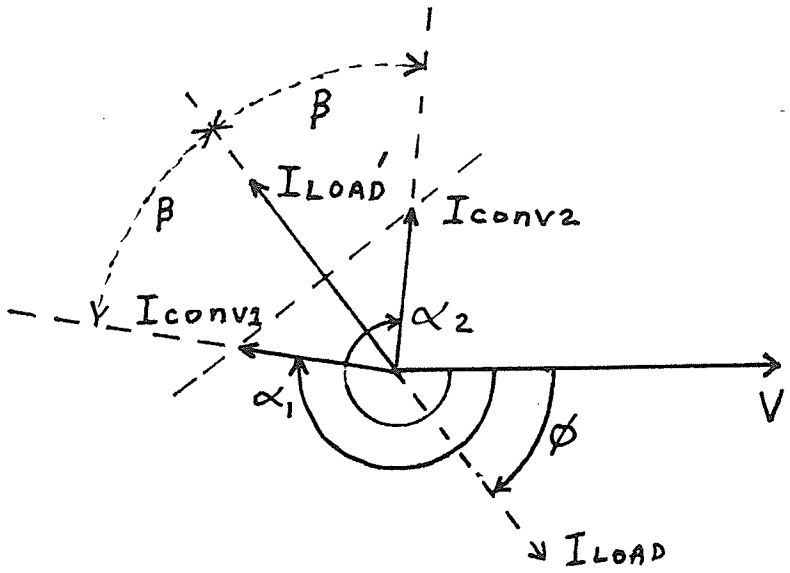

Figure 45 Phasor Diagram Including Delay Angles for the Inverter for the Inverter in the Alternate System

ϕ represents the magnitude of the angle by which current into the load lags the load phase voltage

and β is given by the equation:

$$\beta = + \left| \cos^{-1} \left(\frac{| I_{LOAD} | /2}{| I_{CONV1} |} \right) \right| . \tag{3.53}$$

The above analysis ignores the effect of commutation angle and therefore represents only a first approximation of actual delay angles.

We can relate power into the inverter to the power into the a.c. load by the simplifying assumption of lossless converters. The resulting equation is as follows:

$$I_d \; V_{dRE} = 3VI_{LOAD} \cos \phi \tag{3.54}$$

Continuous adjustment of α_1 and α_2 in the dual inverters maintains V at a desired magnitude as has been described in the literature [37]. For constant V, $I_{LOAD} \cos \phi$ is recognizable as being proportional to load power. Therefore V_{dRE} is also propor-

tional to load power for a given value of I_d. The V_{dRE} produced at the input to the chopper inverter apparatus is also proportional to power for a given I_d. Therefore a controller operating to regulate the a.c. load voltage in a series capacitor dual inverter arrangement would have the same effect on V_{dRE} as a controller operating to regulate voltage on the smoothing capacitor in the chopper inverter apparatus.

3.8.3.2 VOLTAGE RATINGS OF THYRISTORS AND SERIES CAPACITORS

The fixed size of the capacitors in a normal series capacitor commutated Graetz bridge inverter presents a limitation tending against operation at variable values of d.c. current. Figure 46

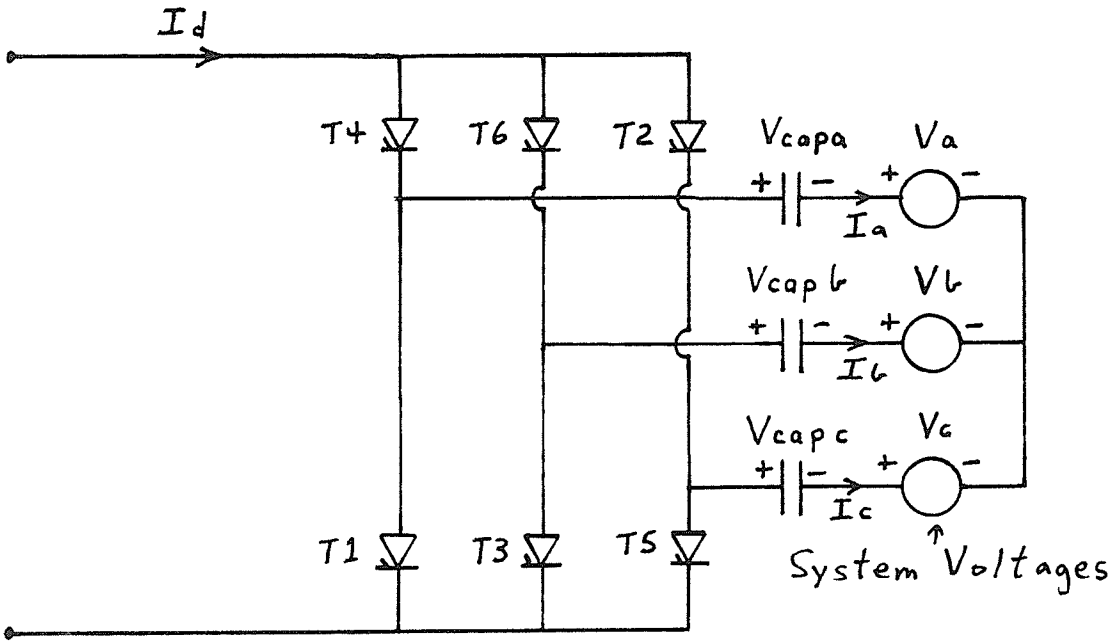

Figure 46 A Schematic for a Series Capacitor Commutated Graetz Bridge Inverter

illustrates a schematic of a series capacitor commutated Graetz bridge inverter. Figure 47 illustrates the waveform of current in phase "a". The dotted line represents the current waveform assuming zero commutation angle and the solid line represents the fundamental frequency current components for phase "a". Commutation of phase

"a" current occurs at 60° based on the reference angle for phase "a" current of 0° at t = 0 illustrated in Figure 47. A phasor diagram of currents and

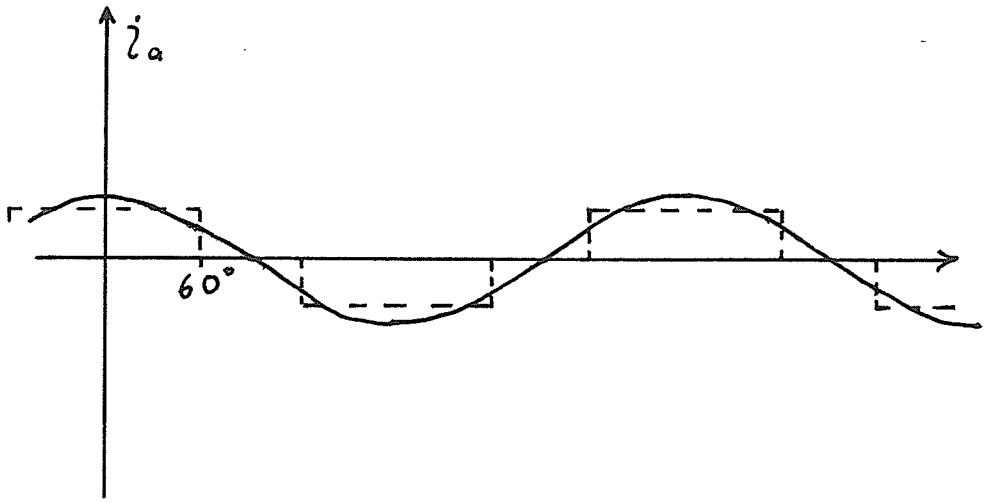

Figure 47 Reference Angle for Phase A Current in Figures 48, 49, and 50

capacitor voltages at the time of commutation is illustrated in Figure 48. All currents and voltages in Figure 48 are based upon the reference angle used in Figure 47. At that commutation T4 must cease to conduct in favour of T6 (see Figure 46). In order for the commutation to take place $V_{ab}\ (effective)$ must be positive at the time of commutation. $V_{ab}\ (effective)$ is defined as $V_{ab}\ (cap)$ plus $V_{ab}\ (system)$ and thus represents the appropriate line to line voltage phasor on the valve side of the series capacitors. $V_{ab}\ (cap)$ is illustrated in Figure 48. $V_{ab}\ (system)$ is developed in Figures 49 and 50. Figure 49 illustrates system voltages for supplying a load with a power factor angle of 45° lagging. A power factor angle of 45° lagging corresponds to an inverter delay angle of 225°. Figure 50 illustrates line to line system voltages with reference to the inverter delay angle. Figure 51 illustrates $V_{ab}\ (effective)$ as made up of $V_{ab}\ (system)$ plus $V_{ab}\ (cap)$ at the instant of firing of T6. From Figure 51 it is observed the $|\ V_{ab}\ (cap)\ |$ must be larger than some minimum value in order that $V_{ab}\ (effective)$ should be positive and thus cause the commutation. That minimum value depends upon $|\ V_{ab}\ (system)\ |$ and the extent

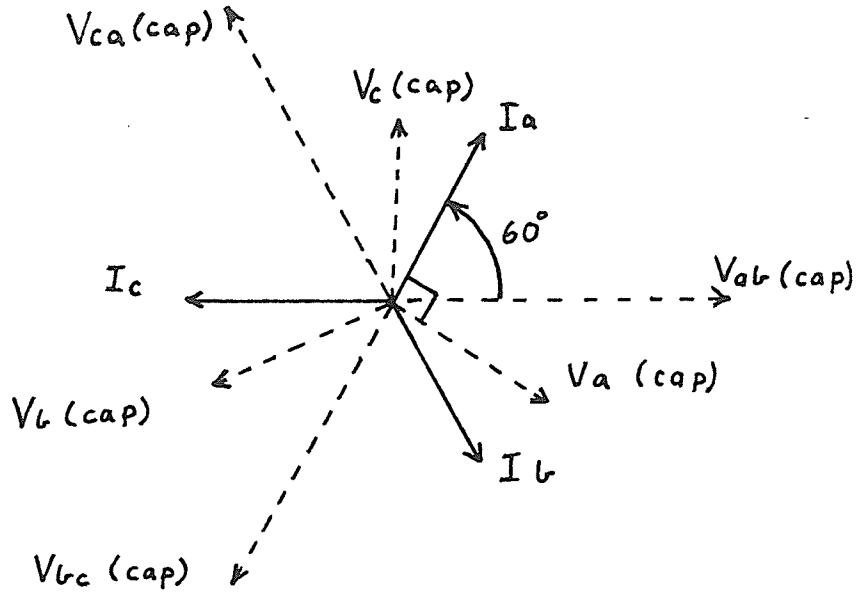

Figure 48 A Phasor Diagram of Capacitor Currents and Voltages at Commutation of Phase A in the Series Capacitor Commutated Inverter

to which α is allowed to be greater than 180°. However, a minimum value of $|V_{ab}(cap)|$ can be determined for a given $|V_{ab}(system)|$ and a particular maximum value of α. Each series capacitor must be of sufficiently small capacitance to generate $1/\sqrt{3}$ times the minimum value of $V_{ab}(cap)$ when I_d is at it's minimum level. Once the size of the capacitor is determined for minimum I_d then any subsequent increase in I_d will cause a proportional increase in $|V_{ab}(cap)|$. The increase in $|V_{ab}(cap)|$ in turn causes $V_{ab}(effective)$ to increase. That increase implies higher valve stresses. We will therefore conclude that the price for facilitating variable d.c. current operation is paid in providing valves and capacitors which have higher voltage ratings.

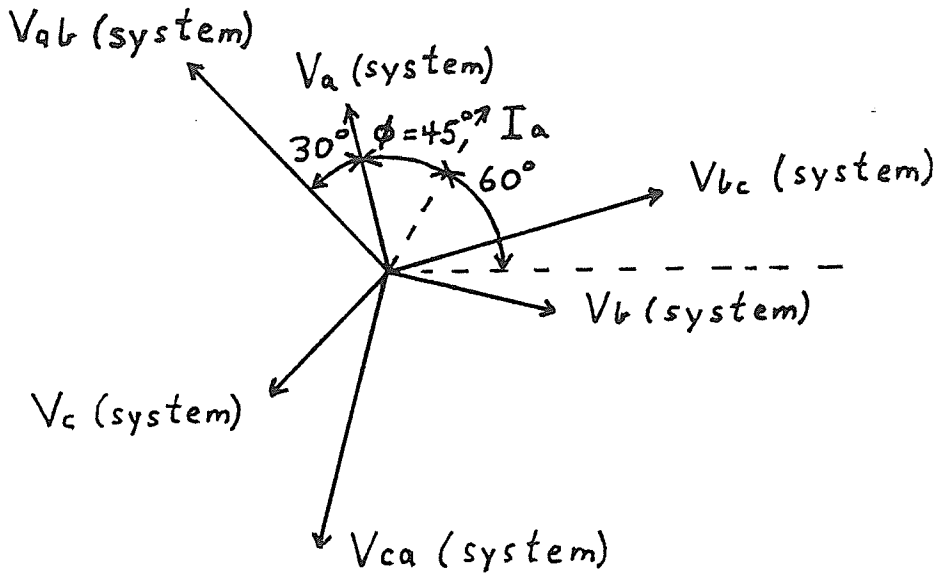

Figure 49 System Voltages in Figure 46 Required to Supply 45° Lagging Load

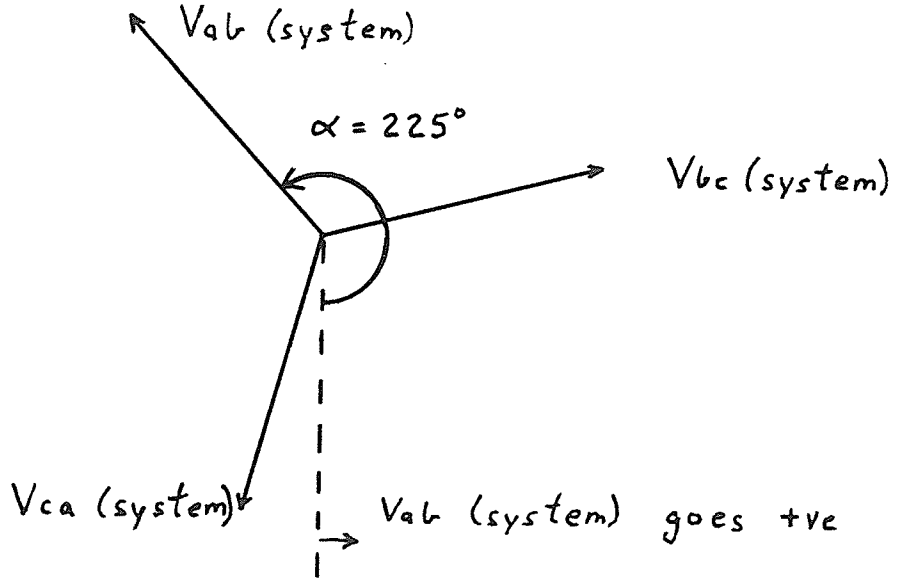

Figure 50 Relation of L-L System Voltages to α at the "Off" Commutation pf "A" Phase

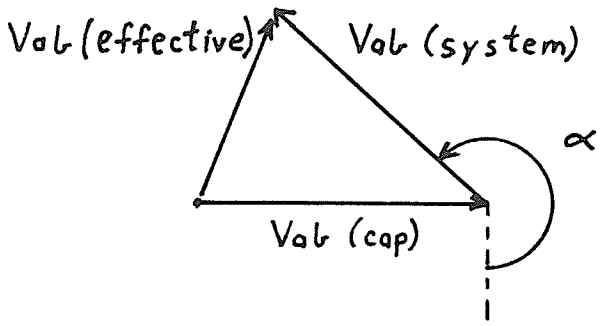

Figure 51 The Relation of V_{ab}(effective) to α, V_{ab}(cap), and V_{ab}(system) at the Time of the "Off" Commutation of "A" Phase

CHAPTER 4

PRELIMINARY INVESTIGATIONS INTO TRANSIENT OPERATION AND CONTROL OF THE RECTIFYING AND INVERTING APPARATUS

4.1 INTRODUCTION

In this chapter the results of three ancillary investigations are presented.

The first investigation relates to a transients simulation of the chopper and inverter apparatus of chapter 3 supplying a load through filters. The simulation which was conducted demonstrates some basic points in the operation of such a circuit. The subroutine CHPINV created for the transients simulation is listed in App. 7 of [43] and the approach to creating the subroutine is explained.

The second investigation relates to a transients simulation of a simplified system including an inductor current controller and a capacitor voltage controller. The controllers are based on the principles described in section 3.8.2.4.

The third investigation relates to a transient simulation of a self-excited induction generator undergoing a change in load while operating in a basically unsaturated mode.

4.2 A TRANSIENT SIMULATION OF A CHOPPER INVERTER APPARATUS SUPPLYING A LOAD THROUGH FILTERS

As mentioned above, the first investigation to be related in this chapter is concerned with the simulation of the chopper inverter apparatus of Figures 37 and 38.

The approach to creating an EMTDC simulation subroutine for the chopper inverter apparatus is presented first and is followed by a brief discussion of the results of the simulation.

The central block in Figure 52 illustrates the connection of the chopper inverter apparatus to the rectifier and load.

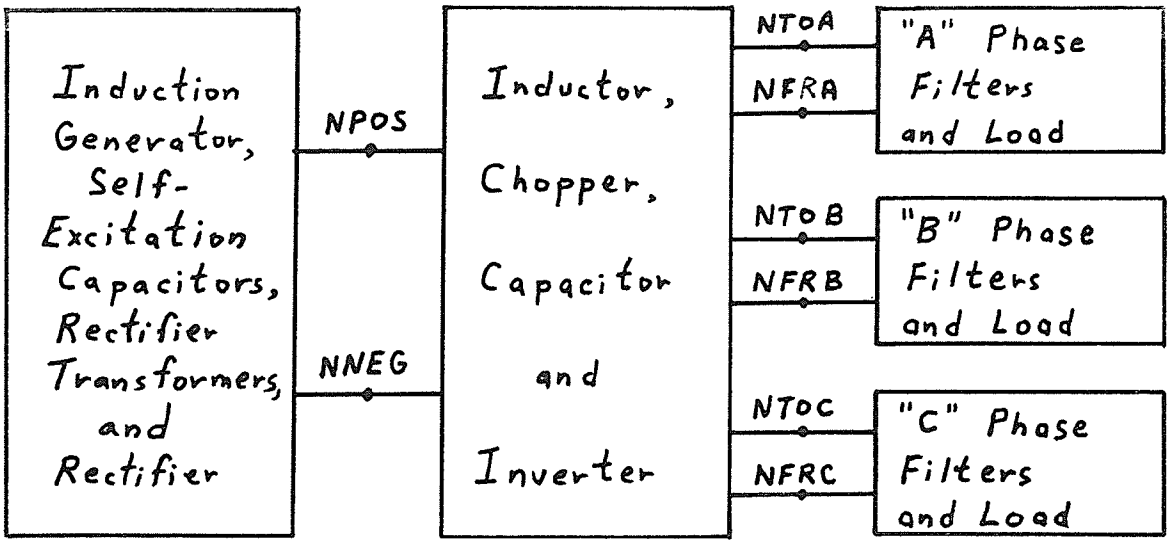

Figure 52 Block Diagram Showing the Connection of the Subroutine CHPINV with the Rest of the System

Figure 53 is presented to illustrate the method of interfacing [41,42] the simulation subroutine CHPINV with the EMTDC node pairs which represent the connections to the rectifier and each load phase. At the beginning of a time step CHPINV reads the voltage V_d at the output of the rectifier between EMTDC nodes NPOS and NNEG. Likewise, the EMTDC branch currents flowing into each phase of the load are measured. The measured magnitudes are used as source quantities at the beginning of a time step in the model of the chopper inverter. The chopper inverter model has two state variables IL and VC and their magnitudes are known at the beginning

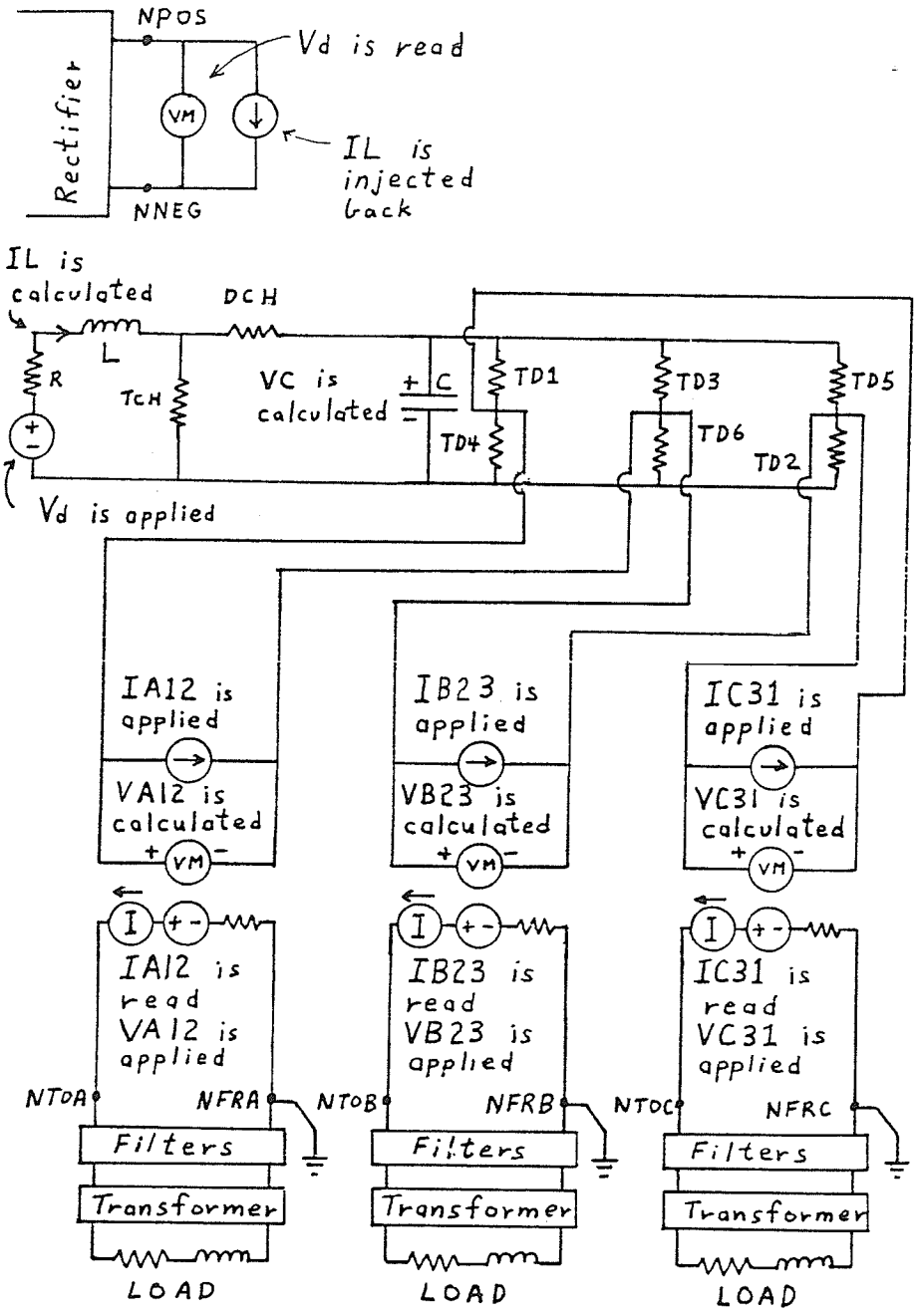

Figure 53 Schematic for the Circuit Modelled in the Subroutine CHPINV

of each time step. TCH, DCH, TD1, TD2, TD3, TD4, TD5, and TD6 denote resistances used to represent thyristors and diodes in the model. Logic is used to switch the resistances between high and low ohmic values to represent blocking or conducting states. Given the above information the state at the end of the time step is determined by the predictor corrector approach. The new value of IL is injected into the EMTDC rectifier output nodes at the beginning of the next time step. Likewise, given the new value of VC, the model calculates VA12, VB23, VC31 referenced in Figure 53 and those values are applied in the next time step as source voltages between EMTDC nodes leading to the individual phases.

The logic used to change the device representing resistances in the CHPINV subroutine is primarily the logic of operation for diodes, thyristors, and diode thyristor anti-parallel pairs. For instance, a resistance representing a diode goes to a low value when the diode is forward biased. Some additional logic was added to make the simulation stable. For instance, if IL is positive and the chopper diode DCH is blocked and the chopper thyristor TCH is conducting then when the chopper thyristor is to be turned "off" it is necessary to turn "on" the chopper diode at the same instant. It is not practical to wait for the diode logic to turn the diode "on" because there will be a one time step delay before the diode can be turned "on" after it is forward biased. During that time step there will be a prohibitively large voltage spike which will disrupt the model. A similar approach was taken to switching of the thyristor diode pairs in the inverter.

The subroutine CHPINV is listed in App. 7 of [43] along with the DSDYN, DSOUT, and data files required for conducting an EMTDC simulation of the chopper inverter apparatus. The rectifier voltage V_d and the chopper duty cycle T_{froff} are maintained constant at 800 volts and 50 % respectively during the simulation. By setting V_d and T_{froff} to these values the model is essentially set running in close to a steady state without control.

Figure 54 illustrates the simulated capacitor voltage and smoothing inductor current. As expected the capacitor voltage oscillated around a value equal to twice the rectifier voltage. It is anticipated that the capacitor voltage could have been closely controlled if a capacitor voltage controller had been controlling chopper duty cycle. The initial inductor current was picked to provide sufficient current to the capacitor to match the current to the inverter with one p.u. voltage applied to a given a.c. load. However, the series filters caused a fundamental frequency voltage drop and thus the a.c. load voltage and current were reduced. The reduced a.c. current corresponds with the reducing I_d which can be noted in Figure 54.

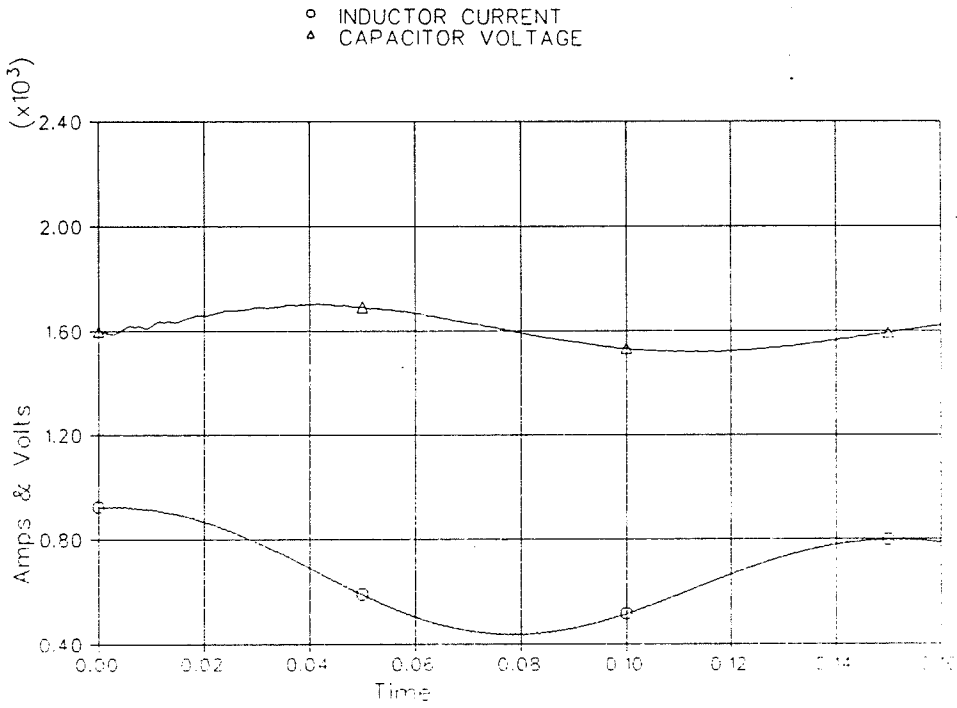

Figure 54 Inductor Current and Capacitor Voltage of the Free Running Chopper Inverter with Fixed V_d and T_{froff}

Figure 55 illustrates three voltage waveforms associated with one phase of the inverter in Figure 53. The rectangular voltage waveform corresponds with the waveform VC31 in Figure 53 and represents the voltage output of the inverter before filtering. The voltage waveform which is of the same approximate magnitude as the

rectangular waveform, is the voltage waveform after the series 5th, 7th, 11th, and 13th harmonic voltage blocking filters but before the transformer. The lower voltage waveform is the load voltage waveform on the low voltage side of the transformer. One can note the dramatic improvement in the voltage waveform due to the effect of filtering. However, the filters have not been optimized with respect to cost or effectiveness.

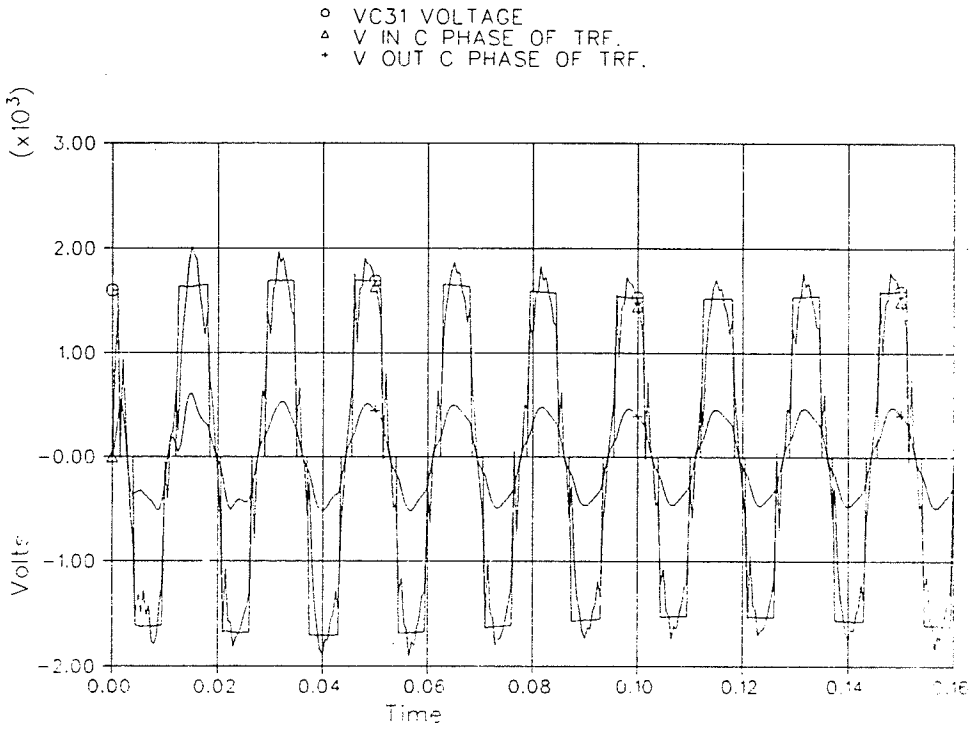

Figure 55 Output Voltages of One Phase of the Inverter

Figure 56 illustrates two current waveforms associated with the inverter of Figure 53. The waveform labelled IC31 is the current in one phase of the inverter output. The current waveform clearly contains a considerable level of harmonic current. A large part of that harmonic current is due to a high pass shunt filter composed of a capacitance to ground on the load side of the transformer leakage impedance. Shunt filters are not a good choice for reducing harmonic voltages because the harmonic currents drawn by those filters are generally excessive. For instance, the 5th harmonic current would be of approximately 0.4 p.u. magnitude for a 20 % 5th

harmonic voltage content with a 10 % transformer impedance. High harmonic currents in the phase currents will translate into increased ripple in the current from the capacitor to the inverter. The second signal in Figure 56 illustrates the current from the capacitor bank to the inverter and some high frequency current harmonics appear to be present.

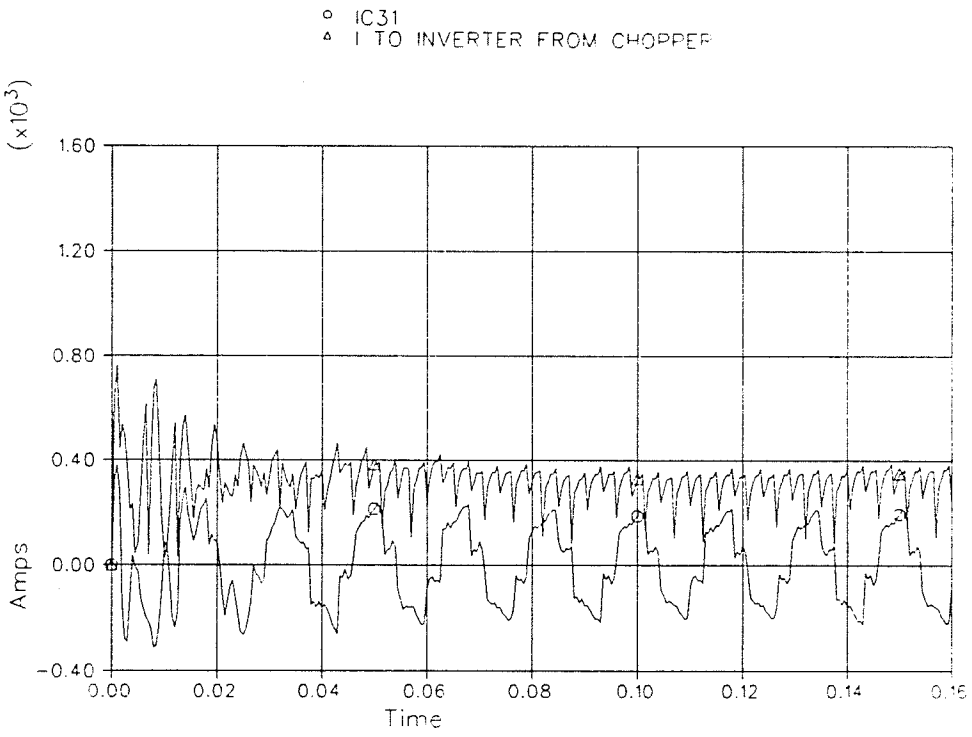

Figure 56 Output Current of One Phase of the Inverter and Current to the Inverter from the Capacitor

It can be noted that the d.c. component of the current to the inverter from the capacitor illustrated in Figure 56 is approximately ½ of the d.c. component of the inductor current illustrated in Figure 54. It was noted earlier that the capacitor voltage was approximately twice the voltage at the input to the smoothing inductor. This confirms that the chopper inverter does indeed operate as a matching circuit is expected to for $T_{froff} = 0.5$.

By way of a summary there are a number of points which should be made.

Stability of the subroutine CHPINV has been provided by logic which initiates

switchings one time step before device logic could provide the switching. This remedy is applied because of the large changes in device representing resistance which occur in one time step.

Consideration was given to representing the chopper inverter model using EMTDC branches and relying on device logic alone to initiate resistance changes using EMTDC subroutine PRLL2. The benefit would arise in avoiding interfacing the subroutine CHPINV to the main EMTDC program and in avoiding the time delays associated with normal interfacing techniques. However, the approach would require a gradual change in resistance over many time steps in a switching period in order to avoid voltage spikes and disruption of the model. Unfortunately this would seem to imply a very short time step and thus a very much increased execution time. For instance, if a switching period is to be 50 μS long then it might be desireable to increase resistance by a factor of 1.4125 on 20 occasions during the period so as to increase resistance by a factor of 1000 in 50 μS. This implies a time step of 2.5 μS. However, the prohibitive increase in execution time could be avoided if EMTDC had two available timesteps. A short time step could be used during switching and a long time step could be used during smooth running. In order to facilitate switching from one step length to another, the long time step could be made a multiple of the short time step. Including the above features into EMTDC would requre a complete re-structuring and re-writing of the program and so the approach was not taken.

Finally, it should be emphasized that shunt filters tend to draw large harmonic currents from the inverter given the rectangular voltage waveshape in Figure 55. It is suggested that use of series harmonic voltage blocking filters alleviates the problem.

4.3 A TRANSIENT SIMULATION OF THE OPERATION OF AN INDUCTOR CURRENT CONTROLLER AND A CAPACITOR VOLTAGE CONTROLLER

A control system similar to that described in section 3.8.2.4 has been simulated using the EMTDC simulation program. Figure 57 illustrates a block diagram of the

system. A full simulation of the induction machine supplying a rectifier has not been undertaken and thus there are a number of simplifications which are discussed in this section.

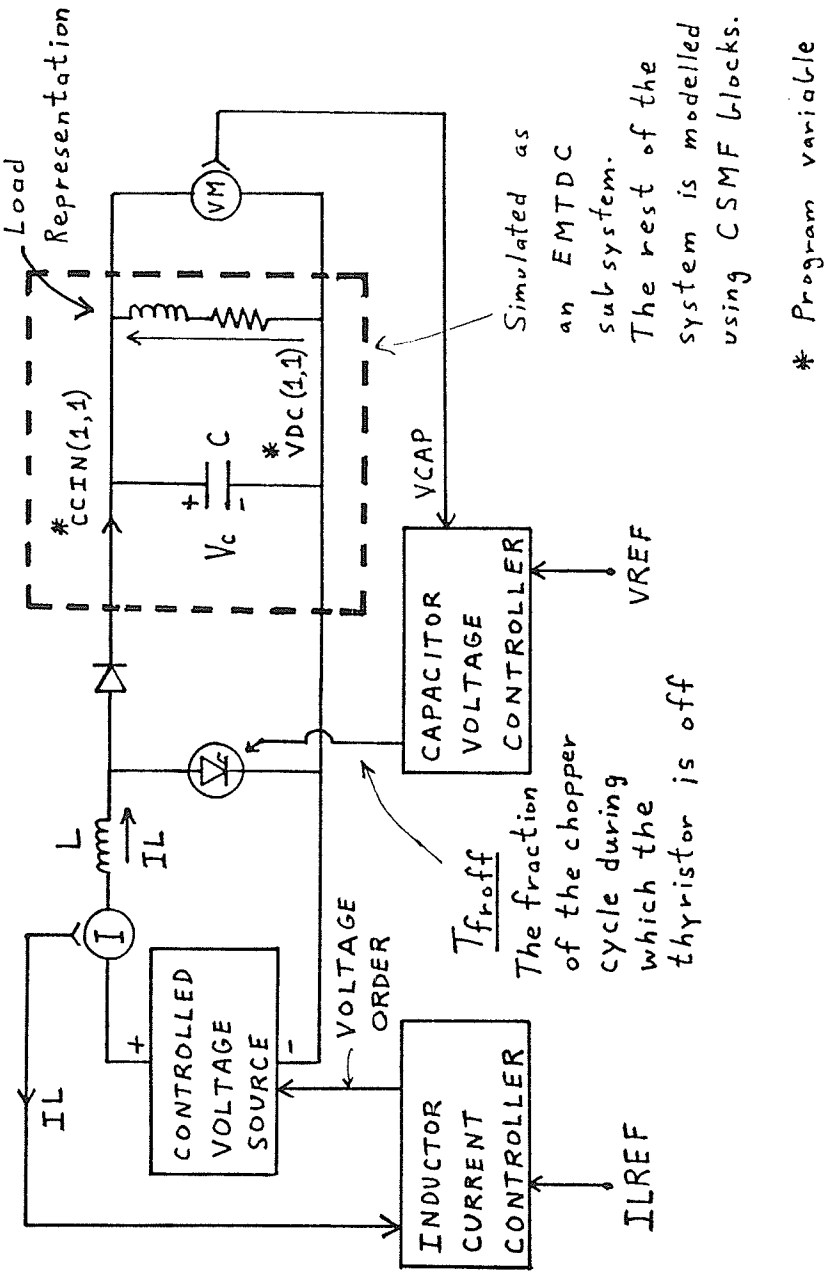

Figure 57 Circuit Simulated in Testing of the Basic Control Concept

The simulation replaces the machine and rectifier with a controlled voltage source. The controlled voltage source responds to a voltage order from the inductor

current controller only after passing through a 0.1 second first order time delay. The time delay is intended to make the response of the controlled voltage source more sluggish than for a real machine and rectifier. In a real system the rectifier output voltage can be expected to respond relatively swiftly to a change in voltage order by means of a swift change to the rectifier delay angle.

As illustrated in Figure 57, the inverter and load have been replaced by a series resistance and inductance. The load circuit has been given a time constant of 0.164 seconds.

The chopper circuit has been idealized as illustrated in Figure 58. This corresponds to a chopper in which the frequency of operation is very high to the point that the voltage at the load end of the inductor can be considered as d.c. and the current into the capacitor can be considered as continuous.

The capacitor voltage controller indicated in Figure 57 is illustrated in more detail in Figure 59. The controller responds to the capacitor voltage to adjust the chopper duty cycle. The controller is a proportional and integral type controller with capacitor voltage as feedback. However, the system introduces a variable gain due to the fact that the current into the capacitor depends upon not only the chopper duty cycle but also the inductor current. The dependance is illustrated in Figure 59.

The inductor current controller indicated in Figure 57 is illustrated in more detail in Figure 60. The controller responds to a current order by producing a voltage order for the rectifier. The capacitor voltage and the capacitor voltage controller affect the task of the inductor current controller because they determine the voltage at the load end of the inductor. The task of the inductor current controller is thus to produce the proper voltage at the source end of the inductor to control inductor current in spite of variation in the voltage at the load end of the inductor.

It is noted that in Figure 60 the voltage on the load end of the inductor is not measured directly. Instead, the inductor current controller is supplied only with a

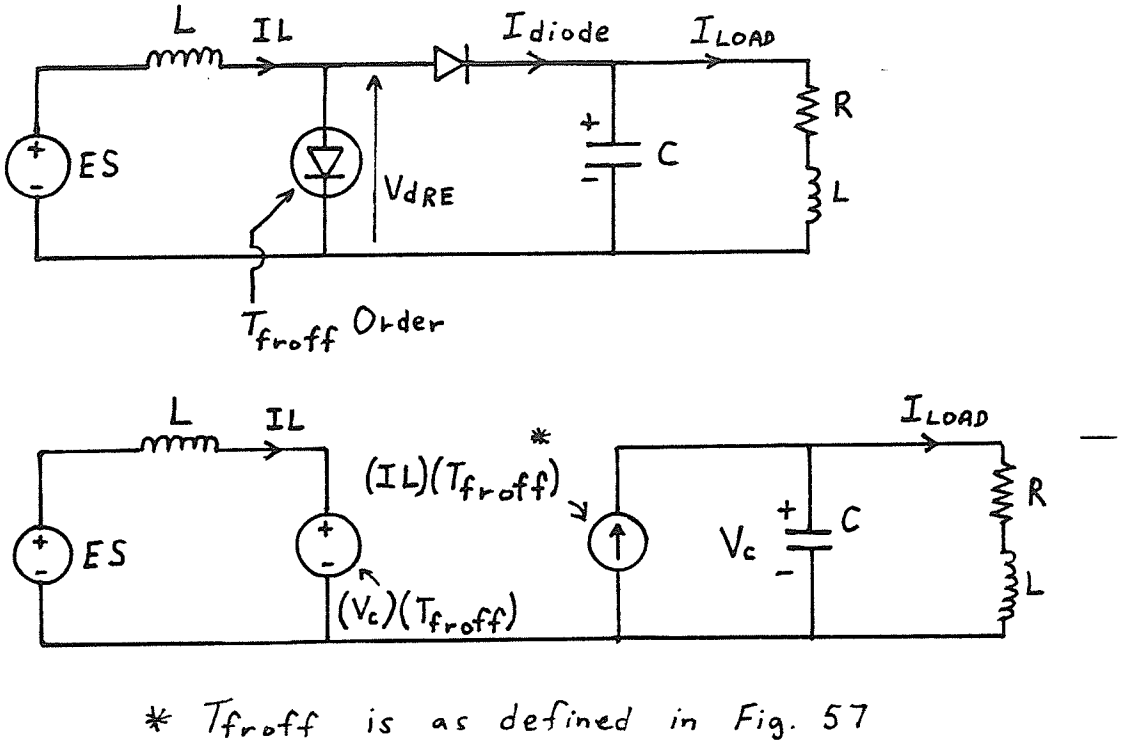

Figure 58 Simplification of the Chopper Circuit for Simulation Purposes

signal indicating current in the inductor. The controller uses the inductor current feedback signal to create a current error signal which is used in three ways. The error signal contributes to the voltage order through proportional and also integral control branches. The third use of the error signal is to create an order for the rate of change of inductor current which is proportional to the error in inductor current. A filtered differentiating device monitors actual inductor current and produces a signal indicating the actual rate of change of inductor current. The differentiating circuit in the simulation has a 0.1 second time constant. An error signal for the rate of change of inductor current is created from the difference between the ordered and actual values of the derivative of inductor current. The error signal for the rate of change of inductor current is then used to create a proportional signal which is

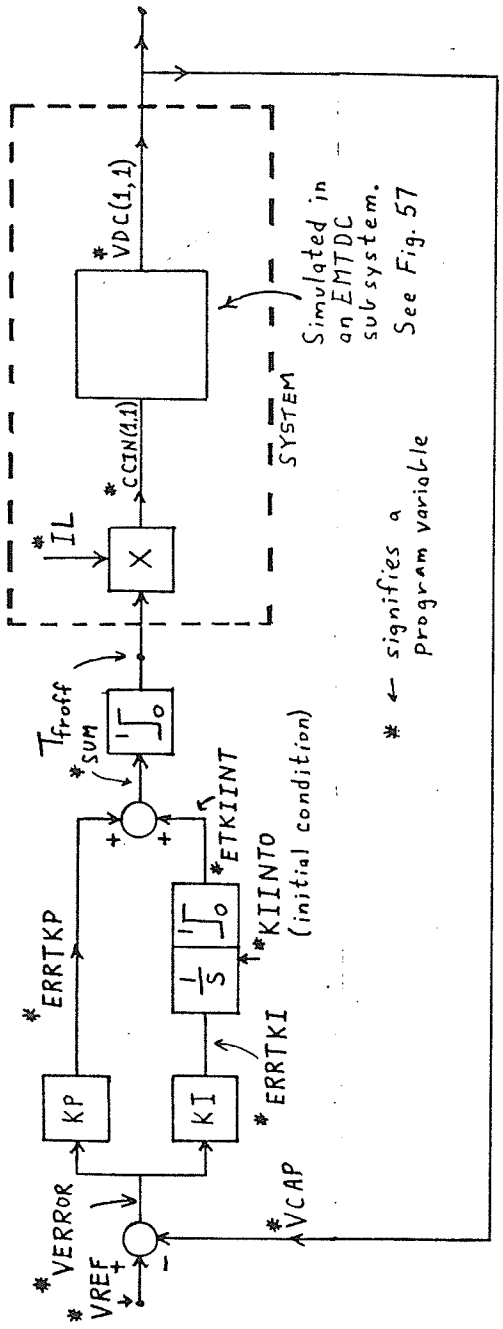

Figure 59 Schematic for Preliminary Capacitor Voltage Controller Used in Simulating Controls

added into the total rectifier voltage order. This addition to the voltage order helps the inductor current controller track rapid changes in the voltage at the load end of the inductor without directly reading that voltage.

Appendix 4 contains EMTDC data and dynamics files for conducting a simula-

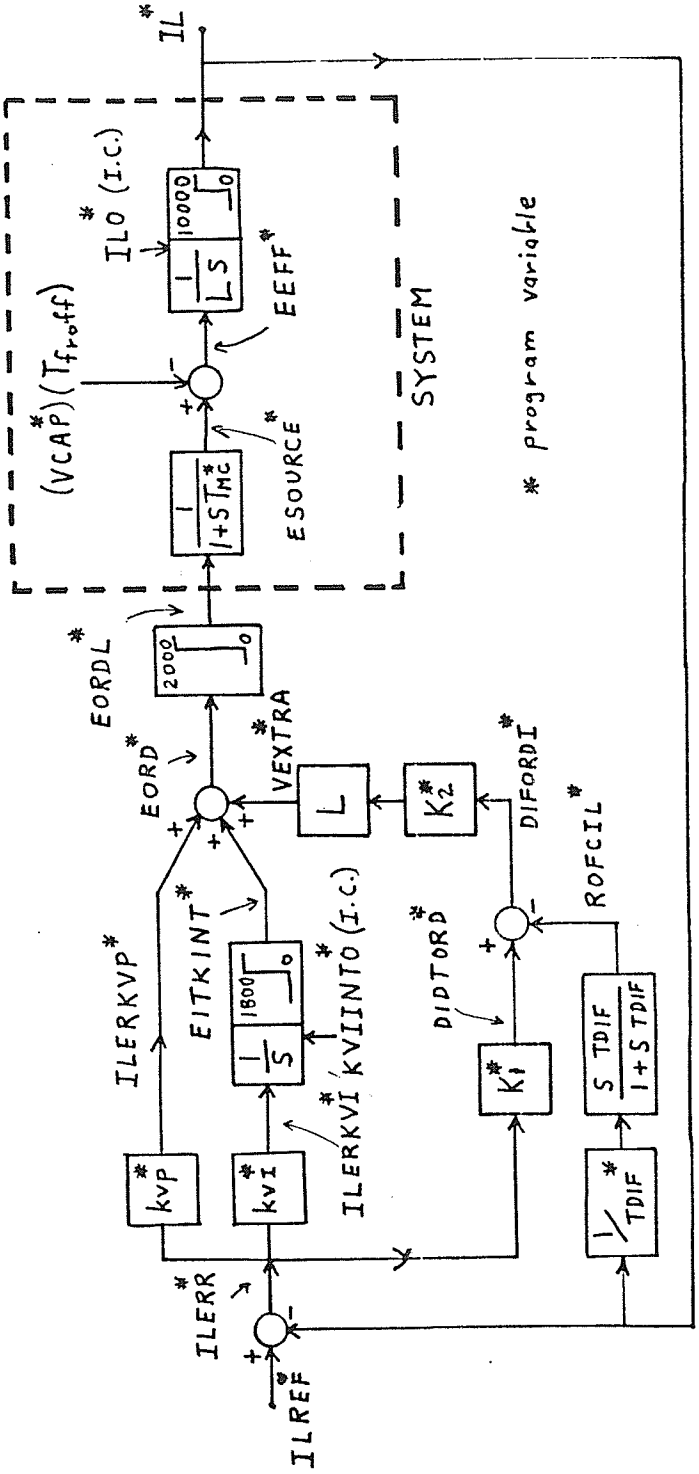

Figure 60 Schematic for Preliminary Inductor Current Controller Used in Simulating Controls

tion commencing with zero capacitor voltage and zero inductor current.

Figure 61 illustrates the rise of capacitor voltage to the reference level from zero. The effective current into the capacitor is also illustrated.

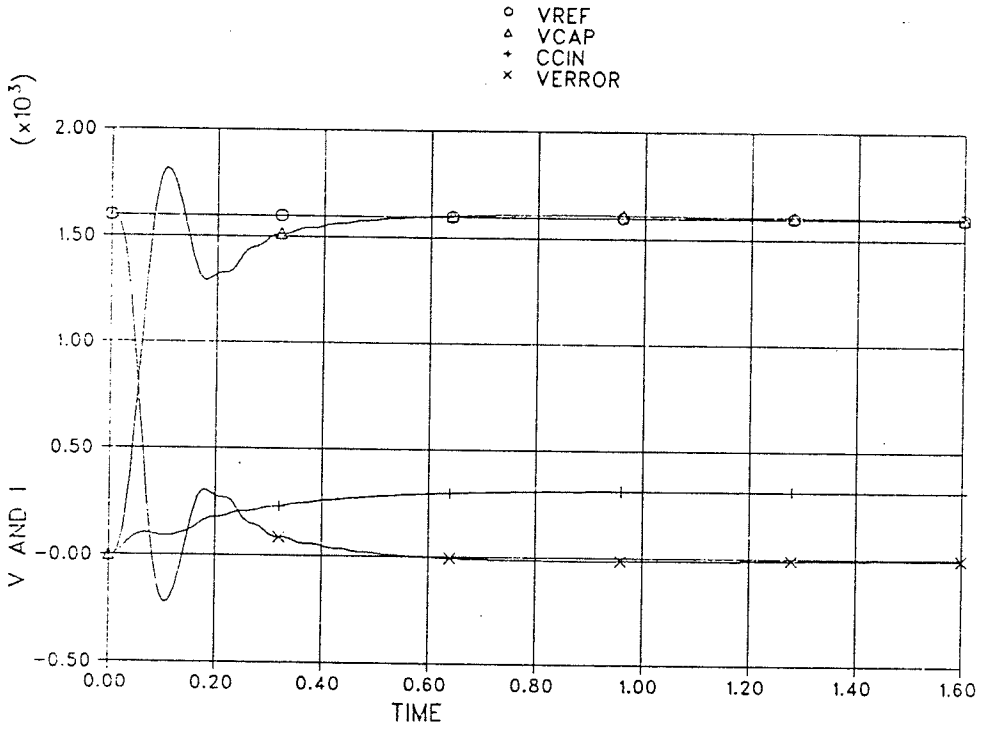

Figure 61 Capacitor Voltage and Current into the Capacitor During Start Up

Figure 62 illustrates the performance of the inductor current controller in attempting to make the controlled voltage source track the voltage at the load end of the inductor (*i.e.* V_{cap} T_{frof}) and at the same time to have the inductor current brought to the reference value. The frequency of the oscillations in the output of the controlled voltage source can be related to the time delays built into the model. When the time constants of the differentiating circuit and the controlled voltage source were reduced by a factor of 5 the frequency of the oscillations increased by a factor of 5. The oscillations represent the inability of the controls to cause the controlled voltage source to track the voltage at the load end of the inductor. It is concluded that tracking could be improved by obtaining an accurate and fast estimate of the actual voltage at the load end of the inductor and incorporating that signal into

the input quantities to the inductor current controller. Then, given a fast acting rectifier firing control, the rectifier output voltage would track the voltage at the load end of the inductor with more precision than that illustrated in Figure 62.

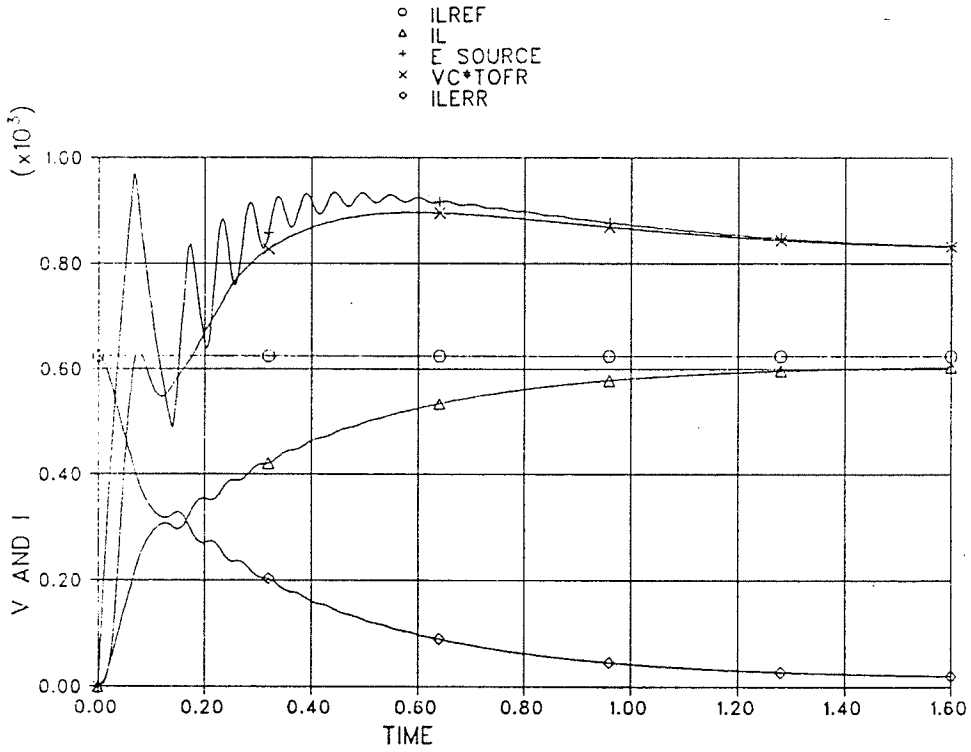

Figure 62 Start Up Response of an Inductor Current Controller Without Benefit of Direct V_{dRE} Input

The simulation is not sufficient for the purpose of finalizing control strategy because of the simplifications in the simulation which replace machine and rectifier dynamics with a first order time delay. However, as a preliminary investigation, the simulation is useful because it demonstrates that an inductor current controller can operate in parallel with a capacitor voltage controller. Furthermore, the inductor current controller used in the simulation was able to function even though it did not receive a direct signal as to the voltage at the load end of the inductor. In addition, the controls were able to respond to simultaneous orders for step increases from zero for inductor current and capacitor voltage. In a real system the task of the controls could be eased by ramping up inductor current and then capacitor voltage.

4.4 A TRANSIENT SIMULATION OF A LIGHTLY SATURATED INDUCTION MACHINE DURING A 50 % LOAD INCREASE

A premise for the discussion in section 4.3 is that a rapid change in rectifier output voltage can be accomplished by a rapid change in rectifier delay angle. The premise can only be true if the machine terminal voltage does not suffer a large immediate increase or decrease due to the transient change in rectifier delay angle.

This section will describe the simulation of a 0.5 p.u. load increase for the example system which includes the machine of Appendix 2. The load change occurs when the machine is running in steady state at 0.25 p.u. rated power and 1.8 p.u. machine speed which corresponds to a relatively unsaturated machine magnetic state. A single line diagram of the simulated circuit is illustrated in Figure 63. The EMTDC subroutine and data files used to produce the simulation are available in Appendix 5. Subroutine MIMSET17 was written to place the machine into steady state operation. The steady state rectifier load is represented by the resistance and inductance on the right in the figure. The single line diagram shows a 50 ohm resistance added in parallel to the iron loss resistance at time equals 0.08 seconds. In the simulation parallel resistances are not used but in fact the iron loss resistance is reduced by a factor of 47.4 by means of EMTDC subroutine PRLL2.

The load current existing after an instantaneous rectifier delay angle decrease is compared in Figure 64 to the load current existing after the addition of the resistive load used in the simulation. It is noted that the magnitude of the simulated currents into the impedance representation of the rectifier will be larger than the constant magnitude of the actual currents into the rectifier (i.e 145.1 amps) until the machine voltage drops to 145.1 / 159.1 of the initial machine voltage (i.e to 2134 volts). Figures 65, 66, and 67 illustrate that the quasi-sinusoidal voltage is not reduced to that level until about 0.2 seconds into the simulation or about 0.12 seconds after the load change. Thus, until about 0.2 seconds into the simulation, voltage is dropping more

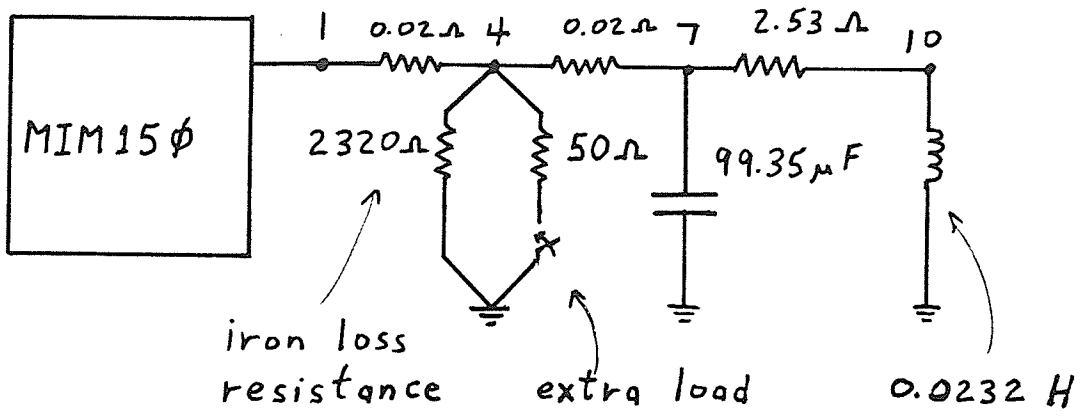

Figure 63 Circuit Simulated in EMTDC to Study the Transient Effect of a 50 % Load Increase on Machine Voltage

quickly than it would due to a comparable rectifier delay angle reduction. The figures therefore illustrate that loss of self-excitation through load suppression of the quasi-sinusoidal voltage is a comparatively slow phenomena.

Figures 65, 66, 67, and 68 also illustrate a short term system transient that occurs when the load power changes. As illustrated in Figures 66 and 67, the machine terminal voltage begins to reduce quickly upon application of the load increase. That effect can be attributed to the discharging of capacitors through the purely resistive additional load which occurs before the machine reacts. Figure 68 illustrates the reaction in the combined magnitude of the direct and quadrature axis machine currents. The reaction of the machine current is initiated by the momentary reduction in machine terminal voltage. The voltage dip simulated was of approximately a 10 % magnitude and lasted about 10 μS. However, even during the 10 % machine voltage dip, the rectifier voltage output could be expected to more than double due to the rectifier delay angle decrease. The voltage dip illustrated in Figure 67 would likely have been of smaller magnitude if the additional load had not been

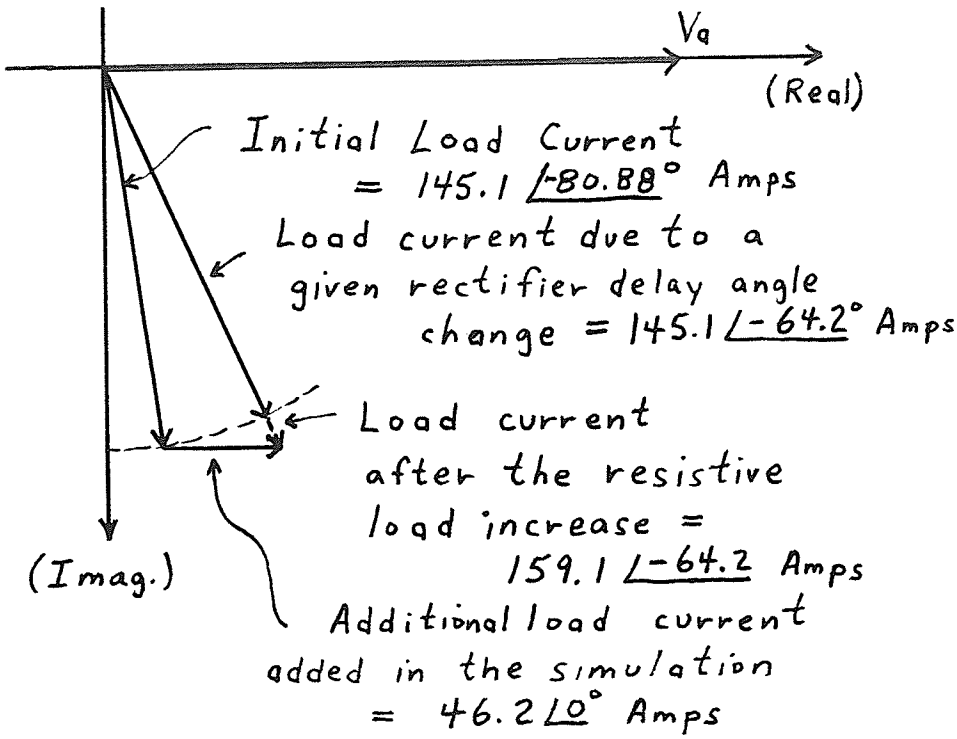

Figure 64 Currents into the Simulated Impedance Representation of the Rectifier Compared to Phase Shifted Constant Magnitude Rectifier Current

purely resistive. The purely resistive nature of the additional load caused load current to build up instantly.

In summary, two points can be noted. We can note that loss of self-excitation through load suppression of the quasi-sinusoidal voltage is a comparatively slow phenomenom. As the second point, we can also note that there will be a minor short term transient in the machine voltage brought on by significant load changes (in this case 0.5 p.u.). These short term voltage transients can be expected to be of only a slightly different character for a delay angle change on an actual rectifier.

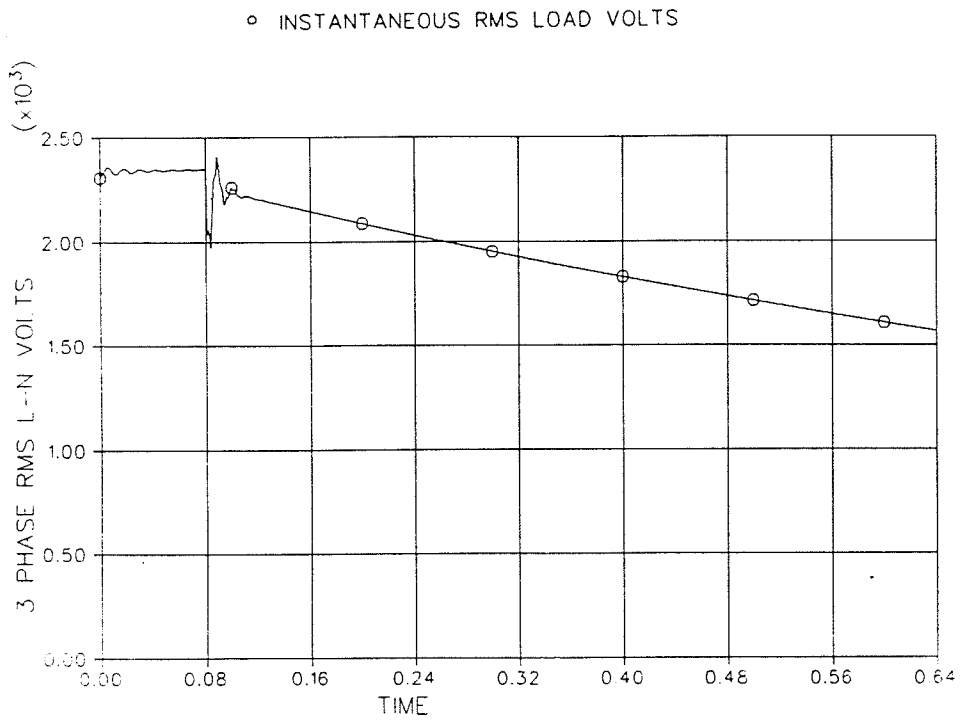

Figure 65 Three Phase Generator Voltage During a 0.5 p.u. Resistive Load Increase

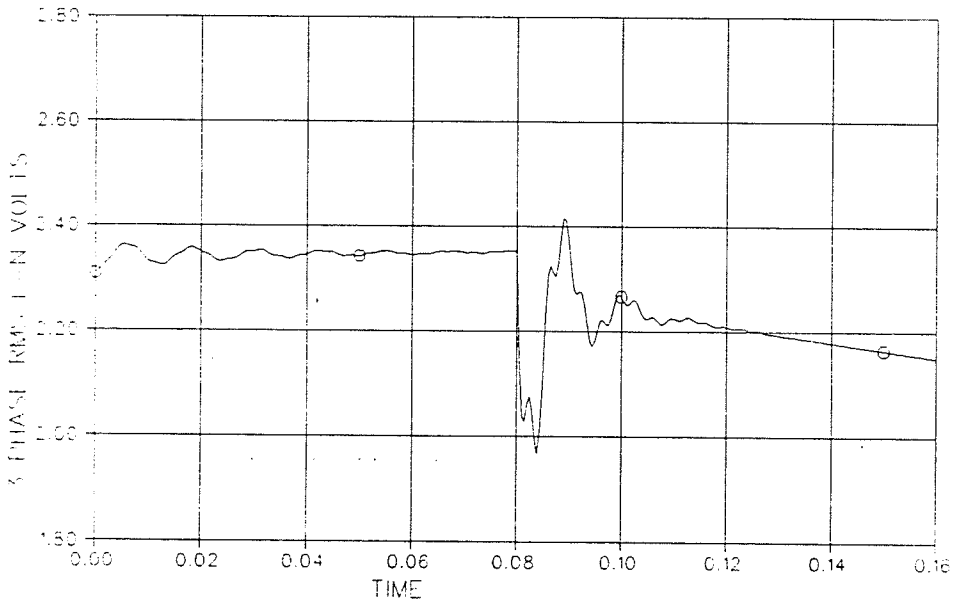

Figure 66 Detail of Figure 65

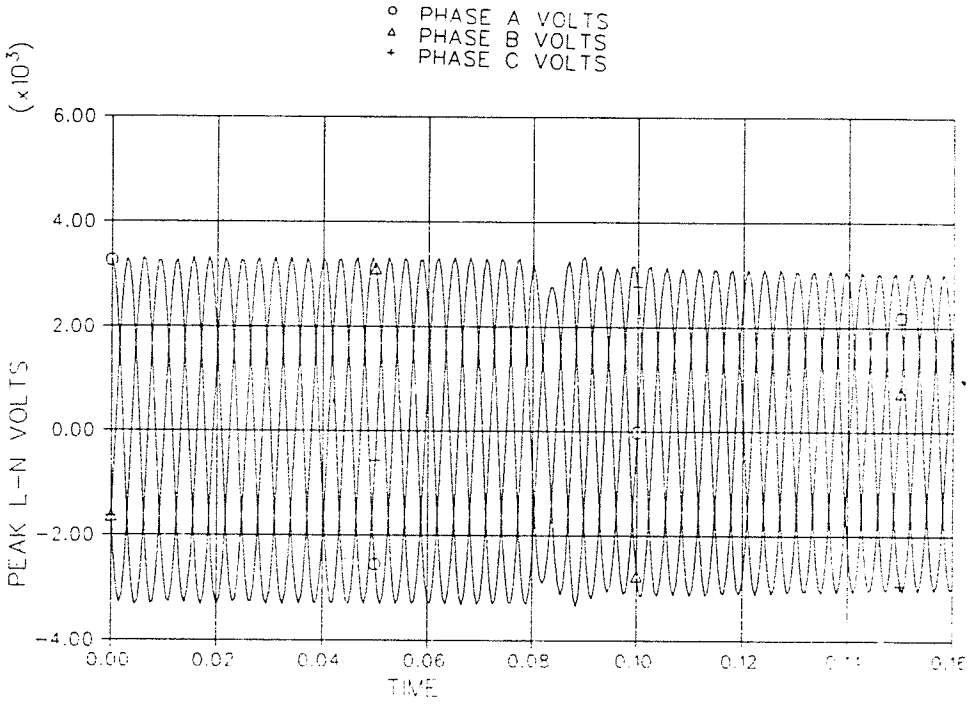

Figure 67 Individual Phases of Generator Voltage During a 0.5 p.u. Resistive Load Increase

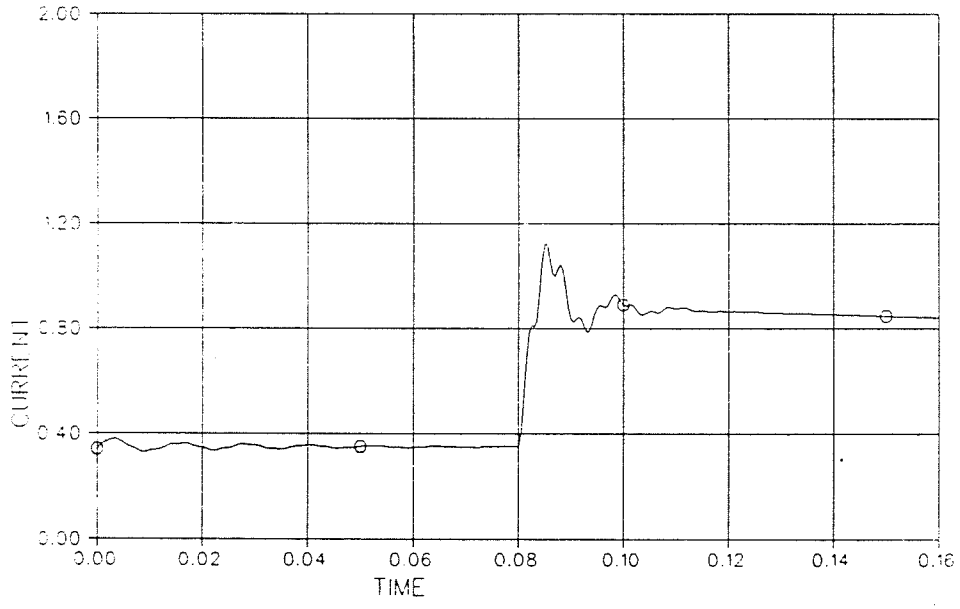

Figure 68 Response of Machine Current to a 0.5 p.u. Resistive Load Increase

CHAPTER 5

SUMMATIONS AND CONCLUSIONS

5.1 SELF-EXCITATION AND OPERATING CURVES FOR A SELF-EXCITED MACHINE

Self-excitation in an induction machine occurs when sufficient terminal capacitance is connected to the output terminals of the machine while the machine is being mechanically driven at sufficient speed having regard to the load.

Program I was developed to determine the capacitance and machine speed required in order to produce a specified terminal voltage and frequency for a given load.

It was determined that the induction machine could advantageously be operated at the rated voltage level over a range of speed and a range of power. For, a given voltage level, the self-excitation capacitors provide the least excitation current at low frequency. Furthermore, real load current depresses the self-excitation voltage. Moreover, the rectifier will be set at minimum delay angle to minimize reactive loading when all the capacitive current is required by the machine in order to maintain voltage. Therefore, Program I was used to pick a capacitance according to that capacitance required to maintain the desired voltage at the anticipated maximum power level and the anticipated minimum machine speed. The calculation assumed that the rectifier would not be drawing any reactive power during that particular operating condition. By this approach the minimum capacitance was determined which would be sufficient to supply the machine over the range of anticipated speed and power levels.

The maximum power level is chosen as the electrical output power level which corresponds to an input of rated motor torque at rated speed. The minimum speed is chosen to be a small fraction below rated speed and it can be determined for a particular machine according to how slow the machine can be driven at the maximum power level before overcurrent occurs in the machine due to increasing magnetizing current.

Referring to Figure 7, Program I searched over XC, XM, and machine speed (MSPD) with all other parameters fixed until terminal voltage was at the desired value and the impedance looking into the machine terminals was equal in magnitude but 180° out of phase with the impedance looking out of the terminals.

Program II was developed to produce a set of operating curves descriptive of the operation of a machine with one value of capacitance XC on the output terminals. The operating curves developed are families of constant value curves in the terminal voltage VT versus RL plane. Quantities which can be plotted in the VT versus RL plane are: frequency F, machine speed MSPD, machine terminal current, capacitor current, total load current, load power, and slip S. For each quantity several planes must be developed corresponding to different values of load reactance XL. RL and XL are as defined in Figure 7.

Program II canvasses a range of RL for each of many values of XM while preparing a plot of a quantity for a given value of XL. At each canvassed combination of RL and XM the program searches over frequency F and slip S for a valid steady state operating condition. Each valid steady state operating point can be located in the VT versus RL plane. The location of a constant value curve in the VT versus RL plane can be determined by interpolation between the locations of the steady state points in the plane.

The choice of plotting a characteristic quantity in several VT vs. RL planes corresponding to different values of XL does not produce a result which emparts

information in the most compact form possible. This detriment arises from the fact that the existence of one true steady state solution for a given combination of RL, XM, XL, and XC automatically implies the existence of a second solution. The consequence of the duplicity of solutions is that two VT versus RL planes must be prepared for each value of XL in order to fully describe a particular quantity. The first VT vs. RL plane corresponds to a slow speed solution (mode I) and the second corresponds to a higher speed solution (mode II). It is possible to keep the two modes of solution separate by careful choice of initial conditions in the search routines. In future the doubling of the number of required plots might be avoided by chosing to plot a characterisitic quantity in several VT vs. RL planes corresponding to different values of machine speed MSPD. In such planes, constant value curves would be plotted for different values of XL. Thus, for a given machine speed, each point in the VT vs. RL plane would correspond to a different value of load RL and XL.

The curves generated by program II were checked against laboratory measurements for the case of a purely resistive load. The calculated values of voltage were within 7 % of the experimentally determined values except at low values of RL at which terminal voltage drops rapidly with lowering of load resistance. In practical circuits, control of reactive power loading will be used to bring the voltage to the desired level. Small variations in circuit parameters caused a much better match between the experimental and calculated curves. This demonstrated the importance of having accurate estimations of machine and capacitance parameters.

The method of program II requires that in order to fully describe a characteristic quantity one must produce two VT vs. RL planes for each XL cross-section of interest. Thus, it could easily require ten VT vs. RL planes to describe voltage as a function of RL, XL, and machine speed (MSPD) rather than say five. Because of the number of curves required by the program II method it was decided to produce a

reduced set of curves which described the characteristic quantities of the circuit at the rated voltage cross-section of the operating space (VT, RL, XL).

Program III was written to produce a reduced set of operating curves which describe steady state quantities associated with operation at a specific level of terminal voltage (ex. rated voltage). In the reduced set of curves each quantity of interest can be described in one plane. For a given quantity, the axes of the plane are the quantity of interest and the power level. Constant machine speed curves are plotted in that plane to describe the quantity of interest as a function of machine speed and power level as illustrated in figure 32. Quantities plotted for an example system are: total load current, load power factor angle, the real component of current into the load, the reactive component of current into the load, the machine terminal current, magnetizing current, and airgap voltage.

Program III investigates one combination of machine speed and power in a given program execution. For a given machine speed and power level, the program searches over F, XM, and XL until the program converges on a valid operating point at the desired terminal voltage. By solving for XL, the program determines the reactive loading that the load must place on the self-excited machine in order to control terminal voltage to the desired level for the particular combination of machine speed and power level investigated in the program execution.

The program III curve which describes machine terminal current as a function of machine speed and power level can be used to determine the upper limit of acceptable machine speed at full power for the investigated voltage level. That curve illustrates that the machine terminal current increases with speed at full load for speed above a certain level. Therefore, the maximum acceptable machine speed corresponds with the speed at which maximum allowable terminal current is reached.

The capacitance used in generating the program III curves is the minimum capacitance which can supply the reactive power requirements of the machine over the

anticipated ranges of machine speed and power level at a specified terminal voltage. However, additional capacitance must be provided because the reactive load of practical rectifiers cannot be reduced to zero when it would be advantageous to do so in order to support self-excitation. Reactive load which cannot be eliminated in practical rectifiers is the reactive load due to the rectifier transformer magnetization current; the commutation angle; and the minimum firing delay angle (ex. $\alpha_{min} = 5°$). By setting α to α_{min} in equation 3.26, it is possible to determine the minimum reactive load presented by the rectifier for each combination of machine speed and power level. Extra terminal capacitance is necessary whenever the minimum reactive load presented by the rectifier is in excess of the reactive load determined by program III for a given combination of machine speed and power level. The minimum required extra terminal capacitance can be determined by canvassing the anticipated ranges of machine speed and power. For the example system, the required extra capacitance was largest at the lowest machine speed and the highest power level.

The addition of capacitance at the terminals of the machine requires some adjustment and augmentation of the reduced set of curves produced using program III. At each combination of machine speed and power level it is necessary to determine in order:

the real and reactive load current from the program III curves;
the additional capacitor current;
the reactive current which must be drawn by the rectifier;
the magnitude of the current into the rectifier transformer;
the power factor of the current into the transformer;
the magnitude of I_d;
the magnitude of V_d;
and finally rectifier delay angle α.

In that regard equation 3.26 is useful. Using the information obtained in this manner one can prepare descriptive graphs for capacitor current magnitude; required converter current magnitude; required d.c. voltage; required d.c. current; and required rectifier delay angle α. Figure 35 gives examples of these graphs for an example sys-

tem in which the machine voltage is maintained at the rated level.

The higher capacitance required by a practical rectifier leads to higher required ratings for rectifier transformers and thyristors as can be seen for the example system by comparing Figures 32 a) and 35 b). It is therefore recommended that rectifier minimum α and the commutating reactance of the rectifier transformer should be kept as small as practically possible in order to minimize the capacitor, transformer, and thyristor ratings.

Figure 35 c) and d) illustrate that for each machine speed and power level there is a unique combination of I_d and V_d. It can therefore be concluded that I_d should certainly not be held constant if we wish to be able to operate the generator over a broad ranges of machine speed and power level while maintaining 1.0 p.u. machine voltage. The apparatus interposed between the rectifier and the load in Figure 1 must be able to receive generated power at the required levels of I_d corresponding to different machine speeds and power levels.

For low power, figures 35 c) and e) illustrate that the higher d.c. voltage required at slow speed is accompanied by a reduced α. This is rather unexpected but arises due to the high commutating reactance and high rectifier current associated with high speed operation. It is because of this characteristic that the preliminary controls proposed in the thesis develope an order for V_d and then translate that order into an α order in a way that compensates for the effect of computating reactance.

5.2 HARMONIC CURRENTS IN THE MACHINE DUE TO THE RECTIFIER

The capacitor bank for a self-excited induction machine typically would have sufficient capacitance to reduce 11th and higher order rectifier generated harmonics in the machine to generally acceptable levels. A low (ex. 0.8) power factor machine supplying a rectifier with a typical commutating reactance and minimum α would

have sufficient capacitance to also cause some attenuation of the 5th and 7th harmonic currents generated by the rectifier. However, a high power factor machine supplying close to an ideal rectifier (i.e. low α_{min} and commutating reactance) would require such a low capacitance that the 5th and 7th harmonic currents into the machine could actually be higher than those generated by the rectifier due to the presence of the self-excitation capacitors. From equation 3.28 and the converter current for the example system illustrated in Figure 32 b), it appears that the highest level of machine harmonic current would arise at full load power and slow speed. This conclusion is based on the fact that the largest rectifier current for any slow speed operation occurs at maximum load and the capacitor bank is much more efficient in attenuating machine harmonic current at high frequency than at low frequency.

For a high power factor machine and close to an ideal rectifier as described above, it may be necessary to use a 12 pulse rectifier to avoid excessive 5th and 7th harmonic currents in the induction generator. The possibility of using tuned shunt filters to ground is to be avoided because of the variable frequency generated on the machine terminals.

5.3 THE CHOPPER-INVERTER APPARATUS

The chopper-inverter apparatus of Figure 37 was the first apparatus considered for interposition between the rectifier and the load as illustrated in Figure 1. The chopper circuit was shown to act in the steady state as a matching circuit which matchs the V_d and I_d out of the rectifier to the smoothing capacitor voltage V_{cap} and the the average current to the inverter from the smoothing capacitor.

In order to make the chopper work properly as a matching circuit, it is necessary to choose to control V_{cap} to a voltage level which is higher than the value of V_d for any anticipated machine speed and power level.

The proposed controls comprise a capacitor voltage controller to regulate the chopper duty cycle and an inductor current controller to control α. Variation of the chopper duty cycle is implemented in order to divert the appropriate fraction of I_d to the capacitor in order to maintain the capacitor voltage at a set level. The α order is obtained from a V_d order signal by means of a control block which implements equation 3.49. In formulating a V_d order the inductor current controller must fulfill two purposes. It must be able to accomplish a fast gross adjustment to the V_d order based upon a slightly erroneous estimate of V_{dRE}. Secondly, the inductor current controller must be able to provide feedback control of the machine voltage while compensating for errors in measuring V_{dRE} and errors in implementing the V_d order. Figure 43 illustrates a preliminary schematic which can serve as a starting point in the future design of a functional inductor current controller.

The complete simulation of the system including transient models of the machine, rectifier, chopper, inverter, and controls is left for future work. However, a simplified transient simulation of the system was undertaken and for that simulation the capacitor voltage controller was shown to be compatible in operation with the inductor current controller. The simulation was based on a controller d.c voltage source at the supply end of the smoothing inductor. The source was controlled through a 0.1 second time delay so that it would respond more slowly than the output voltage of a real rectifier. The rectifier voltage will respond quickly because α can be adjusted quickly and the level of self-excitation in an induction machine was shown in chapter 4 to respond comparatively slowly to changes in α. The controls were proven in concept because the simulated controls were able to response acceptably to step increases from zero for both inductor current and capacitor voltage in spite of the sluggish response of the controlled d.c. source voltage.

The chopper action can be expected to induce ripple onto the smoothing inductor current. However, at a chopper frequency of 1000 Hz the chopper induced ripple

is only about 75 % of the ripple induced by the 6th harmonic voltage. The turn-on and turn-off time of GTO thyristors tends against operation of the chopper above 1000 Hz due to the desirability of maintaining switching time to a small fraction of the chopper period. Much faster switching F.E.T. devices could be employed in the chopper of very small systems in order to allow the chopper frequency to be be increased. The ripple caused by the rectifier could be reduced by using a 12 pulse rectifier.

The ripple charge and associated ripple voltage on the smoothing capacitor due to the action of the chopper can be calculated from equations 3.45 and 3.48. If the inverter used to supply the a.c. load is such that it causes a 12 pulse ripple of voltage on the smoothing capacitor then it might be desirable to operate the chopper at 720 Hz and synchronize the phase of the two induced ripples so that they cancel to the greatest extent possible. However, operating the chopper at such a low frequency would increase the inductor current ripple and would likely require the provision of additional smoothing inductance.

5.4 THE DUAL ARRANGEMENT OF SERIES CAPACITOR COMMUTATED GRAETZ BRIDGE INVERTERS

For this alternative apparatus it is the ability to vary I_d with respect to the magnitude of the a.c. load current $| I_{LOAD} |$ which permits the apparatus to act as a matching circuit between the rectifier output and the a.c. load. In the steady state the circuit can thus accept the I_d required for a given combination of machine speed and power level as for instance is illustrated in Figure 35 d).

It has been shown that for a given I_d a controller for the apparatus will cause the inverter input voltage V_{dRE} to vary in proportion to the power level. This is an approximation based on the assumption of lossless inverters. The controller of this apparatus thus has the same effect on V_{dRE} as does the capacitor voltage controller

in the chopper-inverter apparatus.

It is therefore concluded that this apparatus could be used in place of the chopper-inverter apparatus. The price to be paid for the ability to use the required broad range of I_d is that the voltage rating of the inverter thyristors and series capacitors must be increased substantially.

5.5 FINAL CONCLUSION

From a steady state point of view there appears to be no barrier to implementing a self-excited induction generator operable at rated machine voltage supplying an isolated a.c. load through a d.c. link. The d.c. link current I_d must be variable independant of the magnitude of the a.c load current $| I_{LOAD} |$ in order for the machine voltage to be controlled to the desired level. That adjustment of I_d is permitted by the use of either the chopper-inverter apparatus or the dual arrangement of series capacitor commutated Graetz bridge inverters.

The chopper-inverter system should be able to supply a load which varies from a low level to full load while the machine is driven over a large (eg. 0.9 to 1.8 p.u.) range of speed. During that operation machine voltage will be maintained at the rated level. The dual arrangement of series commutated inverters would require a certain minimum level of load to ensure stability of the voltage regulation.

The basic control concepts have been proven in principle in that the capacitor voltage controller has been shown to be compatible in operation with the inductor current controller by means of a simplified transient simulation. However, a full transient simulation of the machine, rectifier, chopper, inverter, and variable load will be required in order to optimize and ensure stability of the controls. This should be followed by the construction of a prototype.

REFERENCES

[1] Wind-driven, Capacitor-excited Induction Generators For Residential Electric Heating, N. Mohan and M. Riaz (University of Minnesota, Minneapolis, MN, U.S.A.), I.E.E.E. 1978 Power Engineering Society Winter Meeting, New York, U.S.A., 29 Jan. - 3 Feb. 1978 (N.Y., U.S.A.: I.E.E.E. 1978), Paper # A 78 050-7

[2] Static Exciters for Induction Generators, M. B. Brennen and A. Abbondanti (Res. Labs., Westinghouse Electric Corp., Pittsburgh, PA, U.S.A.), I.E.E.E. Ind. Appl. Soc. meeting (10th), Sept. 28 - Oct. 2 1975, Atlanta, Georgia, (N.Y., U.S.A.: I.E.E.E. 1975), p. 1020 - 8

[3] Induction Generators for Small Hydro Plants, L. Pereira, International Water Power and Dam Constr. (GB), vol. 33, no.11, p. 30-4 (Nov. 1981)

[4] A System of Induction Generator with Static Exciter and Paralleled to A.C. Power Lines, Noriaki Sato, Yoichi Hayashi, and Hidetoshi Umida (Tokyo Inst. of Technol., Tokyo, Japan), International Semi-conductor Power Conference, Orlando, FL, U.S.A., 24 - 27 May 1982 (N.Y., U.S.A.: I.E.E.E. 1982), p. 295-305

[5] Static Power Conversion from Self-Excited Induction Generators, J. Arrillaga and D. B. Watson (Dept. of Electrical Eng., Univ. of Canterbury, Christchurch, New Zealand), Proc. Inst. Electr. Eng. (GB), vol. 125, no. 8, p. 743 - 6. (Aug. 1978).

[6] Controllable D.C. Power Supply from Wind-driven Self-excited Induction Machines, D. B. Watson, J. Arrillaga, and T. Densem, Proc. Inst. of Electr. Eng. (GB), vol. 126, no. 12, p. 1245 - 8 (Dec. 1979).

[7] Estudo de um Sistema Gerador de Inducao Auto-excitado Acoplado a um Retificador / "Chopper", C. L. Rocha, E. H. Watanabe, and S. Carneiro Jr. 5. Congr. Bras. Automatica / 1. Congr. Lat.-Americ. Automatica - Campina Grande - 1984, p. 293-297 (in Portugese).

[8] The Process of Self-Excitation in Induction Generators, J. M. Elder, J. T. Boys, and J. L. Woodward, I.E.E. Proc. B (GB), vol. 130, no. 2, p. 103 - 8 (March 1983).

[9] Steady State Analysis of Capacitor Self-Excited Induction Generators, A. K. Tandon, S. S. Murthy, and G. J. Berg, I.E.E.E. Trans. on Power Apparatus and Systems, Vol. PAS - 103, No. 3, March 1984, p. 612 - 18.

[10] Analysis of Self-excited Induction Generators, S. S. Murthy, O. P. Malik, and A. K. Tandon, I.E.E. Proc. C (GB), vol. 129, no. 6, p. 260 - 5 (Nov. 1982).

[11] Development Potential for Low-Head Hydro, R. Nair, Int'l. Water Power and Dam Constr. (GB), Dec. 1982, Vol. 34, no. 12, p. 49 - 56; 72.

[12] L. Monition, M. Le Nir, and J. Roux, "Micro Hydroelectric Power Stations", John Wiley, 1984.

[13] Modern Windmills, P. M. Moretti and L.V. Divone, Scientific American, June 1986, vol. 254, no. 6, p. 110 - 118.

[14] E. W. Kimbark, "Direct Current Transmission", vol. 1, John Wiley, 1971 , at p. 77

[15] Dynamic Performance and Voltage Stability of Self-Excited Induction Generator with Voltage Controller, T. Irisa, S. Takata, and R. Ueda, Trans. Inst. Electr. Eng. Japan Sect. E (Japan), vol. 102, no. 1 - 2, p. 1 - 8 (Jan. - Feb. 1982).

[16] Small Induction Generator and Synchronous Generator Constants for D S G Isolation Studies, William B. Gish (Electric Research and Management, Inc., Thomaston, Maine), I.E.E.E. 1985 Power Engineering Society Summer Meeting, Vancouver, B.C., Canada, July 14 - 19 1985, Paper # 85 SM 414 - 8.

[17] The Capacitive Self-Excitation Transients of an Asynchronous Generator Under Load, S. I. Kitsis, Power Eng. (Acad. Sci. USSR) (USA), vol. 15, no. 4, p. 23 - 35 (1977).

[18] A Low-cost, Single Phase Induction Generator, D. J. Bernays Jr. (C. S. Draper Laboratory, Cambridge, Massachusetts 02139), I.E.E.E. Power Electronics Specialists Conference PESC'82 Record, Cambridge, MA, U.S.A., June 14 - 17 1982 (N.Y., U.S.A.: I.E.E.E. 1982), p. 185 - 96.

[19] Performance of Asynchronous Self-excited Generators in Protecting Detanders from Racing, S. I. Kitsis, Soviet Electrical Engineering (USA), vol. 51, no. 12, 1980, p. 30 - 35.

[20] High-Speed Asynchronous Generators in Autonomous Stabilized Power Supply Sources, S. K. Bokhyan and M. I. Simonyan, Soviet Electrical Engineering (USA), vol. 52, no. 2, 1981, p. 32 - 36.

[21] Use of the Third Field Harmonic for Excitation of Induction Machines, V. Kh. Mirimanyan and E.V. Saratovkina, Soviet Electrical Engineering (USA), vol. 52, Issue 2, 1981, p. 58 - 63.

[22] Structural Model of Asynchronous Generator with Voltage Regulation System, Yu. M. Osadchii, V. S. Frishman, and V. S. Zmitrovich, Soviet Electrical Engineering (USA), vol. 49, issue 1, 1978, p. 48 - 53.

[23] Self-Excitation Processes in an Asynchronous Machine, S. I. Kitsis, Power Eng. (Acad. Sci. USSR) (USA), vol. 12, no. 1, p. 78 - 84.

[24] Capacitive Self-excitation of an Asynchronous Generator, S. K. Boyhyan, Power Eng. (Acad. Sci. USSR) (USA) vol. 15, no. 2, p. 37 - 43 (1977).

[25] Asynchronous Self-excited Generator Transients in Sudden Three Phase Short Circuits, S. I. Kitsis, Electric Technology USSR (London), No. 4, pp. 31 -47, 1980.

[26] Small Hydro from Submersible Pump, E. P. Giddens, W. Spittal, and D. B. Watson, Int. Water Power and Dam Constr. (GB), vol. 34, no. 12, p. 33 -34 (Dec. 1982).

[27] Load-shedding and Self-excitation Transients in Autonomous Asynchronous Generator with Undamped Magnetic Field, S. I. Kitsis, Power Eng. (J. Acad. Sci. USSR) (USA), vol. 19, no. 6, p. 34 -45 (1981).

[28] Calculating the No-load Excitation Capacitance of an Asynchronous Generator, S. I. Kitsis, Power Eng. (Acad. Sci. USSR) (USA), vol. 16, no. 5, p. 125 - 9 (1978).

[29] Self-excited Induction Generator/Forced Commutated Rectifier System Operating as a D.C. Power Supply, A. N. Barreto and E. H. Watanabe (Electrical Engineering Department, Federal University of Rio de Janeiro, Rio de Janeiro, Brazil), European Conference on Power Electronics and Applications

[30] Contributions to the Steady State Analysis of Wind-turbine Driven Self-Excited Induction Generators, S. S. Yegna Narayanan and V. J. Johnny (Indian Inst. of Tech., Madras, India), I.E.E.E. 1985 Power Engineering Society Summer Meeting, Vancouver, B.C., Canada, July 14 - 19, 1985, Paper # 85 SM 337-1

[31] E. W. Kimbark, "Direct Current Transmission", Vol. 1, John Wiley, 1971 at p. 88

[32] E. W. Kimbark, "Direct Current Transmission", Vol. 1, John Wiley, 1971 at p. 302

[33] E. W. Kimbark, "Direct Current Transmission", Vol. 1, John Wiley, 1971 at pp. 308 - 312.

[34] E. W. Kimbark, "Direct Current Transmission", Vol. 1, John Wiley, 1971 at pp. 308 - 312.

[35] Block and Double Block Connections Proposed for HVDC Station Infeed, P. C. S. Krishnayya, I.E.E.E. Power Engineering Society Winter Meeting (1973), Paper # C 73 227 - 6.

[36] Analysis of a Small Series Tap on an HVDC System Using Forced Commutation, A. M. Gole' and R. W. Menzies (Univ. of Manitoba), I.E.E. Int'l Conf. on Thyristor and Static Equipment for A.C. and D.C. Transmission; London, U.K., Nov. 1981

[37] Feasibility of D.C. Transmission with Forced Commutation to Remote Loads, H. M. Turanli, R. W. Menzies, and D.A. Woodford, I.E.E.E. 1983 Power Engineering Society Summer Meeting, Los Angelos, CA, U.S.A., 1983

[38] Analysis of Certain Aspects of Forced Commutated HVDC Inverters, A. M. Gole´ and R. W. Menzies, I.E.E.E. Trans. on Power Apparatus and Systems, Vol Pas-100, May 1981, pp. 22285 - 89.

[39] Progress in Self-Commutated Inverters for Fuel Cells and Batteries, G. A. Phillips, J. W. Walton, and F. J. Kornbrust, I.E.E.E. Trans. on Power Apparatus and Systems, Vol. PAS-98, No. 4, July/August 1979, pp. 1466 - 1475.

[40] E. W. Kimbark, "Direct Current Transmission", Vol. 1, John Wiley, 1971 at pp. 314 - 316.

[41] Improved Interfacing of Electrical Machine Models to Electromagnetic Transients Programs, A. M. Gole´, R. W. Menzies, H. M. Turanli, and D. A. Woodford, I.E.E.E. 1984 Power Engineering Society Winter Meeting, Dallas, Texas, U.S.A., Jan. 29 - Feb. 3 1984, Paper # 84 WM 222 - 6.

[42] Digital Modelling of D.C. Links and Synchronous Machines, D. A. Woodford A. M. Gole´ and R. W. Menzies, I.E.E.E. Trans. on P.A.S., vol. PAS-102, no. 6, June 1983, pp. 1616 -1623.

[43] A Report on Preliminary Investigations into a System Comprising a Self-excited Induction Generator Asynchronously Coupled Through a D.C. Link to an Isolated A.C. Load, T. L. Maguire, submitted to the Department of Electrical Engineering, The University of Manitoba, August, 1986.

APPENDICES

APPENDIX 1

Motor # 1 Parameters

Nameplate Data

Power		1.5 hp.
Speed		1165 r.p.m. , 6 pole
Volts (l-l)		208 volts , 60 Hz.
Current		6.4 amps
Cema Design		B
Frame A182T	Type K	
Model 2F1142M	No. BU 1645	
Manufacturer		Canadian General Electric

P.U. Base Values

I_{base} = 6.4 amps
V_{base} = 120 volts
Z_{base} = 18.75 ohms

Equivalent Circuit Parameters

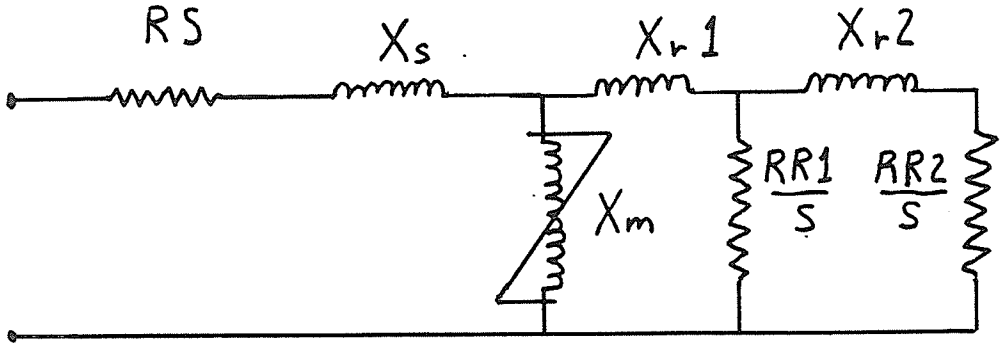

Double Cage Parameters

The following data was obtained from Dr. Ahmad Mohamed Asaad Mahmoud. Dr. Mahmoud conducted the tests on the machine in preparation for his Ph.D. thesis which presented in 1985 at the University of Manitoba.

Parameter	Magnitude (ohms)	Magnitude (p.u.)
RS	1.3207	0.07040
Xs	1.5997	0.08527
Xr1	2.7816	0.14827
RR1	1.7036	0.09081
Xr2	5.0451	0.26893
RR2	2.83711	0.15123

Airgap Volts	Magnetizing Current	Magnetizing Impedance Xm
32.55647	0.92733	35.1078
43.05251	1.22401	35.1733
54.08334	1.55848	34.7026
64.71426	1.91172	33.8513
75.41193	2.27186	33.1939
85.88712	2.69396	31.8814
96.70480	3.32376	29.0950
107.7001	4.22746	25.4763
114.5536	5.67924	20.1706
119.3928	7.75042	15.4047

Single Cage Representation

The double cage representation of the induction machine can be reduced to a single cage representation acceptable for small values of slip simply by paralleling RR1 and RR2 and neglecting Xr2. The resulting equivalent circuit is as given below with RR equal to 1.0644 ohms.

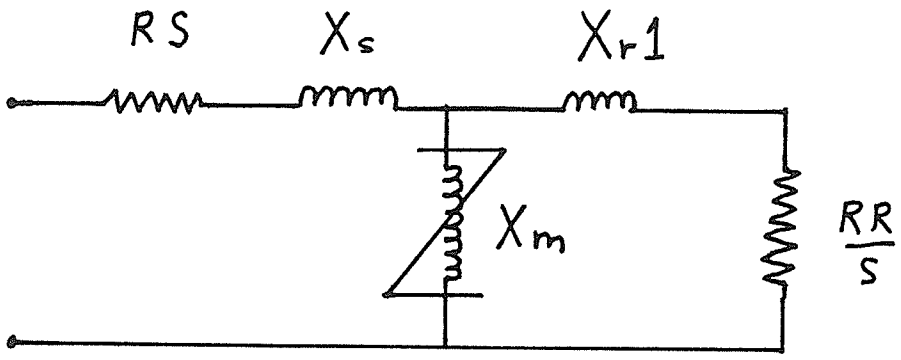

APPENDIX 2

Motor # 2 Parameters

Nameplate Data

Power	900 hp.
Speed	1800 r.p.m. , 4 pole
Volts (l-l)	4000 volts , 60 Hz.
Current	111 amps
Full Load Efficiency	95.3 %
Full Load Power Factor	0.915
Frame Size	H688F
Ser. No.	1 - 1753401
Manufacturer	Canadian Westinghouse Co. Ltd.

Single Cage Representation

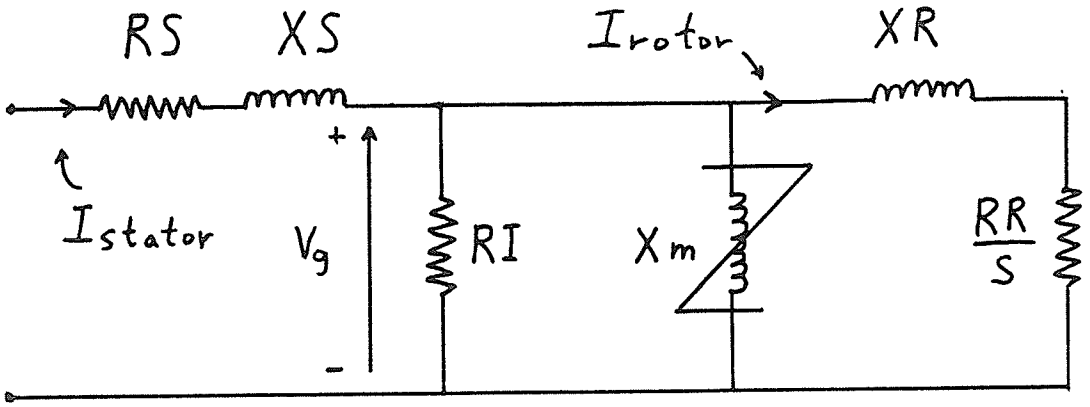

An induction motor design program, executed by the manufacturer in respect of motor #2, provided the following information:

RS = 0.32 ohms
XS = 1.92 ohms
XR = 3.83 ohms
RR = 0.175 ohms
Windage and Friction = 4.7 kW

The saturation curve and a representation of the iron loss resistance were obtained from a running light test reported by Mr. B. J. Quartermaine, P.Eng. The test was conducted in 1971 prior to acceptance of motor #2 by Byron Jackson Division for use by the Hydro Electric Power Commission of Ontario. The test results were as follows:

Voltage (l-l rms)	Current (amps)	Power (3 ph. watts)
4788	31.6	15200
4401	24.4	12800
4000	19.4	11200
3200	14.0	8400
2000	8.6	6400
1200	5.6	5120
721	5.1	4640
665	5.3	4640

In the running light test, the machine speed remains approximately constant so that to a close approximation we can say that the power used in windage and friction remains constant at 4.7 kW during the test. It is possible to estimate rotor current $\vec{I}_{rotor}$ as a function of $\vec{V}_g$ from the relation:

$$\frac{RR}{S} = \frac{\vec{V}_g{}^2}{P_{F \text{ and } W}}$$

Stator current $\vec{I}_{stator}$ can be calculated as a function of V_g from the results of the running light test. Given $\vec{I}_{stator}$ and $\vec{I}_{rotor}$, the real and reactive magnetizing branch current can be obtained as a function of $\vec{V}_g$. A 60 hz representation of iron loss resistance (RI) turns out to be 2320 ohms. Likewise, consideration of reactive current as a function of airgap voltage yields the following curve data:

Airgap Volts (l-n rms)	Magnetizing Current (amps)	Magnetizing Impedance Xm (ohms)
376	3.16	119.0
408	3.29	124.0
683	4.99	136.9
1135	8.4	135.1
1821	13.92	130.8
2271	19.33	117.5
2494	24.34	102.5
2703	31.55	85.7

A reasonable extension of the magnetizing curve yields:

Airgap Volts (l-n rms)	Magnetizing Current (amps)	Magnetizing Impedance Xm (ohms)
2860	39.0	73.0

From this information it is possible to produce a $\vec{V}_g/F$ versus XM curve as was discussed in Chapter 2.

When this machine is run with rated torque input at rated speed electrical power output can be expected of approximately:

$$900\ hp. \times 0.746\ \frac{kW}{hp.} \times 0.953\ efficiency = 639.84\ kW$$

This will be referred to as rated electrical output power. That electrical output power corresponds to a real component of output current of 92.35 amps. An RL = 25.0 ohms in Figure 7 of Chapter 2 will give that real component of current.

APPENDIX 3

Mode I and Mode II Sets of Graphs Descriptive of Machine # 2 Self-excited and Supplying a Resistive Load

This appendix contains mode I and mode II sets of graphs descriptive of machine number 2 supplying a resistive load (i.e. XL very large). The machine has 60 microfarads on each terminal. Note that the rated voltage of the machine is 2.309 kV (l-n rms)and that this graph plots voltage to 25 kV. The voltage axis on all graphs is in volts l-n rms. Above 6000 volts the graphs are inaccurate because the leakage saturation has not been modelled and the terminal current will be greater than 3.5 p.u. at those voltages.

This appendix contains, in order:

1. The mode I graph descriptive of the operating condition associated with a given machine speed and RL with XL very large. For definitions of RL and XL see Figure 7.

2. The mode I graph descriptive of the frequency F associated with a given coordinate in the VT versus RL plane of 1.

3. The mode I graph descriptive of the machine terminal current associated with a given coordinate in the VT versus RL plane of 1.

4. The mode I graph descriptive of the capacitor current associated with a given coordinate in the VT versus RL plane of 1.

5. The mode I graph descriptive of the total load current associated with a given coordinate in the VT versus RL plane of 1. Total load current does not included the capacitor current. It only includes current into RL and XL which are parallel in Figure 7. Thus with XL large the lines in this graph radiate from the origin.

6. The mode I graph descriptive of the load power associated with a given coordinate in the VT versus RL plane of 1.

7. The mode I graph descriptive of the slip S associated with a given coordinate in the VT versus RL plane of 1.

8. The general input data file DATACIR and the data file CRVDATA1 descriptive of the $\vec{V}_g$/F curve which were used to produce the mode I and mode II curves in this appendix.

9. The mode II graph descriptive of the operating condition associated with a given machine speed and RL with XL very large. See Figure 7 for definitions of RL and XL.

10. The mode II graph descriptive of the frequency F associated with a given coordinate in the VT versus RL plane of 9.

11. The mode II graph descriptive of the machine terminal current associated with a given coordinate in the VT versus RL plane of 9.

12. The mode II graph descriptive of the capacitor current associated with a given coordinate in the VT versus RL plane of 9.

13. The mode II graph descriptive of the total load current associated with a given coordinate in the VT versus RL plane of 9. Total load current does not included the capacitor current. It only includes current into RL and XL which are parallel in Figure 7. Thus with XL large the lines in this graph radiate from the origin.

14. The mode II graph descriptive of the load power associated with a given coordinate in the VT versus RL plane of 9.

15. The mode II graph descriptive of the slip S associated with a given coordinate in the VT versus RL plane of 9.

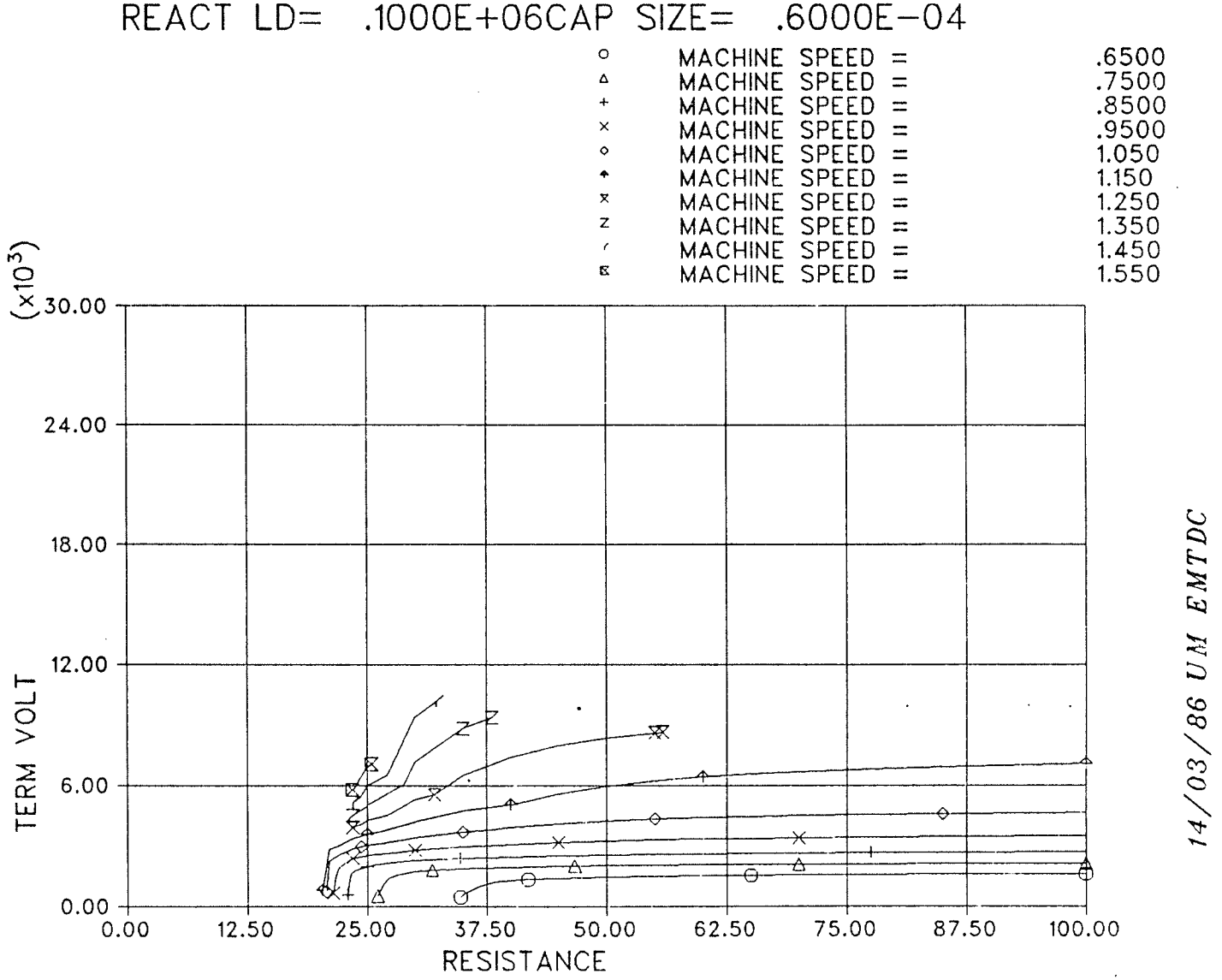

14/03/86 UM EMTDC

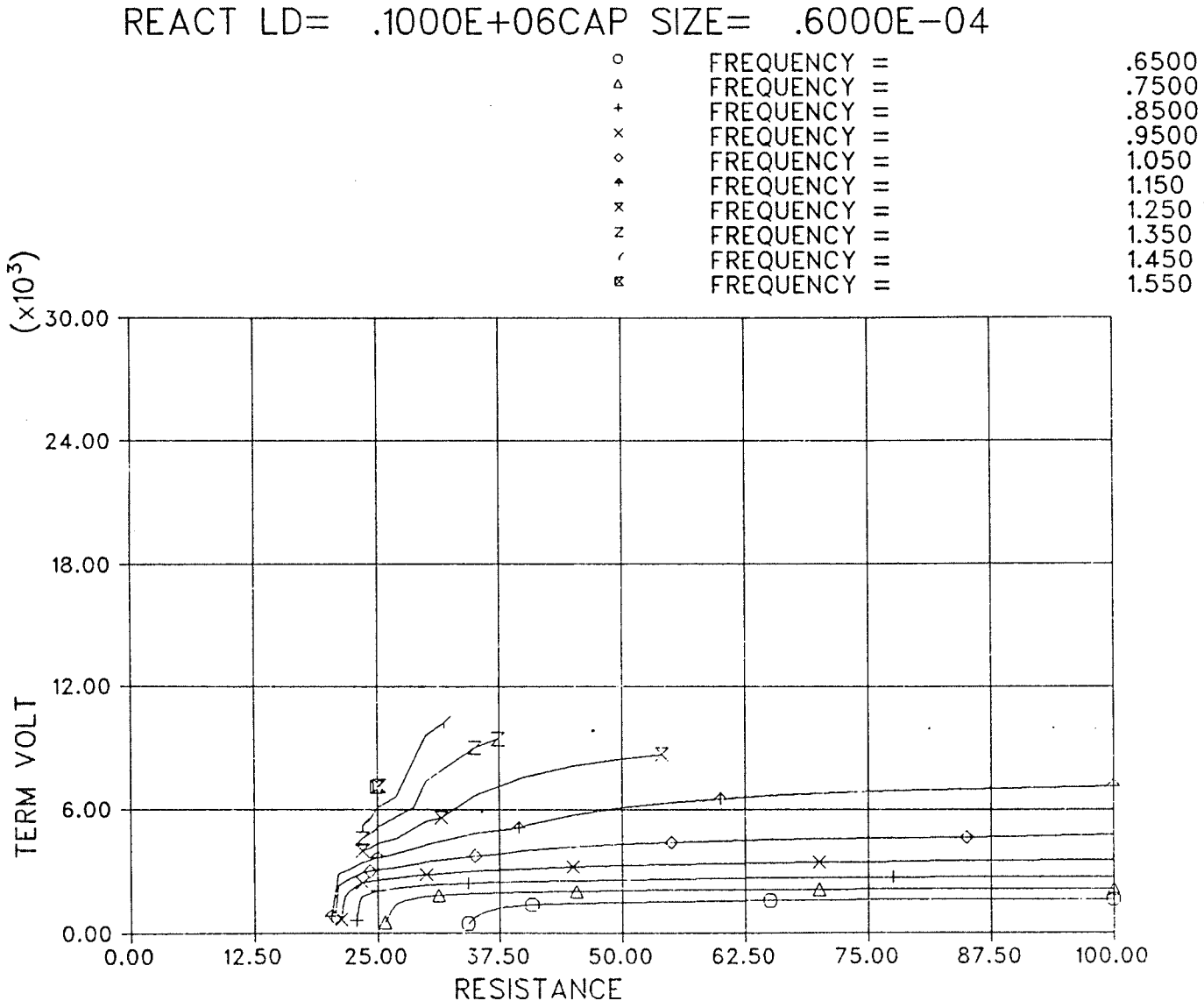

14/03/86 UM EMTDC

REACT LD= .1000E+06CAP SIZE= .6000E-04

○	CAPACITOR CURRENT =	50.00
△	CAPACITOR CURRENT =	100.0
+	CAPACITOR CURRENT =	150.0
×	CAPACITOR CURRENT =	200.0
◇	CAPACITOR CURRENT =	250.0
✦	CAPACITOR CURRENT =	300.0
×	CAPACITOR CURRENT =	350.0

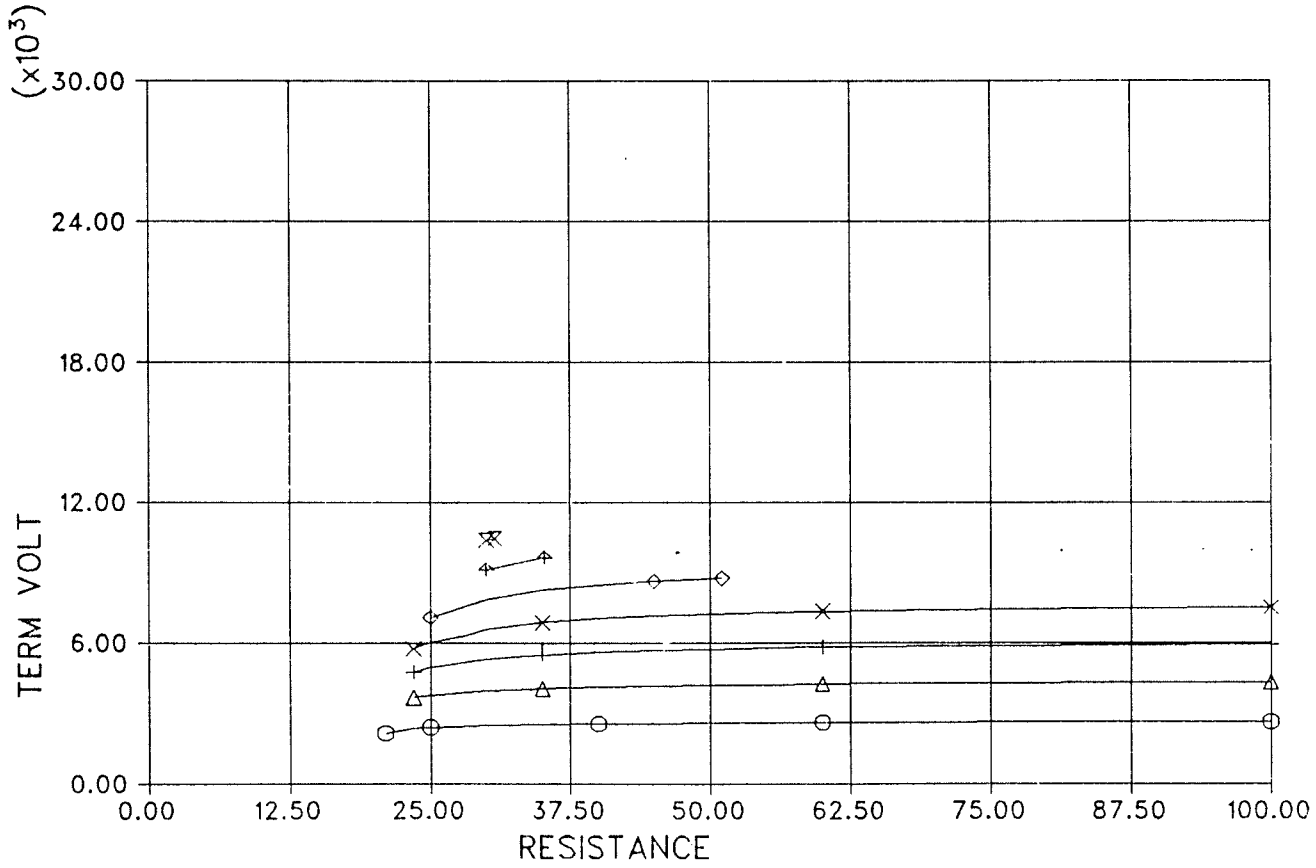

14/03/86 UM EMTDC

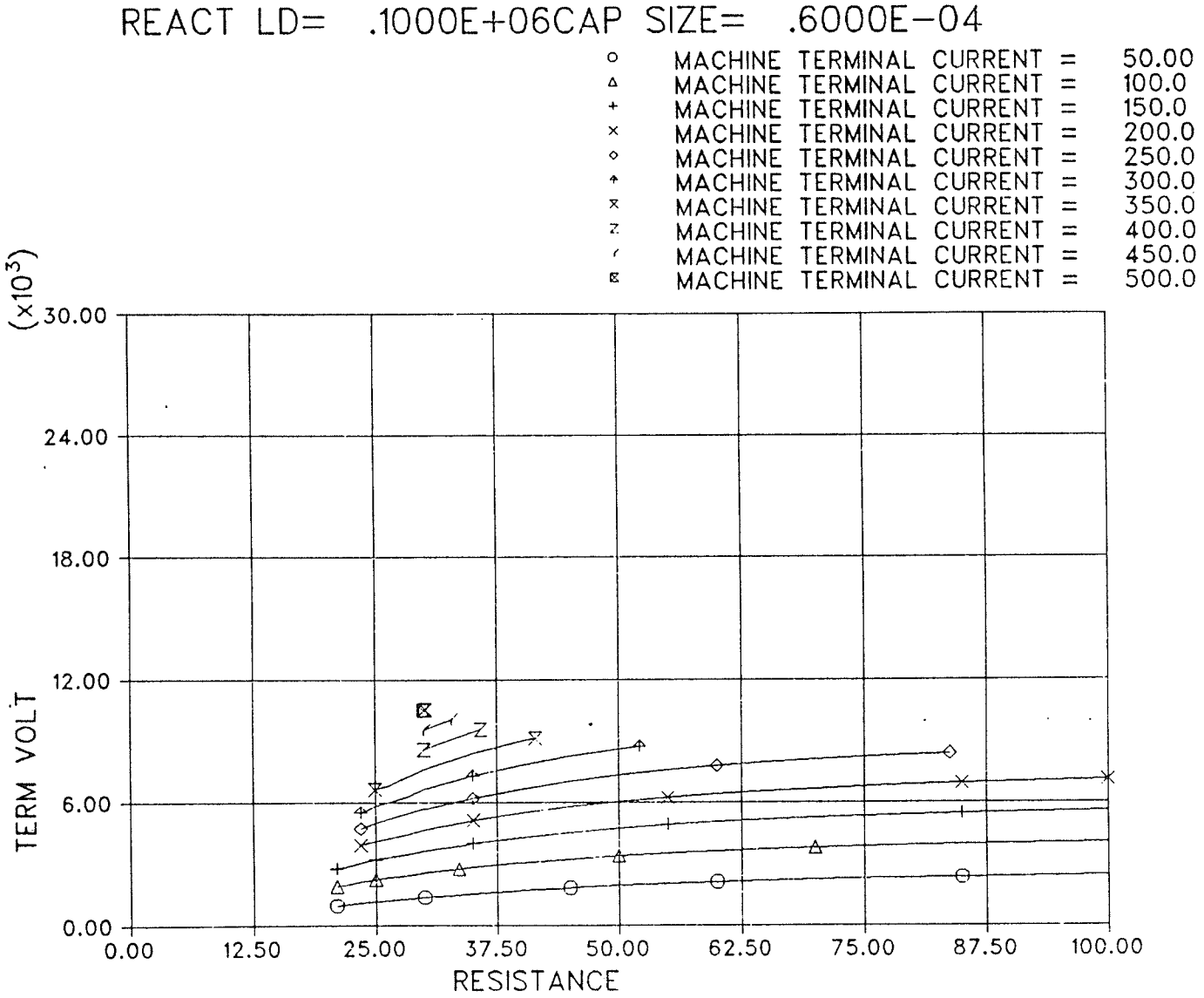

14/03/86 UM EMTDC

REACT LD= .1000E+06CAP SIZE= .6000E-04

○	TOTAL LOAD CURRENT	=	50.00
△	TOTAL LOAD CURRENT	=	100.0
+	TOTAL LOAD CURRENT	=	150.0
×	TOTAL LOAD CURRENT	=	200.0
◇	TOTAL LOAD CURRENT	=	250.0
✦	TOTAL LOAD CURRENT	=	300.0
⋇	TOTAL LOAD CURRENT	=	350.0

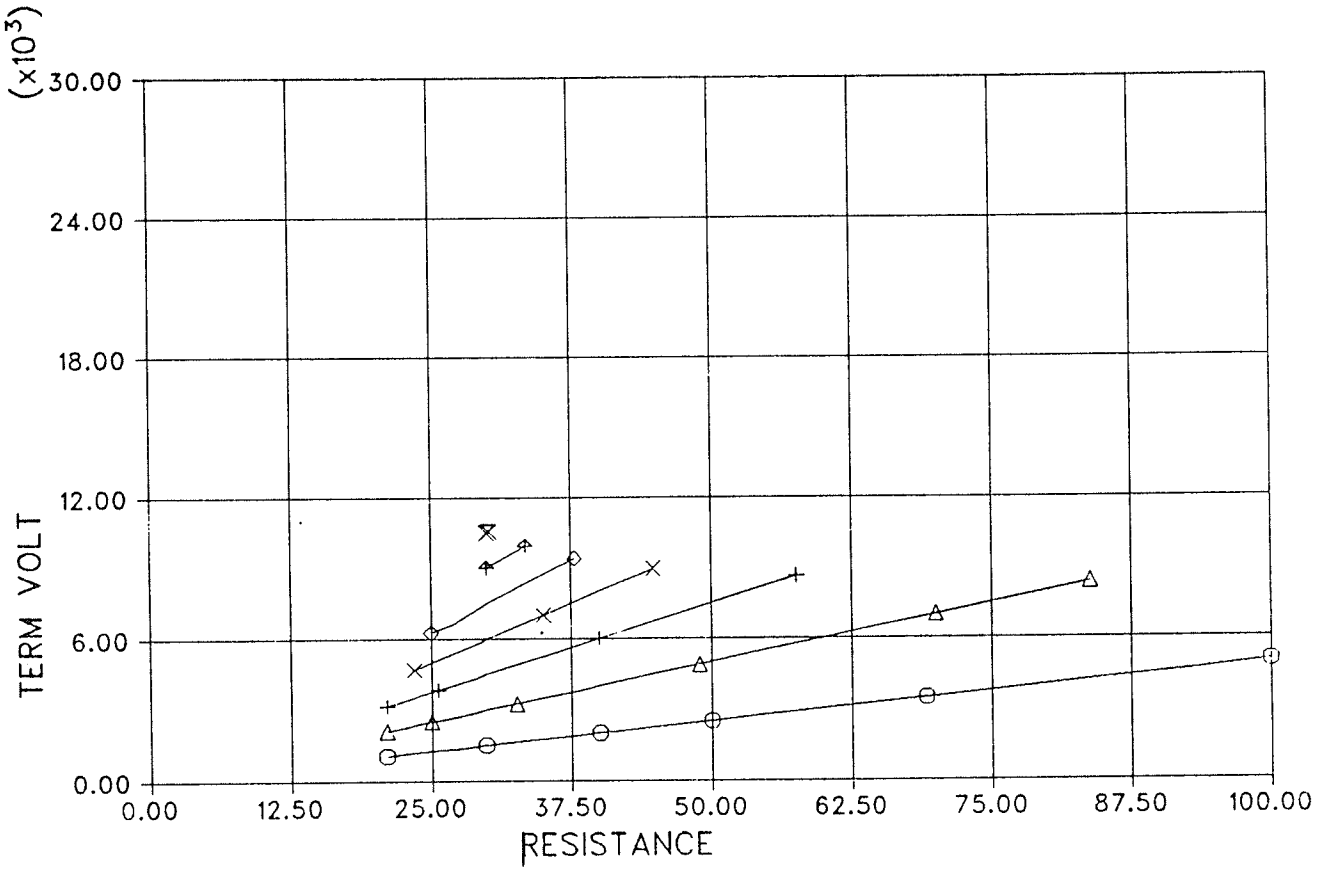

14/03/86 UM EMTDC

REACT LD= .1000E+06CAP SIZE= .6000E-04

o	LOAD POWER =	.2000E+07
Δ	LOAD POWER =	.3000E+07
+	LOAD POWER =	.4000E+07
×	LOAD POWER =	.5000E+07
◇	LOAD POWER =	.6000E+07
✦	LOAD POWER =	.7000E+07
✕	LOAD POWER =	.8000E+07
Z	LOAD POWER =	.9000E+07
◜	LOAD POWER =	.1000E+08
⊠	LOAD POWER =	.1100E+08

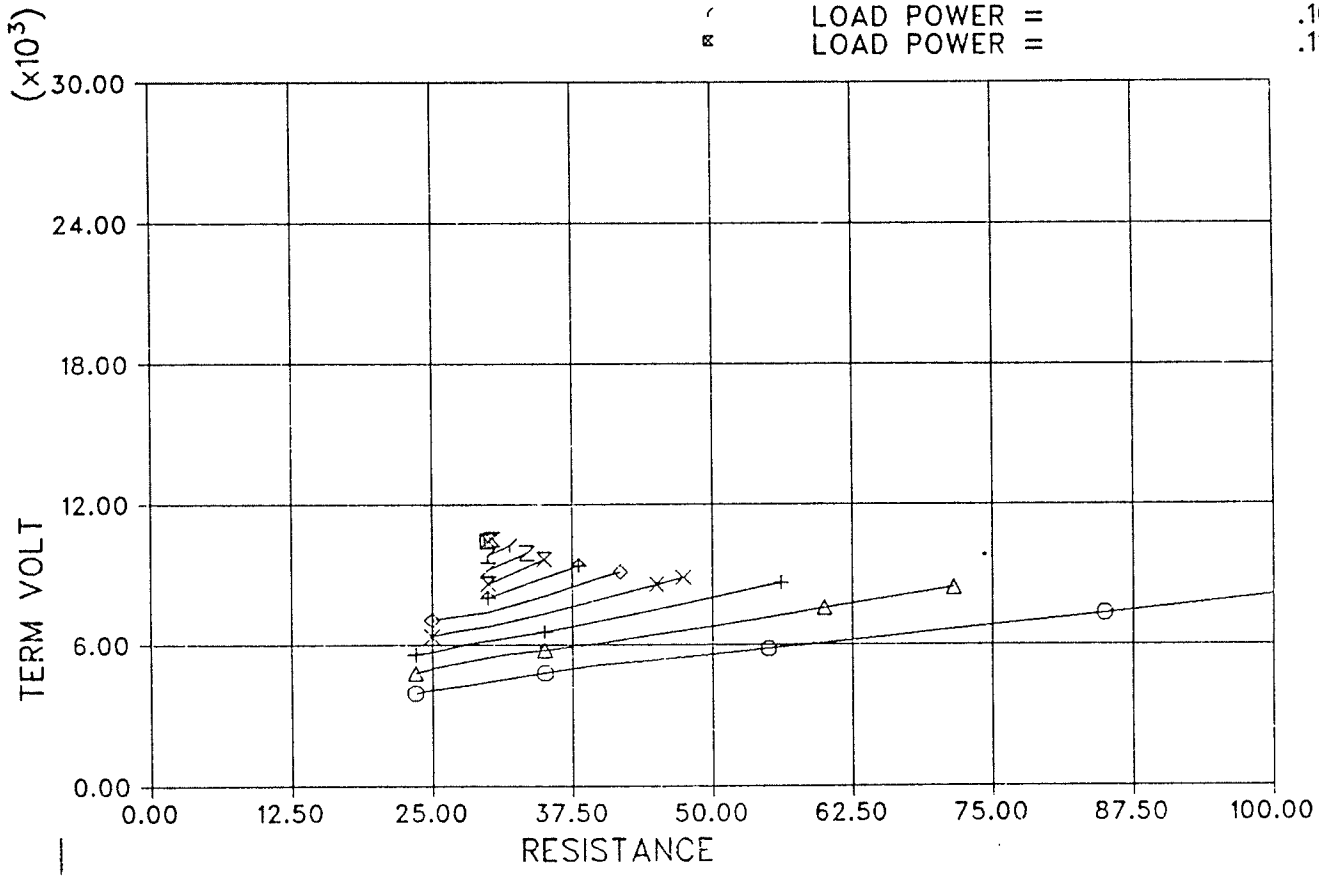

14/03/86 UM EMTDC

REACT LD= .1000E+06CAP SIZE= .6000E-04

○	SLIP =	-.2000E-02
△	SLIP =	-.4000E-02
+	SLIP =	-.6000E-02
×	SLIP =	-.8000E-02
◇	SLIP =	-.1000E-01

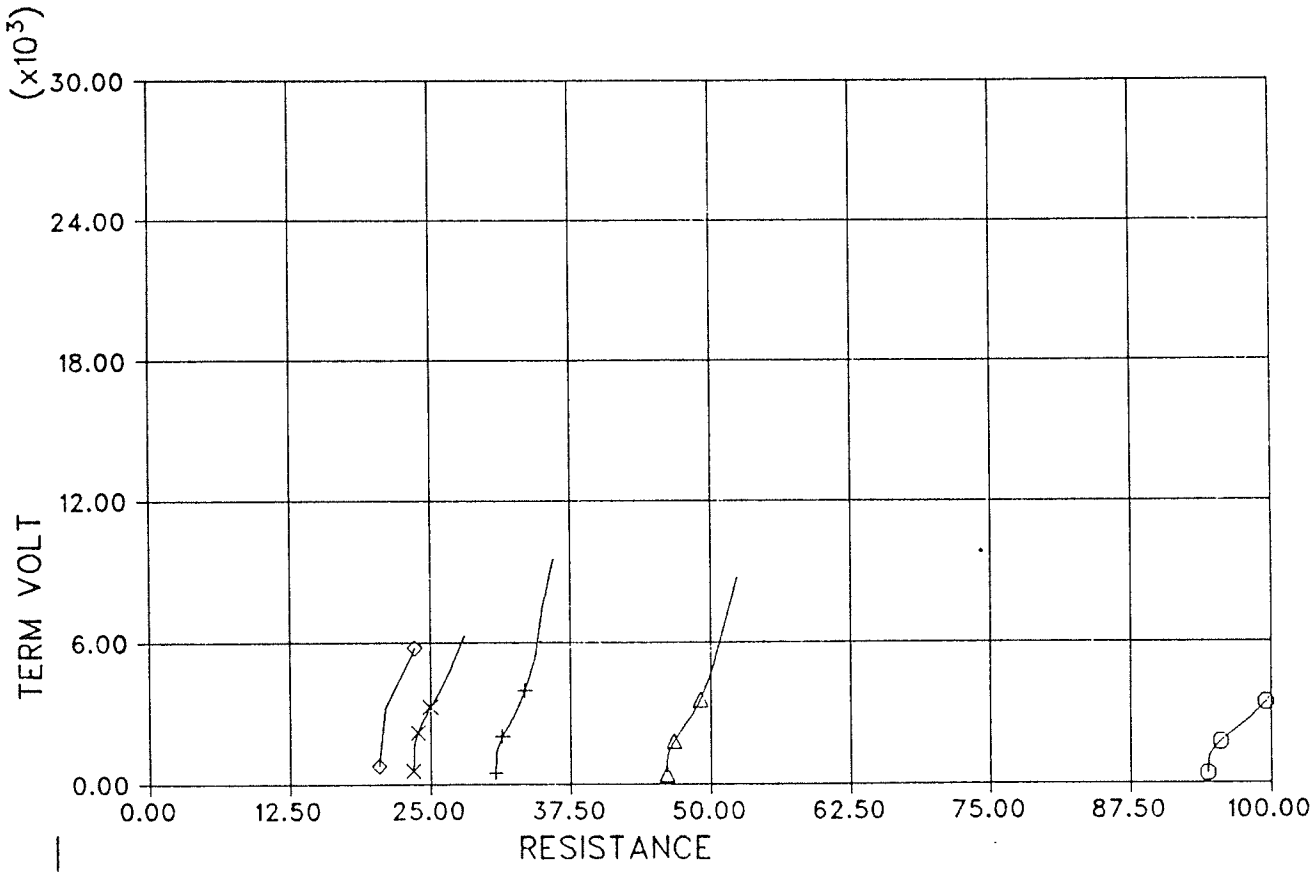

14/03/86 UM EMTDC

File DATACIR page 1 of 1

```
100000. /
13 136.87 133. 130. 125. 110. 100. 90. 80. 70. 60. 50. 40. 30. /
20   100. 85. 77.5 70. 65. 60. 55. 50. 45. 40. 35. 30.
25.0 23.5 21.0 20.0 19. 18. 17. 16. /
44.13 1.92  .32 2320.0 3.827  .175 9999.0 9999.0 /
299  .001 /
```

File CRVDATA1 page 1 of 1

```
10 /
2860.0 2703.0 2494.0 2271.0 2060.0 1821.0 1500.0 1135.0 683.  0.0 /
73.0   85.7    102.5 117.5  125.0  130.8 133.0 135.12 136.87 139.14 /
```

REACT LD= .1000E+06CAP SIZE= .6000E-04

o	MACHINE SPEED =	1.500
Δ	MACHINE SPEED =	1.700
+	MACHINE SPEED =	1.900
×	MACHINE SPEED =	2.100
◇	MACHINE SPEED =	2.300
✦	MACHINE SPEED =	2.500
⧖	MACHINE SPEED =	2.700
Z	MACHINE SPEED =	2.900

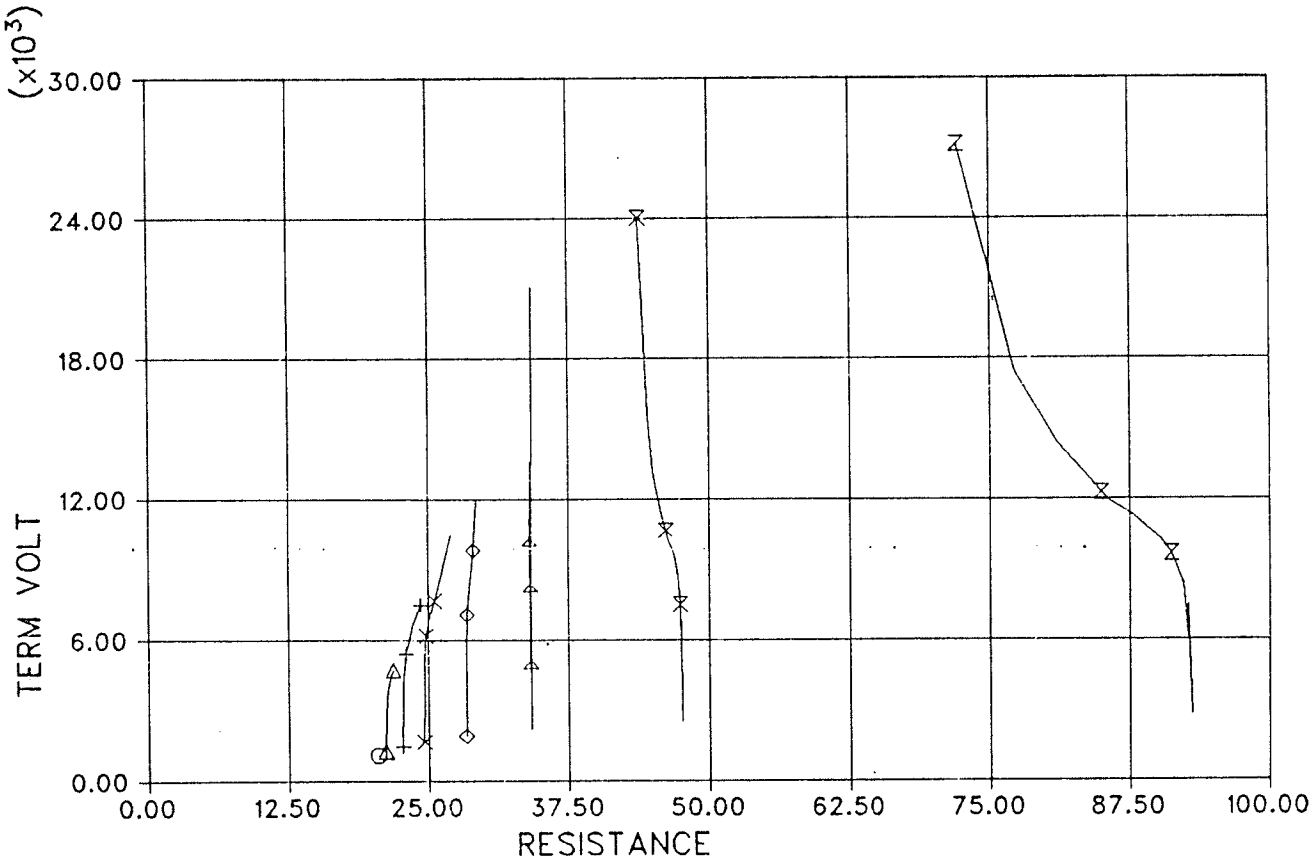

14/03/86 UM EMTDC

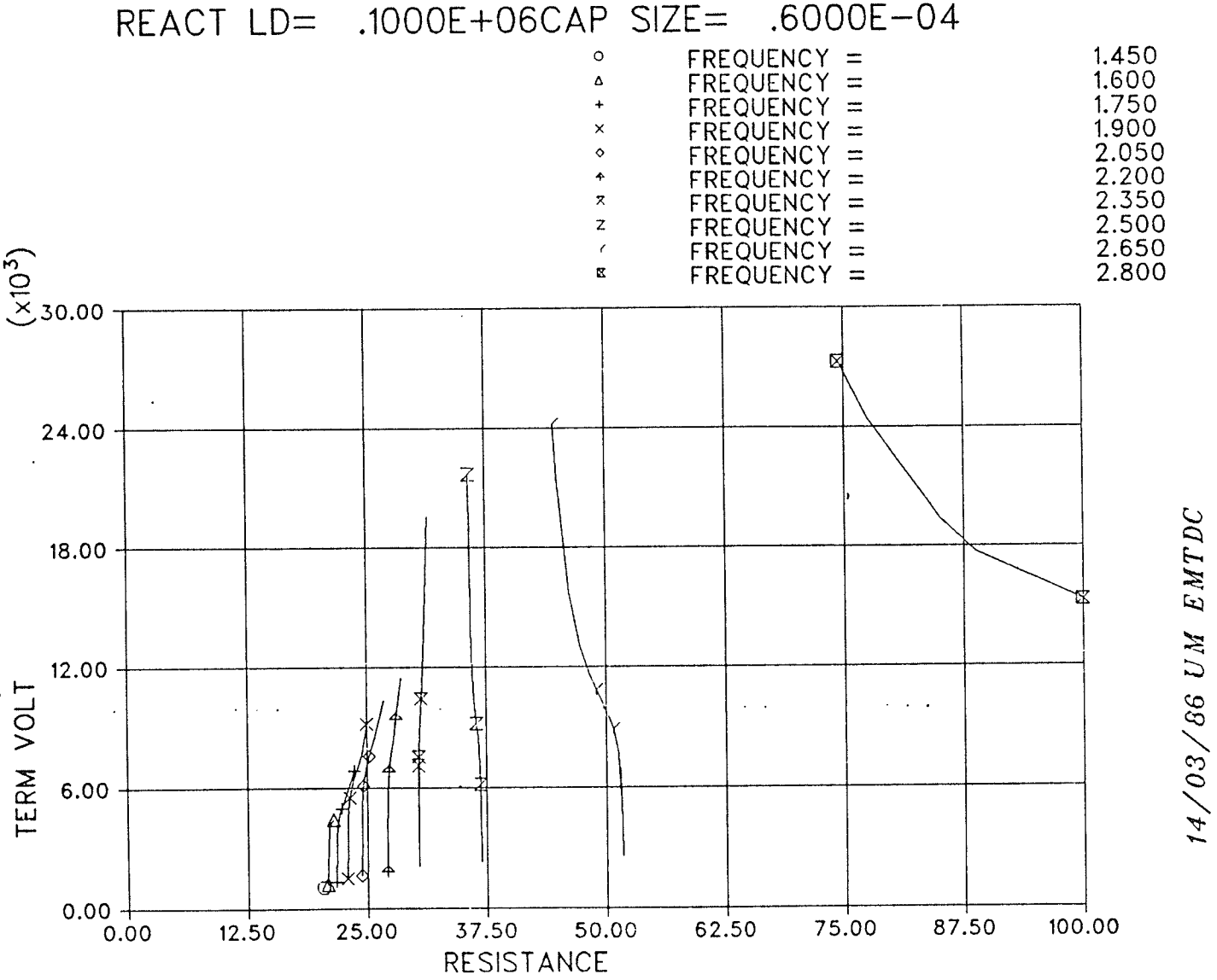
REACT LD= .1000E+06CAP SIZE= .6000E-04
FREQUENCY = 1.450
FREQUENCY = 1.600
FREQUENCY = 1.750
FREQUENCY = 1.900
FREQUENCY = 2.050
FREQUENCY = 2.200
FREQUENCY = 2.350
FREQUENCY = 2.500
FREQUENCY = 2.650
FREQUENCY = 2.800
(x10³)
30.00
24.00
18.00
12.00
6.00
0.00
TERM VOLT
0.00
12.50
25.00
37.50
50.00
62.50
75.00
87.50
100.00
RESISTANCE
14/03/86 UM EMTDC

REACT LD= .1000E+06CAP SIZE= .6000E-04

o	MACHINE TERMINAL CURRENT =	200.0
Δ	MACHINE TERMINAL CURRENT =	400.0
+	MACHINE TERMINAL CURRENT =	600.0
×	MACHINE TERMINAL CURRENT =	800.0
◇	MACHINE TERMINAL CURRENT =	1000.
✦	MACHINE TERMINAL CURRENT =	1200.
✕	MACHINE TERMINAL CURRENT =	1400.
Z	MACHINE TERMINAL CURRENT =	1600.
◜	MACHINE TERMINAL CURRENT =	1800.

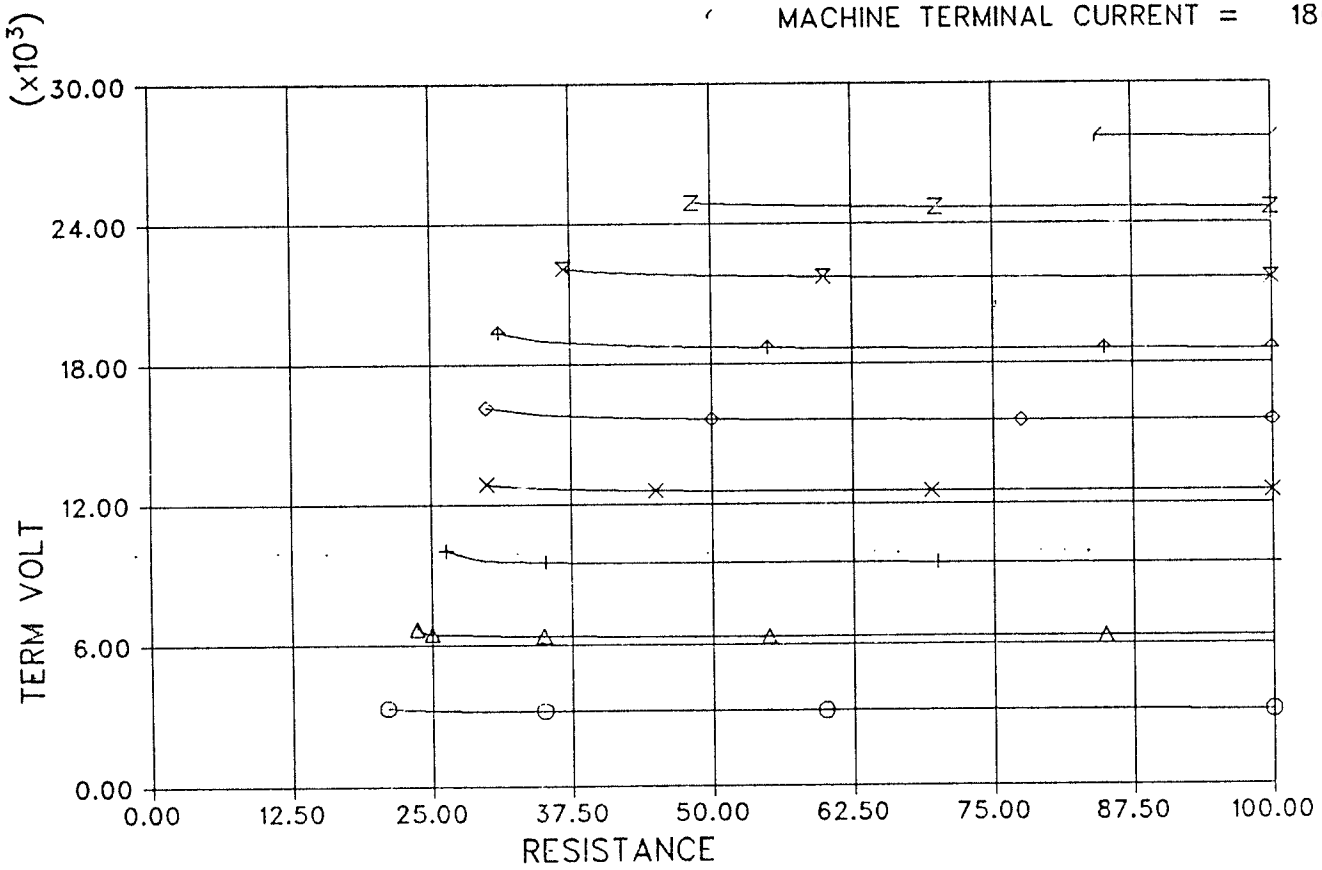

14/03/86 UM EMTDC

REACT LD= .1000E+06CAP SIZE= .6000E-04

o	CAPACITOR CURRENT =	200.0
Δ	CAPACITOR CURRENT =	400.0
+	CAPACITOR CURRENT =	600.0
×	CAPACITOR CURRENT =	800.0
◇	CAPACITOR CURRENT =	1000.
✦	CAPACITOR CURRENT =	1200.
⧖	CAPACITOR CURRENT =	1400.
Z	CAPACITOR CURRENT =	1600.
⌐	CAPACITOR CURRENT =	1800.

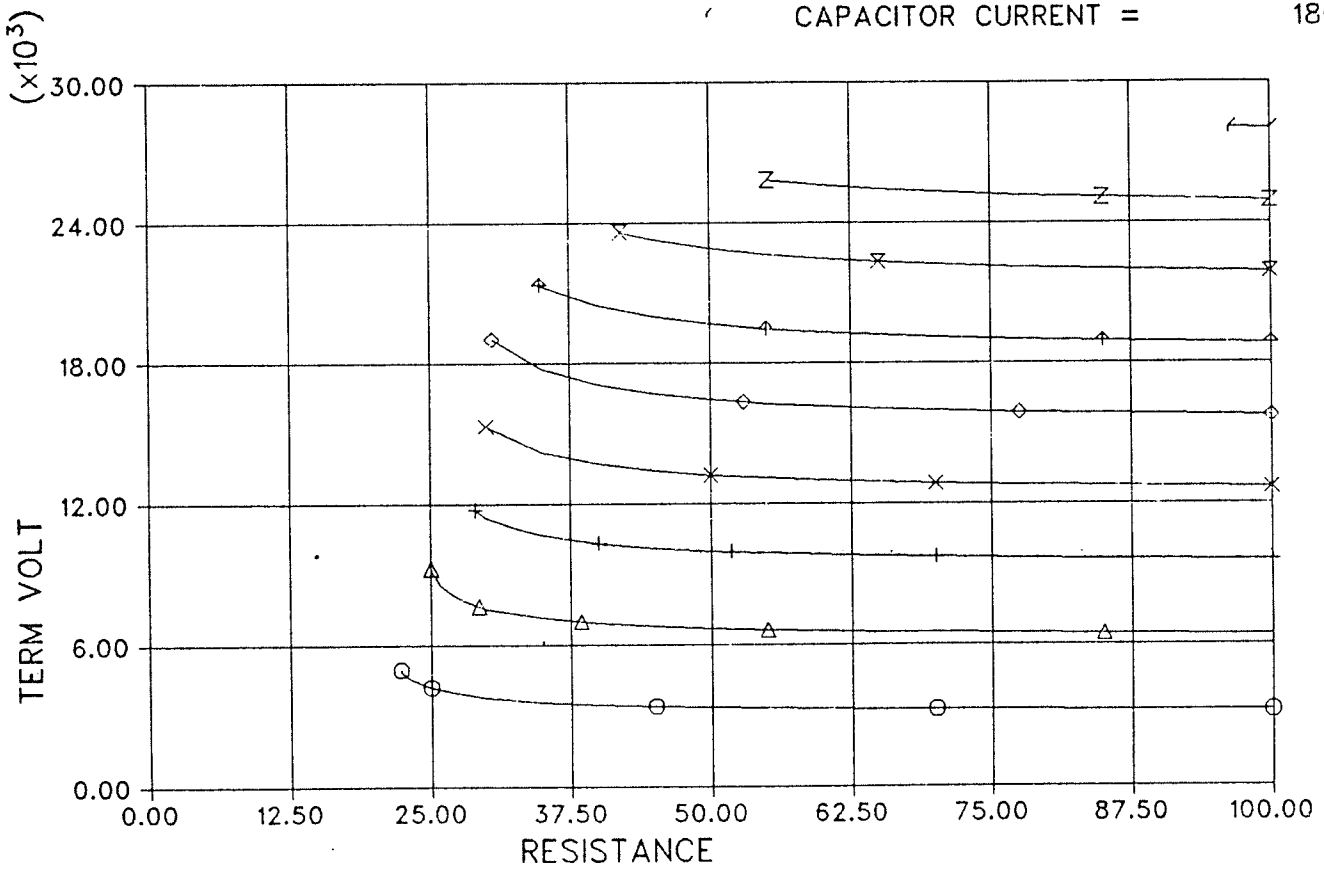

14/03/86 UM EMTDC

REACT LD= .1000E+06CAP SIZE= .6000E-04

○	TOTAL LOAD CURRENT	=	100.0
△	TOTAL LOAD CURRENT	=	200.0
+	TOTAL LOAD CURRENT	=	300.0
×	TOTAL LOAD CURRENT	=	400.0
◇	TOTAL LOAD CURRENT	=	500.0
✦	TOTAL LOAD CURRENT	=	600.0

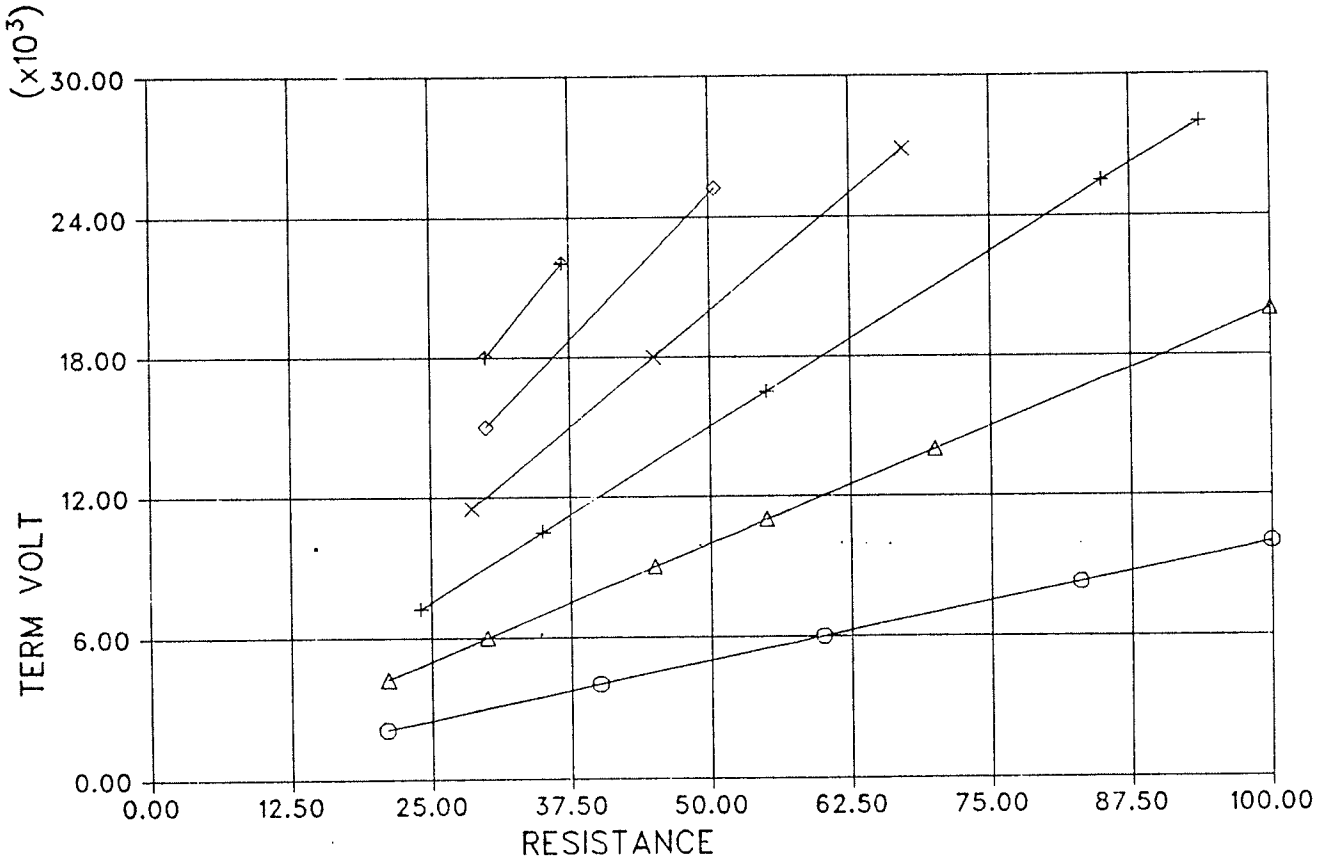

14/03/86 UM EMTDC

REACT LD= .1000E+06CAP SIZE= .6000E-04

o	LOAD POWER =	.4000E+07
Δ	LOAD POWER =	.8000E+07
+	LOAD POWER =	.1200E+08
×	LOAD POWER =	.1600E+08
◇	LOAD POWER =	.2000E+08
✦	LOAD POWER =	.2400E+08
⧖	LOAD POWER =	.2800E+08
Z	LOAD POWER =	.3200E+08
⟋	LOAD POWER =	.3600E+08
⧓	LOAD POWER =	.4000E+08

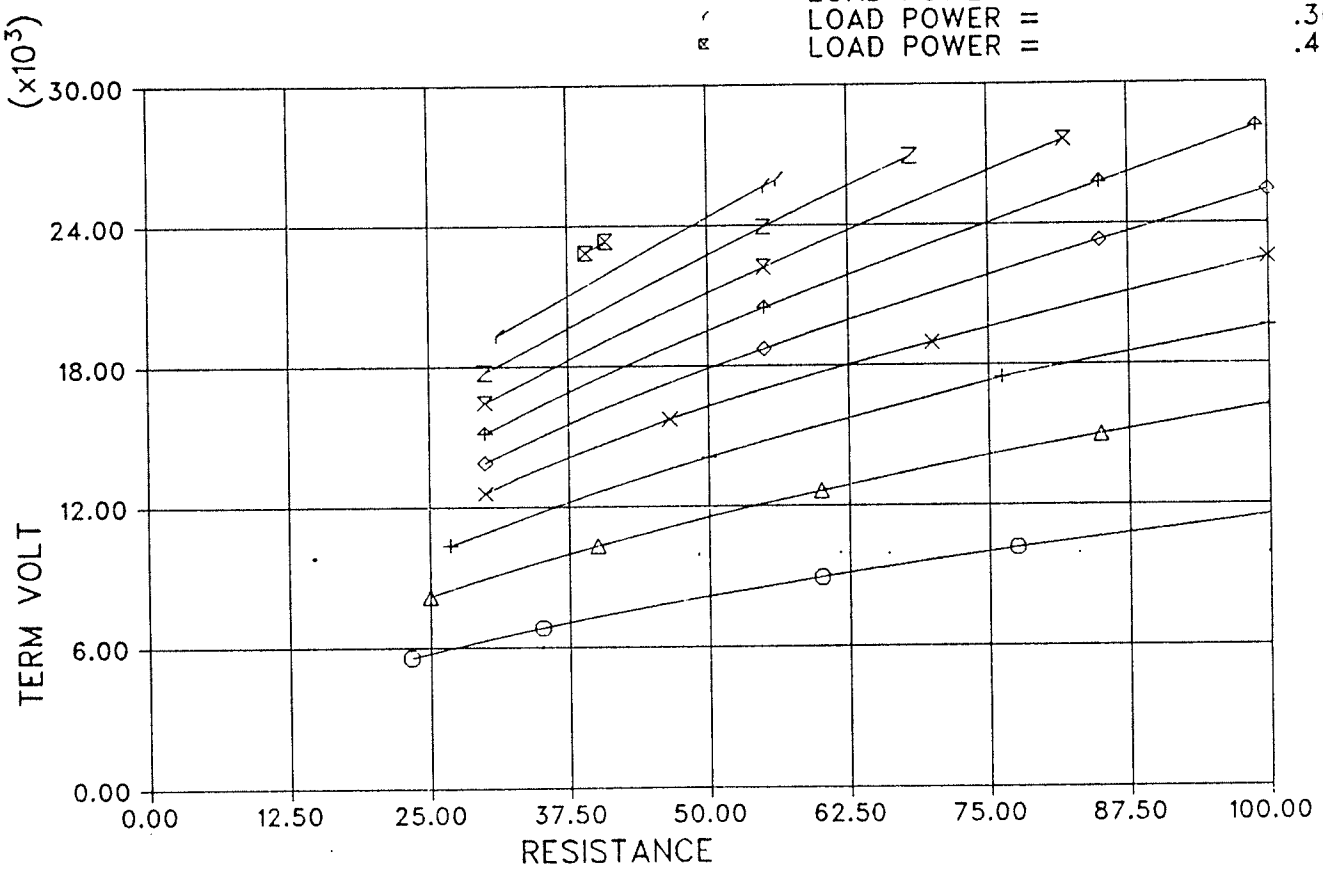

14/03/86 UM EMTDC

REACT LD= .1000E+06CAP SIZE= .6000E-04

○	SLIP =	-.1500E-01
△	SLIP =	-.2500E-01
+	SLIP =	-.3500E-01
×	SLIP =	-.4500E-01
◇	SLIP =	-.5500E-01

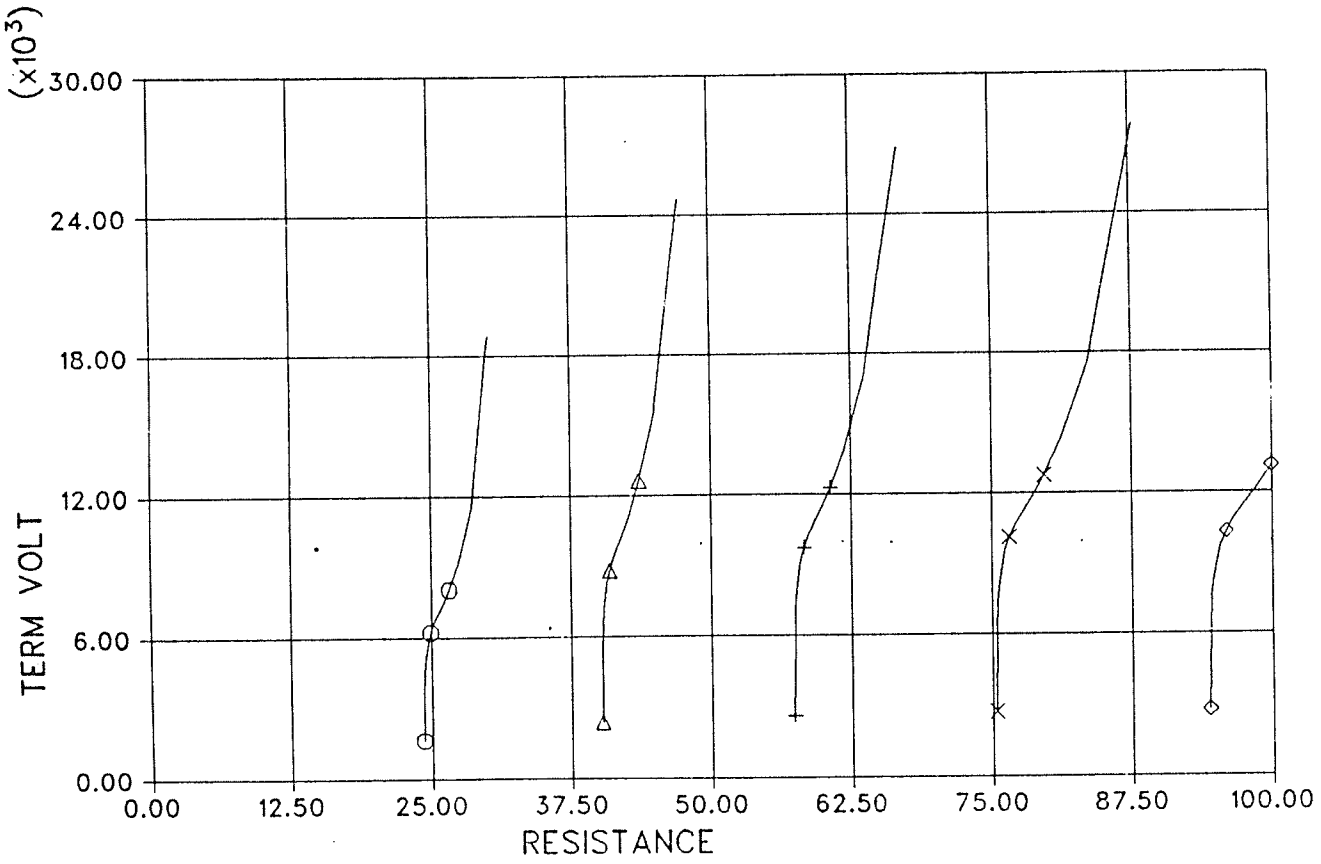

14/03/86 UM EMTDC

APPENDIX 4

EMTDC files for the Control Simulation

This appendix contains the DSDYN, DSOUT, and data files in order to run the transient simulation of the controls discussed in Chapter 4. The files presented in order are:

1. DSD2 - This is the dynamics file.
2. DSO2 - This is the file for specifying output.
3. DATA2 - This file contains the data.

The control system parameters and initial conditions for the simulation in Chapter 4 are:

EEFF at t=0	= VAR(1)	= 0.0
ILO	= VAR(2)	= 0.0
L	= VAR(3)	= 0.1
VREF	= VAR(4)	= 1600.0
KP	= VAR(5)	= 0.3125E-03
KI	= VAR(6)	= 0.46875E-02
KIINTO	= VAR(7)	= 0.0
ILREF	= VAR(8)	= 625.0
KVP	= VAR(9)	= 1.5
KVI	= VAR(10)	= 0.75
KVIINTO	= VAR(11)	= 0.0
TMC	= VAR(12)	= 0.1
TDIF	= VAR(13)	= 0.1
K1	= VAR(14)	= 4.0
K2	= VAR(15)	= 100.0

```
      SUBROUTINE DSDYN
C   SUBROUTINE TO ASSEMBLE SOURCE DATA, SPECIAL CONTROLS,
C   VARIOUS SUBROUTINES, AND ANY FORTRAN STATEMENTS.
C
%INCLUDE 'EMTE'
C
      REAL INTGL3,LIMIT,IL,ILREF,ILERR,KVP,KVI,ILERKVP
      REAL ILERKVI,ILO,KVIINTO,KIINTO,ILDTDIF
C
      COMMON /S1/TIME,DELT,ICH
      COMMON /S2/STOR(5000),NEXC/S3/GVLV(4,4,24),NVLV
      COMMON /S4/VAR(100),CON(100),PGB(25)
C
      IF(TIME.EQ.0.0) STOR(NEXC+1) = VAR(1)
C
      EEFF = STOR(NEXC+1)
      NEXC = NEXC + 1
      ILO = VAR(2)
      IL = INTGL3(ILO,0.0,10000.0,VAR(3),EEFF)
C
C*************************************************
C
      VREF = VAR(4)
      VERROR = VREF - VDC(1,1)
C
      ERRTKP = VERROR * VAR(5)
      ERRTKI = VERROR * VAR(6)
C
      KIINTO = VAR(7)
      ETKIINT = INTGL3(KIINTO,0.0,1.0,1.0,ERRTKI)
C
      SUM = ERRTKP + ETKIINT
      TOFFFR = LIMIT(0.0,1.0,SUM)
C
      CCIN(1,1) = IL * TOFFFR
C
C*************************************************
      ILREF = VAR(8)
      ILERR = ILREF - IL
C
      KVP = VAR(9)
      KVI = VAR(10)
C
      ILERKVP = KVP * ILERR
      ILERKVI = KVI * ILERR
C
      KVIINTO = VAR(11)
      EITKINT = INTGL3(KVIINTO,0.0,1800.0,1.0,ILERKVI)
C
C*************************************
      TDIF = VAR(13)
      ILDTDIF = IL/TDIF
      ROFCIL = DIFPL2(TDIF,ILDTDIF)
      DIDTORD = VAR(14) * ILERR
      DIFORDI = DIDTORD - ROFCIL
      VEXTRA = VAR(3)*VAR(15)*DIFORDI
C
      EORD = ILERKVP + EITKINT + VEXTRA
C*************************************
      EORDL = LIMIT(0.0,2000.0,EORD)
C
      TMCH = VAR(12)
      IF(TIME.EQ.0.0) EORDL = 0.0
      ESOURCE = REALP2(1.0,TMCH,EORDL)
C
      EEFF = ESOURCE - VDC(1,1) * TOFFFR
      STOR(NEXC-14+1) = EEFF
C
      CON(1) = VREF
      CON(2) = VDC(1,1)
      CON(3) = ILREF
      CON(4) = IL
      CON(5) = ESOURCE
      CON(6) = CCIN(1,1)
      CON(7) = VDC(1,1)  * TOFFFR
      CON(8) = VERROR
      CON(9) = ILERR
C
       RETURN
        END
```

File DS02 page 1 of 1

```
      SUBROUTINE DSOUT
C   SUBROUTINE TO ASSEMBLE SOURCE DATA, SPECIAL CONTROLS,
C   VARIOUS SUBROUTINES, AND ANY FORTRAN STATEMENTS.
C
C
%INCLUDE 'EMTE'
      COMMON /S1/TIME,DELT,ICH
      COMMON /S2/STOR(5000),NEXC/S3/GVLV(4,4,24),NVLV
      COMMON /S4/VAR(100),CON(100),PGB(25)
C
      PGB(1) = CON(1)
      PGB(2) = CON(2)
      PGB(3) = CON(3)
      PGB(4) = CON(4)
      PGB(5) = CON(5)
      PGB(6) = CON(6)
      PGB(7) = CON(7)
      PGB(8) = CON(8)
      PGB(9) = CON(9)
C
        RETURN
        END
```

File DATA2 page 1 of 1

```
TEST OF CAP V CONTROL /
0.000050 1.60  0.0032 /
1 /
2 /
0.0  0.00  /
1 0 0.0 0.0 2600.0 /
-1 -2 5.12 /
2 0 0.0  0.84  /
999 /
999 /
999 /
999 /
-400.0 2000.0 /
10 /
0.0 0.0 0.10 1600.0 0.3125E-03 0.46875E-02 0.0 625.0 1.5 .75 0.0 .100
0.1 4.0 100./
999 /
```

APPENDIX 5

EMTDC files for the Simulation of the Shift of Rectifier Angle

This appendix contains the following files:

MIM150 — This file shows just the changes required in MIM100 in order to allow MIMSET17 to set MIM100 in a specified steady state running condition.

MIMSET17 — This file contains a subroutine for setting MIM100 in a specified steady state running condition. The subroutine requires data as specified in comment statement contained in the source code. It should be noted that the saturated value of the magnetizing reactance must be found independantly. XM in ohms at 60 Hz is produced by Programs I, II, and III. However, it could be produced in a small search program if it is desired to set MIM100 for operation as a motor.

CS0DYN — This file contains the dynamics file used in the final simulation in Chapter 4 during which a 0.5 p.u. load increase was placed upon an almost unsaturated machine.

DSOUT — This file contained the output specifying file for the simulation which used CS0DYN.

CS0DAT — This file contained the data input file for the last simulation in chapter 4.

```
      SUBROUTINE MIM150(MS,NA,NB,NC,ANOM,EFD,TMECH,FLD,ITER,FREAL,
     +  PREACT,CONSPD,OMEGA,IKD,IKQ,IROTOR)
C
C*****************************************************************
C MAIN MACHINE SIMULATION PROGRAM. SUBROUTINES XDINV & XQINV USED TO
C INVERT D & Q AXIS INDUCTANCE MATRICES.FUNCTION SATRN GIVES THE
C SATURATION CURVE,SUB AXIS GIVES DX/DT FOR THE AXIS DIFF.EQS.SUB
C TRDQO DOES THE ABC TO DQO XFORMATION (IDIR=1) OR THE DQO TO ABC
C XFORMATION (IDIR=-1).THE PROGRAM TAKES IN VA,VB,VC,VF,TMECH AND
C OUTPUTS IA,IB,IC ETC.
C IF ANOM.LT.0,THE PROGRAM IS JUMPED OVER
C IF CONSPD.GT.0.0, THEN M/C RUNS AT CONSTANT SPPEED=CONSPD
C IF CONSPD.LE. ZERO M/C SPEED IS AFFECTED BY INPUT TORK
C
C FOR ANY ENQUIRIES CONTACT ANIR GOLE AT 474 -9959
C
C*****************************************************************
```

CHANGES TO MIM100 TO ALLOW MIMSET17 TO INITIALIZE IT.

```
      READ (50,*) (STOR(NEXC+I),I=1,5)
      READ (50,*) STOR(NEXC+8),STOR(NEXC+75),STOR(NEXC+9),
     . STOR(NEXC+72)
      READ (50,*) STOR(NEXC+70),STOR(NEXC+7),STOR(NEXC+74)
     1 ,STOR(NEXC+6),STOR(NEXC+10)
      READ (50,*) STOR(NEXC+61),STOR(NEXC+60),STOR(NEXC+71)
      READ (50,*) (STOR(NEXC+I),I=111,140)
      READ (50,*) STOR(NEXC+51),STOR(NEXC+52)
C     READ (50,*) STOR(NEXC+62),STOR(NEXC+54),STOR(NEXC+55),
C    1 STOR(NEXC+57)
      WRITE(6,143) STOR(NEXC+61),STOR(NEXC+60)
C     STOR(NEXC+59)=STOR(NEXC+60)
C *****
```

← COMMENT OUT THE LAST READ STATEMENT AND REMOVE THAT DATA FROM THE DATA FILE.

← COMMENT OUT THE INDICATED STATEMENT WHICH INITIALIZES "OMEGA" TO "OMO".

```
      SUBROUTINE MIMSET17
%INCLUDE 'EMTE'
      COMMON/S1/TIME,DELT/S2/STOR(5000),NEXC
      COMMON/S4/VAR(100),CON(100),PGB(25)
C
C*****************************************************************
C  THIS PROGRAM MUST BE PLACED IMMEDIATELY BEFORE
C                  MIM150
C
C    DATA:
C     LINE1:- TSET , THE TIME WHEN MACHINE CURRENTS,SPEED
C                  AND THETA WILL BE SET.
C             THETASET , THE ANGLE IN RAD. THAT THE D-AXIS LEADS
C                        THE A-AXIS AT TIME = TSET.
C                        ( D-AXIS LEADS Q-AXIS )
C             VTSET , THE L-N VOLTAGE IN RMS VOLTS
C             VANGT0 , THE ANGLE IN RADIANS OF THE A-PHASE
C                      VOLTAGE AT TIME = 0.0
C             FSET , THE P.U. FREQUENCY OF THE TERMINAL VOLTAGE
C             SPDSET , THE P.U. SPEED OF THE MACHINE
C             OMEGAB , THE BASE ANGULAR FREQ. ( USUALLY 376.991 )
C     LINE2:- XS IN OHMS AT 60HZ
C             RS IN OHMS
C     LINE3:- XM IN OHMS AT 60HZ
C     LINE4:- XR1 IN OHMS AT 60HZ
C             XR1XTRA IN OHMS AT 60HZ
C             RR1 IN OHMS
C     LINE5:- XR2 IN OHMS AT 60HZ
C             RR2 IN OHMS
C     LINE6:- CBASE , CURRENT BASE  USED IN MIM150
C
C
C        --- RS --- XS-----XR1-----------
C                      )        )       )
C                     XM      XR1XTRA   XR2
C                      )        )       )
C                      )       RR1      RR2
C                      )        )       )
C        ---------------------------------
C
C       IF YOU ONLY HAVE ONE CAGE  IN YOUR REPRESENTATION THEN
C         USE RR1 = RR2 = 2*RR
C             XR1 = 0.0
C             XR1XTRA = XR2 = XR
C           WHERE RR AND XR DESCRIBE THE SINGLE CAGE.
C
C*****************************************************************
C
      REAL OMEGAB
C
      COMPLEX ROT2C,RR1C,XR1C,XMDC,STATC
      COMPLEX CMPLX
      COMPLEX ZROTORS,ZAIRGAP,ZMACH
      COMPLEX VMACH,IMACH,IROTORS,IROT1,IROT2
C
      IF(TIME.GT.0.0) GO TO 10
C
      READ(50,*) (STOR(NEXC+I),I=1,7)
      READ(50,*) (STOR(NEXC+7+I),I=1,2)
      READ(50,*)  STOR(NEXC+10)
      READ(50,*) (STOR(NEXC+10+I),I=1,3)
      READ(50,*) (STOR(NEXC+13+I),I=1,2)
      READ(50,*)  STOR(NEXC+16)
C
      STOR(NEXC+17) = 0.0
C
   10 CONTINUE
C
      IF(STOR(NEXC+17).GT.1.0) GO TO 1000
C
      TSET = STOR(NEXC+1)
      IF(TIME.GE.TSET) THEN
       STOR(NEXC+17) = 2.0
       TCALC = TIME
       GO TO 20
      ELSE
       GO TO 1000
      END IF
C
   20 CONTINUE
C
```

```
      THETASET = STOR(NEXC+2)
      VTSET    = STOR(NEXC+3)
      VANGT0   = STOR(NEXC+4)
      FSET     = STOR(NEXC+5)
      SPDSET   = STOR(NEXC+6)
      OMEGAB   = STOR(NEXC+7)
C
      XS       = STOR(NEXC+8)
      RS       = STOR(NEXC+9)
C
      XMD      = STOR(NEXC+10)
C
      XR1      = STOR(NEXC+11)
      XR1XTRA  = STOR(NEXC+12)
      RR1      = STOR(NEXC+13)
C
      XR2      = STOR(NEXC+14)
      RR2      = STOR(NEXC+15)
C
      CBASE    = STOR(NEXC+16)
C
      S = ( FSET - SPDSET ) / FSET
      F = FSET
C
      ROT2C = CMPLX(RR2/S,XR2*F)
      RR1C  = CMPLX(RR1/S,XR1XTRA*F)
      XR1C  = CMPLX(0.0,XR1*F)
      XMDC  = CMPLX(0.0,XMD*F)
      STATC = CMPLX(RS,XS*F)
C
      ZROTORS = XR1C + RR1C*ROT2C/(RR1C+ROT2C)
      ZAIRGAP = ZROTORS*XMDC/(ZROTORS+XMDC)
      ZMACH   = STATC + ZAIRGAP
C
      VMACH = CMPLX(VTSET,0.0)
      IMACH = VMACH/ZMACH
C
      IROTORS = IMACH*XMDC/(XMDC+ZROTORS)
      IROT1   = IROTORS*ROT2C/(ROT2C+RR1C)
      IROT2   = IROTORS - IROT1
C
      TRMIMAG = CABS(IMACH)
      CG1IMAG = CABS(IROT1)
      CG2IMAG = CABS(IROT2)
C
      RLITRM  = REAL(IMACH)
      RLICG1  = REAL(IROT1)
      RLICG2  = REAL(IROT2)
C
      XITRM   = AIMAG(IMACH)
      XICG1   = AIMAG(IROT1)
      XICG2   = AIMAG(IROT2)
C
      TRMIANG = ATAN2(XITRM,RLITRM)
      CG1IANG = ATAN2(XICG1,RLICG1)
      CG2IANG = ATAN2(XICG1,RLICG2)
C
      WRITE(6,*) TRMIMAG , TRMIANG
      WRITE(6,*) CG1IMAG , CG1IANG
      WRITE(6,*) CG2IMAG , CG2IANG
C
      SQR2  = SQRT(2.0)
      WDUM    = OMEGAB*FSET*TCALC + VANGT0 - THETASET
C
      CDSET  =  TRMIMAG*COS( WDUM + TRMIANG )/CBASE*SQR2
      CQSET  = -TRMIMAG*SIN( WDUM + TRMIANG )/CBASE*SQR2
C
      CFDSET  = -CG1IMAG*COS( WDUM + CG1IANG )/CBASE*SQR2
      CKQ1SET =  CG1IMAG*SIN( WDUM + CG1IANG )/CBASE*SQR2
C
      CKDSET  = -CG2IMAG*COS( WDUM + CG2IANG )/CBASE*SQR2
      CKQ2SET =  CG2IMAG*SIN( WDUM + CG2IANG )/CBASE*SQR2
C
      NEXM = NEXC + 17
C
      STOR(NEXM + 62) = THETASET
      STOR(NEXM + 59) = SPDSET*OMEGAB
      STOR(NEXM + 54) = CDSET
      STOR(NEXM + 55) = CQSET
      STOR(NEXM + 57) = CFDSET
      STOR(NEXM + 58) = CKDSET
```

```
      STOR(NEXM + 67) = CKQ2SET
      STOR(NEXM + 76) = CKQ1SET
C
 1000 CONTINUE
C
      NEXC = NEXC + 17
C
      RETURN
       END
```



```
       SUBROUTINE DSDYN
C   SUBROUTINE TO ASSEMBLE SOURCE DATA, SPECIAL CONTROLS,
C   VARIOUS SUBROUTINES, AND ANY FORTRAN STATEMENTS.
C
      REAL LIMIT,INTGL3,LDLAG2
C
C**TEMPORARILY IGNORE THIS %INCLUDE STATEMENT
C
%INCLUDE 'EMTE'
      COMMON /S1/TIME,DELT,ICH
      COMMON /S2/STOR(5000),NEXC/S3/GVLV(4,4,24),NVLV
      COMMON /S4/VAR(100),CON(100),PGB(25)
C
C    THIS PROGRAM IS MEANT TO TEST THE SELF EXCITATION OF
C         THE 900 h.p. INDUCTION MACHINE
C
      CALL MIMSET17
C
      CONSPD = VAR(1)*376.991
      TCHANG = VAR(2)
      PNEW   =  VAR(3)
C
      CALL MIM150(1,1,2,3,1.0,0.0,TMECH,FLD,1,
     &  P,Q,CONSPD,OMEGA,CD,CQ,ROT)
C
      CALL PRLL2(TCHANG,1,4,4,1.0,PNEW,0)
      CALL PRLL2(TCHANG,1,5,5,1.0,PNEW,0)
      CALL PRLL2(TCHANG,1,6,6,1.0,PNEW,0)
C
        PGB(1)=VDC(1,1)
        PGB(2)=VDC(2,1)
        PGB(3)=VDC(3,1)
        PGB(4)= RMS3PH(VDC(1,1),VDC(2,1),VDC(3,1))
        PGB(5) = CDC(4,7,1) - CDC(7,10,1)
        PGB(6) = CDC(7,10,1)
C
          RETURN
           END
```

```
      SUBROUTINE DSOUT
C   SUBROUTINE TO ASSEMBLE SOURCE DATA, SPECIAL CONTROLS,
C   VARIOUS SUBROUTINES, AND ANY FORTRAN STATEMENTS.
C
%INCLUDE 'EMTE'
      COMMON /S1/TIME,DELT,ICH
      COMMON /S2/STOR(5000),NEXC/S3/GVLV(4,4,24),NVLV
      COMMON /S4/VAR(100),CON(100),PGB(25)
C
C    FOR 900 h.p. INDUCTION MACHINE SELF EXCITATION TEST
C
        RETURN
        END
```



```
SELF EXCITATION OF LAB M/C /
0.00005  0.16 0.0005   /DELT FINTIM PRTSTEP
1 /NO OF SUBSYSTS
12 /NO OF NODES IN SS 1
3265.43 -1632.71 -1632.71 3265.43 -1632.71 -1632.71
3265.43 -1632.71 -1632.71 3182.74 -1147.11 -2033.87 / INIT NODE VOLTS
1 4 0.02 0.0 0.0 0.0 34.07 /
2 5 0.02 0.0 0.0 0.0 -2.22 / MACHINE BREAKER
3 6 0.02 0.0 0.0 0.0 -31.85 /
4 0 2320.  0.0 0.0 0.0 1.41 /
5 0 2320.  0.0 0.0 0.0 -.71  / IRON LOSS
6 0 2320.  0.0 0.0 0.0 -.71 /
4 7 0.02   0.0 0.0 0.0 32.65 /
5 8 0.02   0.0 0.0 0.0 -1.51 /  NODE SEPARATOR
6 9 0.02   0.0 0.0 0.0 -31.14 /
7 0   0.0 0.0  99.35 0.0 0.0  /
8 0   0.0 0.0  99.35 0.0 190.28 /  EXCITATION CAPACITOR IN MICROF
9 0   0.0 0.0  99.35 0.0 -190.28 /
7 10 2.53 0.0 0.0 0.0 32.51 /
8 11 2.53  0.0 0.0 0.0 -191.74 / RES. PART OF LOAD
9 12 2.53 0.0 0.0 0.0 159.23 /
10 0 0.0  0.02319  0.0 0.0  32.51 /
11 0 0.0  0.023197 0.0 0.0 -191.74 / IND. PART OF LOAD
12 0 0.0  0.023197 0.0 0.0 159.23 /
999 /END OF NODEDATA
999 /NO SOURCEDATA
999 /NO XFORMERDATA
999 /NO TLINEDATA
-5000.  5000. /
10 /#CHANNELS
1.8 0.08 47.4 / MSPD , CHANGE TIME, PNEW
0.0 0.0 2309.0 0.0 1.796597  1.8 376.991 /
1.92 0.32 /
134.3522 /
0.0  3.827 0.35 /
     3.827 0.35 /
111.0 /
0.0923 5.0923 0.0   0.18399 0.18399 /XA XMDO XKF XKD XF
       5.0923 0.0   0.18399 0.18399 / AND CORRESPONDING Q AXIS THINGS
0.01538 0.0168 0.0168 0.0168 0.0168 /RA RFD RQF RKD RKQ
2.0 376.991 0.0 /MECHANICAL THINGS
0.0     0.0       0.0825  0.0780  0.1500  0.1628  0.2289  0.2958
0.3853  0.4916    0.5046  0.6496  0.6385  0.7887  0.7064  0.8922
0.8867  0.9835    1.0000  1.0000  1.1165  1.0801  1.4472  1.1706
1.7890  1.2386    2.2706  1.2689  2.7523  1.2993 /
2309.0   111.0 /  VBASE IBASE
```